



Technische Universität München

Lehrstuhl für Entwicklungsgenetik

Generation and analysis of *FUS* and *TMEM106B* mouse models

Michaela Anna Bosch

Vollständiger Abdruck der von der Fakultät Wissenschaftszentrum Weihenstephan für Ernährung, Landnutzung und Umwelt der Technischen Universität München zur Erlangung des akademischen Grades eines

Doktors der Naturwissenschaften

genehmigten Dissertation.

Vorsitzender: Univ.-Prof. Dr. H. Luksch

Prüfer der Dissertation:

1. Univ.-Prof. Dr. W. Wurst

2. Univ.-Prof. Dr. H. Lickert

Die Dissertation wurde am 13.04.2015 bei der Technischen Universität München eingereicht und durch die Fakultät Wissenschaftszentrum Weihenstephan für Ernährung, Landnutzung und Umwelt am 15.10.2015 angenommen.

Eidesstattliche Erklärung

Ich erkläre an Eides statt, dass ich die bei der promotionsführenden Einrichtung bzw. Fakultät Wissenschaftszentrum Weihenstephan für Ernährung, Landnutzung und Umwelt der TUM zur Promotionsprüfung vorgelegte Arbeit mit dem Titel:

„Generation and analysis of FUS and TMEM106B mouse models“

in Entwicklungsgenetik unter der Anleitung und Betreuung durch Prof. Dr. W. Wurst ohne sonstige Hilfe erstellt und bei der Abfassung nur die gemäß § 6 Abs. 6 und 7 Satz 2 angegebenen Hilfsmittel benutzt habe.

Ich habe keine Organisation eingeschaltet, die gegen Entgelt Betreuerinnen und Betreuer für die Anfertigung von Dissertationen sucht, oder die mir obliegenden Pflichten hinsichtlich der Prüfungsleistungen für mich ganz oder teilweise erledigt.

Ich habe die Dissertation in dieser oder ähnlicher Form in keinem anderen Prüfungsverfahren als Prüfungsleistung vorgelegt.

Die vollständige Dissertation wurde in veröffentlicht. Die promotionsführende Einrichtung..... hat der Vorveröffentlichung zugestimmt.

Ich habe den angestrebten Doktorgrad **noch nicht** erworben und bin **nicht** in einem früheren Promotionsverfahren für den angestrebten Doktorgrad endgültig gescheitert.

Ich habe bereits am bei der Fakultät für der Hochschule unter Vorlage einer Dissertation mit dem Thema die Zulassung zur Promotion beantragt mit dem Ergebnis:

Die öffentlich zugängliche Promotionsordnung der TUM ist mir bekannt, insbesondere habe ich die Bedeutung von § 28 (Nichtigkeit der Promotion) und § 29 (Entzug des Doktorgrades) zur Kenntnis genommen. Ich bin mir der Konsequenzen einer falschen Eidesstattlichen Erklärung bewusst.

Mit der Aufnahme meiner personenbezogenen Daten in die Alumni-Datei bei der TUM bin ich einverstanden nicht einverstanden

München, den

CONTENT

1 ZUSAMMENFASSUNG	1
2 SUMMARY	3
3 INTRODUCTION.....	5
3.1 NEURODEGENERATIVE DISEASES	5
3.1.1 <i>Amyotrophic Lateral Sclerosis (Lou Gehrig’s Disease)</i>	5
3.1.2 <i>Frontotemporal Lobar Degeneration (Pick’s Disease)</i>	10
3.1.3 <i>Link between ALS and FTLD</i>	12
3.2 FUSED IN SARCOMA (FUS).....	15
3.2.1 <i>Structure and Function of FUS</i>	15
3.2.2 <i>FUS in ALS and FTLD</i>	18
3.2.3 <i>Posttranslational Modifications of FUS</i>	21
3.2.4 <i>FUS Rodent Models</i>	22
3.3 TRANSMEMBRANE PROTEIN 106B (TMEM106B).....	24
3.3.1 <i>Structure and Function of TMEM106B</i>	25
3.3.2 <i>TMEM106B in the Human Brain</i>	26
3.3.3 <i>TMEM106B as a Modulator of FTLD</i>	27
3.4 MOTIVATION AND OBJECTIVE OF THE THESIS.....	28
4 MATERIAL	30
4.1 CONSUMABLE MATERIAL	30
4.2 INSTRUMENTS	31
4.3 CHEMICALS AND CONSUMABLE SUPPLIES	33
4.4 KITS.....	38
4.5 VECTORS AND PLASMIDS.....	39
4.6 ENZYMES	40
4.7 OLIGONUCLEOTIDES.....	41
4.7.1 <i>Oligonucleotides for Genotyping</i>	41
4.7.2 <i>Oligonucleotides for RT-PCR</i>	42
4.7.3 <i>Oligonucleotides for Probes</i>	43
4.8 TAQMAN ASSAYS.....	43

4.8.1 Taqman Gene Expression Assay	44
4.8.2 Taqman Copy Number Assay.....	44
4.9 MOUSE STRAINS.....	45
4.9.1 Used Mouse Strains	45
4.9.2 Generated Mouse Strains.....	45
4.10 STOCK SOLUTIONS	46
4.11 WORK WITH BACTERIA.....	47
4.11.1 <i>E. coli</i> Strains.....	47
4.11.2 Solutions.....	47
4.12 CELL CULTURE.....	48
4.12.1 Cell Lines.....	48
4.12.2 Media and Solutions.....	48
4.13 GENERATION OF MICE.....	49
4.14 WESTERN BLOT ANALYSIS.....	49
4.14.1 Solutions.....	49
4.14.2 Antibodies.....	50
4.15 IMMUNOHISTOCHEMISTRY	53
4.15.1 Solutions.....	53
4.15.2 Antibodies.....	53
4.16 WHOLE MOUNT IN SITU HYBRIDIZATION (WISH).....	55
5 METHODS	58
5.1 MOLECULAR BIOLOGY METHODS	58
5.1.1 Cloning and Plasmid Preparation.....	58
5.1.2 Analysis of Genomic DNA.....	60
5.1.3 Analysis of RNA.....	63
5.1.4 Analysis of Protein Samples	65
5.2 CELL CULTURE	67
5.2.1 ES Cells.....	67
5.2.2 Generation of Fibroblasts.....	68
5.2.3 Splitting of Cells.....	68
5.2.4 Freezing and Thawing of Cells.....	68
5.2.5 Electroporation of ES Cells.....	69
5.2.6 Selection and Picking of Resistant ES Cell Clones.....	70
5.2.7 PCR Screening of Resistant ES Cell Clones.....	70
5.2.8 Karyotyping of ES Cell Clones.....	70

5.2.9 Immunofluorescence	71
5.2.10 Seahorse Mito Stress Test	71
5.3 MOUSE HUSBANDRY	72
5.3.1 Generation of Mice	72
5.3.2 Establishment of New Mouse Lines	73
5.3.3 Mouse Facilities	73
5.4 HISTOLOGY	74
5.4.1 Immunohistochemistry of Mouse Tissue	74
5.4.2 Motor Neuron Staining	79
5.4.3 Transmission Electron Microscopy (TEM)	79
5.5 GERMAN MOUSE CLINIC (GMC)	80
5.6 STATISTICS	80
6 RESULTS	82
6.1 <i>FUS</i> MOUSE MODELS	82
6.1.1 Mouse Model lacking <i>Fus</i>	82
6.1.1.1 Generation of <i>Fus</i> deficient mice	82
6.1.1.2 Lethality of <i>Fus</i> ^{-/-} mice	83
6.1.1.3 <i>Fus</i> expression levels <i>in vivo</i>	84
6.1.1.4 Pathological analysis of <i>Fus</i> GT mice	85
6.1.1.5 Phenotypical analysis of <i>Fus</i> GT mice	89
6.1.1.6 Homozygous survivor mice	94
6.1.2 Humanized <i>FUS</i> ^{R521G} Mouse Model	99
6.1.2.1 Generation of h <i>FUS</i> ^{R521G} mice	99
6.1.2.2 Homozygous lethality of h <i>FUS</i> ^{R521G} mice	102
6.1.2.3 Expression of h <i>FUS</i> ^{R521G} <i>in vivo</i>	103
6.1.2.4 Subcellular mislocalization of <i>FUS</i> protein	105
6.1.2.5 Pathological analysis of h <i>FUS</i> ^{R521G+/-} mice	109
6.1.2.6 Phenotypical analysis of h <i>FUS</i> ^{R521G+/-} mice	114
6.1.3 Expression of Different ALS-Associated Mutations <i>in Vivo</i>	118
6.1.3.1 Generation of TALEN mice expressing mutant <i>Fus</i>	118
6.1.3.2 Viability of <i>Fus</i> TALEN mice	119
6.1.3.3 Subcellular mislocalization of <i>Fus</i> protein	120
6.1.3.4 Pathological analysis of <i>Fus</i> TALEN mice	123
6.1.3.5 Phenotypical analysis of <i>Fus</i> ^{R513G+/-} mice	129

6.2 <i>TMEM106B</i> MOUSE MODELS	134
6.2.1 <i>Transgenic Overexpression of Tmem106b in vivo</i>	134
6.2.1.1 Generation of <i>Tmem106b</i> transgenic mice	134
6.2.1.2 Expression levels of <i>Tmem106b</i> in transgenic mice	137
6.2.1.3 Subcellular localization of TDP-43 in <i>Tmem106b^{BACTg}</i> mice	137
6.2.1.4 TEM analysis of <i>Tmem106b^{BACTg}</i> mice	138
6.2.2 <i>Overexpression of Tmem106b on a Mutant hTDP-43^{A513TKi} Background</i>	140
6.2.2.1 Effects of ectopic <i>Tmem106b</i> levels on TDP-43	140
6.2.2.2 Effects of ectopic <i>Tmem106b</i> on protein levels	143
6.2.2.3 TEM analysis of <i>Tmem106b^{BACTg} x hTDP-43^{A315TKi}</i> mice	144
6.2.2.4 Effects of ectopic <i>Tmem106b</i> on mitochondrial proteins and activity	145
7 DISCUSSION	149
7.1 ALS-ASSOCIATED POINT MUTATIONS: LOSS OR GAIN OF FUNCTION?	149
7.1.1 <i>Depletion of Fus</i>	150
7.1.2 <i>Humanized FUS Mouse Model</i>	153
7.1.3 <i>Fus TALEN Mice</i>	157
7.1.4 <i>Comparison of Mouse Models for ALS-Associated Point Mutations</i>	161
7.1.5 <i>Loss or Gain of Fus Function?</i>	164
7.2 OVEREXPRESSION OF <i>TMEM106B</i> <i>IN VIVO</i>	167
7.3 LESSONS FROM MOUSE MODELS GENERATED FOR ALS AND FTLD	170
8 REFERENCES	172
9 APPENDIX	199
9.1 ABBREVIATIONS	199
9.2 INDICES	209
9.2.1 <i>Tables</i>	209
9.2.2 <i>Figures</i>	209
9.3 SUPPLEMENTARY DATA	211
9.3.1 <i>Videos of Fus GT^{-/-} Survivor Mice</i>	211
9.3.2 <i>Comparison of hFUS and mFus</i>	212
9.3.2.1 Subcellular mislocalization of FUS	212
9.3.2.2 Comparison of phenotypical analysis	213
9.3.2.3 Sequenz comparison	215
9.3.3 <i>Comparison of Fus GT, Fus^{R513G} and Fus^{R521G} Mouse Lines</i>	216
9.3.3.1 Comparison of GMC data	216

9.3.3.2 Comparison of pathological results.....	219
9.3.3.3 Comparison of splicing targets.....	220

1 ZUSAMMENFASSUNG

Amyotrophe Lateralsklerose (ALS) und Frontotemporale Lobär Degeneration (FTLD) sind zwei verheerende neurodegenerative Krankheiten, wobei die ersten Symptome meist erst im fortgeschrittenen Alter auftreten. ALS wird durch eine Degeneration von Motoneuronen verursacht, während bei FTLD die frontalen und temporalen Lappen betroffen sind. Charakteristisch für beide Krankheiten sind ungewöhnliche intrazelluläre Proteinaggregate, die zum Beispiel das Protein „Fused in Sarcoma“ (FUS) enthalten. Mutationen im entsprechenden Gen *FUS* wurden in ALS Patienten als primär ursächlich identifiziert. Bei FTLD jedoch scheinen die Aggregate ein sekundärer Effekt zu sein. Als ein Risikofaktor für die pathologisch häufigste Form von FTLD mit TDP-43-positiven Aggregaten wurde *TMEM106B* identifiziert. Bis heute konnten die genauen krankheitsverursachenden Mechanismen allerdings nicht vollständig geklärt werden.

Um eine genauere Vorstellung davon zu bekommen, sollten in dieser Arbeit Mausmodelle für *FUS* und *TMEM106B* etabliert und analysiert werden. Was *FUS* betrifft, sollten die Mäuse verschiedene mit ALS assoziierte Mutationen exprimieren um die Auswirkungen *in vivo* zu verstehen. Im ersten Mausmodell wurde die humane *FUS* cDNA mit der R521G Mutation direkt in den endogenen *Fus* Locus integriert. Zusätzlich wurden Mäuse generiert, die die entsprechende murine Mutation R513G tragen, einen P517L Austausch (entspricht der humanen P525L Mutation), oder eine Insertion an Position 511, die zu einer veränderten Aminosäuresequenz in der Kernlokalisierungssequenz führt (Panda et al., 2013). In Fibroblasten von allen Mauslinien konnte eine veränderte Lokalisierung von FUS im Zytoplasma beobachtet werden, was zeigt, dass die Konstrukte prinzipiell funktionierten wie erwartet. In embryonalen Fibroblasten war diese Mislokalisierung nicht vorhanden. Dies stimmt mit einem sich entwickelnden Phänotyp mit steigendem Alter überein. In Embryonen der hFUS^{R521G}-Linie war die Methylierung von FUS verringert, während in erwachsenen Tieren das Gegenteil der Fall war. Die Mutation könnte durch weniger Methylierung in der Embryogenese und der Kindheit kompensiert werden. In Neuronen jedoch konnten die Beobachtungen zur Lokalisierung nicht bestätigt werden: in keinem der Mausmodelle wurden FUS-Aggregate oder andere pathologische Anzeichen für ALS, wie vermehrt DNA Schäden, detektiert. Fus^{R513G}-Mäuse zeigten erhöhte Level für p62 und AIF, was für Störungen in der Autophagie und Apoptose spricht. In homozygoten Tieren wurde eine reduzierte Anzahl an Motoneuronen gefunden. Homozygote

Tiere der hFUS^{R521G}-Linie waren nicht lebensfähig und Verhaltenstests bei Heterozygoten ergaben einige Bewegungsdefizite. Fus^{R513G}-Mäuse waren dagegen unauffällig.

Um zu klären ob *FUS*-Mutationen zu einem Funktionsverlust im Kern oder zu einer Überfunktion im Zytoplasma führen, sollten zusätzlich Fus-defiziente Mäuse generiert und die Ergebnisse mit dem Phänotyp der anderen Mausmodelle verglichen werden. Mäuse, die homozygot für den Fus-*knock out* waren, waren nicht lebensfähig. Heterozygote zeigten ebenfalls Schwierigkeiten bei der Bewegungskoordination und eine gestörte Autophagie.

In Publikationen wurde berichtet, dass TMEM106B-Level in Gehirnen von FTLD-Patienten mit TDP-43-Pathologie erhöht waren. Deshalb sollte in dieser Arbeit ein Mausmodell etabliert werden, in dem *Tmem106b* überexprimiert wird, sowohl auf einem Wildtyp-, als auch auf einem mutanten hTDP-43^{A513TKi}-Hintergrund (Stribl et al., 2014). Die Tiere wiesen zytoplasmatisches TDP-43 auf, aber keine Einschlüsse und nicht die erwarteten Veränderungen bezüglich Endo- und Lysosomen. Stattdessen war die Morphologie einiger Mitochondrien verändert. Dies wurde nur in gealterten, nicht in jungen Tieren beobachtet, was für einen progressiven Phänotyp spricht.

Bei einem Vergleich aller etablierten Modelle für FUS wird klar, dass die Analysen in den hFUS^{R521G}- und Fus^{R513G}-Mauslinien teilweise inhomogene Ergebnisse lieferten und dass kein klarer Beweis für ein Modell gefunden wurde, in dem *FUS*-Mutationen zu einem Funktionsverlust im Zellkern führen. Obwohl das mutierte humane FUS nur auf geringem Level exprimiert wurde, scheint es zu einem schwerwiegenderen Phänotyp zu führen als das mutierte murine Fus. Wenn man alle beschriebenen Ergebnisse zusammen nimmt, muss gesagt werden, dass die *FUS*- und *TMEM106B*-Mausmodelle aus dieser Studie wohl weder ALS noch FTLD imitieren konnten. Jedoch gab es Hinweise darauf, dass FUS Auswirkungen auf die Autophagie in Zellen hat. Wenn man bedenkt, dass Mitochondrien eine wichtige Rolle bei der Autophagie spielen und dass FUS und ALS bereits mit einer Fehlfunktion von Mitochondrien in Verbindung gebracht wurden, dann könnten Mitochondrien das fehlende Glied zwischen den beiden Krankheiten darstellen.

2 SUMMARY

Amyotrophic Lateral Sclerosis (ALS) and Frontotemporal Lobar Degeneration (FTLD) are two devastating adult onset neurodegenerative disorders. ALS is a form of motor neuron disease, characterized by the loss of upper and lower motor neurons, while FTLD is caused by the degeneration of frontal and temporal lobes. Hallmark for both, ALS and FTLD, are abnormal intracellular protein aggregates, such as Fused in Sarcoma (FUS) inclusions. In ALS patients *FUS* mutations were found as a primary cause, whereas in FTLD inclusions appeared to be a secondary effect. For FTLD with TDP-43 inclusions, the main portion of FTLD cases, *TMEM106B* was identified to be a risk factor by modulating age of onset and disease progression. However, up to date, the molecular events leading to disease wait to be solved.

In this study, mouse models for *FUS* and *TMEM106B* were generated and analyzed in order to gain more insight into the pathomechanisms of ALS and FTLD. Regarding *FUS*, mice should express different ALS-associated mutations to elucidate the direct consequences *in vivo*. Therefore, one mouse model was established carrying the human *FUS* cDNA with the R521G mutation, which was directly inserted into the endogenous *Fus* locus. Furthermore, the corresponding murine mutation, R513G, the P517L exchange (P525L in humans), or an insertion of one base at position 511, leading to a frameshift and thus a nonsense NLS, were placed in the mouse *Fus* gene by TALEN technology (Panda et al., 2013). In fibroblasts, all mutations led to a mislocalization of FUS to the cytoplasm, indicating that the constructs worked as expected. Though, in embryonic fibroblasts, no mislocalization could be monitored, strengthening the exacerbating effect of *FUS* mutations with progressing age. In addition, a downregulation of FUS methylation could be detected for embryos, whereas in adult animals methylation was partly increased, pointing towards a compensation mechanism during embryogenesis and a progressive development during adulthood. However, in neurons of adult mice, no differences in localization could be observed between wild type and mutant animals. Mice were also inconspicuous concerning other pathological marks of ALS, like enhanced DNA damage. *Fus*^{R513G} animals displayed elevated levels of p62 and AIF, indicating effects on autophagy and apoptosis, and a reduced number of motor neurons was counted in homozygotes. Against this, hFUS^{R521G} animals were homozygous lethal and during behavioral tests some motor deficits were monitored, while *Fus*^{R513G} mice did not show any impairment.

To examine, whether mutations in *FUS* cause ALS via a loss or a gain of function mechanism, mice deficient for *Fus* were generated and effects of this loss of function were compared to those of *FUS* mutations. Homozygous *Fus* deficient mice were not viable. For heterozygotes motor deficits and a possible dysfunction in autophagy were monitored, which fits to some results in mice expressing mutated *FUS*.

Since *TMEM106B* was found to be elevated in FTLD patients with TDP-43 pathology, a mouse model should be generated in this study, overexpressing *Tmem106b* on a wild type and a mutant hTDP-43^{A513TKi} (Stribl et al., 2014) background. The main finding was that aged mice showed cytoplasmatic TDP-43, though did not display inclusions or the expected abnormalities concerning endo- and lysosomes, but instead of mitochondria, which appeared to be a progressive phenotype.

Comparing the models for *FUS*, h*FUS*^{R521G} and *Fus*^{R513G} mouse lines were partly inhomogenous in results and there is no clear evidence for a loss of function model. Furthermore, mutations in the human *FUS* gene seem to implicate a more severe phenotype than the mutated endogenous *Fus*, although it was expressed at very low levels. Taken all together, *FUS* and *TMEM106B* mouse models could not mimic ALS or FTLD. Nevertheless, results provided evidence that *FUS* has an effect on autophagy. Considering the fact that mitochondria play an important role in autophagy and that *FUS* and ALS were already connected with mitochondrial dysfunction, mitochondria could be the missing link between both diseases.

3 INTRODUCTION

3.1 NEURODEGENERATIVE DISEASES

The hallmark of neurodegenerative diseases is the progressive loss of neurons in the brain and/or spinal cord. Since damaged or dead neurons cannot be replaced, this results in disturbances of memory (dementia) or movement (ataxia). The first symptoms are recognized when the majority of neurons are dead which means that these are normally late onset diseases, whereby the underlying reasons can be familiar or sporadic. The most known neurodegenerative diseases are Alzheimer's disease (AD), Parkinson's disease (PD), or Huntington's disease (HD). In this thesis the focus was set on Amyotrophic Lateral Sclerosis (ALS) and Frontotemporal Lobar Degeneration (FTLD).

3.1.1 AMYOTROPHIC LATERAL SCLEROSIS (LOU GEHRIG'S DISEASE)

In cases of ALS, the affected neurons are upper (UMN) and lower motor neurons (LMN) of the motor cortex, brainstem, and spinal cord. Degeneration of UMN results in hyperreflexia, extensor plantar response, and increased muscle tone. Symptoms of lost LMN in ALS are weakness, atrophy (muscle wasting), hyporeflexia, muscle cramps, and fasciculations. The lifetime risk for developing ALS amounts to one in 1000 persons (Boillee et al., 2006).

ALS was first described by Jean-Martin Charcot in 1869 (Charcot and Joffroy, 1869). It is also called 'Lou Gehrig's disease' after the famous US baseball player, who was diagnosed with ALS in 1939. He died within two years. The incidence of ALS is one to two per 100 000 persons with males being more often hit by the disease than females (Robberecht and Philips, 2013). The European male : female incidence ratio is 1.4 (Logroscino et al., 2010) and the prevalence is four to six per 100 000 persons (Boillee et al., 2006). The first symptoms of ALS can vary. Physicians differentiate between bulbar onset, which accounts for 20% of ALS cases, with speech disturbances and swallowing difficulties (progressive bulbar palsy), and limb onset ALS (80%) (Chen et al., 2013). In familiar ALS (fALS), the mean age of onset is 46 years (Juneja et al., 1997),

whereas in sporadic cases (sALS) the first symptoms are recognized with an average age of 56 years (Testa et al., 2004). However, the main course of the disease is then very typical: atrophy and weakness spreads out and in the end, patients are paralyzed and caught in themselves. In most cases, patients succumb to the disease within two to four years because of respiratory failure (Chio et al., 2009).

About 10% of ALS cases are inherited, mainly in a dominant manner (fALS) (Lagier-Tourenne and Cleveland, 2009; Dormann and Haass, 2011). In 1991, chromosome 21 was associated with ALS (Siddique et al., 1991) and two years later *Superoxide dismutase 1 (SOD1)* was the first gene that was found to be linked to ALS (Rosen et al., 1993). Mutations in *SOD1* cause 1-2% of all ALS cases and about 20% of fALS (Tab. 1) (Boillee et al., 2006; Lagier-Tourenne and Cleveland, 2009; Robberecht and Philips, 2013). The protein consists of 153 amino acids, encoded by five exons. More than 150 different mutations have been reported to be pathogenic (Andersen and Al-Chalabi, 2011). The mechanism behind is not yet known, but mutant SOD1 seems to have a toxic effect due to influencing pathways of protein degradation (Bendotti et al., 2012). Typically, aggregates containing ubiquitinated misfolded SOD1 are found in affected neurons of patients.

Tab. 1: Heterogeneity of ALS.

Molecular classification	Aggregated protein	Proposed causative dysfunction	Associated gene	Estimated % of		Reference
				fALS	sALS	
ALS-SOD (ALS1)	Superoxide dismutase 1 (SOD1)	Protein aggregation, oxidative stress, mitochondrial disruption, apoptosis, microglia activation, metabolic disturbance, axonal dysfunction	<i>SOD1 (21q22.1)</i>	20%	1-2%	(Rosen et al., 1993)
ALS2*	Alsin	Oxidative stress	<i>Alsin</i>	<1%	NA	(Hadano et al., 2001; Yang et al., 2001)
ALS3	Unknown		<i>Unknown (18q21)</i>			(Hand et al., 2002)
ALS4*	Senataxin (SETX)	Aberrant RNA processing	<i>SETX (9q34)</i>	Unknown		(Chen et al., 2004)
ALS5*	Spatacsin (SPG)	Axonal dysfunction	<i>SPG11 (15q15-21)</i>	Unknown		(Orlacchio et al., 2010)
ALS-FUS* (ALS6)	Fused in sarcoma (FUS)	Aberrant RNA processing	<i>FUS (16p11.2)</i>	1-5%	1%	(Kwiatkowski et al., 2009; Vance et al., 2009)
ALS7	Unknown		<i>Unknown (20ptel-p13)</i>	Unknown		(Sapp et al., 2003)
ALS8	Vesicle-associated membrane protein-associated protein B and C (VAPB)	Apoptosis, metabolic disturbance	<i>VAPB (20q13.3)</i>	<1%	NA	(Nishimura et al., 2004)
ALS-TDP (ALS9)	Angiogenin (ANG)	Aberrant RNA processing	<i>ANG (14q11.2)</i>	<1%	NA	(Greenway et al., 2006)

ALS-TDP (ALS10)	TAR-DNA binding protein (TDP-43)	Aberrant RNA processing	<i>TARDBP (1p36.2)</i>	1-5%	1%	(Rutherford et al., 2008; Sreedharan et al., 2008)
ALS11	Phosphatidylinositol 3,5bisphosphate 5-phosphatase	Apoptosis	<i>FIG4 (6q21)</i>	Unknown		(Chow et al., 2009)
ALS-TDP (ALS12)	Optineurin (OPTN)	Protein aggregation	<i>OPTN (10p15-p14)</i>	<1%	<1%	(Maruyama et al., 2010)
ALS-TDP (ALS14)	Valosin-containing protein (VCP)	Protein aggregation, apoptosis	<i>VCP (9p13)</i>	<1%	1%	(Johnson et al., 2010)
ALS-TDP* (ALS15)	Ubiquilin 2 (UBQLN2)	Protein aggregation	<i>UBQLN2 (Xp11)</i>	<1%	<1%	(Deng et al., 2011)
ALS-TDP	Ataxin 2 (ATXN2)	Repeat expansion	<i>ATXN2 (12q24)</i>	<1%	NA	(Elden et al., 2010)
ALS-TDP	Profilin 1 (PFN1)	Cytoskeleton/cellular transport deficits	<i>PFN1 (17p13.2)</i>	<1%	<1%	(Wu et al., 2012)
ALS-DPR	Dipeptide repeat proteins (DPR) / TDP-43	Hexanucleotide repeat expansion	<i>C9orf72 (9p21)</i>	40-50%	7%	(DeJesus-Hernandez et al., 2011; Renton et al., 2011)
NA	Dynactin (DCTN1)	Axonal dysfunction	<i>DCTN1 (2p13)</i>	Unknown		(Munch et al., 2004)
NA	Charged multivesicular body protein 2b (CHMP2B)	Unknown	<i>CHMP2B (3p11)</i>	Unknown		(Parkinson et al., 2006)

* indicates a (possible) juvenile disease onset. NA, not applicable; (Chen et al., 2013; Robberecht and Philips, 2013; Deng et al., 2014a; Renton et al., 2014)

Accumulation of misfolded or damaged proteins in neurons and/or glial cells is a hallmark of ALS. These intracellular protein inclusions are often Ubiquitin-positive and in most cases the protein is not SOD1, but Transactive Response DNA binding Protein with 43 kDa (TDP-43), a DNA/RNA binding protein, which is involved in several cellular processes, including gene transcription, RNA splicing, microRNA processing, and stabilization, as well as mRNA transport. Mutations in the corresponding gene *TARDBP* were first reported in 2008 (Rutherford et al., 2008; Sreedharan et al., 2008) and till today more than 40 mutations have been identified, accounting for about 1-5% of fALS cases (Tab. 1) (Robberecht and Philips, 2013). However, not only mutations in *TARDBP* lead to TDP-43 pathology. With about 40-50% a hexanucleotide repeat expansions in *C9orf72* is the most important reason for fALS with TDP-43 inclusions (Robberecht and Philips, 2013) (Tab. 1; see also chapter 3.1.3). Other causative genes for ALS-TDP are for example *Optineurin* (*OPTN*, <1% of fALS), coding for an inhibitor of Nuclear Factor- κ B (NF- κ B), or *Ubiquilin 2* (*UBQLN2*, <1% of fALS) (Tab. 1) (Robberecht and Philips, 2013). Mutations in *OPTN* lead to neurotoxicity by a loss of protein function (Chen et al., 2013), whereas *UBQLN2* is a member of the proteasome degradation machinery and mutations cause X-linked fALS (Robberecht and Philips, 2013). Besides protein aggregation, ALS-associated mutations in different genes have further disease causing effects, like axonal dysfunction (e.g. *SPG11*, *DCTN1*), metabolic disturbances (e.g. *VAPB*), microglia activation (e.g. *SOD1*), apoptosis (e.g. *FIG4*, *VCP*), mitochondrial disruption (e.g. *SOD1*), oxidative stress (e.g. *Alsin*), repeat expansions (e.g. *C9orf72*, *ATXN2*), cytoskeleton/cellular transport deficits (*PFN1*), or aberrant RNA processing (e.g. *TARDBP*, *ANG*, *SETX*, *FUS*) (Tab. 1). All these malfunctions then end up in motor neuron degeneration and finally ALS symptoms (Chen et al., 2013).

Certainly, patients with the same gene mutation show variation in age of onset and disease duration, what implicates that there are modifying genetic factors in ALS, such as *KIFAP3* or *EPHA4* (Landers et al., 2009; Van Hoecke et al., 2012), whereas another group doubted the impact of *KIFAP3* on the survival of patients (Traynor et al., 2010). The age of disease onset appeared to be also regulated by a locus on the short arm of chromosome 1 (Ahmeti et al., 2013). Additionally, several environmental factors have been proposed to be involved in the development of ALS like farming products, mercury, manganese, or diets (Wicklund, 2005). Gulf war veterans were found to sicken more often ALS (Haley, 2003; Horner et al., 2003) and on the pacific island Guam the incidence for the so called 'ALS, Parkinson's disease and dementia' (the ALS/PDC complex) was sometimes about 50 to 100 times higher than in the rest of the world (Plato et al., 2003). It was presumed that perhaps cyanobacteria are the reason for this cumulative occurrence of ALS/PDC complex (Bradley and Mash, 2009).

Although we have learnt a lot about ALS in the last years, there is no effective therapy available. During the last weeks ALS gained public awareness due to the 'ALS Ice Bucket Challenge', where people, also a lot of celebrities, are encouraged to donate for ALS and/or to be whelmed with a bucket of ice water.

3.1.2 FRONTOTEMPORAL LOBAR DEGENERATION (PICK'S DISEASE)

FTLD is the name for a cluster of molecular pathologies (McKhann et al., 2001; Josephs, 2008), whereas Frontotemporal Dementia (FTD) is the clinical term for the cluster of syndromes due to the pathological damage (Englund et al., 1994; Neary et al., 1998).

FTD is the second most common cause of presenile dementia after AD. Disease progression goes along with changes in behavior, personality, and/or language. In FTD the affected neurons are those of the frontal and temporal lobes of the brain. Researchers of the TU in Munich presumed that King Ludwig II of Bavaria suffered from a beginning FTD due to his behavior in the last two years of his life and since the autopsy yielded a clear shrinkage of the frontal brain areas (Schmidhofer, 2007).

In 1892, the neurologist Arnold Pick was the first, who reported about symptoms of FTD from a patient (Pick, 1892). Today, the term 'Pick's Disease' is only used for a subtype of FTD. In 1911, Alois Alzheimer reported about neuronal aggregates, later known as 'Pick bodies' (Alzheimer, 1911). Like in ALS, a characteristic of FTD are abnormal intracellular protein inclusions. 3.5 to 4.1 new diagnosed cases in 100 000 persons between 45 and 64 years are reported per year (Knopman et al., 2004; Mercy et al., 2008), whereas the prevalence is very inconsistent: ten to 30 persons are affected in 100 000 between the ages of 45 to 65 years (Sieben et al., 2012) with no gender specific difference in frequency (Ratnavalli et al., 2002; Rosso et al., 2003; Johnson et al., 2005). The average age of onset is 58 years (Johnson et al., 2005), although also patients in their thirties have been described (Mackenzie et al., 2008), and patients die two to 20 years after diagnosis (Hodges et al., 2003; Seelaar et al., 2008). These numbers show that FTD is a many-faceted disease with a high variation in disease onset and duration. Clinically, physicians distinguish between two syndromes according to the early and predominant symptoms: behavioral-variant frontotemporal dementia (bvFTD) and primary progressive aphasia (PPA), which is subdivided into progressive non-fluent aphasia (PNFA) and semantic dementia (SD).

Two third of patients are diagnosed with bvFTD (Bennion Callister and Pickering-Brown, 2014; Riedl et al., 2014).

Tab. 2: Heterogeneity of FTLD.

Molecular classification	Aggregated protein	Causative dysfunction	Associated gene	Estimated % of fFTLD	Reference
FTLD-tau	tau	Impaired microtubule assembly, impaired axonal transport, pathological tau filament aggregation	<i>MAPT</i>	50%	(Hutton et al., 1998; Brandt et al., 2005)
FTLD-TDP	TDP	Unknown	<i>(TARDBP)</i>	(<1%)	(Van Langenhove et al., 2012)
	TDP	Haploinsufficiency	<i>GRN</i>	3-26%	(Baker et al., 2006)
	TDP, DPR	Hexanucleotide repeat expansion	<i>C9orf72</i>	29%	(DeJesus-Hernandez et al., 2011; Renton et al., 2011; van der Zee et al., 2013)
	TDP	Protein aggregation, apoptosis	<i>VCP</i>	<1%	(Watts et al., 2004)
FTLD-FUS	FUS		<i>(FUS)</i>	(<1%)	(Van Langenhove et al., 2010)
FTLD-UPS	Ubiquitin positive	Unknown	<i>CHMP2B</i>	<1%	(Skibinski et al., 2005)

ND, not defined; (Van Langenhove et al., 2012; Dormann and Haass, 2013; Bennion Callister and Pickering-Brown, 2014; Riedl et al., 2014)

Pathologically, FTLD is classified in four subtypes according to the aggregated protein (Tab. 2). Almost half of FTLD cases show accumulation of hyperphosphorylated tau protein in neurons and glial cells (FTLD-tau). The majority of tau-negative cases exhibit neuronal Ubiquitin-positive inclusions (FTLD-U), among these 90% have TDP-43 inclusions (FTLD-TDP). Nearly the rest of FTLD-U cases display inclusions positive for FUS (FTLD-FUS). The last subtype is FTLD-UPS (ubiquitin proteasome system), characterized by dementia lacking distinctive histology (Seelaar et al., 2011; Riedl et al., 2014).

About 40% of FTLT cases are inherited (Tab. 2) (Riedl et al., 2014). The causative gene for FTLT-tau is *MAPT*. FTLT-TDP and FTLT-FUS are rarely triggered by mutations in the corresponding genes (<1% of fFTLT), but in other genes like *GRN* (3-26% of fFTLT) or *C9orf72* (29% of fFTLT, see also chapter 3.1.3) (Perry and Miller, 2013; Bennion Callister and Pickering-Brown, 2014; Riedl et al., 2014). However, the pathology is the same, which means that often secondary pathways seem to be accountable for FTLT. Aside, modifying factors like *TMEM106B* have been associated with the development of FTLT (Van Deerlin et al., 2010) (see also chapter 3.3.2).

Till now, there is no treatment available for FTD, although a lot of drugs have been tested so far. For a summary of clinical trials see the review of Riedl and colleagues (Riedl et al., 2014).

3.1.3 LINK BETWEEN ALS AND FTLT

ALS and FTLT show a lot of common features, not only abnormal intracellular protein inclusions as a hallmark of both diseases, but also the underlying genetic reasons (Tab. 3). Furthermore, the symptoms of both are overlapping in a high rate of patients, so that nowadays ALS and FTLT are not divided in two single diseases anymore, but are characterized as two ends of one disease spectrum (Fig. 1) (Al-Chalabi et al., 2012; Robberecht and Philips, 2013).

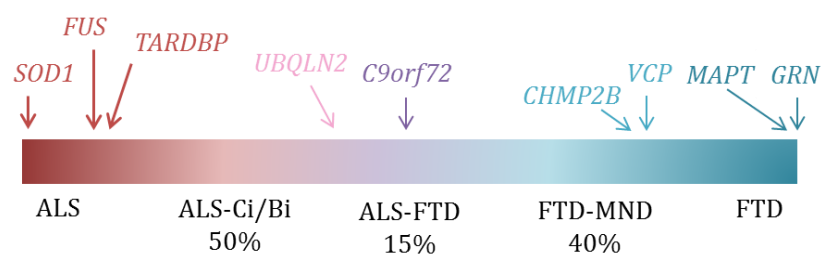


Fig. 1: ALS and FTD as two ends of one disease spectrum. 50% of ALS patients develop cognitive or behavioral symptoms. 15% of these meet the characteristics of FTD. At the other end, 40% of FTD patients show also motor deficits. Mutations in *SOD1*, *FUS* and *TARDBP* are rarely or never found in FTD patients, whereas mutations in *MAPT* and *GRN* are a frequent cause for FTD and *C9orf72* is the major trigger for both. ALS-Ci/Bi, ALS with cognitive or behavioral impairment; MND, motor neuron disease; (Ling et al., 2013; Robberecht and Philips, 2013)

Up to 50% of ALS patients present cognitive or behavioral impairment (ALS-Ci/Bi), 15% of whom meet the features of FTD (Lomen-Hoerth et al., 2003; Ringholz et al., 2005; Lillo and

Hodges, 2009). At the other end of the spectrum, about 40% of FTD patients display motor deficits and are diagnosed with FTD-MND (FTLD with motor neuron disease). Among these, 15% have clear ALS symptoms (Lomen-Hoerth et al., 2002; Burrell et al., 2011).

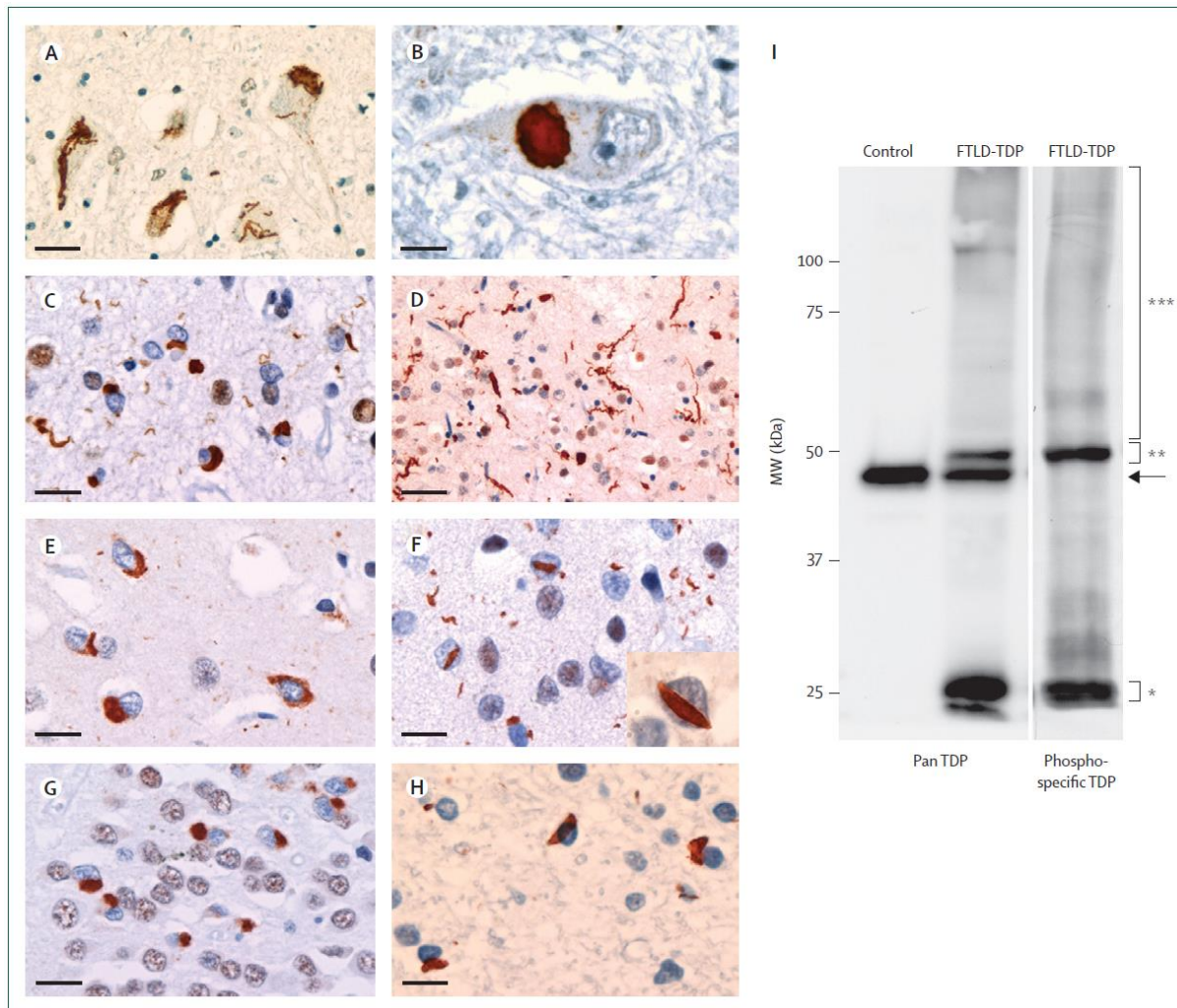


Fig. 2: Pathological features in ALS-TDP and FTLD-TDP. TDP-43 immunohistochemistry on paraffin-embedded tissue showing (A) TDP-43-immunoreactive skein-like and (B) round inclusions in motor neurons in ALS-TDP. FTLD-TDP pathology is subdivided into four distinct morphological subtypes: (C) type 1 is characterised by compact neuronal cytoplasmic inclusions and short neurites; (D) type 2 is characterised by long neurites; (E) type 3 is characterised by compact and granular cytoplasmic inclusions; and (F) type 4 is characterised by numerous neuronal intranuclear inclusions. (G) Cytoplasmic inclusions in the dentate granule cells of the hippocampus. Nuclear staining is absent in inclusion-bearing cells. (H) Glial cytoplasmic inclusions. Scale bars: 40 μ m (D), 20 μ m (A, C, G), 15 μ m (E, F), and 10 μ m (B, H). (I) Immunoblot analysis of urea fractions isolated from brain tissue, showing the highly characteristic biochemical signature of TDP-43 in FTLD-TDP, with pathological bands of approximately 25 kDa (*) and 45 kDa (**), and a high-molecular-weight smear (***) that are not detected in controls. The arrow indicates the wild-type 43 kDa TDP-43 band present in controls and in patients with FTLD-TDP. Notably, only pathological TDP-43 is detected by a phosphorylation-specific TDP-43 antibody against phosphorylated serine residues 409 and 410.45 ALS=amyotrophic lateral sclerosis. ALS-TDP=TDP-43-positive ALS. FTLD-TDP=TDP-43-positive frontotemporal lobar degeneration.

Reprinted from *The Lancet Neurol* 2010, Vol. 9; Ian R A Mackenzie, Rosa Rademakers, Manuela Neumann; **TDP-43 and FUS in amyotrophic lateral sclerosis and frontotemporal dementia**, Pages 995–1007, Copyright 2010, with permission from Elsevier.

Pathologically, 97% of ALS and 45% of FTL cases display TDP-43 inclusions (Fig. 2), whereas FUS pathology is found in 1% and 9% of patients respectively (see also chapter 3.2.2) (Ling et al., 2013). TDP pathology in ALS is characterized by small granules, compact inclusions, and filamentous skeins in neurons and glia of the primary motor cortex, brainstem motor nuclei, spinal cord, and white matter (Fig. 2A, B) (Mackenzie et al., 2010). In FTL, TDP pathology manifests with cytoplasmic inclusions and neurites in the frontotemporal neocortex and dentate granule cells of the hippocampus (Fig. 2G, H) (Mackenzie et al., 2010). Thereby, FTL-TDP is divided into four pathological subtypes according to the anatomical distribution, morphology, and types of inclusions: type 1 is mainly observed in bvFTD and PFNA with *GRN* mutations and neuronal cytoplasmic inclusions (NCI) and dystrophic neurites are the general pathological features. Type 2 shows numerous dystrophic neurites and is found in SD. Type 3 demonstrates only a moderate number of NCIs and is diagnosed with bvFTD and FTD with ALS. Thereby, a connection was made between Type 3 and *C9orf72*. Inclusion body myopathy, associated with Paget disease of bone and FTD with numerous dystrophic neurites and neuronal intranuclear inclusions (NII), represents type 4 (Fig 2C-F) (Mackenzie et al., 2010). Another hallmark of TDP pathology is the presence of a 25 kDa, C-terminal fragment of TDP-43, which seems to be the main component of insoluble, ubiquitinated and phosphorylated cytoplasmic aggregates (Fig. 2I) (Neumann et al., 2006).

Genetically, the major cause for both, ALS and FTD, is a hexanucleotide repeat expansion on chromosome 9p, with around 50% mutation frequency in ALS, 29% in FTD and 88% in ALS-FTD (Gijselinck et al., 2012; Cruts et al., 2013; van der Zee et al., 2013). The function of the associated gene on locus *C9 open reading frame 72* (*C9orf72*) waits to be identified (DeJesus-Hernandez et al., 2011; Renton et al., 2011). Healthy persons carry two to 24 copies of the GGGGCC repeat expansion (Gijselinck et al., 2012; van der Zee et al., 2013), whereas up to thousands of copies were reported from patients (Dols-Icardo et al., 2014). These noncoding repeats in intron 1 seem to be bidirectionally translated into five distinct dipeptide repeat proteins (DPR) due to a missing start codon and form, besides TDP-43 inclusions, DPR aggregates in patients (Mori et al., 2013). These DPR inclusions are TDP-43-negative and p62-positive (van der Zee and Van Broeckhoven, 2014). There was also evidence for haploinsufficiency due to loss of gene expression (Gijselinck et al., 2012; Cruts et al., 2013; van der Zee et al., 2013) and/or RNA toxicity due to sequestration of RNA-binding proteins (DeJesus-Hernandez et al., 2011; Lagier-Tourenne et al., 2013).

3.2 FUSED IN SARCOMA (FUS)

A number of neurodegenerative diseases are caused by the dysfunction of several RNA-binding proteins with prion-like domains. One of these proteins is Fused in Sarcoma/Translocated in Liposarcoma (FUS/TLS) (Gitler and Shorter, 2011; Shelkovernikova, 2013). The gene *FUS* was first described in 1993 as a fusion oncogene (*FUS-CHOP*) in human liposarcomas (Croizat et al., 1993; Rabbitts et al., 1993). In 2009 and 2010, mutations in *FUS* were reported to be a causative factor for ALS and very rare forms of FTD (Kwiatkowski et al., 2009; Vance et al., 2009; Broustal et al., 2010; Van Langenhove et al., 2010). *FUS* variants are also involved in essential tremor (Merner et al., 2012) and aggregation of FUS-protein has been observed, additionally to ALS and FTLD, in HD, spinocerebellar ataxia, and dentatorubropallidolusian atrophy (Neumann et al., 2009b; Doi et al., 2010; Woulfe et al., 2010).

3.2.1 STRUCTURE AND FUNCTION OF FUS

FUS forms together with Ewing sarcoma RNA-binding protein (EWS) and TATA-binding protein-associated factor 15 (TAF15) the FET-protein family (Tan and Manley, 2009). The human protein consists of 526 amino acids and is encoded by the corresponding gene on chromosome 16 with 15 exons (Fig. 3). The N-terminal QGSY-rich region operates as a transcriptional activation domain after binding to transcription factors (Prasad et al., 1994; Zinszner et al., 1994) and was reported to have prion-like properties (Cushman et al., 2010; Gitler and Shorter, 2011; Udan and Baloh, 2011; King et al., 2012). *FUS* binds RNA, as well as single- and double-stranded DNA via the three arginine-glycine-glycine (RGG) motifs, an RNA recognition motif (RRM), and a zinc finger motif (Burd and Dreyfuss, 1994; Zinszner et al., 1997; Baechtold et al., 1999). It was found that mainly GU-rich regions are recognized by the RGG2-Zn-RGG3 domains (Lerga et al., 2001; Iko et al., 2004; Bentmann et al., 2012; Lagier-Tourenne et al., 2012). The C-terminus functions as a nuclear localization signal (NLS). Proline-tyrosine (PY) motifs were described as atypical NLS, which are bound by the nuclear import receptor Transportin (Lee et al., 2006; Dormann et al., 2010).

FUS is ubiquitously expressed and shuttles continuously between the nucleus and the cytoplasm (Zinszner et al., 1997). However, its main function is in the nucleus, where it is involved in

several cellular processes like cell proliferation, DNA repair, transcription regulation, and RNA processing (Lagier-Tourenne et al., 2010). The precise role of FUS in these processes still needs to be assessed, but there were several hints in the past: in 1999, FUS was found to be involved in DNA damage response upon DNA double strand breaks and denatured single-stranded RNA by promoting homologous DNA pairing and D-loop formation (Baechtold et al., 1999; Bertrand et al., 1999). It was also shown that FUS is recruited to sites of double strand breaks by poly (ADP-ribose) polymerase (PARP-1), which binds to the RGG domains and that the prion-like domain mediates an accumulation of FUS at sites of DNA damage. Depletion of FUS led to a reduction of DNA repair via homologous recombination and non-homologous end joining (Mastrocola et al., 2013; Rulten et al., 2014). In *Fus* deficient mice chromosomal instability and a lack of chromosomal pairing was observed (Hicks et al., 2000; Kuroda et al., 2000) (see also chapter 3.2.4). Additionally, Wang et al. suggested that the repair is initiated by a direct interaction of FUS with histone deacetylase 1 (HDAC1) (Wang et al., 2013).

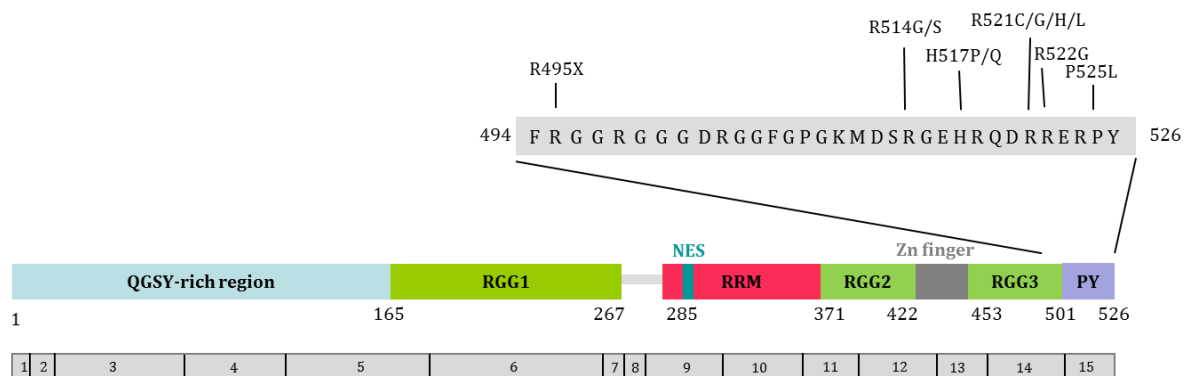


Fig. 3: Structure of FUS. The QGSY-rich region functions as a transcriptional activation domain. The RGG domains, Zn finger and the RRM are DNA/RNA-binding domains. Additionally, the third RGG motif represents along with the PY motif the nuclear localization signal. The encoding exons of each domain are depicted. Majority of ALS-associated mutations are localized at the extreme C-terminus. Here only a few are shown. For detailed information see (Deng et al., 2014a) and (Dormann and Haass, 2013). QGSY, glutamine-glycine-serine-tyrosine; RGG, arginine-glycine-glycine; NES, nuclear export signal; RRM, RNA recognition motif; Zn finger, zinc finger motif; PY, proline-tyrosine nuclear localization signal; X, STOP-codon; adapted from (Dormann and Haass, 2013; Deng et al., 2014a)

Several publications reported an interaction of FUS with the human spliceosome (Hackl and Luhrmann, 1996; Rappsilber et al., 2002; Zhou et al., 2002; Tsuiji et al., 2013), splicing complexes (Calvio et al., 1995), like the Drosha complex mediating the genesis of microRNAs (Gregory et al., 2004; Morlando et al., 2012), and splicing factors, like the heterogeneous ribonucleoproteins hnRNP-A1 and hnRNP-C1/C2 (Zinszner et al., 1994). FUS is involved in alternative splicing and the processing of long intron-containing transcripts found by CLIP analyses (crosslinking and immunoprecipitation followed by high-throughput sequencing)

(Hoell et al., 2011; Ishigaki et al., 2012; Lagier-Tourenne et al., 2012; Rogelj et al., 2012). Its targets are cumulative genes for neurogenesis, neuronal integrity, gene expression regulation, and DNA damage response (Lagier-Tourenne et al., 2012; Zhou et al., 2014). FUS was also found to bind to the 3' UTR of several transcripts, which were associated with the development of ALS, like *SOD1* or *UBQLN2* (Lagier-Tourenne et al., 2012). One famous splice target is *microtubule associated protein Tau (MAPT)*, which is involved in several neurodegenerative diseases like AD, FTL and PD (Lagier-Tourenne et al., 2012; Orozco et al., 2012). A loss of FUS led to an increase of the neurodegeneration associated four-repeat tau isoform (4R tau) (Orozco et al., 2012). FUS regulates not only several thousands of target genes, but also its own gene expression by repressing its mRNA. Lagier-Tourenne and group noted binding of FUS to its own pre-mRNA in a region with a high sequence conservation in mammals and which was annotated as intron 8 or an alternative 3' UTR (Lagier-Tourenne et al., 2012). Zhou et al. proposed upon an alternative splicing of exon 7. The exon 7-skipped splice variant then undergoes nonsense mediated decay (NMD) (Zhou et al., 2013). FUS was also ascertained to be linked to miR-141 and miR-200a in a feedback-loop, as these microRNAs recognize the 3' UTR of FUS (Dini Modigliani et al., 2014). In the study, FUS controlled miR-141/200a expression and the microRNAs in turn the expression of FUS. In ALS-patients, mutations were identified in the 3' UTR of FUS, being pathogenic by increasing FUS expression (Sabatelli et al., 2013). One of these mutations is localized in the binding sequence of miR-141/200a and therefore disrupts the feedback loop (Dini Modigliani et al., 2014).

Several studies reported a role of FUS as a component of the transcriptional pre-initiation complex (PIC) in transcription initiation and/or elongation (Bertolotti et al., 1996; Bertolotti et al., 1999; Das et al., 2007). Tan and colleagues observed a recognition of specific single-stranded DNA sequences in the promoter region of FUS target genes (Tan et al., 2012). FUS can also influence the expression of target genes by acting as a co-regulator of nuclear hormone receptors (Powers et al., 1998) or transcription factors, like nuclear factor NF- κ B (Uranishi et al., 2001) or the transcription repressor ZFM1 (Zhang et al., 1998).

Further, FUS functions also outside of the nucleus. In neurons, FUS is localized to dendritic spines, regulates spine morphology and the axonal distribution of target RNAs, like the mRNA of an actin-stabilizing protein or of the spinal muscular atrophy disease protein survival motor neuron (SMN), which is essential for local protein synthesis and synaptic plasticity. (Belly et al., 2005; Fujii et al., 2005; Fujii and Takumi, 2005; Yoshimura et al., 2006; Aoki et al., 2012; Tolino et al., 2012; Groen et al., 2013).

For a review and a scheme of the diverse functions of FUS see the publication of D. Dormann and C. Haass (Dormann and Haass, 2013).

3.2.2 FUS IN ALS AND FTLD

In 2009, mutations in *FUS* were found to be associated with the development of ALS and to account for about 1-5% of fALS and about 1% of sALS cases (Kwiatkowski et al., 2009; Vance et al., 2009). ALS-FUS or ALS6 includes also juvenile forms of ALS (Baumer et al., 2010) and shows a wide range of disease onset from 26-80 years with a mean course of 33 months (Pasinelli and Brown, 2006). Mutations are mainly autosomal dominant and two third are clustered at the extreme C-terminus (Dormann and Haass, 2013; Deng et al., 2014a). The consequence is a nonfunctional NLS, an impairment of Transportin binding, and thus of nuclear import. This leads to an accumulation of FUS in the cytoplasm and a recruitment of mislocalized FUS into stress granules upon cellular stress (Bosco et al., 2010; Dormann et al., 2010; Gal et al., 2011; Ito et al., 2011; Kino et al., 2011; Bentmann et al., 2012; Niu et al., 2012; Zhang and Chook, 2012; Bentmann et al., 2013). Evidence was provided that also wild type- (WT) FUS is pulled into cytoplasmic stress granules by mutant FUS protein (Vance et al., 2013; Qiu et al., 2014). Stress granules are formed transiently in order to store already transcribed mRNA of housekeeping genes in cases of cellular stress. Hence, stress response factors, like heat shock proteins, can be efficiently expressed and when stress conditions are gone, the stored mRNAs can be immediately translated (Anderson and Kedersha, 2009). Dormann and Haass formulated the two-hit-hypothesis, which declares that a second hit like cellular stress and/or protein degradation defects may then lead to an aggregation of FUS into insoluble inclusions (Dormann et al., 2010; Bentmann et al., 2013; Dormann and Haass, 2013). The group around Shelkovernikova has another hypothesis. They claimed that FUS granules are different from stress granules and suggested a model of multistep FUS aggregation including RNA-dependent and -independent stages (Shelkovernikova et al., 2014).

Concerning FTLD, only scattered *FUS*-mutations were found (Van Langenhove et al., 2010), even if none of those could be identified in autopsy-confirmed FTLD-FUS patients (Urwin et al., 2010; Snowden et al., 2011; Rademakers et al., 2012). However, about 5-10% of FTLD patients are diagnosed with FTLD-FUS (Riedl et al., 2014). FTLD-FUS is subdivided concerning the clinicopathological entity into atypical FTLD-U (aFTLD-U), neuronal intermediate filament inclusion disease (NIFID), and basophilic inclusion body disease (BIBD) (Mackenzie et al., 2009).

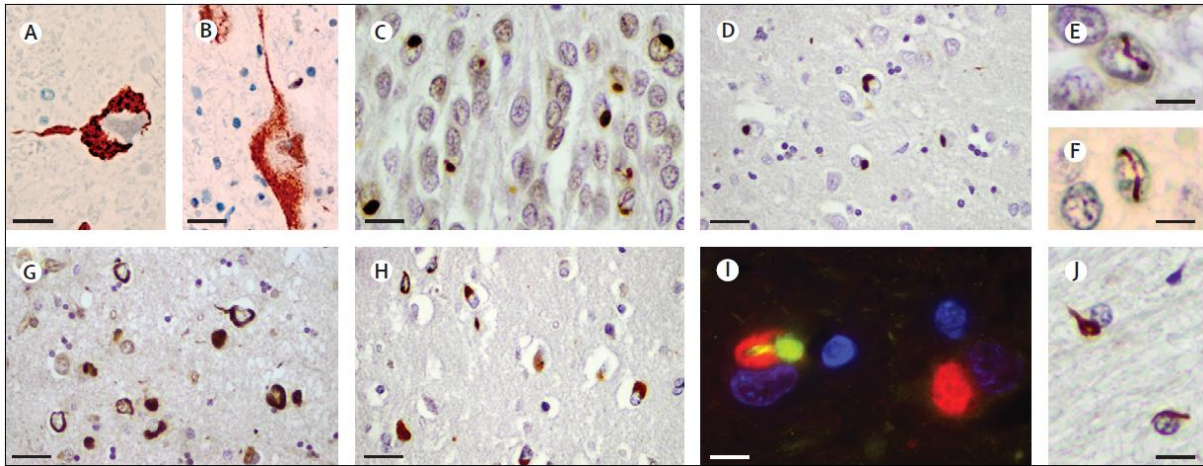


Fig. 4: Pathological features in ALS-FUS and FTLD-FUS. FUS immunohistochemistry on paraffin-embedded tissue showing FUS-immunoreactive cytoplasmic inclusions in lower motor neurons of a familial ALS case with the Arg521Cys FUS mutation, with (A) filamentous or (B) granular morphology. Nuclear FUS staining is present in the inclusion-bearing neuron (B). Three distinct pathological entities of FTLD-FUS can be delineated. In atypical FTLD-U, FUS-immunoreactive cytoplasmic inclusions are detected in (C) the dentate granule cells and (D) the frontal cortex, and (E, F) characteristic vermiform intranuclear inclusions are visible. Numerous FUS-immunoreactive cytoplasmic inclusions are detected with variable morphology in the frontal cortex of (G) basophilic inclusion body disease and (H) neuronal intermediate filament inclusion disease. (I) Many inclusions in the latter disorder are labelled only for FUS, and neurons with α -internexin-positive inclusions always show FUS pathology, with labelling of separate inclusion components as demonstrated by double-label immunofluorescence for FUS (red) and α -internexin (green). (J) FUS-immunoreactive glial cytoplasmic inclusions are present in ALS-FUS and FTLD-FUS. Scale bars: 30 μ m (D, G, H), 20 μ m (C), 15 μ m (A, B), 8 μ m (E, F, I, J). ALS=amyotrophic lateral sclerosis. FTLD=frontotemporal lobar degeneration. FTLD-U=FTLD with ubiquitinated inclusions.

Reprinted from *The Lancet Neurol* 2010, Vol. 9; Ian R A Mackenzie, Rosa Rademakers, Manuela Neumann; **TDP-43 and FUS in amyotrophic lateral sclerosis and frontotemporal dementia**, Pages 995–1007, Copyright 2010, with permission from Elsevier.

The hallmark of both, ALS-FUS and FTLD-FUS is the accumulation of FUS-protein in neurons and/or glial cells. FUS-pathology is characterized by FUS-immunoreactive inclusions in the cytoplasm and less frequently in the nucleus (Fig. 4) (Neumann et al., 2009a; Mackenzie et al., 2010; Josephs et al., 2011). However, the morphology and distribution of FUS inclusions can vary between the different subtypes (Mackenzie et al., 2010; Josephs et al., 2011). In ALS this can depend on the causative mutation and correlates with disease severity (Mackenzie et al., 2011a) (Fig. 4A, B). Mentioning only two examples, juvenile and severe ALS cases (for example with P525L mutation) showed frequent basophilic inclusions and round FUS-immunoreactive NCIs, whereas late onset cases (for example with R521G mutation) had tangle-like NCIs and numerous FUS-immunoreactive glial cytoplasmic inclusions (Mackenzie et al., 2011a). Thereby, long disease duration results in a wide-spread distribution of FUS inclusions in neurons and glia (Suzuki et al., 2012). Concerning FTLD-FUS, the differences reside in the three subtypes (Fig. 4C-H) (Mackenzie et al., 2011b). Autopsy of patients with aFTLD-U displayed neuronal inclusions with a round shape in the hippocampus, neocortex, and the striatum (Neumann et al., 2009a), whereas NIFID and BIBD presented a variety of inclusion morphologies. In the brains of all

aFTLD-U, as well as all NIFID patients, vermiform NIIs were observed in the hippocampus and neocortex (Mackenzie et al., 2011b). BIBD is characterized by basophilic inclusions (Deng et al., 2014a).

Tab. 3: Common features and differences of ALS-FUS and FTLD-FUS.

	Common	Different	
		ALS	FTLD
Clinical reason	Neurodegeneration	Loss of motor neurons	Degeneration of frontal and temporal lobes
Symptoms	Up to 50% of patients with overlap in symptoms	Progressive muscle weakening, atrophy, and spasticity; death due to respiratory failure	progressive behavioral and/or language deficits
Pathological	FUS inclusions; co-localization with p62, Ubiquitin, and stress granule markers	Inclusions with methylated FUS	Inclusions with unmethylated FUS, EWS, TAF15, and Transportin
Genetic		Causative; <i>FUS</i> -mutations (1-5%)	Unknown, no <i>FUS</i> -mutations

ALS-FUS and FTLD-FUS have additional features in common (Tab. 3). Cytosolic FUS inclusions are also immunoreactive for Ubiquitin, p62, and stress granule marker, like Tia1, which suggests that a defect in autophagy, the Ubiquitin-proteasome system and/or cellular stress are common mechanisms in ALS and FTLD (Mizuno et al., 2006; Dormann and Haass, 2013). P62 mediates degradation of polyubiquitinated protein aggregates in autophagosomes (Pankiv et al., 2007) and was also frequently observed in other neurodegenerative diseases, such as AD, PD, and HD (Zatloukal et al., 2002; Kuusisto et al., 2008). Recently, also mutations in the corresponding gene *SQSTM1* (*Sequestosome 1*) were identified in patients with ALS and FTLD (Fecto et al., 2011; Rubino et al., 2012).

However, there are also differences between the two diseases concerning the composition of FUS inclusions (Tab. 3). In ALS, inclusions contain only FUS protein as a direct consequence of *FUS* mutations, whereas in FTLD, the other FET-proteins, EWS and TAF15, are co-deposited, as well as Transportin 1 (Brelstaff et al., 2011; Neumann et al., 2011; Mackenzie and Neumann,

2012; Neumann et al., 2012; Takeuchi et al., 2013). Here the underlying reasons and mechanisms are unknown and FUS-pathology is a secondary effect. Since none of the other Transportin target proteins were affected, a general defect in Transportin-mediated import can be excluded (Neumann et al., 2012). The second variation is the posttranslational modification of deposited FUS protein: in ALS, sequestered FUS is arginine methylated, on the other hand FUS in FTLD is unmethylated (Dormann et al., 2012; Scaramuzzino et al., 2013) (see also chapter 3.2.3).

3.2.3 POSTTRANSLATIONAL MODIFICATIONS OF FUS

As mentioned above, methylation of FUS seems to play a role in the development of ALS and FTLD (Dormann et al., 2012; Tradewell et al., 2012; Yamaguchi and Kitajo, 2012; Scaramuzzino et al., 2013). However, there were also hints that posttranslational phosphorylation is involved (Deng et al., 2014b).

In 2011, Du and colleagues were the first, who found an interaction of FUS and the protein arginine methyltransferase 1 (PRMT1) (Du et al., 2011). They reported that FUS was arginine dimethylated by PRMT1 and that FUS and PRMT1 synergistically coactivated transcription at the survivin promoter and such have an important impact in transcriptional regulation (Du et al., 2011). Survivin is a member of the inhibitor of apoptosis protein (IAP) family and is highly expressed in most human tumours and fetal tissue (Sah et al., 2006). In three publications a decrease of cytoplasmic mislocalization of mutant FUS and inclusion formation was observed after depletion or overexpression of PRMT1 and it was suggested that arginine methylation is involved in the nuclear-cytoplasmic shuttling of FUS and therefore in the pathogenesis of FUS-related ALS (Tradewell et al., 2012; Yamaguchi and Kitajo, 2012; Scaramuzzino et al., 2013). Additionally to PRMT1, asymmetric dimethylation of FUS can also be performed by PRMT8 and an inhibition had the same effects as for PRMT1 (Scaramuzzino et al., 2013). Dormann and colleagues found the reason for these observations: Transportin 1 can also bind to unmethylated RGG3 domain and therefore import mutated FUS into the nucleus (Dormann et al., 2012). The finding from patient autopsies that aggregated FUS is methylated in ALS but not in FTLD suggests the assumption that the pathomechanisms are different in both diseases (Dormann et al., 2012; Dormann and Haass, 2013). Dormann and Haass proposed the hypothesis that in FTLD a defect in methylation leads to hypomethylation of FET-proteins and to inclusions containing unmethylated FET-proteins and Transportin, whereas in ALS, *FUS* mutations result exclusively

in aggregation of methylated FUS (Dormann and Haass, 2013). In contrast, no causative mutations in PRMTs were identified in FTLD patients (Ravenscroft et al., 2013).

This year, another proposal was made concerning the pathomechanism of FTLD-FUS, namely that FUS is phosphorylated and thus translocated to the cytoplasm (Deng et al., 2014b). After induction of double strand breaks, they observed a phosphorylation of FUS at its N-terminus by the DNA-dependent protein kinase (DNA-PK) and an accumulation of FET-proteins and Transportin in the cytoplasm (Deng et al., 2014b). In FTLD-FUS patients, the group found elevated levels of γ H₂AX, a marker for DNA damage (Deng et al., 2014b).

3.2.4 FUS RODENT MODELS

It was often discussed, whether the features found in patients with ALS and FTLD are a consequence of a loss or a gain of FUS function (Haass, 2013). A loss of FUS in the nucleus due to mutations would argue for a loss of function model, whereas also a toxic gain of function model is possible due to too much FUS in the cytoplasm. Sabatelli et al. reported that mutations in the 3' untranslated region (UTR) of *FUS* are associated with ALS by overexpressing FUS (Sabatelli et al., 2013). To answer this question, several animal models overexpressing FUS, lacking FUS, or carrying ALS-associated mutations were generated. In this thesis, the focus is on rodent models. For a broader review see (Lanson and Pandey, 2012) and (McGoldrick et al., 2013).

As early as in 2000, before FUS was connected to ALS and FTLD, the first two mouse models were made (Hicks et al., 2000; Kuroda et al., 2000). Kuroda et al. interrupted the *Fus* coding region inside exon 8, immediately upstream of the RRM, by a promoterless insertion cassette, which created an allele encoding a truncated Fus-Neo fusion protein and was expressed at low levels (Kuroda et al., 2000). They found that homozygous knock out mice were more sensitive to radiation and the male sterility was associated with a lack of chromosomal pairing (Kuroda et al., 2000). The other group disrupted the *Fus* gene in exon 12 by gene entrapment also leading to a Fus-Neo fusion protein (Hicks et al., 2000). Homozygous mice failed to suckle and died within 16 hours after birth. Heterozygous animals showed a defect in B-lymphocyte development and activation, as well as high levels of chromosomal instability (Hicks et al., 2000).

In 2012, Mitchell and colleagues established a mouse model overexpressing human WT FUS and therefore mimicking a gain of FUS function (Mitchell et al., 2013). They observed cytoplasmic

FUS inclusions in the brain and spinal cord (SC), as well as a loss of motor neurons. Symptomatically, homozygous mice developed an aggressive phenotype with an early onset tremor, denervation, focal muscle atrophy, progressive hind limb paralysis, and death at the age of twelve weeks (Mitchell et al., 2013).

The first rodents harboring an ALS-associated point mutation were reported in 2011. The rats overexpressed mutant human R521C FUS and displayed features of ALS and FTLD (Huang et al., 2011). The group observed an aggregation of ubiquitin, a degeneration of motor axons, and a loss of neurons in the cortex and hippocampus, which led to progressive paralysis in transgenic mutant rats (Huang et al., 2011). Rats overexpressing the WT human FUS also showed a significant loss of cortical and hippocampal neurons and were conspicuous concerning spatial learning and memory (Huang et al., 2011). Three years later, another group published mice with the R521C FUS mutation (Qiu et al., 2014). These transgenic animals expressed human mutant FUS under the control of a Syrian hamster prion promoter at a comparable level to the endogenous Fus protein. Here a gain of function was suggested that resulted in enhanced DNA damage and RNA splicing defects, early onset behavioral deficits, and postnatal lethality (Qiu et al., 2014). The group of Sephton et al. put the human WT and R521G FUS under the control of the cytomegalovirus immediate early enhancer-chicken β -actin hybrid (CAG) promoter (Sephton et al., 2014). Both transgenic mouse lines died early around day 30 and developed severe motor deficits, as well as neuroinflammation and denervated neuromuscular junctions. Interestingly, the phenotype of human WT FUS animals was more severe in these points. Mice expressing the human R521G mutation additionally displayed altered sociability and a reduction of dendritic arbors and mature spines (Sephton et al., 2014). Another mouse model, which was lacking the complete NLS, RGG2 and 3, and the zinc finger motif, taught that neuronal aggregation of FUS was sufficient to recapitulate several features of ALS and that this was independent of RNA-metabolism (Shelkovnikova et al., 2013). The construct was expressed under the control of the Thy-1 promoter and abruptly at the age of 2.5 to 4.5 months mice developed a severe motor phenotype and died within days. This was caused by a severe damage of motor neurons and axons and a neuroinflammatory reaction (Shelkovnikova et al., 2013). Somatic brain transgenic (SBT) mice expressing mutant FUS, which means that newly born mice were injected bilateral intracerebroventricularly with a vector encoding human FUS_{R521G} or FUS _{Δ 14} without the PY-NLS, showed a mislocalization of FUS to the cytoplasm to a varying degree, which correlated with disease severity in humans (Verbeeck et al., 2012). Truncation of the NLS resulted in insoluble FUS and NCIs, which were also immunoreactive for other pathologic markers, including ubiquitin, p62, α -internexin, and PABP-1 (Verbeeck et al., 2012).

One rat model appeared to recapitulate some features of FTLD, such as progressive loss of memory, by overexpressing mutant R521C FUS under the CaMKII promoter (Huang et al., 2012). The rats displayed FUS and ubiquitin positive inclusions in the cytoplasm of neurons, a loss of neurons in the dentate gyrus and frontal cortex, abnormal neuritic branching, altered dendritic spine density, progressive golgi fragmentation, and aggregation of mitochondria in degenerating neurons (Huang et al., 2012).

Despite all these models yielded several hints for the pathomechanisms especially behind ALS, till now, a complete picture could not be drawn. Rodent models could also not elucidate, whether disease is caused by loss or gain of FUS function. Phenotypes of models for ALS-associated *FUS* mutations were quite inconsistent and the mutant human FUS was not expressed under the endogenous promoter. Additionally, some models were overexpressing mutant human FUS (Huang et al., 2011; Huang et al., 2012) so that it is not clear, whether the phenotype is caused by the mutation or by the overexpression.

3.3 TRANSMEMBRANE PROTEIN 106B (TMEM106B)

In 2010, a genomewide association study (GWAS) identified three single nucleotide polymorphisms (SNPs) at locus 7p21.3 (rs1020004, rs6966915, and rs1990622), where the gene *TMEM106B* is located, as a risk factor for the development of FTLD-TDP (Van Deerlin et al., 2010). The SNPs lie within introns 3 and 5, and downstream of *TMEM106B*, with rs1990622 downstream being the top SNP (Van Deerlin et al., 2010). *TMEM106B* was found to be >2.5 times higher expressed in the cortex of FTLD-TDP patients compared to healthy controls, indicating that the risk alleles mediate genetic susceptibility by increasing gene expression. This was observed in FTLD-TDP patients with *Progranulin* (*GRN*) mutations to a higher extend than in patients with *GRN*-independent FTLD, suggesting that *GRN* acts upstream of *TMEM106B* (Van Deerlin et al., 2010). Further, the authors observed that homozygotes for the risk allele of rs1020004 in intron 3 displayed shorter disease duration than homozygotes for the minor allele (Van Deerlin et al., 2010). The association of *TMEM106B* variants and *GRN* mutation carriers was confirmed by further studies in a cohort with 640 FTLD patients of Caucasian ancestry, patients from France and Italy, and a Flanders-Belgian cohort (Finch et al., 2011; van der Zee et al., 2011; Lattante et al., 2014). They identified the same top SNP and found that one or two copies of the protective allele C reduced the risk for developing FTLD to 70-50% (van der Zee et al., 2011). Via

exon sequencing, two amino acid substitutions in the coding region of *TMEM106B*, S134N and T185S, were found to be associated with FTLD. T185S (rs3173615) is located in exon 6 and displayed a frequency of 35% in patients and 42% in controls (van der Zee et al., 2011). This SNP was shown to be in perfect linkage disequilibrium with rs1990622 (Cruchaga et al., 2011; Finch et al., 2011) and to correlate with pathogenic *GRN* mutations (Nicholson et al., 2013; Lattante et al., 2014), as well as *C9orf72* expansion (van Blitterswijk et al., 2014). *In vitro*, the risk allele T185 revealed higher levels of TMEM106B due to a faster degradation of the S185 form as a result of a changed N-glycosylation at residue 183, whereas mRNA levels did not differ (Nicholson et al., 2013).

Due to the similarities of ALS and FTLD, it was assumed that these three SNPs could be also involved in the development of ALS. A replication of the GWA study yielded that *TMEM106B* is a risk factor for both, ALS and FTLD (Rollinson et al., 2011), whereas Vass and colleagues found no difference between ALS patients and healthy persons concerning *TMEM106B* SNP genotype frequencies (Vass et al., 2011), and the same was true for MND patients (van Blitterswijk et al., 2014). However, *TMEM106B* seems to be involved in the development of cognitive impairment in ALS (Vass et al., 2011).

3.3.1 STRUCTURE AND FUNCTION OF *TMEM106B*

TMEM106B is an uncharacterized transmembrane protein of 274 amino acids. It is encoded by nine exons and harbors a transmembrane domain, which corresponds to exons 4 and 5. The other domains are of unknown function. Five transcripts of *TMEM106B* are depicted, among these three are protein coding. In 2012, TMEM106B was redescribed as a type 2 integral membrane protein with a luminal (C-terminus) and a cytoplasmic side (N-terminus) (Lang et al., 2012) and being localized to late endosomes and lysosomes (Chen-Plotkin et al., 2012; Lang et al., 2012; Brady et al., 2013). The luminal domain is highly glycosylated, which is required for the transport of TMEM106B (Chen-Plotkin et al., 2012; Lang et al., 2012). This domain is removed via regulated intramembrane proteolysis (Brady et al., 2014). The signal peptide peptidase-like 2a (SPPL2a) processes TMEM106B to an N-terminal fragment containing the transmembrane and intracellular domains, which is further cleaved into a small, rapidly degraded intracellular domain (Brady et al., 2014).

TMEM106B was found to control dendritic branching and trafficking of lysosomes together with microtubule-associated protein 6 (MAP6) (Schwenk et al., 2014), as well as lysosomal size, motility and responsiveness to stress (Stagi et al., 2014). TMEM106B knockdown resulted in a reduction of lysosomal number and diameter in neurons and an increase of transported lysosomes, whereas an overexpression in enlarged lysosomes in the soma, disturbed axonal transport, and altered lysosomal stress signaling (Stagi et al., 2014). Brady and colleagues observed that TMEM106B levels are regulated by lysosomal activities (Brady et al., 2013). They approved that an ectopic expression of TMEM106B correlated with elevated levels of GRN and further morphological changes of lysosome compartments and impairment of the endolysosomal degradation pathway (Brady et al., 2013). Lang et al. could not verify a possible connection between TMEM106B and GRN, though a significant increase of TMEM106B levels due to inhibition of vacuolar H⁺-ATPases, a finding that was also observed for GRN (Lang et al., 2012). By contrast, two studies reported a colocalization of TMEM106B and GRN in late endolysosomes (Chen-Plotkin et al., 2012; Nicholson et al., 2013) and an increase of GRN levels following TMEM106B overexpression (Chen-Plotkin et al., 2012). They also suggested that TMEM106B overexpression could be the result of a depression of the microRNA-132/212 cluster, direct repressors of TMEM106B, by binding to its 3' UTR. Overexpression of TMEM106B yielded an enlargement and acidification of endo-lysosomes and a negative influence on the mannose-6-phosphate pathway (Chen-Plotkin et al., 2012).

Some of these results are contradicting, which could be due to the fact that all these studies were *in vitro* experiments. This year, a GRN deficient mouse model yielded an *in vivo* confirmation of a possible connection of GRN and TMEM106B (Gotzl et al., 2014). The mice showed elevated levels of TMEM106B and recapitulated features of FTLN, as well as neuronal ceroid lipofuscinosis (NCL), a lysosomal storage disorder (Gotzl et al., 2014). In mice lacking the lysosomal protein cathepsin D (CTSD), a model for NCL, both GRN and TMEM106B were found to be increased which strengthens a possible link between FTLN and NCL (Saftig et al., 1995; Gotzl et al., 2014).

3.3.2 TMEM106B IN THE HUMAN BRAIN

In patients, TMEM106B was found to be >2.5 times elevated (Van Deerlin et al., 2010), which could be confirmed by several groups (Chen-Plotkin et al., 2012; Nicholson et al., 2013; Gotzl et

al., 2014). Subcellularly, it is expressed in endosomes and lysosomes (Chen-Plotkin et al., 2012; Lang et al., 2012; Brady et al., 2013).

On cellular and brain region level, TMEM106B is expressed in the majority of all cortical and hippocampal neurons and populations of oligodendrocytes, reactive astrocytes, and microglia (Sato et al., 2014). Busch and colleagues could detect TMEM106B in the cytoplasm of neurons, glia, and in cells surrounding blood vessels in frontal and occipital cortex in healthy human brains (Busch et al., 2013). Frontal cortex is a region where typically TDP pathology is highly pronounced, as opposed to occipital cortex (Geser et al., 2009). TMEM106B was observed in all layers of neocortex, especially in layer 3-5 (Busch et al., 2013). In the hippocampus, it could be stained in the pyramidal neurons of Ammon's horn and in the cerebellum, it was expressed in Purkinje cells (Busch et al., 2013). In FTLD-TDP patients, TMEM106B expression was much more diffuse throughout the cell body, mainly in *GRN* mutation carriers. However, no formation of pathological TMEM106B inclusions could be proven and TDP-43 inclusions were not immunoreactive for TMEM106B (Busch et al., 2013).

TMEM106B was not only linked to FTLD but also to AD: expression of TMEM106B was found to be reduced in brains of AD patients, whereas *GRN* levels were elevated (Sato et al., 2014). Interaction of polymorphisms in *TMEM106B* and *APOE* was reported to be associated with late-onset AD (Lu et al., 2014) and rs1990622 seems to be involved in the pathologic presentation of AD. The C-allele was much more frequent in AD cases with TDP-43 pathology than in other AD patients (Rutherford et al., 2012).

3.3.3 *TMEM106B* AS A MODULATOR OF FTLD

The *TMEM106B* variant rs1990622 was reported to confer risk for the development of FTLD-TDP (Van Deerlin et al., 2010; Finch et al., 2011; van der Zee et al., 2011; Lattante et al., 2014) and, as mentioned above, different publications connected TMEM106B to *GRN* (Van Deerlin et al., 2010; Finch et al., 2011; van der Zee et al., 2011; Chen-Plotkin et al., 2012; Brady et al., 2013; Nicholson et al., 2013; Gotzl et al., 2014; Lattante et al., 2014).

Recent patient based studies characterized *TMEM106B* rather as a modifier of FTLD-TDP. Generally, rs1990622 genotype CC was found to be protective in FTLD-TDP, except in *C9orf72* expansion carriers (Gallagher et al., 2014). In those patients, C depicted the risk allele and was linked to an earlier age of disease onset and death (Gallagher et al., 2014). In *GRN* mutation

carriers, the allele T of rs1990622 was associated with an earlier age of disease onset, in average 13 years (Cruchaga et al., 2011), and decreased GRN levels in patients and controls (Cruchaga et al., 2011; Finch et al., 2011), except again in *C9orf72* expansion carriers (Gallagher et al., 2014). A direct influence of the coding polymorphism T185S on GRN levels seems to be unlikely (Brady et al., 2013; Nicholson et al., 2013). However, the minor allele S185 was shown to be protective in *GRN* mutation (Nicholson et al., 2013; Lattante et al., 2014), as well as *C9orf72* expansion carriers (van Blitterswijk et al., 2014).

In asymptomatic *GRN* mutation carriers, *TMEM106B* SNP genotypes were suggested to modulate brain connectivity (Premi et al., 2014) and *TMEM106B* variant rs1990622 was associated with gray matter volume of left-sided temporal lobe involved in language processing what could explain the language deficits of FTLT-DTP patients (Adams et al., 2014).

Despite all these hints, no *in vivo* studies for *TMEM106B* have been published and the precise mechanism behind FTLT could not be solved till now. However, the modifying effect of *TMEM106B* variants could be the explanation of the wide range of age at onset, disease duration and symptoms in FTLT, partly overlapping with ALS.

3.4 MOTIVATION AND OBJECTIVE OF THE THESIS

The aim of this thesis was to generate and analyze new different mouse models for the ALS- and FTLT-associated genes *FUS* and *TMEM106B*. These models should help to learn more about the pathomechanisms and to open new perspectives in the diagnostic and development of therapeutics for the treatment of these two devastating neurodegenerative diseases. While mutations in *FUS* had been identified to be causative for the development of ALS, so far none of the published mouse models for *FUS* could completely mimic an ALS phenotype. In these models *FUS* was always expressed under an exogenous promoter and therefore under- or overexpressed or perhaps differentially regulated. My hypothesis was that modeling ALS in the mouse can be achieved when employing the endogenous promoter. Thus, in this study, mouse models for *FUS* should be generated using the endogenous murine *Fus* promoter and tested for an ALS phenotype. *TMEM106B* was identified to be a risk factor for FTLT right when this study started and so far the function of *TMEM106B* is quite unclear, not to speak of a successful mouse model. Therefore, in this study, mouse models should be generated in order to get more insight into the functions of *TMEM106B* and its role in the development of FTLT.

In order to analyze the contribution of FUS to the development of ALS, mouse models were made expressing ALS-associated *FUS*-mutations under the endogenous promoter. On the one hand, murine *Fus* was exchanged by human FUS with the R521G mutation via recombinase mediated cassette exchange, on the other hand murine *Fus* was mutated via TALEN technology by the group of Ralf Kühn and mice expressing *Fus* mutations, which correspond to the human mutations R521G or P525L, or lacking a functional NLS were provided (Panda et al., 2013). The mice should be analyzed and compared regarding pathological and behavioral changes. Additionally, to compare the effects of mutated FUS versus a loss of FUS function and thus to answer the question, if ALS is the result of a lost or an enhanced performance, murine *Fus* was interrupted in intron 1 and *Fus* deficient mice were generated. These mice should also be investigated concerning pathology and behavior.

TMEM106B was reported to confer risk for the development of FTLD-TDP by increasing its own gene expression and to modify disease onset and duration in patients. Therefore, mice overexpressing *TMEM106B* to different extents should be made and the effects of such an ectopic expression on proteins like GRN or TDP-43 and those of the endo-/lysosomal pathway should be analyzed pathologically. To possibly enhance these effects, the mouse line was crossed with a model for an ALS-associated TDP-43 mutation (Stribl et al., 2014).

Pathological and phenotypical analyses of these mouse models should lighten the mechanisms behind the development of ALS and FTLD and therefore make an important contribution to a potential treatment or even a prevention of these devastating diseases in the future.

4 MATERIAL

4.1 CONSUMABLE MATERIAL

Consumables	Company
384-well qRT-PCR plates	4titude
μ -Slide 8 Well Glass Bottom	ibidi
Adhesive Seal Applicator	Thermo Scientific
Cell culture dishes	Nunc
Centrifuge tubes	Corning
Coverslips	Roth
Cuvettes for electroporation	BioRad
Embedding pots	Polysciences
Filter paper	Whatman 3mm
Filter tips	Starlab
Gloves	Meditrade, Kimtech Science
Hyperfilm	Amersham
Multiwell plates	Eppendorf
One way needles	Terumo
One way syringes	Terumo
Pasteur pipettes	Brand
PCR reaction tubes 0,2 ml	Biozym
PCR reaction lids	Biozym

Pipette tips	Gilson
Plastic pipettes	Greiner
PVDF membrane	Millipore
Reaction tubes (0.5 ml, 1.5 ml, 2 ml, 5 ml)	Eppendorf
Reaction tubes (15 ml, 50 ml)	Sarstedt
Tissue cassettes	Merck
Tissue embedding molds	Polysciences
Wipes	Kimtech Science

4.2 INSTRUMENTS

Instrument	Type	Company
Autoclave	667-1ST	Aigner
Balances	LC6201S, LC220-S	Sartorius
Centrifuges	Evolution RC	Sorvall
	5417 R, 5424	Eppendorf
	Varifuge 3.0R	Heraeus
Chambers for electrophoresis		Peqlab
Developing machine	Curix 60	Agfa
Digital camera	AxioCam MRc	Zeiss
Electric homogenizer	Ultra-Turrax T25 basic	IKA
Electroporation system	Gene Pulser XCell	BioRad
Freezer (-20°C)		Liebherr

Freezer (-80°C)	HFU 686 Basic	Heraeus
Fridges (4°C)		Liebherr
Gel documentation system	E.A.S.Y.	Herolab
Gel blotting system	XCell SureLock™ MiniCell	Invitrogen
Glass pipettes		Hirschmann
Glassware		Schott
Ice machine	AF 30	Scotsman
Incubators (bacteria)	Innova 4230	New Brunswick Scientific
Incubators (cells)		Heraeus
Light source for microscopy	KL 1500	Leica
Magnetic heater	MR3001	Heidolph
Magnetic stirrer		Heidolph
Microscope	Axioplan2 imaging	Zeiss
Microscope (fluorescent)	Axiovert 200M	Zeiss
Microtom	SM2000R	Leica
Microwave oven		Sharp
Neubauer counting chamber		Brand
PCR machine	MasterCycler Gradient	Eppendorf
Perfusion pump	401U/D1	Watson-Marlow Bredel
pH meter	pH Level 1	InoLab
Photometer	Biophotometer 6131	Eppendorf
Pipette filler, electronic	Easypet	Eppendorf
Pipettes		Gilson

Power supplies for electrophoresis	E443 EC250-90, EC3000-90 EPS200	Consort Thermo Pharmacia Biotech
Real-time PCR system	7900HT	Applied Biosystems
Shaker	Polymax 1040	Heidolph
Slide warmer	BV SW 85	Adamas instrument
Sonifier	Cell disrupter B15	Branson
Software microscope	Axiovision	Zeiss
Thermomixer	Comfort	Eppendorf
UV-lamp	N-36	Benda
UV/Vis-spectral photometer	NanoDrop® ND-1000	Peqlab
Vortex	Vortex genie 2	Scientific industries
Water bath	U3 AQUAline AL 12	Julabo LAUDA
Water conditioning system	MilliQ biocel	Millipore

4.3 CHEMICALS AND CONSUMABLE SUPPLIES

Chemical	Company
3,3'-diaminobenzidine (DAB)	DCS LabLine
5x Sample Loading buffer	Invitrogen
20x NuPAGE® Running buffer	Invitrogen
20x NuPAGE® Transfer buffer	Invitrogen
β-mercaptoethanol	Sigma

Acetic acid	Merck
Ag501-X8	BioRad
Agarose (for gelelectrophoresis)	Biozym
Ampicillin	Sigma
Ampuwa	Fresenius
Antibody dilution buffer	DCS LabLine
Aquapolymount	Polysciences
Bacto agar	Difco
Bis-tris	Sigma
Blocking reagent	Roche Diagnostics-Boehringer
BM Purple Ap substrate	Roche Diagnostics-Boehringer
Boric acid	Merck
Bovine serum albumin	Sigma
Bromphenol blue	Sigma
CHAPS (3-[(3-cholamidopropyl)dimethylammonio]-1-propanesulfonate)	Biomol
Chloramphenicol	Sigma
Chloroform	Sigma
Citric acid	Sigma
Colcemid	Roche
Collagenase type Ia (cell culture tested)	Sigma
Cresyl violet acetate	Sigma
DAPI stain	Carl Roth

DigAb coupled to AP	Roche Diagnostics-Boehringer
Dimethyl formamide	Sigma
Dimethyl sulfoxide (DMSO)	Sigma
Dithiotreitol (DTT)	Roche
DMEM (Dulbecco's Modified Eagle's Medium) (1x)	Gibco
DNA ladder: GeneRuler (100 bp/1 kb)	Fermentas
dNTPs	Fermentas
DPBS (Dulbecco's Phosphate Buffered Saline) (1x)	Gibco
Ethylene diamine tetraacetic acid (EDTA)	Sigma
Ethylene glycol tetraacetic acid (EGTA)	Sigma
Ethanol absolute	Merck
Ethidiumbromide	Fluka
Ethylene glycol	Sigma
Fetal calf serum (FCS)	PAN, Hybond
Formaldehyde	Sigma
Formamide	Sigma
Glutaraldehyde	Sigma
Glycerol	Sigma
Gelatin	Sigma
Goat serum	Sigma
Hematoxylin (according to Mayer)	Sigma
Heparin	Sigma

HEPES Buffer Solution (1M)	Gibco
Hydrochloric acid (HCl)	Merck
Hydrogen peroxide (H ₂ O ₂ , 30%)	Sigma
Hygromycin B (cell culture)	Calbiochem
IPTG (Isopropyl- β -D-thiogalactopyranosid)	Fermentas
Isopropanol	Merck
Kanamycin	Sigma
Levamisol	Sigma
L-Glutamine 200 mM (100x)	Gibco
LIF	Millipore
Magnesium chloride	Merck
Maleic acid	Sigma
MEM nonessential amino acids (NEAA) (100x)	Gibco
Methanol	Merck
Mineral oil	Sigma
Molecular Weight Marker: ECL Full-Range Rainbow	Amersham
MOPS	Sigma
N-laurylsarcosine Sodium Salt Solution	Sigma
Nonidet P40 (NP-40)	Fluka
Paraffin	
Paraformaldehyde	Sigma
Pen Strep (100x)	Gibco

Pertex mounting medium	HDscientific
Phosphatase inhibitor (tablets)	Roche
Polymerase T4	NEB
Potassium hydroxide (KOH)	Sigma
Protease inhibitor (tablets)	Roche
Puromycin (cell culture)	Life Technologies
RNA polymerase T7	Roche
RNase A	Sigma
RNase inhibitor	Roche
RNaseZAP®	Sigma
rNTPs DigMix	Roche
Skim milk powder	BD Biosciences
SOC medium	Invitrogen
Sodium acetate	Merck
Sodium Cacodylate Buffer (0.1M) with 2.5% glutaraldehyde (pH 7.4)	Science Services
Sodium chloride	Merck
Sodium citrate	Sigma
Sodium desoxycholate	Sigma
Sodium dodecyl sulfate (SDS)	Sigma
Sodium hydrogen carbonate	Sigma
Sodium hydroxide	Roth
Stempan E14 GMEM medium	PAN

Streptavidin-peroxidase solution	KPL
Sucrose	Sigma
Thiourea	Invitrogen
TriReagent	Sigma
Tris	Sigma
Triton X 100	BioRad
Trizol	Invitrogen
Trypsin/EDTA (E14)	PAN
Trypsin/EDTA 0.05% (1x)	Gibco
Tween-20	Sigma
Urea	Sigma
X-Gal	Fermentas
Xylol	Roth

4.4 KITS

Kit	Company
5 PRIME MasterMix (PCR)	5 PRIME
ECL Detection Kit	Amersham
Gateway® LR clonase™ II enzyme mix	Invitrogen
iScript™ Select cDNA Synthesis Kit	BioRad
M.O.M.™ Kit	Vector Laboratories

Pierce® BCA Protein Assay Kit	Thermo Scientific
QIAamp DNA Blood Mini Kit	Qiagen
QIAGEN Large-Construct Kit protocol	Qiagen
Qiagen Plasmid Maxi Kit	Qiagen
Qiagen Plasmid MiniPrep Kit	Qiagen
QIAquick Gel Extraction Kit	Qiagen
QIAquick PCR Purification Kit	Qiagen
ReadyPrep™ Protein Extraction Kit (Soluble/Insoluble)	BioRad
RC DC™ Protein Assay	BioRad
RNase-Free DNase Set	Qiagen
RNeasy® Mini Kit	Qiagen
SuperScript® VILO cDNA Synthesis Kit	Life Technologies
TaqMan® Universal Master Mix	Applied Biosystems
TOPO TA Cloning® Kit (Dual promoter)	Invitrogen
Wizard genomic DNA purification Kit	Promega

4.5 VECTORS AND PLASMIDS

Plasmid	Construct from	Description
Caggs-CRE-IRES-Puro		Cre-recombinase and Puromycin resistance expressing vector
FLPo		Flp-recombinase expressing vector
pCRII-TOPO	Invitrogen	TOPO TA cloning vector

pDest ⁺¹	L. Schebelle	Destination vector for Gateway cloning
pENTR4	Invitrogen	Basis for pENTR-EX vectors
pENTR-EX-SA hFUS ^{P525L} pA	D. Dormann	pENTR-EX vector for Gateway reaction containing human <i>FUS</i> cDNA
pENTR-EX-SA hFUS ^{R495X} pA	GeneArt	pENTR-EX vector for Gateway reaction containing human <i>FUS</i> cDNA
pENTR-EX-SA hFUS ^{R521G} pA	D. Dormann	pENTR-EX vector for Gateway reaction containing human <i>FUS</i> cDNA
pENTR-EX-SA hFUS ^{WT} pA	D. Dormann	pENTR-EX vector for Gateway reaction containing human <i>FUS</i> cDNA
pEx-Flp-Hygro-SA hFUS ^{P525L} pA	C. Stribl	Exchange vector for RMCE
pEx-Flp-Hygro-SA hFUS ^{R495X} pA	M. Bosch	Exchange vector for RMCE
pEx-Flp-Hygro-SA hFUS ^{R521G} pA	C. Stribl	Exchange vector for RMCE
pEx-Flp-Hygro-SA hFUS ^{WT} pA	C. Stribl	Exchange vector for RMCE
Plasmid from 129S7AB2.2 BAC clone bMQ263o13	Source BioScience LifeSciences	Containing Sv129 <i>Tmem106b</i> locus

4.6 ENZYMES

Enzyme	Company
Alkaline phosphatase, calf intestinal (CIP)	NEB
Cre recombinase	NEB
DNA polymerase (Taq)	Qiagen
DNase I	Roche
Klenow fragment of DNA polymerase I	NEB

Proteinase K	Roche
Restriction enzymes	NEB, Roche
RNase A	Serva
T4 DNA Ligase	NEB

4.7 OLIGONUCLEOTIDES

4.7.1 OLIGONUCLEOTIDES FOR GENOTYPING

Name	Sequence	Annealing temp.	Product size
SR2	5'-GCCAAACCTACAGGTGGGGTCTTT-3'	60°C	539 bp β geo
TP	5'-ATCAAGGAAACCCTGGACTACTG-3'		262 bp successful exchange
FUS rev	5'-CCATAGCTTTGGGTTGCTTGTGG-3'	60°C	532 bp with SR2 after successful hygromycin excision
B045	5'-CTCCGCCTCCTCTTCCTCCATC-3'		652 bp β geo
B048	5'-CCTCCCCCGTGCCTTCCTTGAC-3'	58°C	907 bp inverted β geo
B050	5'-TTTGAGGGGACGACGACAGTAT-3'		449 bp successful exchange
EUCE_fw1	5'-TCTCGTCTCCTACCAGAACCA-3'		837 bp transgenic allele
EUCE_fw WT	5'-AGACTTGTGGTCCGGTGCT-3'	60°C	651 bp endogenous allele
EUCE_rv	5'-TCAAATACAGATCATCCCTTAAGTTT-3'		

Talen fw	5'-CTATGGAGATGATCGACGTG-3'	59°C	576 bp
Talen rv	5'-TGGTTACAATTAGGGTAGTCTG-3'		
Intron3_ fw	5'-TGGTGAGATTCTGTTTCATTTGC-3'	53-63°C	389 bp
Intron3_rv	5'-CTGAGACAAGTGGCAGTATTGG-3'		
Insert_fw	5'-TTCATGTGGGTCAAACAAATCT-3'	53-63°C	495 bp Sv129
Insert_rv	5'-CCACTTTCCTTGTATTTTCTAGGG-3'		345 bp B6
SNP_upstr eam_fw	5'-GTGACCAGCTATGCTTTGATTG-3'	53-63°C	482 bp; SNPs rs30620182, rs30569103,
SNP_upstr eam_rw	5'-GCTGAAATTGTGTCTGGTTTGA-3'		rs30811046
SNP_upstr eam2_fw	5'-TTCAGAGTGCCCATGTTTCATTA-3'	53-63°C	400 bp; SNP rs30220269
SNP_upstr eam2_rw	5'-ATCCTATTCCACAAATGGCAG-3'		

4.7.2 OLIGONUCLEOTIDES FOR RT-PCR

Name	Sequence	Annealing temperature
hnRNP-D_fw	5'-GACGCCAGTAAGAACGAGGA-3'	60°C
hnRNP-D_rv	5'-TGATCGCCCTGTGATAGGAT-3'	
Ndr2_fw	5'-AGGACAAACACCCGAGACTG-3'	60°C
Ndr2_rv	5'-ATGGTAGGTGAATATCGCCG-3'	
Ptk2b_fw	5'-AGACCTCCTCCACAGACCAA-3'	60°C

Ptk2b_rv	5'-CATCTTTCCTCTCGCCTCAG-3'	
Sort1_fw	5'-CAGGAGACAAATGCCAAGGT-3'	60°C
Sort1_rv	5'-TGGCCAGGATAATAGGGACA-3'	
Tia1_fw	5'-TGAAAGTGAATTGGGCAACA-3'	60°C
Tia1_rv	5'-TGGACTGAGGTCACCAACAA-3'	

4.7.3 OLIGONUCLEOTIDES FOR PROBES

Name	Sequence	Annealing temp.	Product Size
TMEM in Situ fw2	5'-TTGGATTCCAGATAGCAGCA-3'	60°C	696 bp
TMEM in Situ rv2	5'-GCTGTCTGCAGATGTTTTTGA-3'		
TMEM106B_Southern5000 fw	5'-GAAAATGGCTATGGGTTTACAACA-3'	60°C	588 bp
TMEM106B_Southern5000 rv	5'-ACCTCAACCTAATGCCACAGC-3'		

4.8 TAQMAN ASSAYS

All TaqMan® Assays were purchased from Life Technologies™ (prior Applied Biosystems) and were labeled with FAM.

4.8.1 TAQMAN GENE EXPRESSION ASSAY

Gene	Species	Localization	Assay ID
<i>Actb</i> (endogenous reference)	mouse		Mm00607939_s1
<i>FUS</i>	human and mouse	Exon 6/7	HS00192029_m1
<i>Fus</i>	mouse	Exon 1/2	Mm01271304_m1
<i>Tmem106b</i>	mouse	Exon 3/4	Mm00510952_m1

4.8.2 TAQMAN COPY NUMBER ASSAY

Gene	Species	Assay ID
<i>Tmem106b</i>	mouse	Mm00651778_cn
<i>Efnb2</i> (Chromosome 8)	mouse	Mm00256539_cn
<i>Rnf112</i> (Chromosome 11)	mouse	Mm0004107_cn
<i>Uty</i> (Y Chromosome)	mouse	Mm00527282_cn
<i>Tfrc</i>	mouse	Copy Number Reference Assay

4.9 MOUSE STRAINS

4.9.1 USED MOUSE STRAINS

Mouse strain	Description
C57Bl/6J	Wild type mouse line
Gt(ROSA)26Sortm16(Cre)Arte (Taconic)	General deleter knock-in of “Splice-Acceptor – NLSSV40T – Cre polyadenylation site” in the <i>ROSA26</i> locus; ubiquitous and constitutive activity
Fus ^{P511fs}	Mouse model with a frameshift at position 511 in the murine <i>Fus</i> gene leading to a nonsense NLS (side product of Fus ^{R513G} line)
Fus ^{P517L} (Panda et al., 2013)	Mouse model expressing a <i>Fus</i> mutation that corresponds to the human ALS causative <i>FUS</i> point mutation P525L
Fus ^{R513G} (Panda et al., 2013)	Mouse model expressing a <i>Fus</i> mutation that corresponds to the human ALS causative <i>FUS</i> point mutation R521G
hTDP-43 ^{A315TKi} (Stribl et al., 2014)	Mouse model expressing a human ALS causative TDP-43 point mutation (A315T) under the control of the endogenous <i>Tardbp</i> promoter

4.9.2 GENERATED MOUSE STRAINS

Mouse strain	Description
EUCE0290f05	Knock-in of RMCE βgeo cassette in intron 1 of the <i>Fus</i> locus

hFUS ^{R521G}	Mouse model generated by RMCE and carrying a human ALS causative <i>FUS</i> point mutation (R521G) under the control of the endogenous <i>Fus</i> promoter
hFUS ^{R521G} Rosa (in the text: hFUS ^{R521G})	Breeding of hFUS ^{R521G} mice with Gt(ROSA)26Sor ^{tm16(Cre)} Arte (Taconic) mice in order to excise the hygromycin cassette
Tmem106b ^{BACTg} (according to (Vintersten et al., 2008))	Mice containing additional copies of <i>Tmem106b</i> and thus overexpressing Tmem106b
Tmem106b ^{BACTg} x hTDP-43 ^{A315TKi}	Compound mutant mice

4.10 STOCK SOLUTIONS

Solution	Ingredients
Fast digestion buffer (1x)	5 mM KCl 10 mM Tris 0.5% NP-40 0.5% Tween-20
Lysis buffer	1 M Tris HCl, pH 7.5 0.5 M EDTA, pH 8.0 5 M NaCl 20% N-laurylsarcosine Sodium Salt Solution
Loading buffer for agarose gels	15% Ficoll 400 200 mM EDTA 1-2% Orange G
Paraformaldehyde (PFA, 4%)	4% PFA w/v in PBS
PBS (1x), pH 7.4	171 mM NaCl 3.4 mM KCl 10 mM Na ₂ HPO ₄ 1.8 mM KH ₂ PO ₄

Precipitation solution	5 M NaCl 100% Ethanol
SSC (20x)	3 M sodium chloride 300 mM trisodium citrate (pH 7.0)
TAE (10x)	0.4 M Tris base 0.1 M acetate 0.01 M EDTA
TE buffer	10 mM Tris, pH 8.0 1 mM EDTA
Tris-HCl, pH 7.5 or 8.0	1 M Tris base

4.11 WORK WITH BACTERIA

4.11.1 *E. COLI* STRAINS

Strain	Company
DH5 α	Invitrogen
TOP10	Invitrogen

4.11.2 SOLUTIONS

Solution	Ingredients
LB medium	10 g bacto peptone 5 g yeast extract 5 g NaCl ad 1 l H ₂ O
LB agar	98.5% LB medium

	1.5% bacto agar
Ampicillin selection medium	LB medium with 50 µg/ml ampicillin
Kanamycin selection medium	LB medium with 25 µg/ml kanamycin
Ampicillin selection agar	LB agar with 100 µg/ml ampicillin
Kanamycin selection agar	LB agar with 50 µg/ml kanamycin

4.12 CELL CULTURE

4.12.1 CELL LINES

Cell line	Clone
E14TG2A	EUCE0290f05 (MGI:4382244)
Fibroblasts, MEFs (FUS mouse models)	

4.12.2 MEDIA AND SOLUTIONS

Solution	Ingredients
E14 medium	10% FCS (Hybond) 1000 U/ml LIF in E14 GMEM medium
Fibroblast medium	10% FCS (PAN) 1% L-Glutamin 1% MEM NEAA (1-3% Pen Strep) In DMEM medium

Freezing medium (1x)	10% DMSO in medium
Gelatin solution	1% gelatin in H ₂ O

4.13 GENERATION OF MICE

Solution	Ingredients
BAC injection buffer	5 mM Tris 0.1 mM EDTA, pH7.6 filtersterilize and store at 4°C

4.14 WESTERN BLOT ANALYSIS

4.14.1 SOLUTIONS

Solution	Ingredients
Blocking solution	5% skim milk powder in 1x TBS-T
Loading buffer (5x)	5x sample loading buffer 4% β -mercaptoethanol
RIPA buffer	50 mM Tris-HCl 150 mM NaCl 3 mM EDTA 1% Triton-X 100 0.5% SDS 0.5% sodium desoxycholate
Running buffer (1x)	5% 20x NuPAGE® Running buffer in H ₂ O

10 x TBS	0.25 M Tris-HCl pH 7.5 1.37 M NaCl in H ₂ O
1x TBS-T	1x TBS 0.05% Tween-20
TEB (Triton Extraction Buffer)	0.5% Triton X 100 0.02% NaN ₃ in PBS
Transfer buffer (1x)	5% 20x NuPAGE® Transfer buffer 10% methanol in H ₂ O
Urea buffer	7 M Urea 2 M Thiourea 4% CHAPS 30 mM Tris-HCl, pH 8.5 in H ₂ O

4.14.2 ANTIBODIES

Primary Antibodies

Antibody	Ordering Number	Company	Dilution
anti- γ H ₂ AX, mouse monoclonal	05-636	Millipore	1:5000
anti-AIF (D39D2), rabbit monoclonal	5318	Cell Signaling	1:1000
anti-BDNF, rabbit polyclonal	ab46176	Abcam	1:1000
anti-beta Actin (AC-15), mouse monoclonal	GTX26276	GeneTex	1:5000
anti-C9orf72, rat		Developed by Prof. Dr. D.	1:10

Edbauer			
anti-cathepsin D, goat polyclonal		Santa Cruz Biotechnology	1:500
anti-FUS/TLS (4H11), mouse monoclonal	sc-47711	Santa Cruz Biotechnology	1 : 4000
anti-GFAP, rabbit polyclonal	ab7260	Abcam	1:50 000
anti-GRN (8H10), rat monoclonal		(Gotzl et al., 2014)	1:50
anti-H ₃ , rabbit polyclonal	ab1791	Abcam	1:2000
anti-LAMP1 (1D4B), rat monoclonal		Developed by J. Thomas August, distributed by Developmental Studies Hybridoma Bank, NICHD, maintained by the University of Iowa, Department of Biology	1:2000
anti-MeFUS, rat monoclonal		Gift from Dr. E. Kremmer, Molecular Immunology, Helmholtz Center Munich	1:10
anti-NeuN (A60), mouse monoclonal	MAB377	Millipore	1:500
anti-Opa1, mouse monoclonal	612606	BD Bioscience	1:1000
anti-p62 (C-terminal specific), guinea pig polyclonal	GP62-C	Progen	1:1000
anti-Parkin (PRK8), mouse monoclonal	sc-32282	Santa Cruz Biotechnology	1:1000
anti-PRMT1, rabbit monoclonal	ab92299	Abcam	1:5000
anti-TARDBP (2E2-D3) (human), mouse monoclonal	DR1075	Abnova	1:1000
anti-tau (3-repeat isoform RD3),	05-803	Millipore	1:1000

mouse monoclonal			
anti-tau (4-repeat isoform RD4), mouse monoclonal	05-804	Millipore	1:5000
anti-TDP43 (mouse/human), rabbit polyclonal	10782-2-AP	ProteinTech Group	1:1000
anti-Tim44, mouse	612583	BD Bioscience	1:4000
anti-Tmem106b (6F2), rat monoclonal		(Lang et al., 2012)	1:50
anti-Tom20 (FL-145), rabbit polyclonal	SC-11415	Santa Cruz Biotechnology	1:2000
anti- α -tubulin, mouse monoclonal		Sigma-Aldrich	1:5000

Secondary Antibodies (horseradish peroxidase conjugated)

Antibody	Company	Dilution
donkey-anti-goat IgG	Santa Cruz Biotechnology	1:5000
goat-anti-guinea pig IgG	Dianova	1:5000
donkey-anti-mouse IgG	Promega	1:10 000
goat-anti-mouse IgG	Dianova	1:5000
donkey-anti-rabbit IgG	Promega	1:10 000
goat-anti-rabbit IgG	Dianova	1:5000
goat-anti-rat IgG + IgM	Dianova	1:5000
mouse-anti-rat IgG2c	generated	1:1000

4.15 IMMUNOHISTOCHEMISTRY

4.15.1 SOLUTIONS

Solution	Ingredients
Blocking Solution	10% serum in 1x PBS-T
Cresylviolet solution (Nissl staining)	0.5% cresylviolet 2.5 mM sodium acetate 0.31% acetic acid
DAB-solution	Substrate: DAB 25:1
EDTA-T	0.2% EDTA 0.05% Tween 20 in H ₂ O
H ₂ O ₂ -solution (1%)	30% H ₂ O ₂ in methanol
PBS-T	1x PBS 0.5% Triton-X for cells/0.1% Tween 20 for tissue sections

4.15.2 ANTIBODIES

Primary Antibodies

Antibody	Ordering Number	Company	Dilution
anti- γ H2AX, mouse monoclonal	05-636	Millipore	1:400
anti-cleaved Caspase, rabbit polyclonal	9661	Cell Signaling	1:400
anti-FUS, rabbit polyclonal	HPA008784	Sigma	1:300
anti-GFAP, rabbit polyclonal	ab7260	Abcam	1:5000

anti-Hsp27, goat polyclonal	sc-1049	Santa Cruz Biotechnology	1:250
anti-NeuN (A60), mouse monoclonal	MAB377	Millipore	1:200
anti-p62 (C-terminal specific), guinea pig polyclonal	GP62-C	Progen	1:200
anti-TDP-43 (human), mouse monoclonal	ab57105	Abcam	1 : 500
anti-TDP-43 (mouse/human), rabbit polyclonal	10782-2-AP	Proteintech	1 : 500
TIA-1 (C-20), goat polyclonal	sc-1751	Santa Cruz Biotechnology	1:300
anti-Ubiquitin, mouse monoclonal	mab1510	Millipore	1:250

Secondary Antibodies (Fluorescence)

Antibody	Company	Dilution
donkey-anti-rabbit (Alexa 594 (red))	Life Technologies	1:500
donkey-anti-rabbit (Alexa 488 (green))	Life Technologies	1:500
donkey-anti-mouse (Alexa 594 (red))	Life Technologies	1:500
donkey-anti-mouse (Alexa 488 (green))	Life Technologies	1:500
goat-anti-guinea pig (Alexa 594 (red))	Life Technologies	1:500

Secondary Antibodies (DAB)

Antibody	Company	Dilution
goat-anti-rabbit (Biotin SP)	Dianova	1:300
goat-anti-mouse (Biotin SP)	Dianova	1:300

4.16 WHOLE MOUNT IN SITU HYBRIDIZATION (WISH)

Solution	Ingredients
4% PFA/0.2% glutaraldehyde	4% PFA/PBT 0.2% glutaraldehyde in PBT
Alkaline phosphatase buffer	0.1 M NaCl 50 mM MgCl ₂ 0.1% Tween20 0.1 M Tris-HCl, pH 9.0 2 mM Levamisol in H ₂ O
Blocking stock solution	10% blocking reagent (w/v) 0.1% Tween20 in MAB
Citric acid	1 M in H ₂ O
Deionized formamide	10 g Ag501-X8 in 100 ml formamide stirr for 1 h filtrate, store at -80°C
Heparin	100 mg/ml in H ₂ O
Hybe buffer	50% deionized formamide 5x SSC 0.05% heparin solution 0.1% Tween20

	in H ₂ O, adjust to pH 6 with Citric acid
MAB buffer, pH 7.5	100 mM maleic acid 150 mM NaCl
	in H ₂ O, adjust pH with solid NaOH
MABT	0.1% Tween20 in MAB buffer
PBT	PBS with 0.1% Tween20
PBT/glycine	2 mg/ml glycine in PBT
ProteinaseK buffer	2% Tris-Hcl, pH 7.0 1 mM EDTA in H ₂ O
RIPA	see Western Blot Analysis, 4.14.1
RNase A	10 µg/µl in 0.01 M NaAc, pH 5.2 heat to 100°C for 15 min, cool slowly to RT adjust pH by adding 0.1 vol. of 1 M Tris-HCl, pH 7.4
RNase solution	0.5 M NaCl 10 mM Tris-HCl, pH7.5 0.1% Tween20 in H ₂ O
SSC/FA/Tween20	2x SSC 50% formamide 0.1% Tween20 in H ₂ O
Staining solution	BM Purple Ap substrate 2 mM Levamisol 0.1% Tween20
TBST (10x)	0.1 M NaCl 20 mM KCl 250 mM Tris-HCl, pH 7.5 10% Tween20 in H ₂ O
TBST/Levamisol	2 mM Levamisol in TBST

tRNA	10 µg/µl in H ₂ O phenolize 2x, store at -20°C
------	---

5 METHODS

5.1 MOLECULAR BIOLOGY METHODS

5.1.1 CLONING AND PLASMID PREPARATION

TOPO cloning

Cloning of PCR products in the TOPO vector was done with the TOPO TA Cloning® Kit (Dual promoter) from Invitrogen, following manufacturer's instructions. Ampicillin (100 µg/ml) or kanamycin (50 µg/ml) were applied for selection. For 'blue/white selection', 50 µl each X-Gal and IPTG were put on the agar plates to induce β-galactosidase transcription from the TOPO plasmid, resulting in blue colonies. After a successful integration of the PCR product, the β-galactosidase is disrupted and cannot be expressed. Hence, the colonies stay white.

Previously, PCR products were purified using the QIAquick PCR Purification Kit (Qiagen) or were isolated from an agarose gel after gel electrophoresis using the QIAquick Gel Extraction Kit (Qiagen) according instructions. For this purpose, PCR products were supplemented with loading buffer and loaded on 1-2% agarose gels containing ethidium bromide. As a standard the 100 bp or 1 kb GeneRuler standard from Fermentas were applied. After the run in 1x TAE buffer at about 100 V for 30-60 min, the products were visualized on a UV desk at a wavelength of 366 nm and the correct bands were cut out with a scalpel.

Transformation of chemically competent bacteria

To transform plasmids of choice in bacteria, chemically competent *E. coli* DH5α were utilized. Therefore, an aliquot of 100 µl bacteria suspension was slowly thawed on ice. After pipetting 1-5 µl of plasmid to the bacterial suspension, the tube was flipped carefully for mixing and incubated on ice for 30 min. For permeabilization of the plasma membrane, bacteria were exposed to heat shock at 42°C for 30-60 sec and immediately put on ice. Then 250 µl SOC or 700 µl LB medium was added and bacteria were incubated at 37°C for approximately 1 h for recovering. Following centrifugation at 5000 rpm for 3 min, the pellet was resuspended in the return, plated on LB agar plates containing the appropriate antibiotic, and incubated overnight at 37°C.

Gateway® Cloning reaction

For the purposes of RMCE, the Gateway® Cloning System from Invitrogen was used to translocate the human *FUS* cDNA from the pENTR vectors into pDest vectors containing a hygromycin resistance. The following approach was pipetted:

1 μ l pENTR clone (100 ng/ μ l)

1 μ l destination vector (150 ng/ μ l)

6 μ l TE buffer, pH 8.0

LR Clonase™ II enzyme mix was thawed on ice, 2 μ l were applied, and the reaction mix was incubated overnight at 16°C. To stop the reaction, 1 μ l of Proteinase K solution was added. After incubation for 10 min at 37°C, 1 μ l was transformed into DH5 α cells as described above and selected on ampicillin plates (100 μ g/ml).

Preparation of plasmids

In order to purify and test plasmid DNA of transformed bacteria, the following protocol was used: single colonies were picked from the selection plates and were incubated in 5 ml LB medium containing the appropriate antibiotic over night at 37°C. The next day, 2 ml of the bacteria suspension were centrifuged at 10 000 rpm and the pellet was resuspended in 250 μ l P1 buffer taken from the Qiagen Plasmid MiniPrep Kit. 250 μ l of buffer P2 (also from the Kit) were added, the tube was carefully inverted till white flakes appeared, and incubated for 5 min at room temperature (RT). 350 μ l of P3 buffer (from the Kit) were subjoined, the tube was inverted again, and centrifuged at 13 000 rpm for 10 min. The supernatant was tipped into a new tube containing 600 μ l Isopropanol and centrifuged at 13 000 rpm for 15 min. The resulting pellet was washed with 70% ethanol, dried for 10-20 min, and solved in 20-100 μ l EB buffer (Qiagen Plasmid MiniPrep Kit).

For a higher yield plasmid preparation, 1 ml of the Miniprep culture was added to 250 ml LB medium with antibiotic, incubated overnight at 37°C, and the Qiagen Plasmid Maxi Kit was applied according to manufacturer's instructions.

Concentration of the purified DNA was determined with a spectrophotometer, measuring the optical density (OD) at a wavelength of 260 nm. $OD_{260} = 1$ corresponds to 50 μ g/ml of double stranded DNA. Purity of DNA was assessed by the relation of DNA/protein (OD_{260}/OD_{280}), which should not exceed a value of 1.8.

Restriction digest of plasmid DNA

To digest plasmid DNA, enzymes and buffers were used according manufacturer's instructions. In general, for 1 µg of DNA 1 unit (U) of restriction enzyme was applied and incubated at the appropriate temperature for minimum 1 h or overnight. To isolate digested DNA fragments according to their size, a gel electrophoresis and following gel extraction was performed as described above.

If blunt ends were required, Polymerase T4 or the Klenow fragment of Taq polymerase I were used. Together with NTPs the enzyme was added as recommended to the digested DNA and incubated for 15 or 30 min at 37°C. To stop the reaction the solution was heated to 70°C or 75°C for 10 or 20 min respectively.

For dephosphorylation to prevent religation of the digested DNA, 10 U of alkaline phosphatase (CIP) were added and incubated for 10 min at 37°C. To inactivate the enzyme the reaction was heated to 65°C for 10 min.

5.1.2 ANALYSIS OF GENOMIC DNA

Isolation of genomic DNA

In order to isolate genomic DNA from mouse tails, Wizard genomic DNA purification Kit (Promega) was used according manufacturer's instructions. For isolation from cells QIAamp DNA Blood Mini Kit (Qiagen) was applied following manufacturer's instructions.

For a 'quick and dirty' isolation, mouse tails were lysed at 55°C under shaking with fast digestion buffer and Proteinase K (0.1 mg/ml) for minimum 5 h or overnight. After lysis the reaction was inactivated through heating to 95°C for 10 min.

In each case, 1 µl of isolated DNA was utilized for PCR analysis.

Polymerase Chain Reaction (PCR)

To amplify DNA the following basic reaction batch for PCR analysis was applied:

10 μ l 5x MasterMix
 1 μ l forward primer (10 pmol)
 1 μ l reverse primer (10 pmol)
 1 μ l template DNA
 ad 20 μ l H₂O

... and the following basic amplification program was run:

94°C 5 min
 94°C 30 sec
 X °C 1 min
 72°C 1 min
 72°C 10 min
 10°C ∞

} x35

The specific annealing temperatures for each primer pair are listed in Materials, chapter 4.7.

For genotyping of TALEN mice, the following program was used:

94°C 5 min
 94°C 1 min
 59°C 1 min
 72°C 1.5 min
 72°C 10 min
 10°C ∞

} x30

Afterwards, the resulting PCR product of 576 bp was digested as described above with the following restriction enzymes:

TALEN mouse line	Enzyme	WT	Recombined
Fus ^{P511fs} , Fus ^{R513G}	BclI	121 + 455 bp	121 + 192 + 263 bp
Fus ^{P517L}	HaeIII	30+54+172+ 287 bp	30 + 33 +54 + 459 bp

For genotyping of *Tmem106b* SNPs the following program was run and PCR products were sequenced:

94°C 3 min

95°C 15 sec }
63°C 15 sec } x10
72°C 1 min }

95°C 15 sec }
53°C 15 sec } x25
72°C 1 min }

72°C 10 min

10°C ∞

Taqman Copy Number Assay

Genotyping of *Tmem106b*^{BACtg} mice was done by EUCOMM, group Hörlein. They used a FAM labelled TaqMan® Copy Number Assay (Mm00651778_cn; Life Technologies). *Tfrc* (TaqMan® Copy Number Reference Assay, Life Technologies) served as reference gene.

5.1.3 ANALYSIS OF RNA

Isolation of RNA

Prior to RNA isolation, material was treated with RNaseZap®. Mice were sacrificed with CO₂ and dissected. Required organs were immediately frozen on dry ice and stored at -80°C or immediately processed. For this purpose, tissues were homogenized in appropriate amounts of TRIzol® using an electric homogenizer and total RNA was isolated by the RNeasy® Mini Kit from Qiagen following manufacturer's instructions. Total RNA from cells was also gained applying RNeasy® Mini Kit. Therefore, cells were washed with PBS and scraped off from the dish in TRIzol®. RNA concentration was determined with the NanoDrop® ND-1000 UV/Vis spectral photometer from Peqlab. The underlying calculation is based on the principle of Lambert Beer that OD₂₆₀ = 1 corresponds to an RNA concentration of 40 µg/ml. The purity of isolated RNA was stated via the ratio of OD₂₆₀/OD₂₈₀, which should meet a value of about 2.0.

Reverse Transcription Polymerase Chain Reaction (RT-PCR)

For transcription of total RNA into complementary DNA (cDNA) the iScript™ Select cDNA Synthesis Kit from BioRad was used according instructions:

- x µl RNA (1 µg)
- 4 µl 5x iScript select reaction mix
- 2 µl oligo(dT)20 primer
- 1 µl iScript reverse transcriptase
- ad 20 µl nuclease-free H₂O

To perform reverse transcription the reaction was incubated at 42°C for 60 to 90 min, followed by 5 min inactivation of the reverse transcriptase at 85°C. cDNA was stored at -20°C. For RT-PCR analysis 1 µl of cDNA template was utilized following the scheme described above for genomic DNA.

Quantitative RT-PCR (qRT-PCR)

For purposes of qRT-PCR, RNA was transcribed into cDNA using the SuperScript® VILO cDNA Synthesis Kit from Life Technologies following instructions:

x μ l RNA template (1 μ g)
 4 μ l 5x Vilo™ Reaction Mix
 2 μ l 10x SuperScript® Enzyme Mix
 ad 20 μ l nuclease-free H₂O

The reaction batch was incubated at RT for 10 min and then at 42°C for 1 h. Afterwards, reverse transcriptase was inactivated via heating the reaction to 85°C for 5 min. cDNA was diluted to a concentration of 1 ng/ μ l and aliquots were stored at -20°C.

For quantitative analyses of gene expression levels, TaqMan® Gene Expression assays were purchased. The analysis was performed in triplets on 384 well plates and the following approach was applied for each well:

9 μ l cDNA
 10 μ l 2x TaqMan® Universal Master Mix
 1 μ l 20x TaqMan® Assay

The following program was run on a 7900HT Fast Real-Time PCR system with the SDS software v2.3 (Applied Biosystems):

95°C 10 min
 95°C 15 sec }
 60°C 1 min } x40

As an endogenous reference a TaqMan® Gene Expression assay for β -Actin was used.

Ct values of analyzed triplets (technical replicates) were averaged and “fold change” was assessed. Thereby, statistical calculation ($2^{-\Delta\Delta Ct}$) (Livak and Schmittgen, 2001) was done using Microsoft Office Excel (only one biological replicate/genotype) or the statistical program R (more biological replicates/genotype; programmed by Theresia Faus-Keßler). The log delta delta Ct values were compared between groups and fold changes were calculated by back-

transforming the differences. For more biological replicates per genotype Student's t-test was performed (since only two groups were elevated), 95% confidence intervals and p values were calculated and significance was assessed as follows:

- n.s. $p > 0.05$
- * $p \leq 0.05$
- ** $p \leq 0.01$
- *** $p \leq 0.001$

The number of animals used for the single experiments (n) is quoted below the respective figure or table in the results.

Whole Mount *in situ* hybridization (WISH)

In order to check BAC expression *in vivo*, WISH was performed following the protocol described before (Uez et al., 2008) without modifications. Analyzed were WT and transgenic *Tmem106b*^{BACtg} embryos at E12.5. The cDNA probe used for hybridization binds 7 kb downstream of the *Tmem106b* Stop codon and is depicted in Fig. 36A. Primers for the probe are listed in Materials, chapter 4.7.3.

5.1.4 ANALYSIS OF PROTEIN SAMPLES

Isolation of Protein

Mice were sacrificed with CO₂, required organs were extracted, immediately frozen on dry ice, and stored at -80°C or shortly processed. Therefore, tissues were homogenized in RIPA buffer containing protease (and phosphatase) inhibitor(s) (1 tablet/10 ml buffer) with an electric homogenizer, sonicated and centrifuged at 13 000 rpm for 30 min and 4°C. The supernatant was aliquoted and stored at -80°C. To assess protein concentration Pierce® BCA Protein Assay Kit (Thermo Scientific) was used according instructions. For measurements, every protein sample was diluted 1:10, 1:25 and 1:50 on a 96-well plate. The absorption was determined at a

wavelength of 562 nm. In Microsoft Office Excel the concentration of each protein sample was calculated based on the created standard curve.

For isolation of soluble and insoluble protein fractions, the ReadyPrep™ Protein Extraction Kit (Soluble/Insoluble) from BioRad was utilized following manufacturer's instructions. To measure protein concentration, RC DC™ Protein Assay was used as recommended. A 'per hand' method was also applied using the following protocol: homogenized tissues were centrifuged in an ultracentrifuge for 30 min at 50 000 rpm and 4°C. The supernatant was collected as soluble fraction and concentration was determined as described above. The resulting pellet was washed two times with RIPA buffer, sonicated and centrifuged again. The supernatants were collected as S1 and S2 fraction. The pellet from the second washing step was resuspended in Urea buffer, sonicated and centrifuged for 30 min at 12 000 rpm and RT. The resulting supernatant was collected as the insoluble protein fraction and stored at 4°C.

For detection of γ H₂AX, histones had to be isolated in an acid atmosphere. Therefore, the histone extraction protocol from Abcam was used. According this protocol, tissues were homogenized in TEB buffer containing protease inhibitor (1 tablet/10 ml) (no phosphatase inhibitor!), sonicated, and incubated on ice (without movement) for 10 min. After centrifugation for 10 min at 2000 rpm and 4°C the supernatant was discarded, the pellet was washed with TEB buffer, and finally solved in 0.2 M HCl. The histone extraction occurred overnight at 4°C.

Detection of Tmem106b, as well as mitochondrial and lysosomal proteins (Fig. 40, 43) was done by Julia Götzl (Institute of Metabolic Biochemistry, LMU/DZNE, Munich). Therefore, snap frozen brain tissue was pulverized, extracted with RIPA buffer freshly supplemented with protease inhibitor cocktail (Sigma-Aldrich) and phosphatase inhibitor (Roche Applied Science), and analyzed as previously described (Götzl et al., 2014). For quantification, blots were imaged with the LAS-4000 image reader from Fujifilm Life Science and quantified with the Multi-Gauge V3.0 software (Fujifilm Life Science). Graphs were made with GraphPad Prism 5.04 (GraphPad Software).

Western Blot analysis

Via Western Blotting, proteins were separated according to their size by Sodium Dodecyl Sulfate (SDS) Polyacrylamide Gel Electrophoresis (PAGE) (Laemmli, 1970). Therefore, the NuPAGE® Novex gel system and appropriate buffers from Invitrogen were used. 20 µg of total protein (0.5 µg of acid extracted histones) were mixed with 5x sample loading buffer (Invitrogen), heated to 95°C for 5 min, and immediately put on ice til gel loading. SDS-PAGE was performed in Running

buffer at 200 V for 60 min (35 min for histones). For blotting, a PDVF membrane was activated in pure methanol for 1 min prior to use. Blotting was performed in Transfer buffer at 30 V for 90 min (70 min for histones). After blocking of the membrane with 5% milk or BSA in TBS-T for about 1 h, binding of the specific primary antibody diluted in blocking solution was achieved overnight at 4°C. The next day, the membrane was washed three times for about 10 min with TBS-T and then incubated with the appropriate secondary antibody diluted in blocking solution for about 1 h. Following three washing steps with TBS-T the membrane was incubated for about 1 min with ECL reagents (Amersham). For detection, a chemiluminescent film (Amersham) was exposed to the membrane in a hyperfilm cassette for 15 sec to 20 min depending on the signal intensity and developed in the Curix 60 developing machine from Agfa. Quantification of the signal was done in dependence on the loading control using ImageJ and calculated with Microsoft Office Excel. As an endogenous control, β -Actin was used. For statistics see chapter 5.6.

Enzyme Linked Immunosorbent Assay (ELISA)

Mice were sacrificed with CO₂. Blood was taken by bleeding, incubated at RT for 1 to 2 h till it was curdled, centrifuged at 3000 rpm for 15 min, and stored at -80°C. ELISA was performed by Julia Götzl as described before (Capell et al., 2011).

5.2 CELL CULTURE

5.2.1 ES CELLS

The ES cell clone EUCE0290f05 (MGI:4382244) is a feeder independent E14Tg2A (E14) gene trap line and was produced for commercially purpose by the European Conditional Mouse Mutagenesis (EUCOMM) program. It was directly injected into mouse blastocysts to generate a *Fus* deficient mouse line and served as a basis for the generation of mouse lines, expressing ALS-associated mutations in the human *FUS* gene, via Recombinase Mediated Cassette Exchange (RMCE; see chapter 5.1.1, 5.2.5-5.2.8, 5.3.2, 5.3.3) (Schebelle et al., 2010). ES cells were grown on gelatin coated cell culture dishes at 37°C and 5% CO₂. Medium contents are listed in Material 4.12.2. To avoid differentiation, medium was supplemented with Leukemia inhibiting factor (LIF).

5.2.2 GENERATION OF FIBROBLASTS

Mouse embryonic fibroblasts (MEFs) were derived from E12.5 to E14.5 embryos. Therefore, embryos were decapitated and skinned. Heads were used for genotyping (see chapter 5.1.2) and organs were discarded. The skin was cut up small in 0.05% Trypsin/EDTA and incubated at 37°C and 5% CO₂ for 30 min. Afterwards, the pieces were centrifuged for 4 min at 1200 rpm, directly plated on big cell dishes, and grown at 37°C and 5% CO₂.

Fibroblasts from adult mice were derived from small pieces of the ear. Pieces were cut up small in fibroblast medium containing the triple amount of Pen/Strep and 1 mg/ml Collagenase and incubated overnight at 37°C and 5% CO₂. The next day, pieces were centrifuged at 1500 rpm for 7 min, plated on 24-well dishes, and grown at 37°C and 5% CO₂. After 24 h medium was carefully changed.

5.2.3 SPLITTING OF CELLS

ES cells were splitted every two days during expansion phase to avoid differentiation. Fibroblasts were splitted, when cells were dense. Therefore, medium was discarded, cells were washed with PBS, and trypsinized for about 5 min at 37°C. To inactivate the Trypsin an equal volume of medium was added, cells were centrifuged for 4 min at 1200 rpm, and plated on several culture dishes in an adequate ratio.

5.2.4 FREEZING AND THAWING OF CELLS

To freeze cells, the same procedure was applied like for splitting. After trypsination and centrifugation, the cell pellet was resuspended in freezing medium, transferred in 1 ml freezing vials, precooled in freezing containers, and frozen at -80°C for a few days to weeks. For long term storage, the vials were restored in liquid nitrogen. To freeze multi-well plates cells were trypsinized and freezing medium with the double amount of DMSO was added with a final ratio of 1:1. Plates were wrapped in cellulose and frozen at -80°C.

To replat cells, vials or plates were thawed in a water bath (37°C), fresh medium was added, and the suspension was centrifuged at 1200 rpm for 4 min. Cells were resuspended in medium and plated on appropriate dishes.

5.2.5 ELECTROPORATION OF ES CELLS

Within the scope of RMCE technique, pEx-Flp vectors carrying the human FUS cDNA had to be stably integrated into the murine genome. For this purpose, electroporation of mouse ES cells was applied, where short electric impulses lead to a permeabilization of the cell plasma membrane. Along with pEx-Flp vectors, a FlpO recombinase-expressing plasmid was co-electroporated (Schebelle et al., 2010).

Therefore, DNA had to be purified. 30 µg of FlpO-expressing plasmid or 70 µg of pEx-Flp vectors was each mixed with 3 volumes of 100% ethanol and 1/10 volume of NaAc. Hence, the DNA fell out and was incubated overnight at -20°C. The next day, DNA was centrifuged for 30-60 min at 14 000 rpm and 4°C, the resulting DNA pellet was washed with 70% ethanol, and dried under the cell culture hood. Finally, it was solved in 50 µl PBS each. The cells were trypsinized, centrifuged as described before, and the cell pellet was resuspended in PBS. To count the cells, a Neubauer counting chamber was used. After calculation, the volume that corresponds to the required number of 10^7 cells was centrifuged, cells were resuspended in 600 µl PBS, and mixed with the solved DNA in an electroporation cuvette. Following electroporation with 300 V and 500 µF for 2 ms and a recovery time of 10 min at RT, fresh medium was added and cells were plated to equal parts on 3 x 10 cm gelatin coated cell culture dishes. Cells were grown for two days at 37°C and 5% CO₂, with medium change after 24 h.

To excise the hygromycin cassette already in the cells, 15 µg of Cre recombinase-expressing plasmid (Caggs-CRE-IRES-Puro) was purified and electroporated in 3×10^5 cells following the same protocol.

5.2.6 SELECTION AND PICKING OF RESISTANT ES CELL CLONES

For selection of successfully transfected cell clones, medium was changed after two days with one containing 125 U/ml hygromycin or 1 µg/ml puromycin. Hygromycin selection was performed for 9 days with medium change every day, puromycin selection for 3 days followed by 10 days with normal medium. In this time, successfully transfected and thus resistant cells could form colonies which were picked at day 10 or 14 respectively. Therefore, medium was changed with PBS, single colonies were picked using a pipette, and transferred to a 96-well plate containing PBS/Trypsin (4:1). The plate was incubated at 37°C for 10 min. Then, the Trypsin was inactivated by adding fresh medium. Cells were resuspended and plated on gelatin coated 96-well plates. They were grown at 37°C and 5% CO₂ with medium change every two days and gradually expanded up to 10 cm dishes.

5.2.7 PCR SCREENING OF RESISTANT ES CELL CLONES

For screening of successfully transfected ES cells, picked and densely grown clones were washed twice with PBS and 50 µl lysis buffer (plus 1 mg/ml Proteinase K) was added directly to 48-well plates and incubated overnight at 50°C in a humid atmosphere. The next day, plates were centrifuged for 2 min at 2500 rpm. Afterwards, 100 µl precipitation solution per well were added and the plates were shaken for 30 min at RT. The precipitated DNA was washed three times with 70% ethanol, dried and finally solved in TE buffer.

5.2.8 KARYOTYPING OF ES CELL CLONES

Before injection in blastocysts, ES cells were karyotyped. Therefore, cells were treated with colcemid (0.2 µg/ml) for 1 h to depolymerize microtubules. Afterwards, cells were washed, trypsinized, and centrifuged. The pellet was resuspended in returned medium by flipping and a hypotonic solution (75 mM KCl in H₂O) was added drop wise for 10 min. Following centrifugation at 900 rpm for 10 min, the pellet was resuspended again in the return by flipping

and 15 ml fixation solution (methanol/acetic acid 3:1) were added. After incubation for 30 min at -20°C and a second centrifugation the pellet was solved in 1 ml fixation solution, dropped on a water-covered object slide, and dried overnight. The slides were embedded with DAPI staining solution (0.2 µg/ml in PBS) and chromosomes of about 20 cells were counted at an inverted fluorescent microscope (Axiovert 200M, Zeiss).

5.2.9 IMMUNOFLUORESCENCE

To stain cells for specific proteins, immunofluorescence was performed. Therefore, cells were plated on 8-well ibidi slides. When cells were dense, they were washed twice with PBS and fixed for 20 min with 4% paraformaldehyde (PFA). After two washing steps with PBS, cells were blocked for 1 h at RT with Blocking Solution containing 10% FCS and 0.5% Triton X 100 in PBS. The specific primary antibody was diluted in Blocking Solution and incubated overnight at 4°C. The next day, cells were washed twice with PBS and incubated with the secondary antibody diluted in Blocking Solution for 1 h at RT and in the dark. Following two washing steps with PBS, nuclei were stained blue with DAPI (2 µg/ml), cells were washed again twice with PBS and stored in PBS. Staining was examined at an inverted fluorescent microscope (Axiovert 200M, Zeiss).

For quantification of FUS localization, 100 cells per genotype were counted and absolute percentages of different localization patterns were calculated.

5.2.10 SEAHORSE MITO STRESS TEST

To measure mitochondrial respiration of Tmem106b overexpressing mouse lines, a Seahorse Mito Stress Test was performed. Therefore, MEFs were derived from embryos as described above, brought to the Institute of Metabolic Biochemistry at the LMU/DZNE in Munich, and analyzed by Nicole Exner. The analysis was done using the Mito Stress Test Kit and the XF96 Extracellular Flux Analyzer, both from Seahorse Bioscience, according to manufacturer's

instructions. The results of three independent measurements were evaluated by the program “Seahorse Wave”. Error bars represent standard deviation.

5.3 MOUSE HUSBANDRY

5.3.1 GENERATION OF MICE

Generation of mice from ES cells

Within the scope of RMCE, successfully transfected and karyotyped ES cells were injected into blastocysts. For this purpose, cells were trypsinized and centrifuged as described before, solved in 1.5 ml medium, and stored on ice till injection.

The injection was done by the injection team of the Institute of Developmental Genetics (IDG). For the production of blastocysts (E3.5) female mice (C57Bl6/N or BALB/c) were superovulated. Therefore, females were injected intraperitoneal with 7.5 U Pregnant Mare’s Serum Gonadotropin (PMSG), 48 h later with Human Chorion Gonadotropin (HCG), and then immediately mated. Both injections were performed at noon. The next day, matings were separated, plaque was checked, and positive females were sacrificed 3 days post coitum. Blastocysts were dissected from the uteri, flushed with M2 medium, individually fixed with a capillary of the micromanipulator, and 10-20 ES cells were injected into the blastocoel with a second capillary. Up to 10 manipulated blastocysts were transferred into the uterus of a pseudo-pregnant foster mother using a thin cannula. Therefore, CD-1 female mice were mated to sterile, vasectomized males. For the transfer, foster mothers were anesthetized according to their weight and afterwards kept on warming plates until awakening.

Generation of TALEN mice

TALEN mice were generated by the group of Ralph Kühn (Panda et al., 2013).

Generation of *Tmem106b*^{BACtg} mice

For generation of *Tmem106b*^{BACtg} mice the 129S7AB2.2 bacterial artificial chromosome (BAC) clone bMQ263o13 (Source BioScience LifeSciences) was grown as recommended and the plasmid was purified following the Large-Construct Kit protocol (Qiagen). The plasmid was linearized in the backbone using the enzyme BsiWI, solved in BAC injection buffer, and transgenic animals were then generated via pronuclear injection at the Max-Planck-Institute in Dresden as previously described (Vintersten et al., 2008).

5.3.2 ESTABLISHMENT OF NEW MOUSE LINES

Concerning FUS mouse models, pups were born 17 days after the embryo transfer. Chimeras derived from E14 ES cells showed white/agouti fur color. Chimeras are genetically divergent mice, consisting of cells derived from the wildtype blastocysts and to some extent of cells derived from the injected ES cells. The more the contribution of the ES cells, the merrier the fur color of the chimeras. With an age of 8 weeks chimeras were mated to wildtype C57Bl/6J mice. Germline chimeras transmit the genetically modified information of the ES cells to the next generation and produce offsprings consisting to 100% of the mutant cells (germline transmission).

Tmem106b^{BACtg} mice were generated at the Max-Planck-Institute in Dresden and transferred to the quarantine of the Helmholtz Center Munich. There, they were bred a short time and then implanted into the 'C-Streifen' by the injection and mouse team via *in vitro* fertilization.

5.3.3 MOUSE FACILITIES

All mouse models were bred and kept in the 'C-Streifen' of the Helmholtz Center Munich according to national guidelines. As standard, five mice at maximum were grouped in individually ventilated cages (IVC) on a 12 h dark/night cycle and $22 \pm 2^\circ\text{C}$ (relative humidity of $55 \pm 5\%$). Water and food were available *ad libitum*. Pups were weaned at the age of 3 weeks

according to their gender and genotyped by DNA isolation from tail clips. Earmarks were made for identification.

5.4 HISTOLOGY

5.4.1 IMMUNOHISTOCHEMISTRY OF MOUSE TISSUE

Perfusion and dissection

In order to analyze mouse models on cellular level, immunohistochemistry was performed. Therefore, mice were asphyxiated with CO₂, fixed with their paws onto a polystyrene board, and the thorax was opened. The tip of the left heart ventricle was cut and a blunt needle was inserted in the ascending aorta. Blood vessels were rinsed with ice-cold PBS using a perfusion pump. When the liver turned pale PBS was replaced by ice-cold 4% formaldehyde (FA) for about 5 min until the body stiffened. Required organs (mainly brain) were removed and postfixed overnight in 4% FA and at 4°C. Concerning the spinal cord the whole spinal column was dissected, fixed in 4% FA overnight, and prepared the next day.

Dehydration and paraffin embedding

After one day postfixation organs were transferred in 70% ethanol until further progression. Dehydration in an ascending ethanol scale, equilibration and embedding in paraffin was performed as follows:

Reagents	Temperature	Time	
		Brain	SC
4% FA	4°C	overnight	
70 % ethanol	4°C	overnight	
96% ethanol	RT	2 h	30 min
100% ethanol	RT	2 h	30 min

Xylol	RT	1-2 h	30min
Xylol/paraffin	65°C	1 h	30 min
paraffin	65°C	overnight	

After equilibration in paraffin, tissues were embedded in tissue cassettes and stored at 4°C.

For sectioning, paraffin blocks were fixed at a microtome and cut in 8 µm thick sections. Sections were flattened in a 39°C water bath, mounted on slides, dried in an incubator overnight at 36°C, and stored at 4°C until staining.

Nissl- staining

For a cellular overview tissue sections were stained the Nissl reagent cresyl violet. Staining was performed according to the following protocol:

Step	Reagents	Time
Dewaxing	Xylol	30-45 min
Rehydration	100% ethanol	1 min, raising the slide up and down
Rehydration	96% ethanol	1 min, raising the slide up and down
Rehydration	70% ethanol	1 min, raising the slide up and down
Staining	Cresyl violet	30 min
Rinse	H ₂ O	1 min
Differentiation	70% ethanol	2 x 10 sec
Differentiation	96% ethanol + 0.5% acetic acid	5 sec
Dehydration	96% ethanol	2 x 10 sec
Dehydraton	100% ethanol	2 x 10 sec

Embedding	Xylol	2 x 5 min
-----------	-------	-----------

Slides were covered immediately with pertex and dried overnight at room temperature.

Immunohistochemistry

To analyze the expression of specific proteins, tissue sections were stained with 3-3'Diaminobenzidine (DAB) or a fluorescence-coupled secondary antibody was used. The staining was performed according to the following protocol:

Step	Reagent/Solution	Time	Remarks
1. Dewaxing	Xylol	30-45 min	
2. Rehydration	100% ethanol	1 min, raising the slide up and down	Until no shrouds are visible any more
3. Rehydration	96% ethanol	1 min, raising the slide up and down	Until no shrouds are visible any more
4. Rehydration	80% ethanol	1 min, raising the slide up and down	Until no shrouds are visible any more
5. Rehydration	70% ethanol	1 min, raising the slide up and down	Until no shrouds are visible any more
6. Rehydration	60% ethanol	1 min, raising the slide up and down	Until no shrouds are visible any more
7. Rehydration	30% ethanol	1 min, raising the slide up and down	Until no shrouds are visible any more
8. Rinse	VE-H ₂ O	2 min	
9. Antigen-retrieval	EDTA-T	Heat in microwave until cooking (3x)	1 min cool down in between
10. Antigen-retrieval	EDTA-T	10-60 min	Cool down

11. Wash	PBS-T	2 min	
12. Blocking	PBS-T + goat serum (200 ml + 6 ml)	1 h	
13. 1 st antibody	Primary antibody in Antibody Dilution Buffer	overnight	4°C, humid chamber
14. Wash	PBS-T	2 min	
15. 2 nd antibody	Secondary antibody in Antibody Dilution Buffer	1 h	RT, humid chamber
16. Wash	TBS-T	2 min	
17. Intensify	Streptavidin-peroxidase solution	30 min	RT, direct on slides till they are covered
18. Tipping of streptavidin- peroxidase solution			
19. DAB-staining	200 µl DAB- solution/slide	Till tissue turns brown	Humid chamber, dark
20. Wash	H ₂ O	2 min	Stop staining
21. Wash	VE-H ₂ O	2 min	
22. Nuclei staining	Hematoxylin	5 min	
23. Wash	Cold VE-H ₂ O	2 min	
24. Dehydration	70% ethanol	1 min, raising the slide up and down	Until no shrouds are visible any more
25. Dehydration	96% ethanol	1 min, raising the slide up and down	Until no shrouds are visible any more
26. Dehydration	100% ethanol	1 min, raising the slide up and down	Until no shrouds are visible any more

27. Embedding	Xylol	5 min	
---------------	-------	-------	--

Slides were immediately covered with pertex and dried overnight under the flow.

For stainings with mouse primary antibodies the protocol was modified as follows:

Step	Reagent/Solution	Time	Remarks
11.	PBS/Formic acid (1:2.3)	20 min	Pipet directly on slides
12. Stop	VE-H ₂ O	2 min	
13. Quenching	1% H ₂ O ₂ -solution	30 min	
14. Stop	VE-H ₂ O	2 min	
15. Wash	1x PBS	2 min	
16. Blocking	Mouse IgG Blocking Reagent (M.O.M. [™] Kit) in PBS	1 h	RT
17. 1 st antibody	Antibody diluted in protein concentrate (M.O.M. [™] Kit) + PBS	overnight	4°C, humid chamber
18. Wash	PBS-T	2 min	
19. 2 nd antibody	Antibody diluted in protein concentrate (M.O.M. [™] Kit) + PBS	1 h	RT, humid chamber
20. Wash	TBS-T	2 min	
21.			Continue with the normal protocol

For immunofluorescence using fluorescence-coupled secondary antibodies, the DAB protocol was stopped after step 17. Incubation with the 2nd antibody was performed in the dark. Afterwards slides were washed with PBS, covered with aqua polymount, and dried in the dark.

5.4.2 MOTOR NEURON STAINING

For motor neuron counting, mice were sacrificed and perfused as described before. The throat was opened with a scalpel and the spinal column was cut at vortex C2. Spinal cords were postfixed with 4% FA overnight at 4°C. The next day they were transferred to 30% sucrose for dehydration until sinking (usually overnight). Afterwards spinal cords were prepared, frozen in embedding blocks in 30% sucrose on dry ice, and stored at -20°C or immediately cut. Therefore, spinal cords were blocked on a pre-cooled microtome (with dry ice), cut in 40 µm sections till vortex T5, and transferred to 96-well plates containing 30% sucrose. Concerning homozygous Fus GT survivors, the lumbar part was sliced. The plates were frozen at -20°C or immediately processed. Every third section was washed in PBS and pulled on a slide. Sections were dried for 10 min, fixed in 4% PFA for 5 min, and washed 3 times for 5 min each with PBS. After blocking in PBS-T containing 10% horse serum, sections were incubated with the primary antibody Hsp27, diluted in Blocking Solution, for 48 h at 4°C and in a humid chamber. Following 3 washing steps with PBS-T for 5 min each, sections were incubated with the specific secondary fluorescence-coupled antibody, diluted in Blocking Solution, overnight at 4°C in a humid and dark chamber. The next day, sections were washed 3 times with PBS for 5 min each and in the dark, mounted with Mowiol, and dried in the dark. Motor neurons were counted at an inverted fluorescent microscope (Axiovert 200M, Zeiss) and the mean number per section was calculated.

5.4.3 TRANSMISSION ELECTRON MICROSCOPY (TEM)

For TEM analysis, mice were sacrificed and perfused as described before. Instead of 4% FA, a solution of 2.5% and 2.5% glutaraldehyde in PBS was used. Mice were decapitated, brains were prepared, and single brain areas (frontal cortex and cerebellum) were sliced in 1 mm x 1 mm x 1mm big cubes using a razor blade. These cubes were transferred to 2 mm tubes containing 1.5

ml Sodium Cacodylate Buffer (0.1 M) with 2.5% glutaraldehyde (pH 7.4) and incubated overnight at 4°C. Further, TEM was performed by Michaela Aichler from the Institute of Pathology at the Helmholtz Center Munich.

5.5 GERMAN MOUSE CLINIC (GMC)

All behavioral tests were done in the German Mouse Clinic (GMC) of the Helmholtz Center Munich and planned by Lillian Garrett and Lore Becker. Animals were housed in individually-ventilated cages in a temperature (22-24°C) and humidity (50-60%) controlled environment on a 12/12h light/dark cycle (lights on at 7 am). Water and food were available *ad libitum*. All animal testing procedures were executed during the light phase of the cycle and approved by the German animal welfare authorities (Regierungspräsidium Bayern) and in accordance with the Council of European Communities Directive of the 24th November 1986 (86/609/EEC).

Mice were challenged to evaluate basic neurological and motor functions. Cohorts of mice were transferred to the GMC at the age of about 6 months. Tests were performed after a habituation of 2 weeks according to standardized protocols (partially available as EMPReSSslim protocols, see www.eumodic.org) (Carter et al., 2001; Wall et al., 2003; Stanley et al., 2005; Mandillo et al., 2008; Feil et al., 2009). For the Inverted Grid, mice were put on a grid (cage lid) at a height of 40 cm above a soft surface and made attach to the grip by short shaking. Then the grid was inverted upside-down, and the time until they fell down was recorded (mean of three consecutive trials). Statistical analysis was performed using a linear regression model including body mass, since differences in body mass may confound grip force.

5.6 STATISTICS

The number of animals used for the single experiments (n) is quoted below the respective figure or table in the results. In each case standard deviation (S.D.) was determined.

Statistical analysis of two groups was performed by unpaired and two-tailed Student's t-test. Statistical comparison of three or more groups was done by one-way Analysis of Variance (ANOVA; GraphPad Prism). Post hoc analysis for correction of multiple testing after ANOVA calculation was performed applying Dunnett's multiple comparisons test, since every mean was compared to a control mean (WT). Significance was assumed as follows:

n.s. $p > 0.05$

* $p \leq 0.05$

** $p \leq 0.01$

*** $p \leq 0.001$

**** $p \leq 0.0001$

Concerning behavioral tests, data were either reported as mean + standard error of the mean (S.E.M) in bar or line graphs or individually shown in scatterplots with a horizontal line indicating the mean. Sex effects were tested for and since there was no influence, sexes were pooled. Data were statistically analyzed by one-way or two-way ANOVA (considering also the gender besides the genotype) with Bonferroni posthoc tests or by unpaired Student's t-tests. The chosen level of significance was $p < 0.05$. Statistical analysis for the inverted grid test was performed using a linear regression model including body mass as a covariate, since differences in body mass may confound grip force.

For detailed statistical analysis of qRT-PCR see chapter 5.1.3.

6 RESULTS

6.1 *FUS* MOUSE MODELS

In order to gain new insights into the pathomechanism of ALS, different mouse models were generated, expressing ALS-associated *FUS* mutations or lacking *Fus*.

6.1.1 *MOUSE MODEL LACKING FUS*

6.1.1.1 Generation of *Fus* deficient mice

For generation of *Fus* deficient mice, the validated EUCOMM (European Conditional Mouse Mutagenesis) gene trap E14TG2A (E14) embryonic stem (ES) cell clone EUCE0290f05 (MGI:4382244), containing a β geo (β -galactosidase/neomycinphosphotransferase) cassette in intron 1 of the murine *Fus* gene (Fig. 5A, B), was injected into Balb-c blastocysts (IDG3.2) and transferred into the uteri of pseudo-pregnant CD-1 foster mice. Out of three injections, five pups and one male chimera was born (6.7% of pups/injection). For germline transmission, this mouse was bred with C57Bl6/J females.

Arising pups were genotyped by a triple PCR with one reverse (rv) primer in exon 2 of the *Fus* gene (EUCE_rv) and two distinct forward (fw) primers for the endogenous (EUCE_fw WT) and the transgenic (TG) *Fus* allele (EUCE_fw1) (Fig. 5A). The WT *Fus* allele yielded a product of 651 bp, whereas the TG band had a product size of 837 bp. This PCR was also used for further routine genotyping as shown exemplarily on a litter at embryonic day 11.5 (E11.5) (Fig. 5D). Embryos with the number 2, 4, and 7 were WT, #1 and 5 were heterozygous, and #3 homozygous. #6 was not clear and had to be repeated.

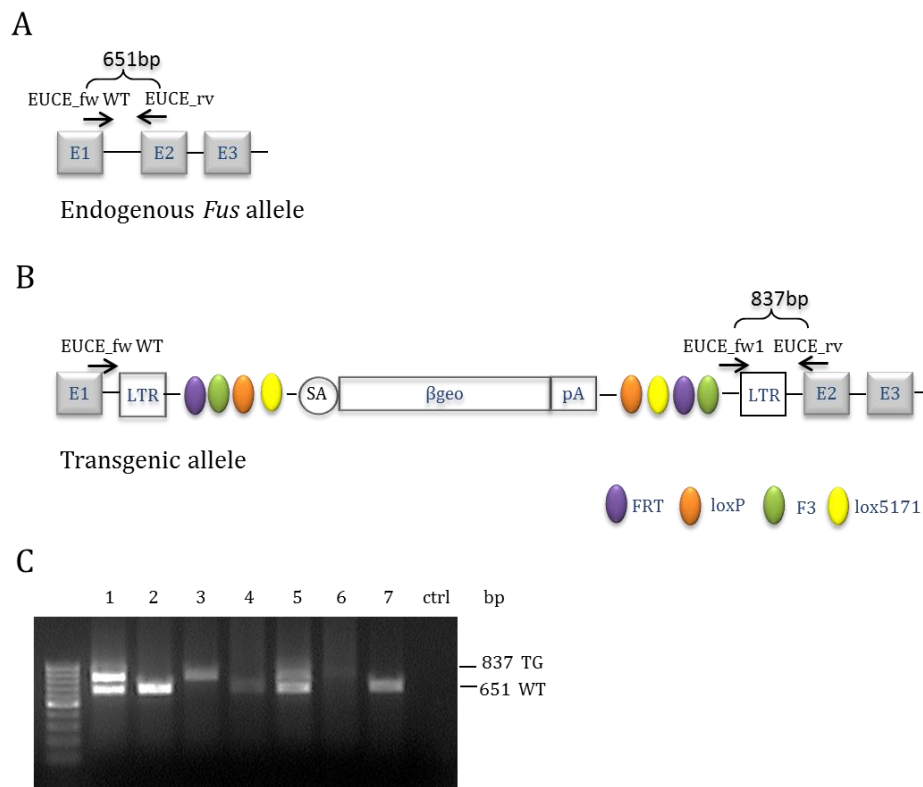


Fig. 5: Illustration and genotyping of the EUCE0290f05 gene trap mice alleles. (A) The endogenous *Fus* allele with primers for genotyping. (B) Concerning the transgenic allele, a gene trap β geo cassette was inserted into the first intron of the murine *Fus* locus. Genotyping primers with corresponding product sizes are depicted. With the recombination sites FRT, loxP, F3, and lox5171 the E14 ES cell clone could be used for possible Flp and Cre recombinations. (C) Genotyping of *Fus* deficient mice by taking the example of E11.5 embryos. The transgenic allele yields a product of 837 bp, the WT allele of 651 bp. Hence, #2, 4, and 7 are WT, #1 and 5 heterozygous for the TG allele, and #3 homozygous. Ladder: Fermentas GeneRuler 100 bp; E, exon; SA, slice acceptor; pA, polyadenylation site;

6.1.1.2 Lethality of *Fus*^{-/-} mice

Presuming Mendelian inheritance, matings of heterozygous *Fus* deficient mice should give an allocation of 25% WT and homozygotes (hom) respectively, and 50% heterozygotes (het). However, genotyping of 181 mice at weaning age yielded a proportional distribution of 36.5% WT, 59.7% het and 3.9% hom, indicating a strongly reduced viability of *Fus*^{-/-} mice (Tab. 4).

To determine the starting point of enhanced lethality, three litters between embryonic day (E) 11.5 (Fig. 5C) and 13.5 were dissected and genotyped. Among 19 embryos, 21.0% were WT, 52.6% het and 26.3% hom (Tab. 4), correlating with Mendelian inheritance. Together with seven adult survivors, this points towards a perinatal lethality of homozygous deficient *Fus* mice.

Tab. 4: Lethality of *Fus*^{-/-} mice.

	WT	<i>Fus</i> ^{+/-}	<i>Fus</i> ^{-/-}	total
embryonic	4	10	5	19
	21.0%	52.6%	26.3%	
adult	66	108	7	181
	36.5%	59.7%	3.9%	

6.1.1.3 *Fus* expression levels *in vivo*

To analyze remaining *Fus* expression levels in *Fus* gene trap (GT) mice, quantitative real-time PCRs (qRT-PCRs) and Western Blots were performed on embryonic and adult tissues (Fig. 6) (see also Bachelor thesis of Loulou Peisl).

For measurement of *Fus* mRNA levels, embryos of het x het matings were sacrificed at E13.5 and mouse embryonic fibroblasts (MEFs) were generated. Subsequently, RNA was isolated, transcribed into cDNA and qRT-PCR was done with a Gene Expression Assay spanning exons 1 and 2 of murine *Fus*. Comparison of WT and GT MEFs revealed a decrease of *Fus* mRNA levels to 56% in heterozygous and 0.06% in homozygous cells (Fig. 6A; Loulou Peisl), indicating that the gene trap is leaky. This could be caused by an alternative splicing around the gene trap cassette, for example. To follow this up, total protein was gained from a litter of E11.5 embryos for detection of *Fus* by Western Blotting. On protein level, heterozygous embryos showed a remaining *Fus* expression of 87% compared to WT and homozygotes of 11% (Fig. 6B), suggesting that *Fus* levels are regulated post-transcriptionally.

To answer the question of *Fus* expression levels in adult mice, brain samples of about three months old mice were used for qRT-PCR (Fig. 6C; Loulou Peisl) and Western Blot (Fig. 6D) analysis. Heterozygous GT mice displayed a reduction of 46% of *Fus* mRNA and 40% of *Fus* protein, supporting a possible regulation on protein level. Additionally, these results indicate that embryos can somehow compensate the depletion of *Fus* on protein level, since for heterozygous embryos remaining *Fus* levels of 87% were observed compared to WT littermates, whereas for adults this was only 60%. This could be the reason why homozygotes survive embryogenesis.

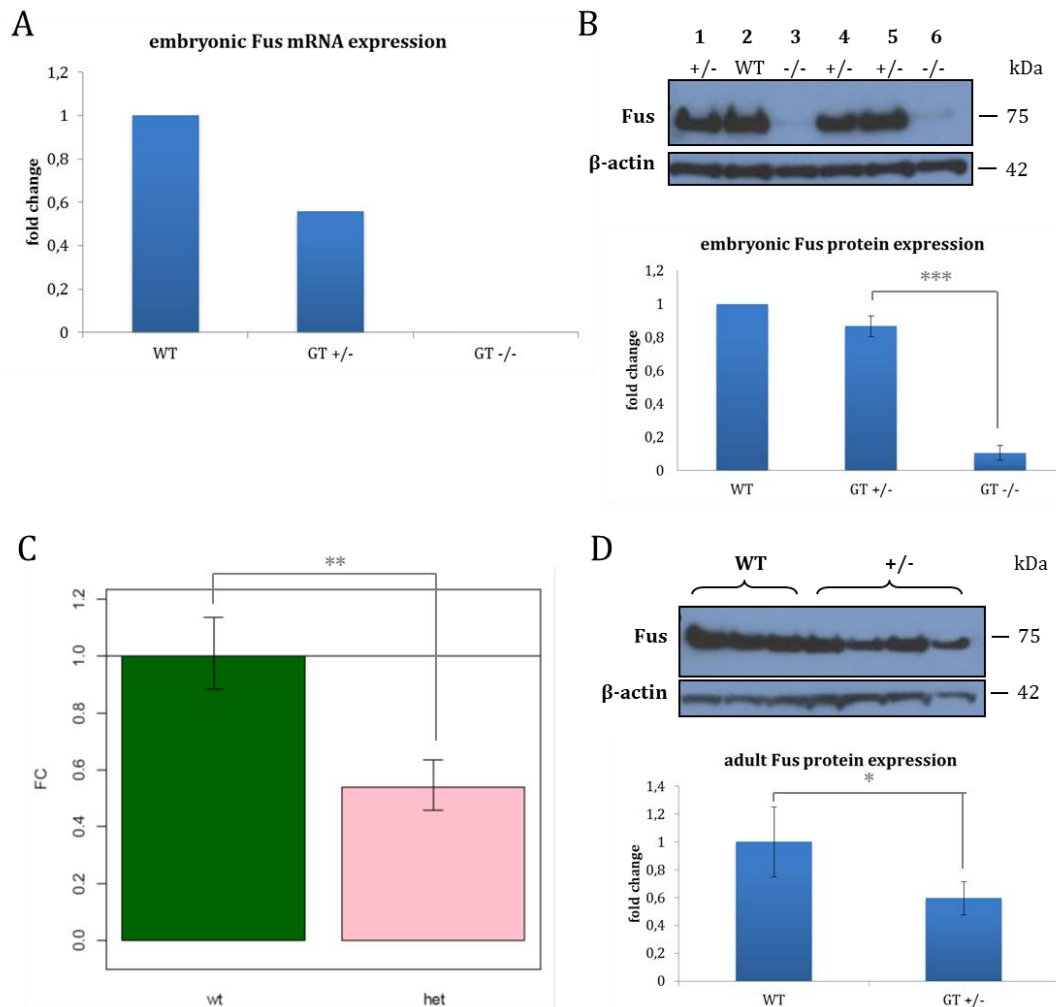


Fig. 6: Embryonic and adult expression levels of *Fus*. (A) qRT-PCR of MEFs from GT E13.5 embryos yielded a reduction of *Fus* mRNA levels to 56% in heterozygous and 0.06% in homozygous cells. A mixture of genotype specific cells was used. Thus, no standard deviation could be assessed. Experiment by Loulou Peisl. (B) Quantification of Western Blot from a litter of E11.5 embryos revealed decreased levels to 87% and 11% respectively. (Error bars represent S.D... Student's t-test was performed between hetero- and homozygous embryos, since only one WT was available in this litter. n(WT)=1; n(GT^{+/-})=3; n(GT^{-/-})=2; p=0.0007; β -actin served as loading control for quantification.) (C) In three months old mice, qRT-PCR of brain samples showed remaining *Fus* expression of 54% on mRNA level. (Delta-delta-Ct with 95% confidence intervals was performed. n(WT)=2; n(het)=3; p=0,0012;) FC, fold change; Graph by Loulou Peisl. (D) On protein level, *Fus* is reduced to 60% in brain lysates of adult GT compared to WT mice. (Error bars represent S.D.. Student's t-test was performed. n(WT)=3; n(GT^{+/-})=4; p=0.03; β -actin served as loading control for quantification.)

6.1.1.4 Pathological analysis of *Fus* GT mice

In order to analyze the effects of diminished *Fus* levels *in vivo*, protein levels of splicing targets, autophagy marker, and marker for astrogliosis and DNA damage were determined via Western

Blot from brain lysates of three months old heterozygous GT mice and compared to WT littermates.

It was reported, that Fus usually becomes arginine methylated by PRMT1 and that the methylation status is important for the development of ALS (Dormann et al., 2012; Tradewell et al., 2012; Yamaguchi and Kitajo, 2012; Scaramuzzino et al., 2013). To determine, whether depletion of Fus influences methylation, Western Blot was performed with an antibody recognizing methylated Fus (MeFus) (Dormann et al., 2012) and MeFus/Fus ratios were calculated. However, low levels of Fus appeared to have no effect on its methylation status (Fig. 7A, B), though PRMT1 was significantly reduced to about 58% (Fig. 7A, C), indicating that PRMT1 expression is regulated by Fus.

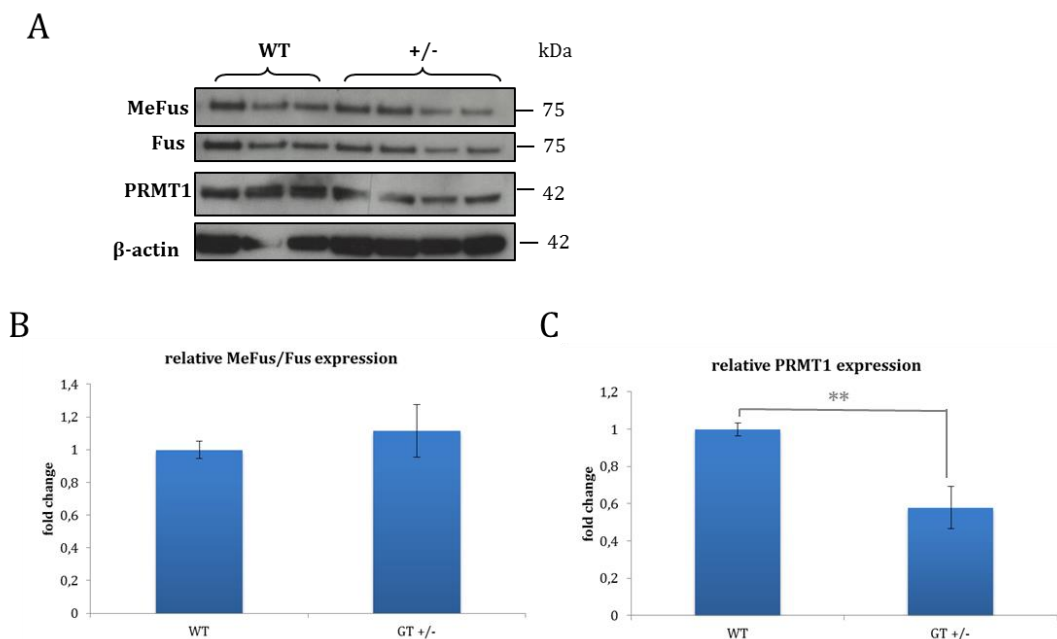


Fig. 7: Fus depletion did not change its methylation status. (A) Western Blots from brain lysates of about three months old heterozygous GT mice and WT littermates. Used antibodies are indicated. β -actin served as loading control for quantification. (B, C) Quantification of (A); Error bars represent S.D.. Student's t-test was performed. $n(\text{WT})=3$; $n(\text{GT}^{+/-})=4$; (B) No changes could be detected in Fus methylation. (C) Levels of PRMT1 were significantly reduced. For quantification, the second WT was excluded due to a bleb on the loading control. $p=0.009$;

Orozco and colleagues showed that *in vitro* a knockdown of FUS resulted in an increase of 4R tau and disturbed cytoskeletal function (Orozco et al., 2012). *In vivo*, however, this could not be confirmed on mRNA (Bachelor thesis of Loulou Peisl) nor on protein level, as Western Blotting with two antibodies distinguishing between the two tau isoforms revealed. 4R tau protein was not changed, whereas hints for an increase of 3R tau were found but nothing significant (Fig. 8A,

C, D). The group around Lagier-Tourenne also identified splicing targets of FUS, among others also tau, and reported about targets, where splicing was changed due to depletion of FUS (Lagier-Tourenne et al., 2012). For this reason, RNA was purified from adult GT brains, transcribed into cDNA, and rtPCRs were performed with primers used in the publication. Primers for tau did not work in mouse brain tissue. For other splicing targets, no significant outcome was observed, but tendentially, results for exon inclusion or exclusion could be confirmed for *Ptk2b*, *hnRNP-D*, *Ndr2* and *Tia1* (Supplementary Data, chapter 9.3.3.3). In terms of *Sort1*, more exclusion of exon 18 could be detected due to less *Fus* in contrast to the findings in the publication (Supplementary Data, chapter 9.3.3.3). There they found only TDP-43 dependent changes (Lagier-Tourenne et al., 2012). *Bdnf* is another splicing target of FUS and important for dendritic growth and synapse formation (Qiu et al., 2014). Nevertheless, no changes could be detected on protein level (Fig. 8A, B).

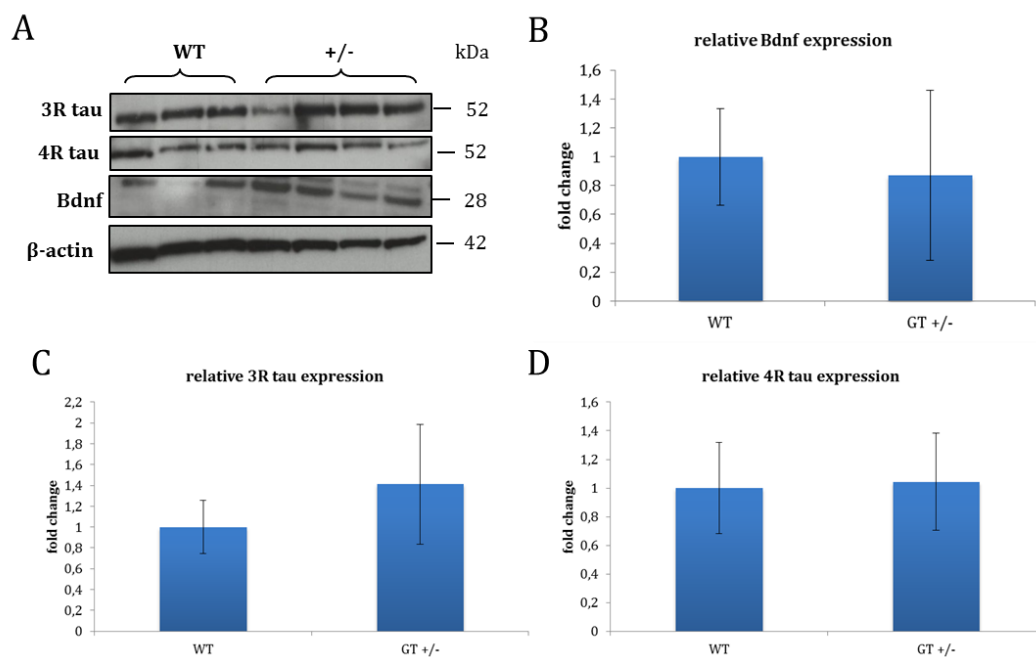


Fig. 8: Splicing targets were not changed on protein level upon depletion of Fus. (A) Western Blots from brain lysates of about three months old heterozygous GT mice and WT littermates. Used antibodies are indicated. β -actin served as loading control for quantification. (B-D) Quantification of (A); Error bars represent S.D.. Student's t-test was performed. $n(\text{WT})=3$; $n(\text{GT}^{+/-})=4$; (B) A high variation could be detected concerning *Bdnf* protein levels, but no significant change upon *Fus* depletion. For quantification, the second WT band was not included due to a bleb. (C, D) Depletion of *Fus* did not alter splicing of tau, though there was a tendency towards more 3R tau (C).

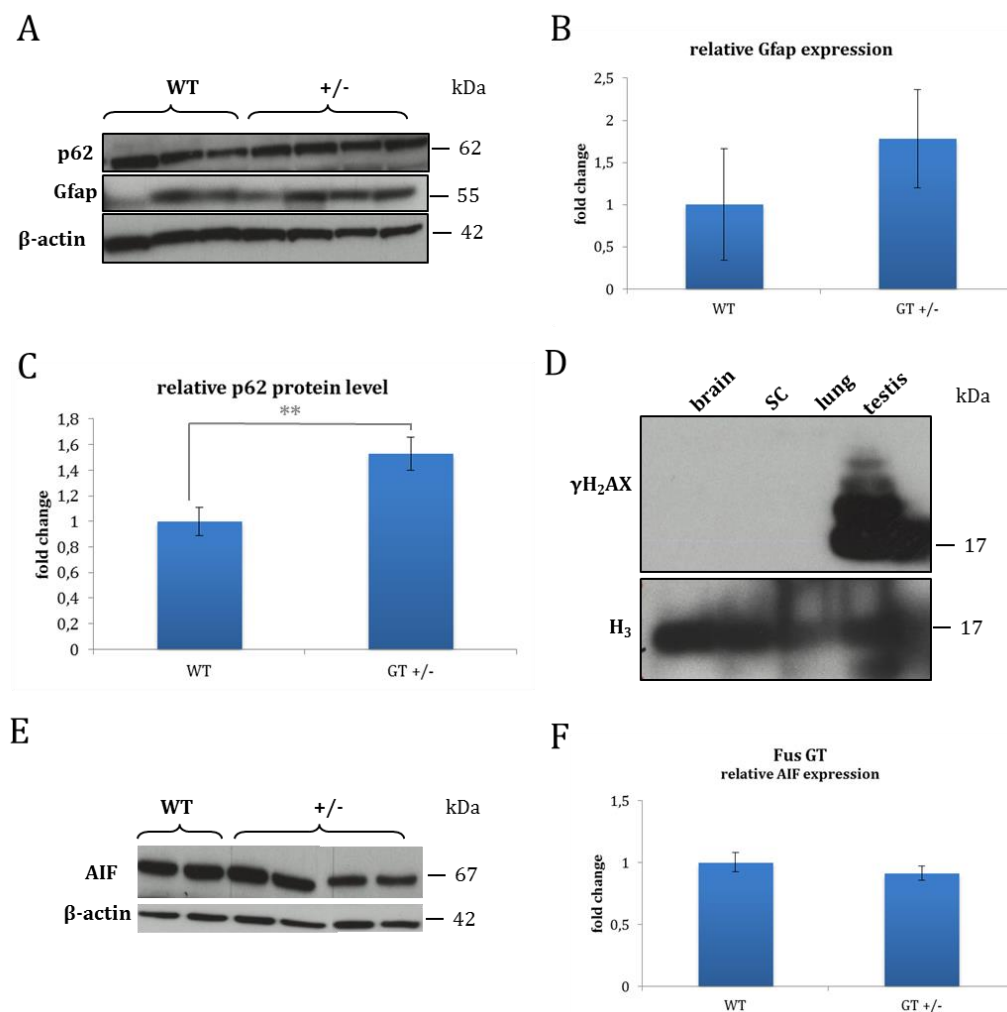


Fig. 9: No DNA damage or neuroinflammation, but enhanced p62 upon depletion of Fus. (A) Western Blots from brain lysates of about three months old heterozygous GT mice and WT littermates. Used antibodies are indicated. β -actin served as loading control for quantification. (B, C) Quantification of (A); Error bars represent S.D.. Student's t-test was performed. $n(\text{WT})=3$; $n(\text{GT}^{+/-})=4$. (B) Gfap levels were not significantly changed. (C) However, levels of autophagy marker p62 were significantly elevated in Fus GT mice to 152%. $p=0.002$; (D) Western Blot from brain, spinal cord, and lung lysates of a three months old heterozygous mouse for γ H₂AX could not detect elevated levels of the DNA damage marker. Testis was used as a positive control and H₃ as loading control. (E) Western Blots from brain lysates of about three months old heterozygous GT mice and WT littermates. Used antibodies are indicated. β -actin served as loading control for quantification. (F) Quantification of (A); No significant change of AIF levels could be observed. (Error bars represent S.D.. Student's t-test was performed. $n(\text{WT})=2$; $n(\text{GT}^{+/-})=4$.)

Additionally, marker for neuroinflammation, autophagy, apoptosis, and DNA damage were applied. Gfap, a marker for astrogliosis, was tendentially elevated but again not significant (Fig. 9A, B). AIF, apoptosis inducing factor in neurons, was unchanged in brain lysates (Fig. 9E, F). These results indicate that there is no neuroinflammation and apoptosis in the nervous system of heterozygous GT mice. P62, which was also observed in AD, PD, and HD (Zatloukal et al., 2002; Kuusisto et al., 2008), was not changed on the first look. However, Western Blots were standardly quantified in relation to the loading control β -actin, which shows that less protein was loaded in the GT traces. Since β -actin was not changed on other blots, it is no target of Fus.

Quantification yielded significant higher p62 levels in GT mice compared to WT littermates (Fig. 9A, C). Accumulation of p62 is caused by lack of autophagy and leads to induction of cellular stress response (Rusten and Stenmark, 2010). Fus is also involved in DNA damage response and a loss of Fus resulted in reduction of DNA repair and chromosomal instability (Baechtold et al., 1999; Bertrand et al., 1999; Hicks et al., 2000; Mastrocola et al., 2013; Wang et al., 2013; Qiu et al., 2014; Rulten et al., 2014). Therefore, heterozygous GT mice were tested for an enhanced expression of γ H₂AX, a marker for DNA damage, but nothing of the sort could be detected in brain, SC or lung lysates (Fig. 9D).

6.1.1.5 Phenotypical analysis of Fus GT mice

Phenotypically, heterozygous GT mice looked inconspicuous at a first glance. There were no changes in weight of male mice, females were a bit heavier at an age of 9.5 months (Fig. 10A). They were healthy and not obviously impaired in walking, posture, and activity. To get a deeper insight into phenotypical effects of a depletion of Fus, mice were analyzed in the German Mouse Clinic (GMC). Starting with seven month of age, a cohort of 28 heterozygous GT mice was challenged regarding activity, strength, coordination, balance, anxiety, and memory and results were compared to those of WT littermates (Fig. 10, 11; Tab. 5).

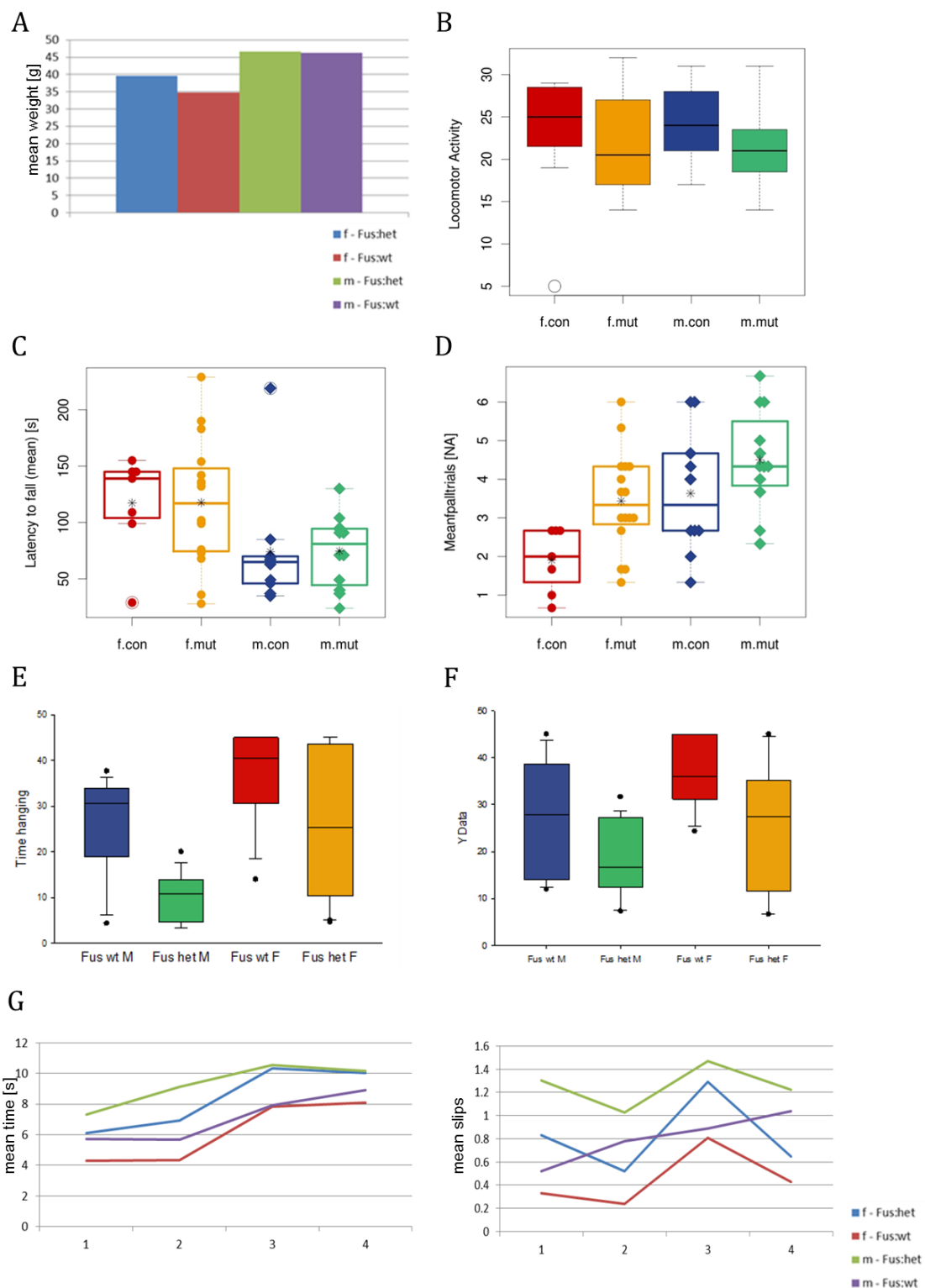


Fig. 10: Sensorimotor impairments in Fus GT mice. (A) Weight of GT male mice was the same as of WT males. Females were about 5 g heavier than WTs. (B-G) Sensorimotor tests of seven to 9.5 months old heterozygous GT mice and WT littermates. GT mice were inconspicuous concerning locomotor activity in the SHIRPA protocol (B) and coordination and balance in the Rotarod test (C). Beam Ladder (D) and Inverted Grid (E) yielded a significant increase of fore paw slips (D) and a reduced latency to fall down (E) in eight months old mice. (F) A repetition of the Inverted Grid 1.5 months later confirmed the results in younger mice. (G) Heterozygous mice showed an increased traversing time and slightly more slips in the Balance Beam test. (Error bars represent S.E.M. Two-way ANOVA or linear

regression (Inverted Grid) was performed. n(WT F)=7; n(het F)=16; n(WT M)=9; n(het M)=12;) F, female; M, male; Graphs by Lore Becker;

Modified SHIRPA, a test of general health and autonomous functions, as well as reflexes, posture, and activity yielded no differences between GT and WT mice (Fig. 10B). This was confirmed by the Open Field, where spontaneous activity in a novel environment was analyzed (Tab. 5). The Grip Strength test for muscle strength of fore limbs and combined fore and hind limbs (no figure available) and Rotarod for coordination and balance (Fig. 10C) revealed no changes in seven months old *Fus* deficient mice. Therefore, mice were put on a grip or a rod and time was measured till they released or fell down. 2.5 months later, a repetition of Grip Strength brought no further results (no figure available). Another test for motor coordination and balance is the Balance Beam, where mice had to traverse beams with different diameters. Time to traverse the beam was recorded, along with falls, foot slips, and stops. The test was inconclusive in eight months old mice, whereas 1.5 months later, heterozygous GT mice showed an increased traversing time and slightly more slips (Fig. 10G). Furthermore, Beam Ladder and Inverted Grid were applied, also trials for motor coordination and sensorimotor function. In Beam Ladder testing the same parameters were defined as for the Balance Beam. Here a significantly increased number of fore paw slips (Fig. 10D) was observed in mutants, but no differences in time and stops. For the Inverted Grid, mice were put on a grid, which was turned, and time was measured till they fell down. A reduced latency to fall down was found in eight months old mice (Fig. 10E), which was approved 1.5 months later (Fig. 10F).

For memory, different trials were applied: in the Open Field apparatus, mice were placed individually in a corner of the arena and allowed to freely explore for 20 min. Spontaneous activity, rearing activity, and time spent in the center were assessed. Spontaneous alternations were determined using the Y-maze. Therefore, each mouse was placed at the end of one arm and allowed to move freely through the maze during a five-minute session. Spontaneous alternations, defined as consecutive entries into all three arms without repetitions, were scored. The last test was the social discrimination test, where mice were exposed to stimulus animals, removed after some time and then put back with an additional unknown animal. The duration of investigatory behavior of the test animal towards the stimulus animals was recorded.

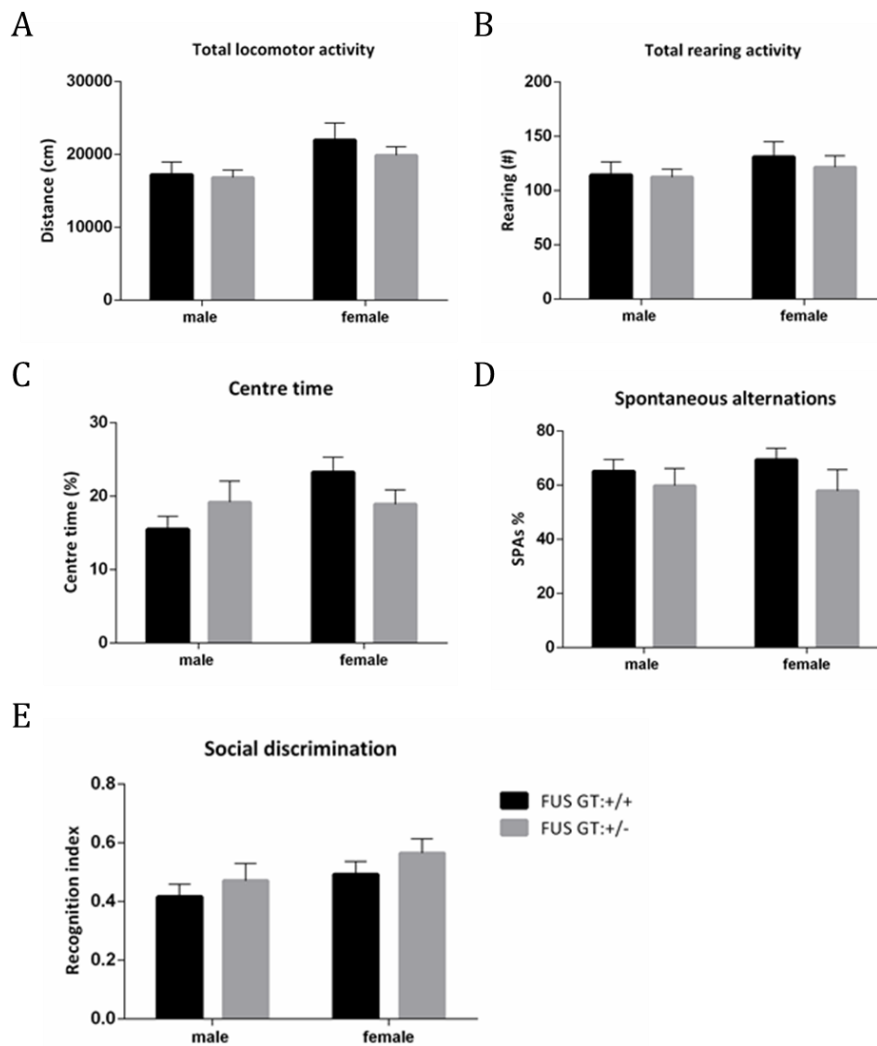


Fig. 11: No memory deficits in *Fus* deficient mice. 13 months old heterozygous GT mice did not show significant changes concerning activity (A, B) time spent in the center of the Open Field apparatus (C), working memory (D) or social discrimination (E). (Error bars represent S.E.M. Two-way ANOVA was performed. $n(\text{GT}^{+/+} \text{ female})=7$; $n(\text{GT}^{+/-} \text{ female})=16$; $n(\text{GT}^{+/+} \text{ male})=9$; $n(\text{GT}^{+/-} \text{ male})=12$;) $\text{GT}^{+/+}=\text{WT}$; Graphs by Lillian Garrett;

In terms of anxiety, memory, and social discrimination, there were no clear genotype effects on either exploratory/rearing activity or anxiety related behavior in the Open Field (Tab. 5, Fig. 11A-C). Additionally, no distinct behavior was noticed at an age of 13 months between GT and WT mice concerning working memory (Y maze; Fig. 11D) or recognition in the olfaction-based social discrimination test (Fig. 11E). There was even a trend towards better memory (Fig. 11).

These results indicate more a motoric than a memory phenotype in heterozygous *Fus* deficient mice.

Tab. 5: Summary of behavioral analyses of Fus GT mice in the German Mouse Clinic.

Behavior test	Parameter measured	<i>Fus</i> GT	
		9 WT M/12 het M/7 WT F/16 het F	
		Age (months)	Result
SHIRPA (Fig. 10B)	General health and autonomous functions, reflexes, locomotor activity, posture, and movement	7	n.d.
Grip Strength	Muscle function	7	n.d.
Rotarod (Fig. 10C)	Coordination and balance	7.5	n.d.
Balance Beam	Motor coordination and balance	8	n.d.
Beam Ladder (Fig. 10D)	Motor coordination	8	Increased number of fore paw slips (p<0.05), no difference in time and stops
Inverted Grid (Fig. 10E)	Sensorimotor function	8	Reduced latency to fall down (p<0.01)
Open field	Locomotion (Fig. 11A)	8	n.d.
	Exploration (Fig. 11B)	8	n.d.
	Anxiety-related (Fig. 11C)	8	n.d.
Balance Beam 2 nd time (Fig. 10G)	Motor coordination and balance	9.5	Increased traversing time and slightly more slips, no difference in stops
Inverted Grid 2 nd time (Fig. 10F)	Sensorimotor function	9.5	Reduced latency to fall down (p<0.01)
Grip Strength 2 nd time	Muscle function	9.5	n.d.
Y maze (Fig. 11D)	Working memory	13	Trend to less alterations
Social discrimination (Fig. 11E)	Olfaction-based social memory/discrimination	13.5	Trend to more social discrimination

n.d., no difference; het, heterozygous; hom, homozygous; F, female; M, male; in red: significant

6.1.1.6 Homozygous survivor mice

As mentioned above, seven homozygous survivors arose after more than half a year of het x het breeding with varying degree of impairment. Two were found dead with about one month of age. The phenotype of the other five mice ranged from inconspicuous concerning fertility, mobility, health, and viability (Fig. 12A) to a strong interference regarding these aspects (Fig. 12B-E), pointing to a varying degree of remaining Fus expression or modifying aspects. However, this could not be proven due to the limited number of available mice. Some mice were very small at weaning age (Fig. 12C) and three had no clear gender (Fig. 12E, F). Primary sexual organs were not developed till the age of about three months (Fig. 12E).

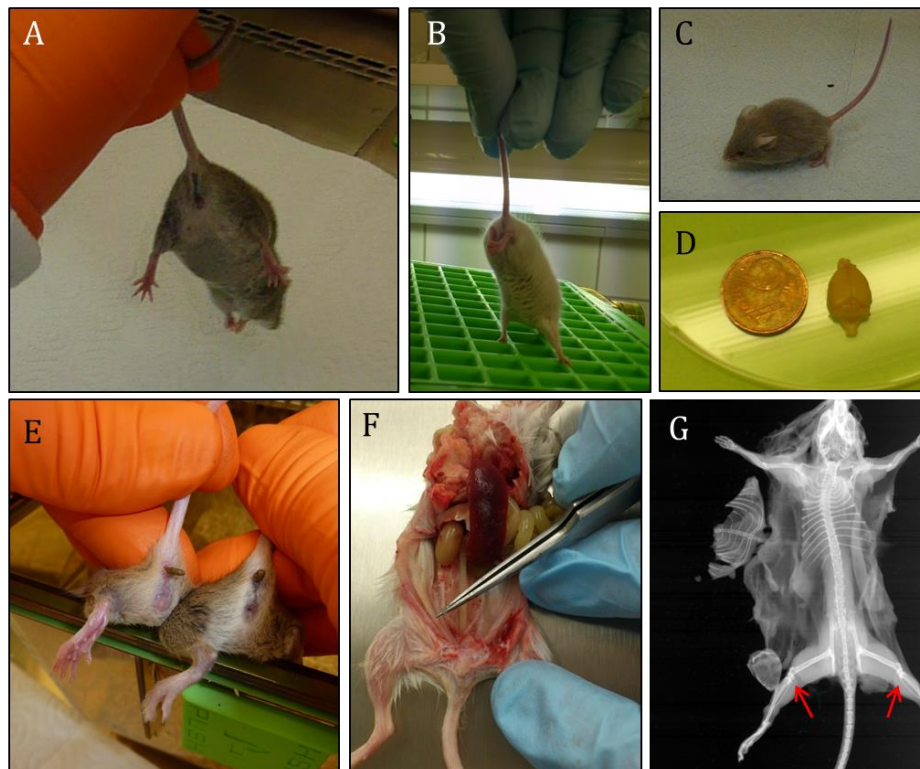


Fig. 12: Morphological heterogeneity of homozygous survivor mice. (A) Inconspicuous pregnant homozygous mouse (#211) with normal posture when hold at its tail. (B) Limb claspings of a symptomatic homozygous GT mouse (#253). Some homozygotes were smaller than their littermates at weaning age (#274; C) with abnormal brain morphology (#253; D), no clear gender (#274 left, in comparison with a age-matched WT; E), stunted uterus (#253; F), arthrosis (arrow), and scoliosis (“211; G, by Thomas Floss).

One female mouse born in September 2013 (#211) was healthy and produced three litters in three months with four pups in average, though no homozygotes among them (Fig. 12A). In October 2014, this mouse was still alive but has not produced offspring anymore since March

2014 and displayed some abnormalities in walking. X-ray film (by Thomas Floss, Irina Rodionova, and Frauke Neff) at the age of 13 months revealed scoliosis, some consolidated vertebrae, pelvic bones, arthrosis of the knees, probably less bone lime (Fig. 12G), and stunted muscles. The other phenotypic extreme was observed with one mouse born in February 2014 (#253) (Fig. 12B). This homozygote was half as sized as its littermates and showed abnormalities in posture and walking, as well as sexual organs and brain morphology. It had a hump, displayed a toddling gait, characterized by bilateral external torsion of the tibia, and clasped its hindlimbs when hold at its tail (Fig. 12B). Dissection revealed again scoliosis, a small brain with an unlikely morphology of the cerebellum (Fig. 12D), and a stunted uterus (Fig. 12F). The latter might explain why the sex could not be ascertained at weaning age. In the digital appendix a video of this mouse at the age of seven weeks is provided, in which the abnormal posture and gait can be seen (see also chapter 9.3.1). The second video shows the homozygote with the number 274 (Fig. 12C) at the age of three weeks. These were the two survivors with the strongest phenotype. It is also obvious that #274 was very small, even for this young age.

Tab. 6: Chromosomal Copy Number Assay of homozygous GT survivors.

Mouse ID	Sex	Genotype	Y-Chromosome	Chromosome	Chromosome	Results
				8	11	
163	M	hom	1.4	2	1.8	pass
211	F	hom	0	2.6	1.3	fail
240	F	hom	0	2.7	1.6	fail
253	F	hom	0	2.4	1.4	fail
270	M	WT	1	2.3	1.5	pass
271	M	het	0.8	2.3	1.5	pass
272	M	het	1.3	2	1.6	pass
273	F	het	0	2	1.5	pass
274	F	hom	0	2.4	1.8	fail

het, heterozygous; hom, homozygous; M, male; F, female

A Copy Number Assay for chromosome 8, 11, and Y yielded a female gender for this mouse, as six of the seven survivors were female and the gender of three of them had to be determined via

Copy Number Assay (Tab. 6). This qRT-PCR also brought some deviations to light that hint at a chromosomal instability like only one chromosome 8 or triple chromosome 11 (Tab. 6). Just one of the five genotyped homozygous survivors passed the assays. For a precise statement this has to be further analyzed.

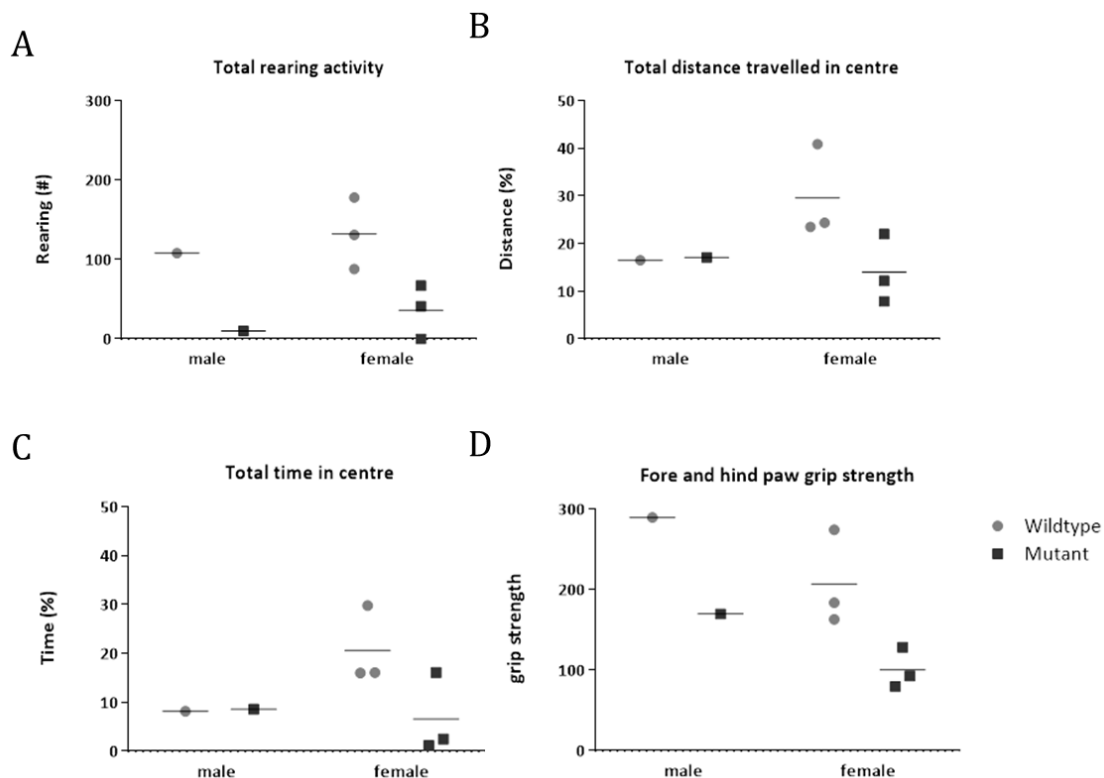


Fig. 13: Phenotypical analysis of homozygous survivors. (A-C) The Open Field yielded a decreased total rearing activity (A), less total distance travelled (B), and less time spent in the center (C) in homozygous GT survivor mice compared to WT littermates. (D) Grip Strength testing revealed less strength in both, fore and hind paws. (Error bars represent S.E.M. n(WT female)=3; n(het female)=3; n(WT male)=1; n(het male)=1;) Graphs by Lore Becker and Lillian Garrett;

With a small group of mice, four homozygotes and WT's each, some tests were done in the GMC concerning strength, locomotor and exploratory activity, and motor coordination. Due to an insufficient number of animals nothing could be said regarding significance. These are only first hints for a possible phenotype, effected by loss of Fus. The Open Field yielded less rearing activity (Fig. 13A) and, for females, less total distance travelled and less time spent in the center (Fig. 13B, C). This could point towards more exploration and less anxiety, but also strength impairment as indicated by the results of the Grip Strength test (Fig. 13D). In the Beam Walk no clear genotype effects could be observed (data not shown).

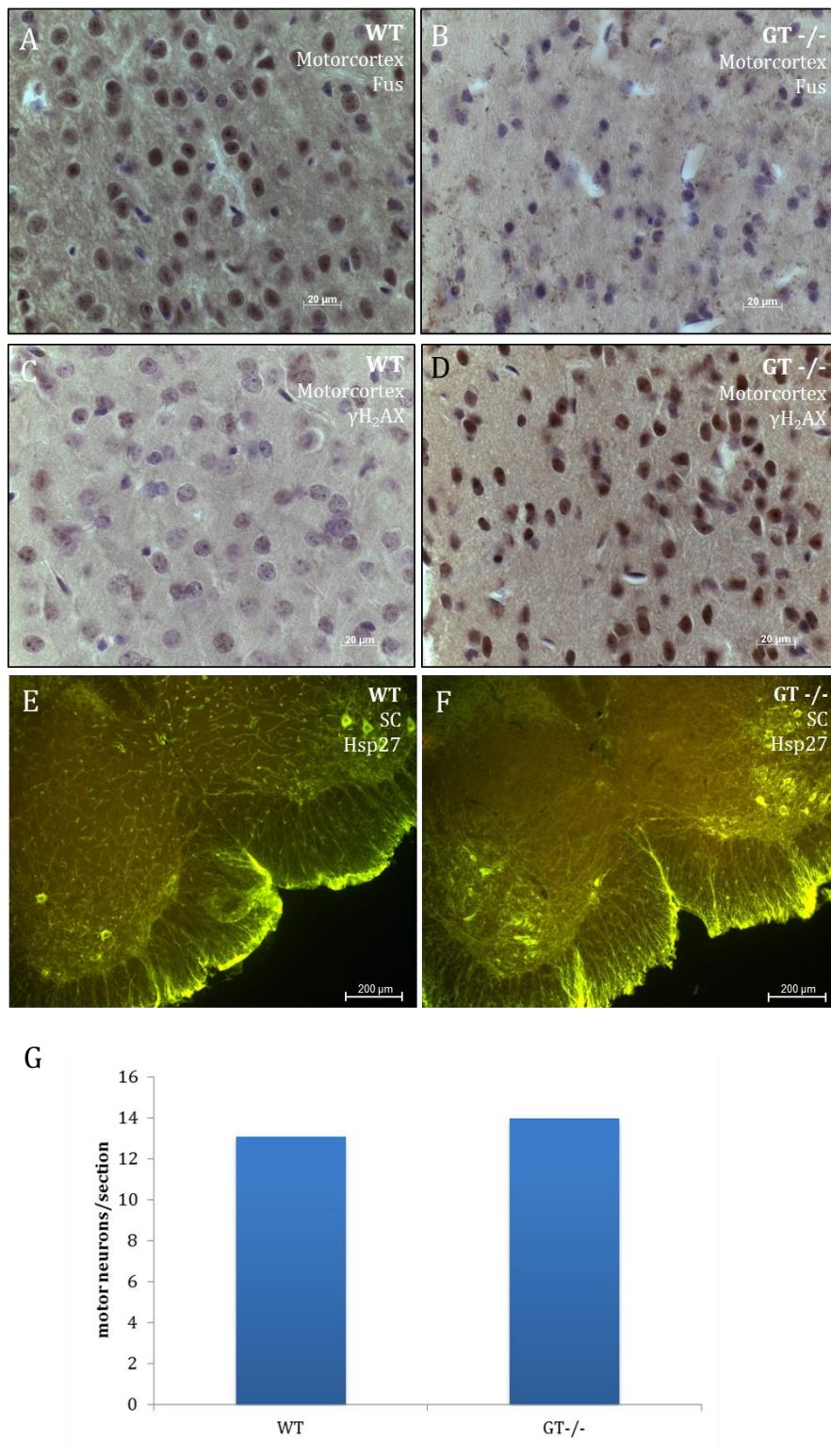


Fig. 14: Pathological analysis of homozygous GT survivors. (A-D) Immunostaining for Fus (A, B) and γ H2AX (C, D) of brain sections from the homozygous survivor mouse with the biggest walking deficit (#253) and a WT littermate. The Fus GT^{-/-} mouse showed less Fus (B) and an increased staining for γ H2AX in the motorcortex (D) compared to WT control (A, C). Scale bar: 20 μ m; (E-G) Immunostaining for Hsp27 and counting of SC sections from the homozygous GT mouse #253 (F) and a WT littermate (E). There was no difference obvious in number of motor neurons (G) (n/genotype=1). Scale bar: 200 μ m;

Due to the „ballerina walk“, the SC of the mouse #253, along with a WT littermate, was prepared, sliced, and the lumbar part containing neurons for hind limb innervation were stained for Hsp27, a marker for motor and sensory neurons (Plumier et al., 1997). Since sensory neurons are located in dorsal root ganglia and motor neurons in the ventral horn of the SC, Hsp27 was an appropriate marker for this study. Motor neurons were blindly counted and the average number of neurons per section was calculated. Motor neuron numbers did not indicate a difference between the homozygous and the WT mouse (Fig. 14E-G). Additionally, brains of these mice were cut and stained for Fus, γ H₂AX, NeuN, and Gfap. The only difference, besides reduced levels of Fus protein (Fig. 14A, B), could be observed concerning γ H₂AX with an enhanced staining of the DNA damage marker in the homozygous GT survivor compared to WT control (Fig. 14C, D).

6.1.2 HUMANIZED *FUS*^{R521G} MOUSE MODEL

6.1.2.1 Generation of hFUS^{R521G} mice

Generation of hFUS mouse embryonic stem cells

For expression of human ALS-associated mutations *in vivo*, the EUCOMM ES cell clone EUCE0290f05 (see chapter 6.1.1.1) was taken as a basis. Applying Recombinase Mediated Cassette Exchange (RMCE) technology (Schebelle et al., 2010), the β geo cassette of EUCE0290f05 was exchanged by human *FUS* cDNA.

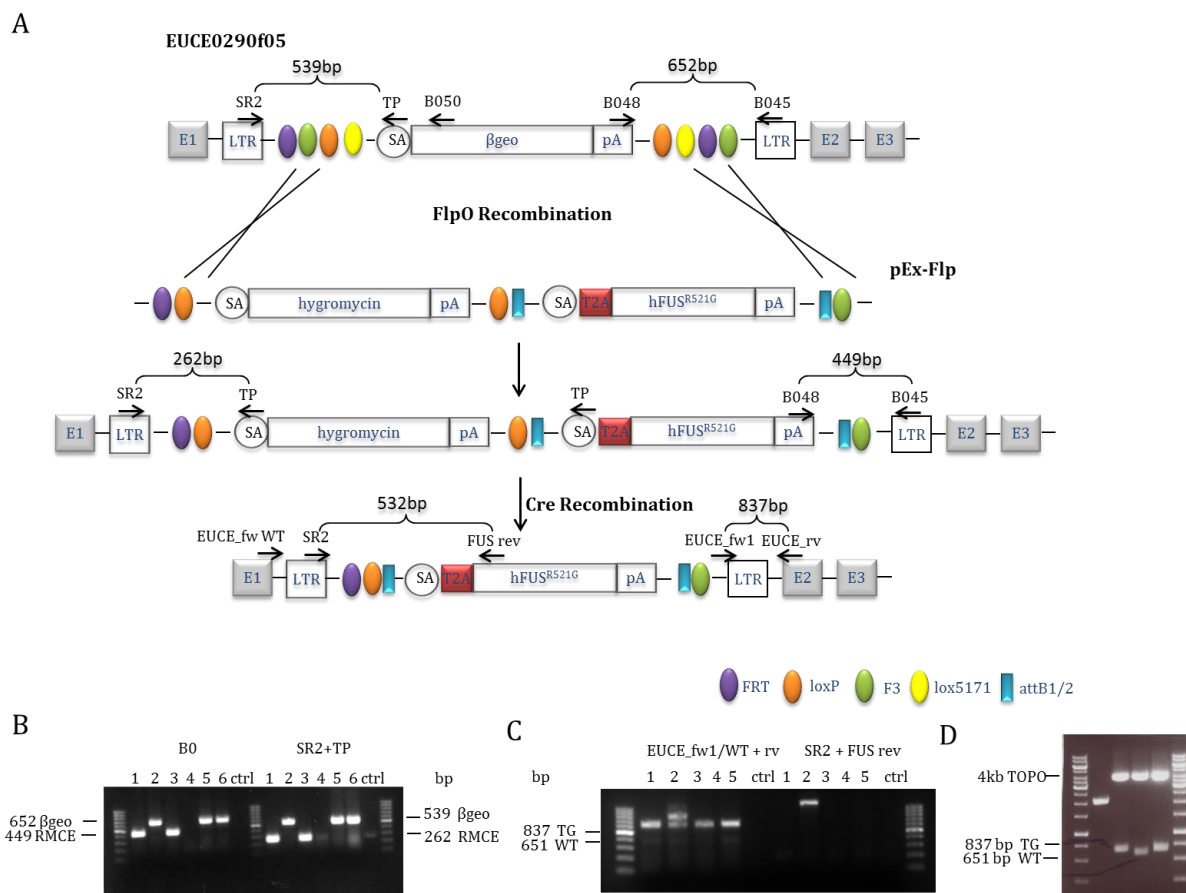


Fig. 15: Generation of mice carrying ALS-associated *hFUS* mutations. (A) Schematic outline of the generation of hFUS expressing mice by applying RMCE technology. pEX-Flp vectors containing a hygromycin cassette and *hFUS* cDNA were electroporated into the EUCOMM ES cell clone EUCE0290f05. Via FlpO recombination, the original β geo cassette was exchanged by the recommended construct. Cre recombinase cut the hygromycin cassette for a successful expression of hFUS. Primers for genotyping with product sizes are indicated. (B) Genotyping of ES cell clones for a correct exchange. Positive clones showed a band of 449 bp in the triple B0-PCR and 262 bp in the SR2/TP-PCR (clones 1 and 3). (C) After excision of hygromycin, combination of SR2 and FUS rev primers gave a product, whereas PCR of other original transgenic clones did not. Routine genotyping was further done with EUCF_fw1/EUCF_fw WT and EUCF_rv primers which yielded bands at 837 bp and 651 bp, respectively. The third bigger band was cloned in TOPO.

Plasmid preparation und digestion with EcoRI revealed the original two bands again (D), indicating that this third band appeared because of adherence of the TG and WT band.

Corresponding pENTR vectors were kindly provided by Dorothee Dormann and Christian Haass. The first vector harbors the WT *FUS* cDNA sequence beginning with the ATG and ending with the stop codon, the second carries the R521G mutation, reported to be a mild mutation with a late disease onset, and the third the P525L exchange as a severe mutation (Dormann et al., 2010). A pENTR vector with the R495X mutation was purchased from GeneArt® Gene Synthesis. This mutation was identified in a family with early-onset ALS and was found to truncate the final 32 amino acids from the C-terminus (Bosco et al., 2010). The four vectors provided all recombination sites, which are necessary for RMCE. In front of the *FUS* sequence, a T2A site was inserted. Due to its ribosome skipping effect, 2A or 2A-like oligoprotein sequences lead to a cleavage of polyproteins (Luke et al., 2008). In the construct, the T2A site was used to prevent a *FUS* fusion protein with a duplicated exon 1.

Via Gateway cloning, *FUS* cDNAs were brought into the pDest vector carrying a hygromycin resistance (Schebelle et al., 2010). The resulting pEx-Flp vectors were then electroporated along with a FlpO recombinase-expressing plasmid into the gene trap clone EUCE0290f05. FlpO recombination should substitute the β geo cassette by the hygromycin/*FUS* cassette (Schebelle et al., 2010) (Fig. 15A). Therefore, the human *FUS* cDNA was directly imported into the mouse *Fus* locus by RMCE and should be expressed instead.

Following hygromycin selection (125 U/ml) for ten days, 25-40 hygromycin positive clones were picked for each construct, grown, and further screened by PCR. Two different PCR strategies were applied: triple B0-PCR and SR2/TP-PCR as published before (Schebelle et al., 2010). The B0-PCR was performed with primer B045, a rv primer binding in the 3' LTR sequence, primer B048, a fw primer binding in the poly adenylation site (pA), and primer B050, a second rv primer binding in the β geo cassette (Fig. 15A). This PCR provided information about the orientation of the gene trap vector (Schebelle et al., 2010) and gave product sizes of 652 bp for the original β geo insertion, 907 bp for an inverted β geo cassette, and 449 bp for a successful exchange (Fig. 15A, B). The SR2/TP-PCR with the corresponding primers in the 5' LTR and the splice acceptor (SA) revealed a product with 539 bp for the directly oriented β geo cassette and 262 bp for the exchange (Fig. 15A, B). Hence, clones that showed bands of 449 bp and 262 bp respectively were considered as positive for the recommended exchange, which was one out of 17 in case of the WT *FUS* (5.9%), two out of 25 for *FUS*^{R521G} (8%), and one out of 23 for the *FUS*^{P525L} construct (4.3%). Concerning *FUS*^{R495X}, two positive ES cell clones out of 28 analyzed could be identified (7.1%). The number of tested clones was fewer than the number of picked

clones, since not all grew after picking. However, efficiencies did not meet those described by Schebelle et al. due to unknown reasons. All PCR products were purified and checked for completeness by sequencing, so this was not the point.

Generation of hFUS mice

Positive ES cell clones were expanded, karyotyped, injected into blastocysts, and transferred into the uteri of pseudo-pregnant CD-1 foster females. Born male chimeras were mated with female C57Bl6/J mice. Only for one construct, the hFUS^{R521G} construct, germline transmission was obtained (Tab. 7). For excision of the hygromycin cassette, flanked by loxP sites for Cre recombination, the arising F1 generation was bred with Rosa26-Cre-expressing mice. Since Rosa26-Cre is ubiquitously expressed, hFUS was activated in all tissues. For the sake of simplicity these hFUS^{R521G} Rosa mice are further named as hFUS^{R521G} mice. In order to check hygromycin excision, offsprings were genotyped using two distinct PCRs: (I) Combination of the forward primers in exon 1 of murine *Fus* or within the transgenic construct (EUCE_fw1/EUCE_fw WT) and one reverse primer in exon 2 of the endogenous *Fus* (EUCE-rv) (see also chapter 6.1.1.1) gave product sizes of 651 bp for the WT or 837 bp for the TG allele (Fig. 15A, C). Later, this PCR was used for routine genotyping. When these primers were combined in one single PCR tube, a third bigger band appeared. Sequencing yielded mixed sequence information of WT and TG. After cloning this PCR product into a TOPO vector and digestion with EcoRI to cut the insert out again, only the two original WT and TG products were detectable indicating that an adherence of both products was here observed (Fig. 15D). (II) A PCR with the SR2 primer and a reverse primer at the very beginning of *hFUS* sequence (FUS rev) resulted only in a detectable product, if the hygromycin cassette is removed. Otherwise the product was too big. The estimated size after hygromycin excision would be 532 bp (Fig. 15A). However, there was a band with more than 1 kb observed. TOPO cloning and sequencing suggested that again an adherence of WT and TG sequence took place (data not shown).

Especially, there was no germline transmission for the hFUS^{WT} construct, what would be important for comparison. To overcome this problem, hygromycin cassette of positive ES cell clones was cut out *in vitro* by electroporating a Cre recombinase-expressing plasmid. After selection with puromycin (1 µg/ml) for three days and growing with normal medium for another ten days, picked clones were tested by PCRs as described above and positive clones were expanded, karyotyped, and injected into blastocysts. Though, no germline transmission was achieved for the WT construct or the other ones (Tab. 7).

Tab. 7: Injected *hFUS* ES cell clones before or after Cre Recombination and resulting germline transmission.

Construct	Number of injections	Born pups	Chimeras (males)	Chimeras (males) (% of pups per injection)	Germline transmission
hFUS ^{WT}	21	82	21 (14)	1.2 (0.8)	no
hFUS ^{R521G}	2	16	11 (8)	34.3 (25)	yes (1)
hFUS ^{P525L}	4	15	13 (8)	21.7 (13.3)	no
hFUS ^{R495X}	9	61	19 (15)	3.5 (2.7)	no
hFUS ^{WT} + Cre	12	35	2 (2)	0.5 (0.5)	no
hFUS ^{R521G} + Cre	3	9	1 (0)	3.7 (0)	no
hFUS ^{P525L} + Cre	4	19	9 (5)	11.8 (6.6)	no

6.1.2.2 Homozygous lethality of hFUS^{R521G} mice

In correlation with Mendelian inheritance, one would expect 25% of WT and homozygous transgenic mice respectively, and 50% of heterozygotes. However, among 93 offsprings of het x het matings 25.8% were WT and 73.1% heterozygous, indicating embryonic lethality of homozygous hFUS^{R521G} mice. At weaning age, one homozygous survivor was identified (1.1%), but was dead within the next two weeks (Tab. 8).

To learn more about the stage of lethality, litters at different embryonic days were dissected and genotyped. Embryos seem to die between E11.5 and 13.5 (Tab. 8). At E12.5 for example, four litters were sacrificed with 31 embryos altogether. Among two litters no homozygotes could be detected. The other two litters harbored one homozygous embryo each (Tab. 8).

Tab. 8: Lethality of homozygous hFUS^{R521G} mice.

	WT	+/-	-/-	total
E7.5	-	3	2	5
E8.5	1	3	5	9
E9.5	-	2	2	4
E11.5	-	4	3	7
E12.5 (4 litters, 2 litters without homs)	10	19	2	31
E13.5	2	6	2	10
E14.5	1	4	-	5
Adult (21 litters)	24	68	1	93
	25.8%	73.1%	1.1%	

hom, homozygote;

6.1.2.3 Expression of hFUS^{R521G} *in vivo*

In order to check expression of human FUS *in vivo*, qRT-PCRs were performed with species-specific probes. Concerning protein level, only total FUS levels could be determined due to default of species-specific antibodies.

By a Gene Expression Assay with exon-spanning probes, recognizing either both, mouse *Fus* and human *FUS* mRNA, or distinguishing between both, relative mRNA levels were determined in different aged heterozygous hFUS^{R521G} mice and compared to WT littermates. A probe only binding to human *FUS* mRNA could not be used, since it was complementary to exon 1 and 2. Exon 1 is non-coding and was therefore not included in the *hFUS* cDNA cassette. Thus, only total and murine mRNA levels were assessed. Quantification yielded reduced mRNA levels of murine *Fus* to 70.9% (Fig. 16B) and total *FUS* to 81.9% (Fig. 16A) respectively, indicating that hFUS^{R521G} is only expressed at minimal levels.

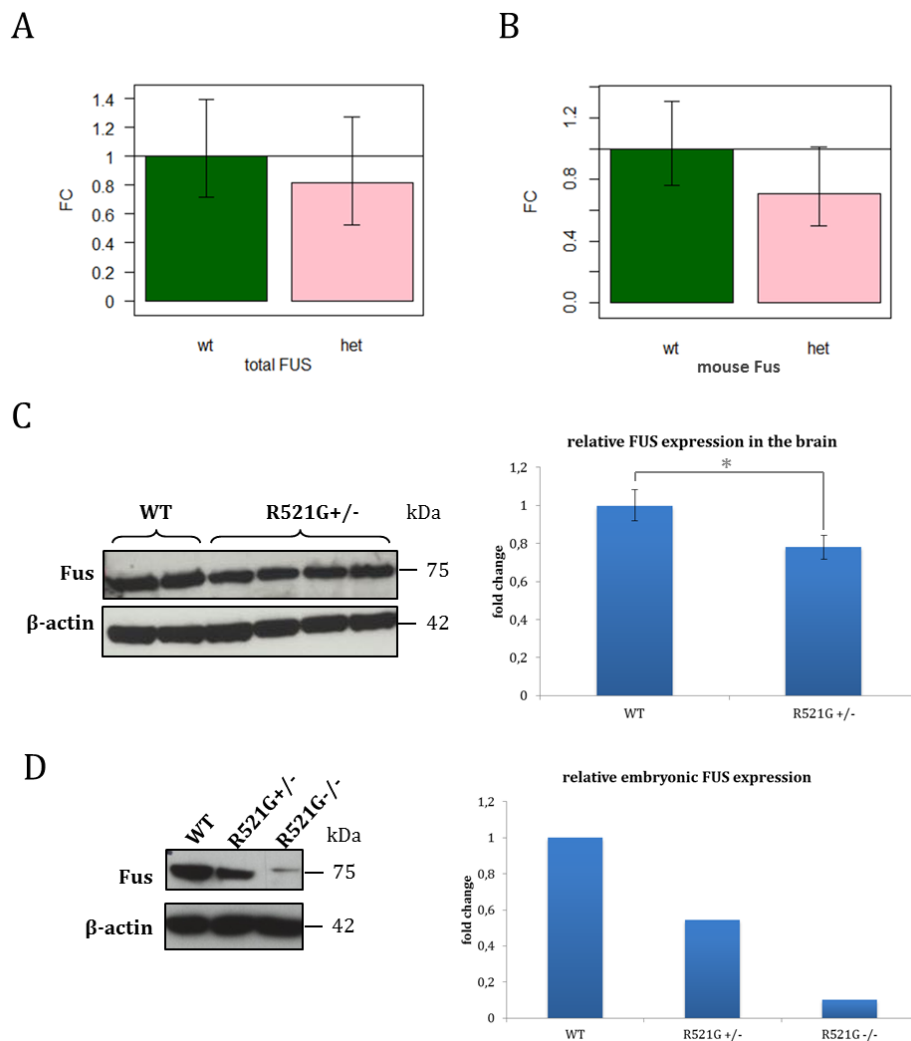


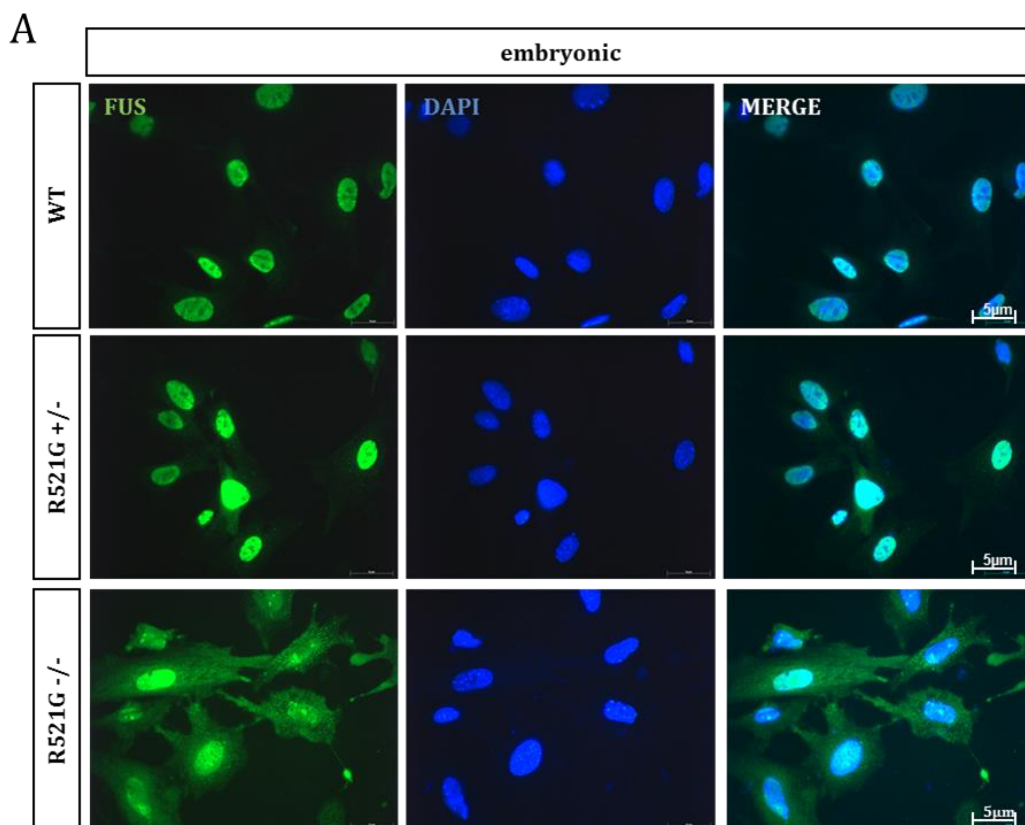
Fig. 16: Expression of hFUS^{R521G} in vivo. (A, B) qRT-PCR from brain samples of different aged heterozygous hFUS^{R521G} transgenic mice and their littermates. (Delta-delta-Ct with 95% confidence intervals was performed. n (WT)=3; n (het)=4;) FC, fold change; (A) On mRNA level, total *FUS* is reduced to 81.9% compared to WT. p=0.30; (B) Murine *Fus* mRNA in heterozygotes constituted 70.9% of the WT *Fus* level. p=0.055; (C) Western Blot for total FUS from brain lysates of 6-15 months old TG mice and WT littermates. On protein level, total FUS is significantly reduced to 78.1% in heterozygous mice compared to WT. (Error bars represent S.D.. Student's t-test was performed. n(WT)=2; n(R521G^{+/-})=4; p=0.02;) (D) Exemplary Western Blot from E11.5 embryos yielded reduced total FUS levels in TG embryos. (n/genotype=1; Therefore, no statistics were performed.)

Western Blotting for total FUS from brain lysates revealed a significant reduction of protein levels to 78.1% in transgenic mice compared to WT littermates (Fig. 16C), confirming the results of the qRT-PCR (Fig. 16A). Exemplary Western Blot from E11.5 embryos also showed less total FUS levels of 54.5% for a heterozygous and 10.2% for a homozygous embryo compared to a WT (Fig. 16D). In *Fus* GT mice, *Fus* protein appeared to be regulated post-transcriptionally and protein levels were upregulated compared to mRNA (see chapter 6.1.1.3; Fig. 6). For hFUS^{R521G} mice, less FUS protein than mRNA was detected. Since the antibody purchased from Santa Cruz Biotechnology is raised against the C-terminus of human FUS, the mutation could reduce

antibody binding and effective total protein levels could be higher. The Gene Expression Assay recognizes exons 6/7. However, two other antibodies from Sigma (used for immunostaining) and Hycult Biotech did not give specific bands. This was the reason why this antibody was further used.

6.1.2.4 Subcellular mislocalization of FUS protein

It was reported in different publications that expression of ALS-associated mutations leads to mislocalization of FUS to the cytoplasm (Bosco et al., 2010; Dormann et al., 2010; Gal et al., 2011; Ito et al., 2011; Kino et al., 2011; Niu et al., 2012; Zhang and Chook, 2012) and that mutant FUS also interacts with WT FUS and pulls it out of the nucleus (Vance et al., 2013; Qiu et al., 2014). In order to investigate subcellular localization of FUS in hFUS^{R521G} transgenic mice, fibroblasts were established and stained for FUS protein (Fig. 17).



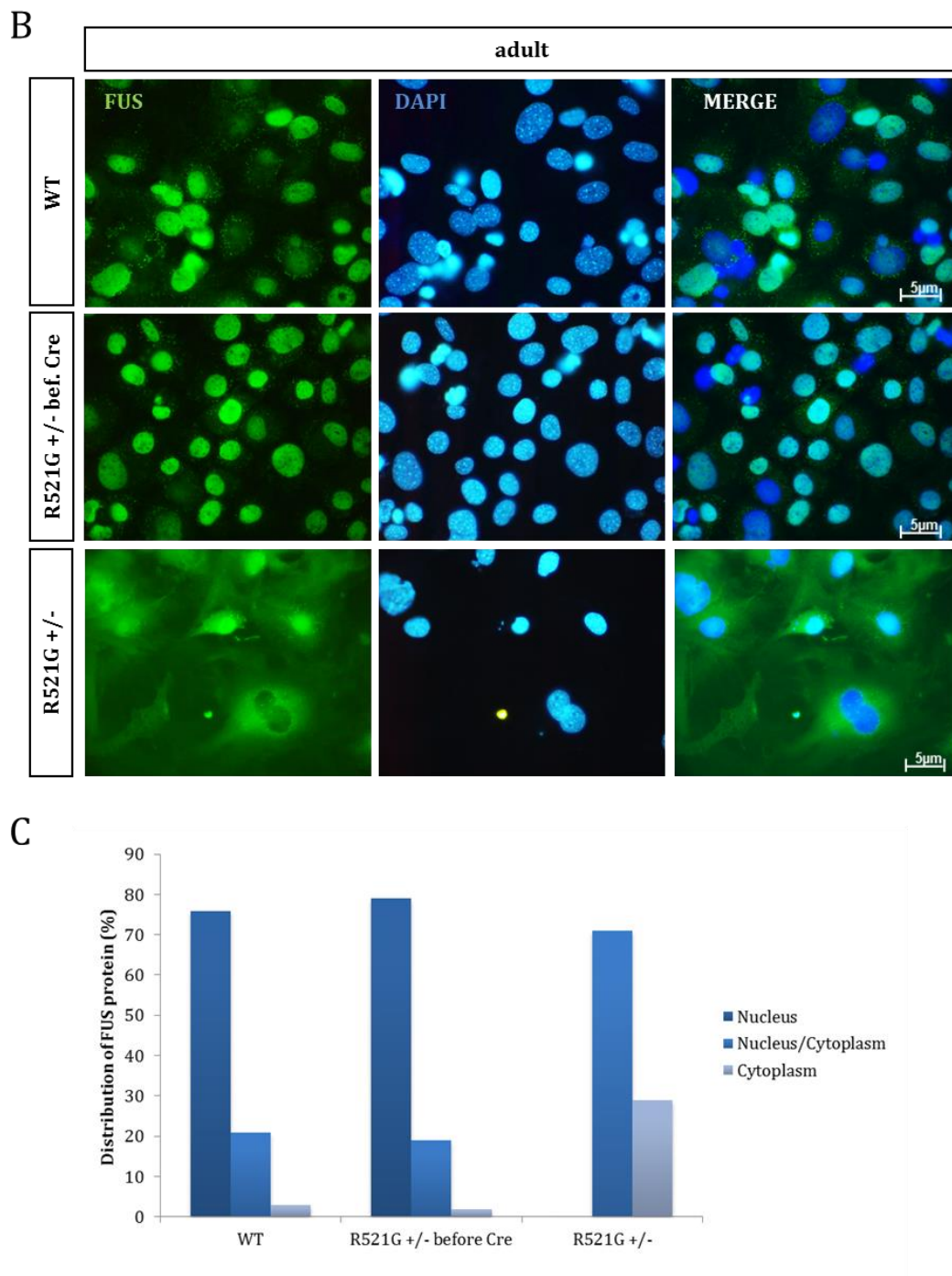


Fig. 17: Mislocalization of FUS in fibroblasts derived from heterozygous adult mice, but not in embryonic fibroblasts. (A) FUS staining of MEFs. In WT and heterozygous cells, all FUS was localized to the nucleus, whereas in homozygous cells a portion of FUS protein could be observed in the cytoplasm. Scale bar: 5 µm; (B) FUS staining of fibroblasts derived from an adult heterozygous hFUS^{R521G} mouse, an adult mouse before Rosa26-Cre pairing and a WT littermate. While in WT cells and cells, where hFUS expression has not been induced yet, all FUS was found in the nucleus, heterozygous hFUS expressing cells showed a high degree of FUS mislocalization to the cytoplasm. Scale bar: 5 µm; (C) Quantification (%) of adult fibroblasts with FUS only in the nucleus or cytoplasm and cells where FUS was observed in both compartments. In heterozygotes no single cell was detected, where FUS staining was only found in the nucleus, in contrast to WT cells and those before hygromycin excision. (100 cells/genotype were counted. n/genotype=1) bef. Cre, before Cre recombinase

For this purpose, E12.5 embryos were dissected and Mouse Embryonic Fibroblasts (MEFs) were grown. For lack of an antibody distinguishing between murine and human FUS, only localization of total FUS could be determined. Immunostaining revealed mainly a nuclear FUS localization in WT and heterozygous MEFs. In homozygous cells a portion of FUS protein was found to be redistributed to the cytoplasm (Fig. 17A). For immunostaining, an anti-FUS antibody from Sigma was used, which binds to the N-terminus of FUS, whereas the one used for Western Blots recognizes the C-terminus, where the mutation is located. This could be the reason why in homozygous cells a high degree of FUS protein could be detected in contrast to the Western Blot from embryos (Fig. 16D).

To test whether also granule formation could be observed upon cellular stress, as observed in several studies (Bosco et al., 2010; Dormann et al., 2010; Gal et al., 2011; Ito et al., 2011), MEFs were treated with sodium arsenite for one hour to induce oxidative stress. Subsequently, cells were stained for FUS and Tia1, a marker for stress granules (Fig. 18). Both stress granule formation and recruitment of FUS into these granules could be monitored to an increasing degree from WT to homozygous cells (Fig. 18).

To see, if the situation is the same with cells derived from adult mice, fibroblasts were cultivated from a piece of ear and again stained for FUS. Herein, a mislocalization to the cytoplasm could be observed to a high degree already in heterozygous cells, whereas the WT showed nuclear localization (Fig. 17B). For quantification of cells with FUS localized only to the nucleus or cytoplasm respectively and cells with FUS in both compartments, 100 cells for each genotype were counted and absolute percentages of different localization patterns were calculated. Concerning WT cells, 76% of cells displayed nuclear localization, 21% nuclear and cytoplasmic localization recapitulating shuttling of FUS between both compartments, and only 3% exclusive cytoplasmic localization (Fig. 17C). In contrast, no single heterozygous cell could be found with exclusive nuclear localization. In 29% of cells, FUS was solely observed in the cytoplasm and 71% exhibited FUS in the nucleus and cytoplasm (Fig. 17C). Since total FUS protein was stained, this suggests an influence of mutant FUS on endogenous FUS localization.

Due to low expression levels of hFUS^{R521G} (Fig. 16) the question arised if this phenotype was really affected by the human FUS mutation or perhaps by insertion of a gene trap cassette in the murine *Fus* locus. For this reason, fibroblasts were generated from adult transgenic mice before Cre recombination. In these animals, expression of the gene trap ended at the poly A of hygromycin and hFUS has not been expressed yet. FUS staining of those cells revealed the same picture as in WT cells, meaning a primarily nuclear FUS localization (Fig. 17B). Counting yielded percentages of 79% for nuclear localization, 2% for cytoplasmic localization and 19% for

detection in both compartments, nearly the same as for WT cells (Fig. 17C). These data recommend that mislocalization of Fus was due to expression of mutant protein and that also endogenous Fus was extracted to the cytoplasm, and consequently, that the construct worked.

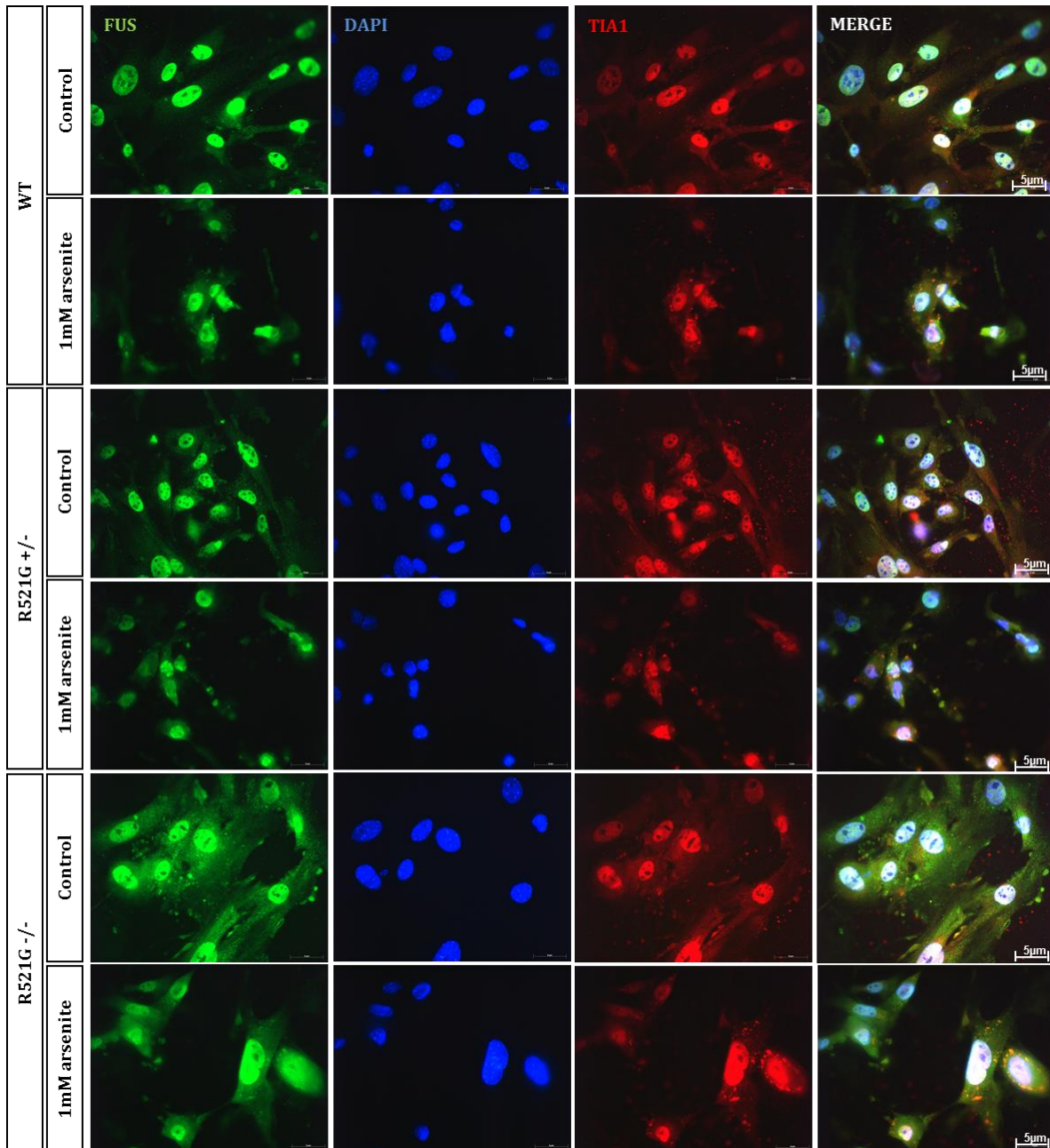


Fig. 18: FUS is recruited into stress granules upon oxidative stress. To induce cellular stress WT, heterozygous and homozygous hFUS^{R521G} MEFs were treated with 1 mM sodium arsenite for 1 hour. Untreated cells were used as a control. Staining for FUS and Tia1 revealed formation of stress granules and recruitment of FUS into these granules in correlation with the degree of FUS mislocalization. Scale bar: 5 µm;

6.1.2.5 Pathological analysis of hFUS^{R521G}^{+/-} mice

Except for embryonic lethality of hFUS^{R521G}^{-/-} mice, human *FUS* mutation did not seem to affect health or motoric function. To further examine the effects of an ALS-associated *FUS* mutation *in vivo* different pathological analyses were performed.

First, it was interesting to know if the subcellular mislocalization of FUS, as seen in adult fibroblast cells *in vitro*, could be also observed *in vivo*, since a hallmark of ALS-FUS is FUS mislocalization and inclusion formation in neurons and/or glial cells (Mackenzie et al., 2010). For this reason, four and 15 months old heterozygous hFUS^{R521G} mice and WT littermates were perfused, brains and SC were prepared, cut and immunostained for FUS protein (Fig. 19A, B). However, even in the aged mutant mice no FUS inclusions could be detected, either in SC or brain tissue (Fig. 19B). The same was true for p62 and ubiquitin (data not shown), which are colocalized in FUS inclusions in patients (Mizuno et al., 2006; Dormann and Haass, 2013). Western Blot from brain and SC lysates of 15 months old mice did also not hint to altered p62 levels (Fig. 20B, D). Fractionation of soluble and insoluble protein and subsequent western blotting revealed no insoluble FUS protein in brain or SC (Fig. 20A).

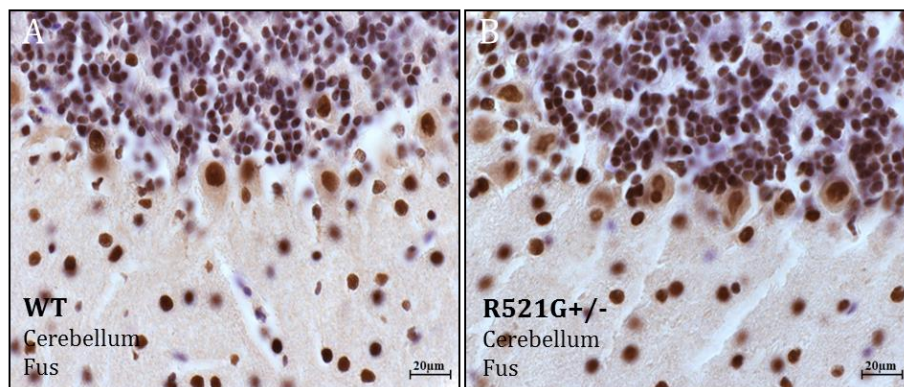


Fig. 19: No FUS mislocalization or inclusions in hFUS^{R521G}^{+/-} mice. Example (cerebellum) for FUS immunostaining of a 15 months old heterozygous hFUS^{R521G} mouse (B) and WT control (A). No FUS inclusions could be detected in the brain. Scale bar: 20 μ m;

Rodent models for ALS-associated *FUS* mutations, overexpressing hFUS^{R521G}/hFUS^{R521C} or lacking the entire NLS, showed enhanced expression of Gfap indicating astrogliosis and neuroinflammation (Huang et al., 2011; Huang et al., 2012; Shelkovernikova et al., 2013). Though, under the endogenous promoter, *FUS* mutation R521G did not result in an increase of Gfap in

immunostaining or Western Blot (Fig. 20B, C). Western Blot for apoptosis-inducing factor AIF yielded a trend towards increased apoptosis (Fig. 20E, F).

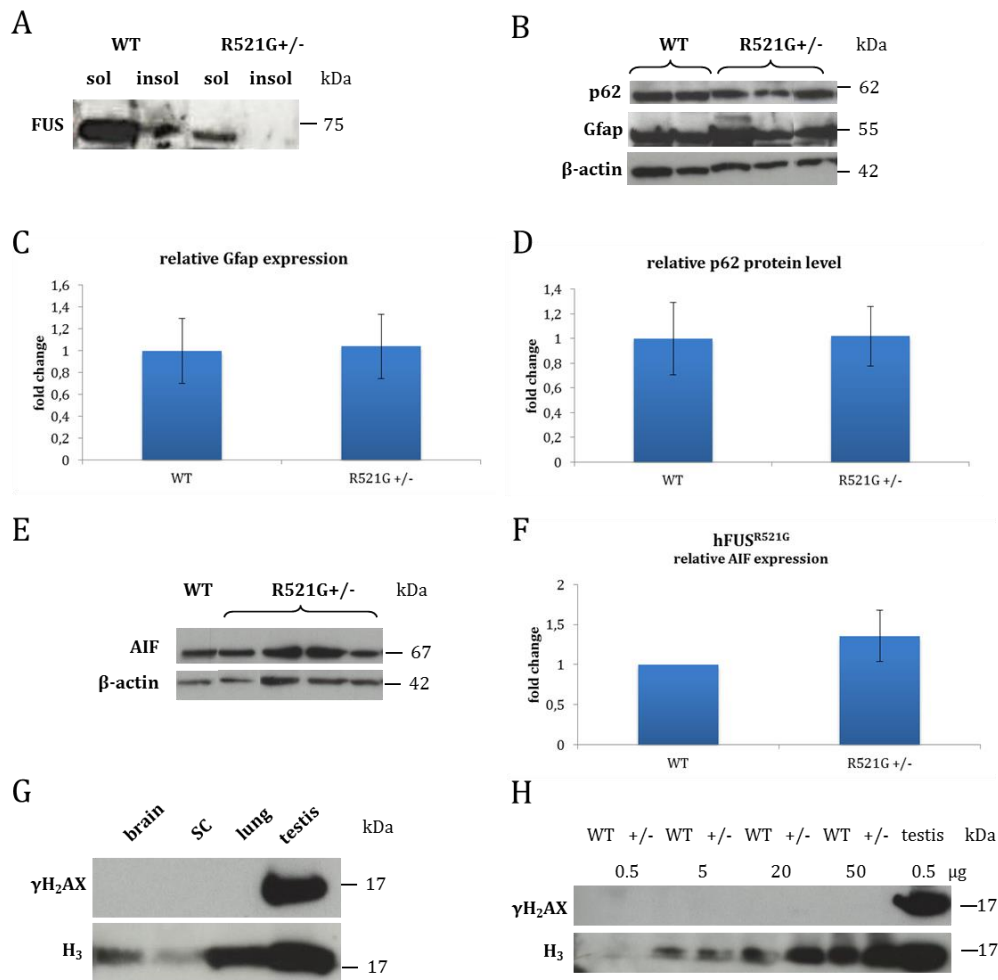


Fig. 20: Expression of hFUS mutation R521G *in vivo* did not cause insoluble FUS, DNA damage, or other pathological features. (A) Exemplary Western Blot from SC lysates of a WT and a heterozygous hFUS^{R521G} mouse. In the 15 months old animal no insoluble FUS could be detected. (B) Western Blots from brain lysates of 15 months old heterozygous hFUS^{R521G} mice and WT littermates. Used antibodies are indicated. β-actin served as loading control for quantification. (C, D) Quantification of (B); Error bars represent S.D.. Student's t-test was performed. n(WT)=2; n(R521G^{+/-})=3; No changes were observed concerning protein levels of Gfap (C) or p62 (D). (E) Western Blot for AIF from brain lysates of 15 months old heterozygous hFUS^{R521G} mice and WT littermates. β-actin served as loading control for quantification. (F) Quantification of (E) showed no changes in levels of apoptosis-inducing factor AIF. (S.D.(R521G^{+/-}) is quoted. n(WT)=1; n(R521G^{+/-})=3;) (G) Western Blot for γH₂AX from lysates of different tissues from a heterozygous hFUS^{R521G} mouse did not provide evidence for DNA damage. (H) Western Blot with increasing amounts of brain lysates did also not yield a signal indicating DNA damage. Testis was used as a positive control and H₃ as loading control. sol, soluble; insol, insoluble;

DNA damage was another common finding *in vitro* or *in vivo* after manipulating FUS (Hicks et al., 2000; Mastrocola et al., 2013; Rulten et al., 2014) and Qiu and colleagues measured enhanced levels of γH₂AX, a marker for double strand breaks upon overexpression of R521C mutation (Qiu

et al., 2014). Herein, immunostaining from 15 months old mice (data not shown) and western blotting from seven months old mice (Fig. 20G) for γ H₂AX did not give evidence for DNA damage in the brain, SC, or lung. To assure that enough protein lysate was used, Western Blot was repeated with increasing amounts of brain lysates (Fig. 20H). Nevertheless, even with 100 fold brain lysate, compared to testis as positive control, no signal could be detected.

ALS-associated loss of motor neurons was also recapitulated by some rodent models (Huang et al., 2011; Huang et al., 2012; Shelkovernikova et al., 2013). Hereof, for this model, nothing could be observed by Nissl staining or immunostaining for the neuronal marker NeuN in brain or SC (data not shown). Blind counting of motor neurons in the cervical part of the SC, innervating fore-paws and stained by Hsp27, did also not yield differences between 13 months old WT and heterozygous hFUS^{R521G} mice (Fig. 21). In contrast, there was rather a tendency towards more motor neurons (Fig. 21C).

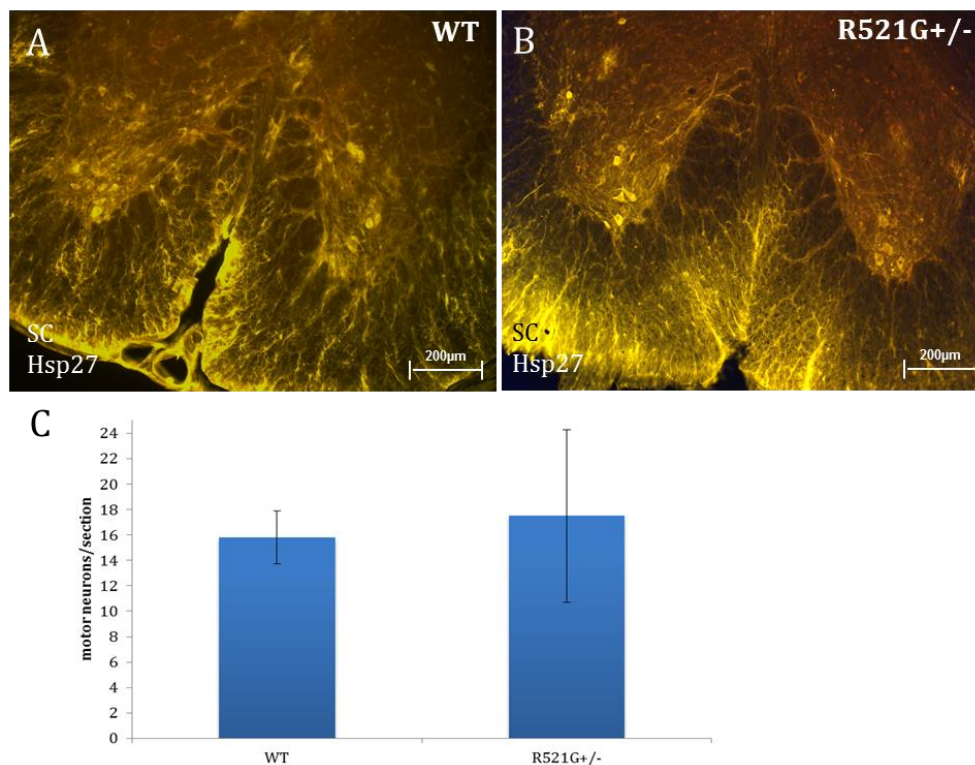


Fig. 21: No loss of motor neurons in hFUS^{R521G}+/- mice. Example for immunostaining of cervical motor neurons in the SC of 13 months old heterozygotes (B) and WT littermates (A). (C) Quantification yielded no significant difference in number of motor neurons. (Error bars represent S.D.. Student's t-test was performed. n=3/genotype; p=0.7;) scale bar: 200 μm;

Qiu and colleagues reported in their publication reduced levels of brain-derived neurotrophic factor (BDNF) as a FUS target and less activation of the receptor TrkB, which resulted in

dendritic and synaptic defects (Qiu et al., 2014). Concerning the current mouse model, Western Blot for Bdnf yielded a tendency towards reduced protein levels in the brain compared to WT (Fig. 20B), but simultaneously tendentially increased levels of phospho-TrkB (Fig. 20C). tau was also found to be a splicing target of FUS (Orozco et al., 2012). In brain lysates of aged hFus^{R521G} mice, significantly decreased levels of tau were detected (Fig. 20A, D, E). However, no shift towards the 4R tau isoform was observed, as it was the case in the publication after FUS depletion (Orozco et al., 2012). 3R tau was decreased to 38.7% (Fig. 20 D) and 4R tau to 26.0% (Fig. 20D).

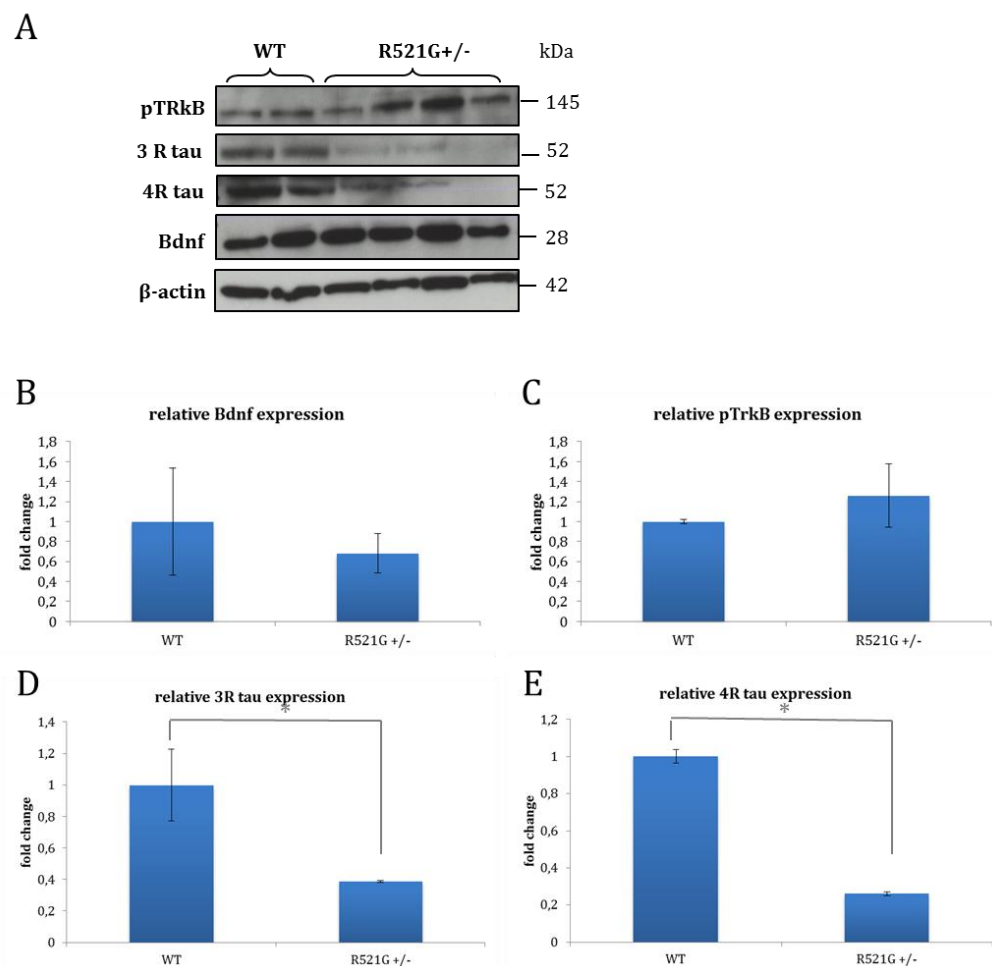


Fig. 22: Expression of hFUS mutation R521G *in vivo* did not change levels of the splicing target *Bdnf*. (A) Western Blots from brain lysates of 15 months old heterozygous hFUS^{R521G} mice and WT littermates. Used antibodies are indicated. β-actin served as loading control for quantification. (B-E) Quantification of (A); Error bars represent S.D.. Student's t-test was performed. n(WT)=2; n(R521G^{+/-})=4; No significant changes could be observed concerning protein levels of Bdnf (B) and its activated receptor pTrkB (C). (D, E) Levels of 3R tau (p=0.02) as well as 4R tau (p=0.01) were significantly decreased.

Methylation of FUS was suggested to play an important role in the development of ALS and that this is mediated by PRMT1 (Dormann et al., 2012; Tradewell et al., 2012; Yamaguchi and Kitajo, 2012; Scaramuzzino et al., 2013). Analysis of methylation status of FUS by Western Blot revealed an interesting difference between embryos and adult hFUS^{R521G} mice compared to WT littermates (Fig. 23), although it was not significant in embryos due to only one WT per litter. Whereas in E13.5 heterozygous embryos MeFUS was downregulated to 75.7% relative to total FUS levels (Fig. 23A, B), in adult mice the opposite was observed. Compared to WT littermates, heterozygotes showed a highly significant elevation of methylation about 72.5% (Fig. 23D, E). Contemporary, no changes in PRMT1 levels could be detected in embryos (Fig. 23A, C). In adult brain lysates, PRMT1 levels were significantly decreased to 80.2% (Fig. 23D, F). The same was noticed when repeated with MEFs and adult fibroblasts established for immunostaining (see chapter 6.1.2.4), suggesting that methylation could be involved in FUS localization and that this is not mediated by PRMT1.

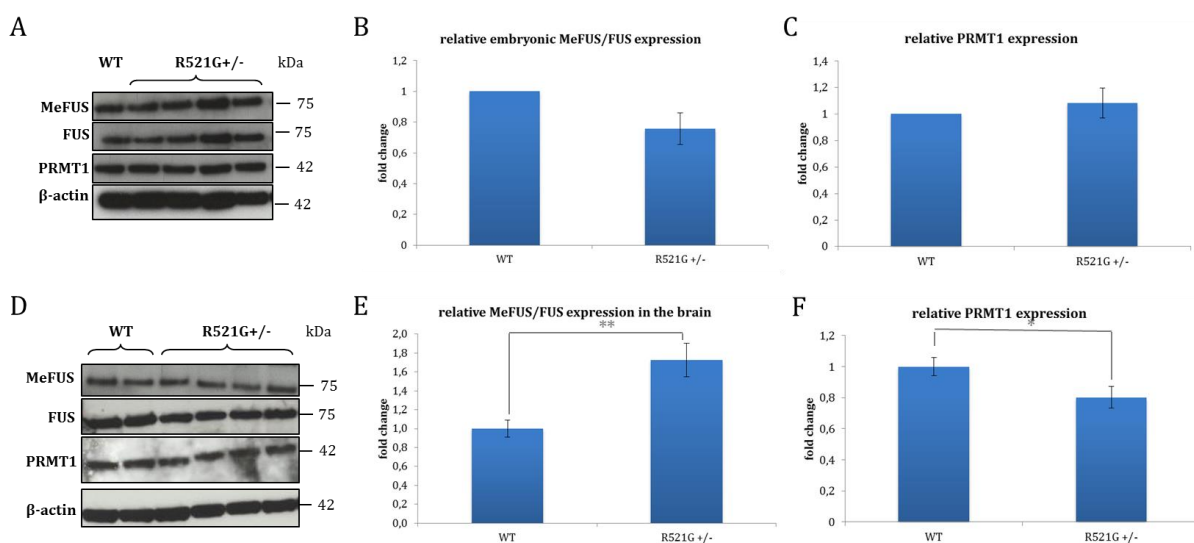


Fig. 23: Differences in FUS methylation status in embryos and adult hFUS^{R521G}/⁺/⁻ mice. (A) Western Blot from head lysates of E13.5 embryos. Used antibodies are indicated. β -actin served as loading control for quantification. (B, C) Quantification of (A); S.D.(R521G^{+/+}) is quoted. n(WT)=1; n.(R521G^{+/+})=4; (B) Methylation of FUS is reduced to 75.7% compared to WT control, whereas PRMT1 levels were not changed (C). (D) Western Blots from brain lysates of 15 months old heterozygous hFUS^{R521G} mice and WT littermates. Used antibodies are indicated. β -actin served as loading control for quantification. (E, F) Quantification of (D); Error bars represent S.D.. Student's t-test was performed. n(WT)=2; n.(R521G^{+/+})=4; Quantification of a Western Blot from adult brain revealed an increase of methylated FUS relative to total FUS to 172.5% compared to WT littermates (E; p=0.006;) and a decrease of PRMT1 levels to 80.2% (F; p=0.03;).

6.1.2.6 Phenotypical analysis of hFUS^{R521G}^{+/-} mice

For phenotypical analysis, a cohort of 17 heterozygous hFUS^{R521G} mice and the same number of controls were tested in the workflow for locomotion and sensorimotor function described above for heterozygous GT mice (see chapter 6.1.1.5) (Tab. 9). The first observation was a distinction in body weights: female heterozygotes were heavier than their WT littermates, males by contrast were lighter (Fig. 24A).

Regarding locomotor activity, heterozygotes showed reduced activity in the SHIRPA test (Fig. 24B), whereas in the Open Field no clear genotype effects were detected (Fig. 25A). On the other hand, Open Field yielded increased exploratory activity (Fig. 25B) and more time spent in the center (Fig. 25C).

Tab. 9: Summary of behavioral analyses of hFUS^{R521G} mice in the German Mouse Clinic.

Behavior test	Parameter measured	<i>hFUS^{R521G}</i> <i>7 WT M/9 het M/10 WT F/8 het F</i>	
		<i>Age</i> <i>(months)</i>	<i>Result</i>
SHIRPA (Fig. 24B)	General health and autonomous functions, reflexes, locomotor activity, posture and movement	7	Reduced locomotor activity
Grip Strength (Fig. 24G)	Muscle function	7	n.d.
Rotarod (Fig. 24E)	Coordination and balance	7.5	More falling from the rod
Balance Beam (Fig. 24C, D)	Motor coordination and balance	7.5	Trend to more time and slips
Beam Ladder (Fig. 24F)	Motor coordination	7.5	Slightly less traversing time
Inverted Grid	Sensorimotor function	8	Latencies reduction
Open field	Locomotion (Fig. 25A)	9	n.d.
	Exploration (Fig. 25B)	9	Increase in total rearing activity (p=0.01)
	Anxiety-related (Fig. 25C)	9	More time in the center (p=0.03)
Balance Beam 2 nd time	Motor coordination and balance	9.5	Slightly more time
Y maze	Working memory	10	n.d.
Social discrimination (Fig. 25D)	Olfaction-based social memory/discrimination	12.5	Trend towards more social discrimination
Inverted Grid 2 nd time	Sensorimotor function	13.5	Latencies reduction
Grip Strength 2 nd time	Muscle function	13.5	n.d.

n.d., no difference; het, heterozygous; hom, homozygous; F, female; M, male; in red: significant

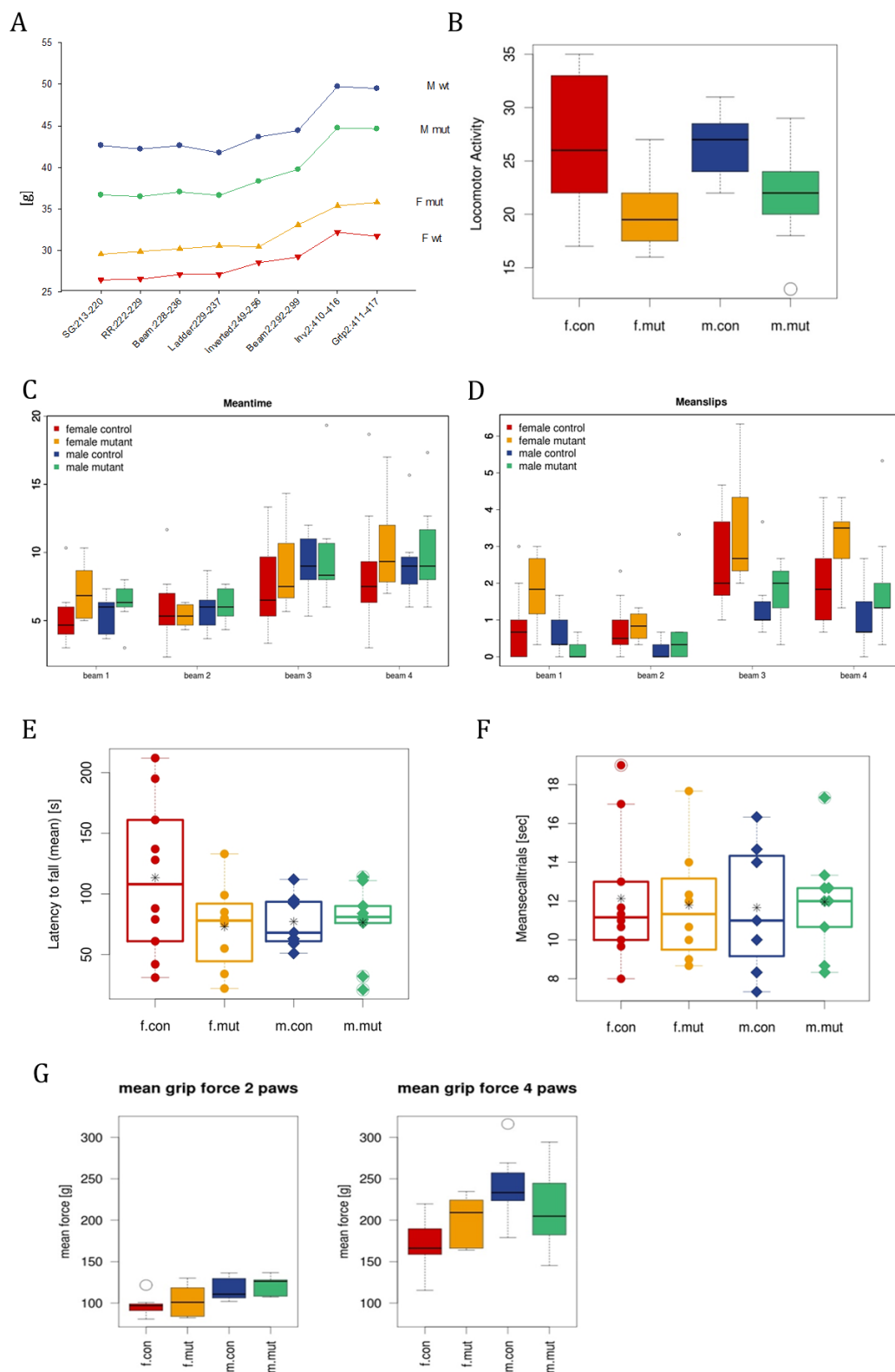


Fig. 24: *hFUSR521G^{+/-}* mice showed hypoactivity but were inconspicuous concerning strength and motor coordination. (A) Differences in body weight: female mutants were heavier than WT controls, males lighter. Tests and ages (days) are depicted. (B) SHIRPA test with seven months old heterozygous TG mice revealed a decrease in locomotor activity. Two-way ANOVA was performed; $p < 0.05$; (C, D) Balance Beam test yielded a trend to more time in females (C) and more slips, which did not reach significance due to high variation (D). (E) In the Rotarod test a tendency to reduced latencies was observed in females. (F) The Beam Ladder test resulted in slightly less traversing times. (G) Grip Strength of seven months old mice did not show differences in muscle function of fore limbs or fore

and hind limbs combined. (Error bars represent S.E.M. Two-way ANOVA was performed. n(WT F)=10; n(het F)=8; n(WT M)= 7; n(het M)=9;) Graphs by Lore Becker;

No clear differences could be noted in Grip Strength in mice with seven or 13.5 months of age (Fig. 24G). Concerning motor coordination and balance, only Inverted Grid revealed significant genotype effects: eight as well as 13.5 months old hFUS^{R521G} mice fell more often from the grid (Supplementary Data, chapter 9.3.2.2). Challenging the mice by Rotarod (Fig. 24E), Balance Beam (Fig. 24C, D), and Beam Ladder (Fig. 24F) resulted in a trend to more falls (Fig. 24E), and increase in time needed (Fig. 24C) and slips (Fig. 24D), but not in stops, or slightly less traversing time (Fig. 24F), but not in number of slips or stops, respectively in 7.5 months old mice (Tab. 9). A repetition of Balance Beam two months later brought no new outcome (data not shown). Together, these data suggest hypoactivity and an increase in curiosity in heterozygous TG mice compared to WT littermates.

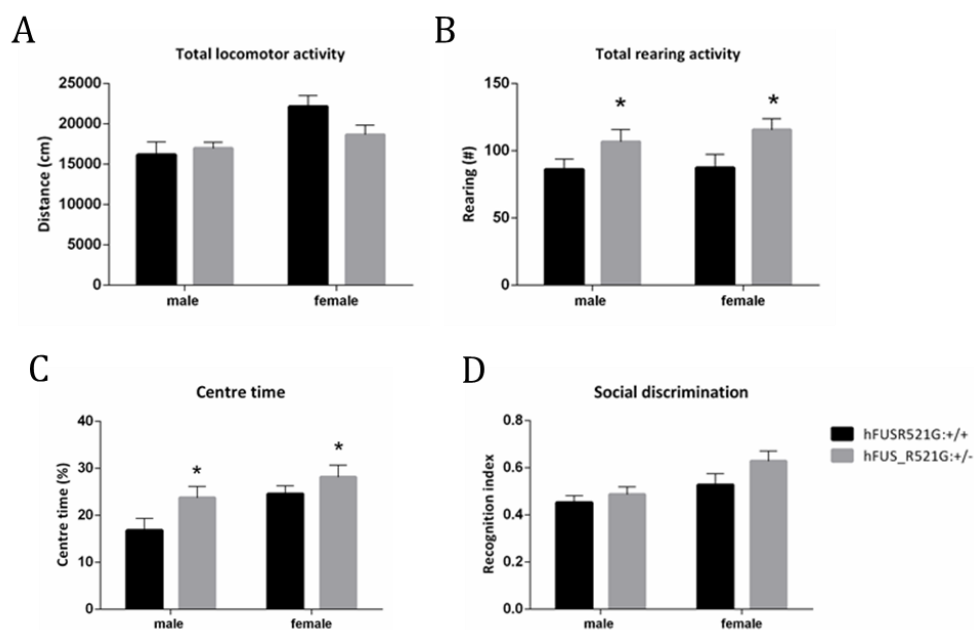


Fig. 25: Enhanced curiosity in hFUS^{R521G}+/- mice. (A-D) Open Field analyses yielded no changes in total activity (A), but a significantly increased rearing activity (B; p=0.01) and time spent in center (C; p=0.03). (D) No significant changes could be observed concerning social discrimination. (Error bars represent S.E.M. Two-way ANOVA was performed. n(hFUSR521G^{+/+} female)=10; n(hFUSR521G^{+/-} female)=8; n(hFUSR521G^{+/+} male)= 7; n(hFUSR521G^{+/-} male)=9;) hFUSR521G^{+/+}=WT; Graphs by Lillian Garrett;

6.1.3 EXPRESSION OF DIFFERENT ALS-ASSOCIATED MUTATIONS IN VIVO

6.1.3.1 Generation of TALEN mice expressing mutant Fus

Due to lack of hFUS^{WT} control mice for the humanized ALS-associated mutation R521G, mice with the corresponding mutations in the endogenous *Fus* should be generated and analyzed.

Murine *Fus* protein consists of 519 amino acids and shares 90.7% homology with human FUS. The R495X mutation in humans is adequate to R487X mutation in the mouse, and human R521G to murine R513G. The murine P517L exchange matches to the human P525L mutation. Mice were produced by Sudeepta Panda and Benedikt Wefers via TALEN technology (Wefers et al., 2013; Kuhn and Wefers, 2014; Wefers et al., 2014) and published in 2013 (Panda et al., 2013) (see also PhD thesis of Sudeepta Panda). The R487X mutation did not achieve germline transmission, R513G and P517L were successfully exchanged and stably inherited (Fig. 26). As a side effect within generation of Fus^{R513G} mice, one founder mouse occurred with a frameshift at position P511 (Fig. 26). This led to a nonsense NLS and a shift of the stop codon 61 amino acids backwards (Fig. 26B).

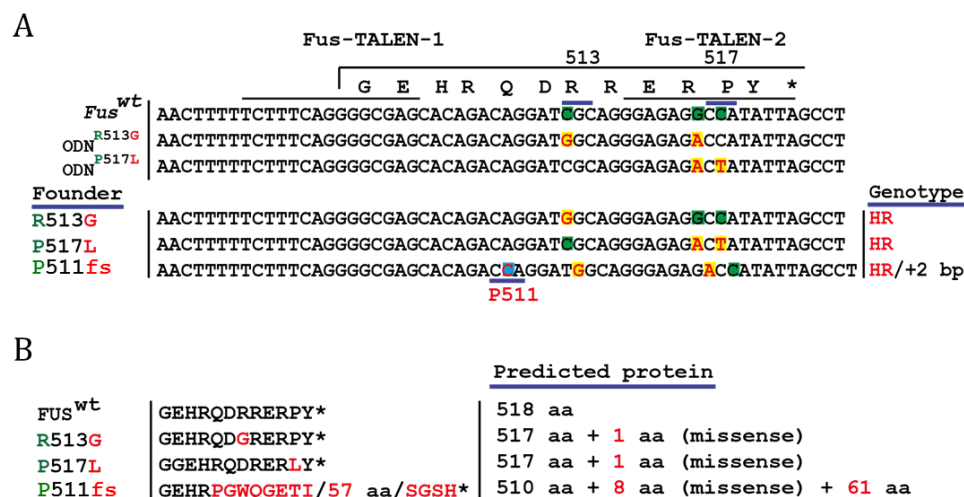


Fig. 26: Generation of mutant *Fus* mice applying TALEN technology. (A) Sequences of TALEN constructs are depicted. Germline transmission was achieved for Fus^{R513G} and Fus^{P517L} via homologous recombination. Among pups for the R513G construct, one founder occurred with a frameshift at position 511. (B) Predicted proteins for all three exchanges. The frameshift leads to a nonsense prolonged amino acid sequence. aa, amino acid; fs, frameshift; HR, homologous recombination; (kindly provided by Sudeepta Panda) (Panda et al., 2013)

6.1.3.2 Viability of Fus TALEN mice

According to Mendelian inheritance, offsprings from het x het matings should be to a quarter WT and homozygotes, and half heterozygotes. However, this was not observed in TALEN mutated Fus mice (Tab. 10).

Regarding Fus^{R513G} mice, percentages were 16.7% for WT, 63.7% for heterozygous, and 19.6% for homozygous pups respectively (Tab. 10). Fus^{P517L} mice showed a distribution of 43.4% for WT mice and 56.6% for heterozygotes. Among 99 offsprings till now, no homozygote came up (Tab. 10). The Fus^{P511fs} line produced 112 descendants till now with only one homozygote among them (0.9%). 31.9% were WT and 67.3% heterozygous (Tab. 10). The survivor was sacrificed with 1.5 months of age and used for immunostainings (see chapter 6.1.3.4). Thus, no point could be made about the viability or phenotype of this survivor.

Considering these results, a shift of genotypes was observed for all three lines. Numbers suggest an enhanced lethality especially in the Fus^{P517L} line. At a first glance, all living mice looked healthy and not impaired concerning mobility.

Tab. 10: Viability of mutant Fus TALEN mice. Depicted are numbers from het x het matings.

	WT	+/-	-/-	total
R513G	40	153	47	240
	16.7%	63.7%	19.6%	
P517L	43	56	-	99
	43.4%	56.6%		
P511fs	36	76	1	113
	31.9%	67.3%	0.9%	

6.1.3.3 Subcellular mislocalization of Fus protein

To check *in vitro*, if Fus mutations in the NLS lead to a disturbance of nuclear import and thus a mislocalization to the cytoplasm, MEFs and fibroblasts from adult mice were generated and stained for Fus (Fig. 27).

Embryonically, no shift of Fus localization from the nucleus to the cytoplasm could be detected. Even in homozygous Fus^{P511fs} MEFs, carrying the putative most severe mutation, only a very rare cytoplasmic staining could be seen (Fig. 27A). Treatment with 0.5 mM sodium arsenite to induce oxidative stress resulted in more export of Fus to the cytoplasm, stress granule formation, and recruitment of Fus to these granules according to the amount of Fus mislocalization. This was enhanced applying 1 mM sodium arsenite. Most cytoplasmic Fus staining was observed in homozygous Fus^{P511fs} MEFs (Fig. 28) (Experiment performed by Sudeepta Panda).

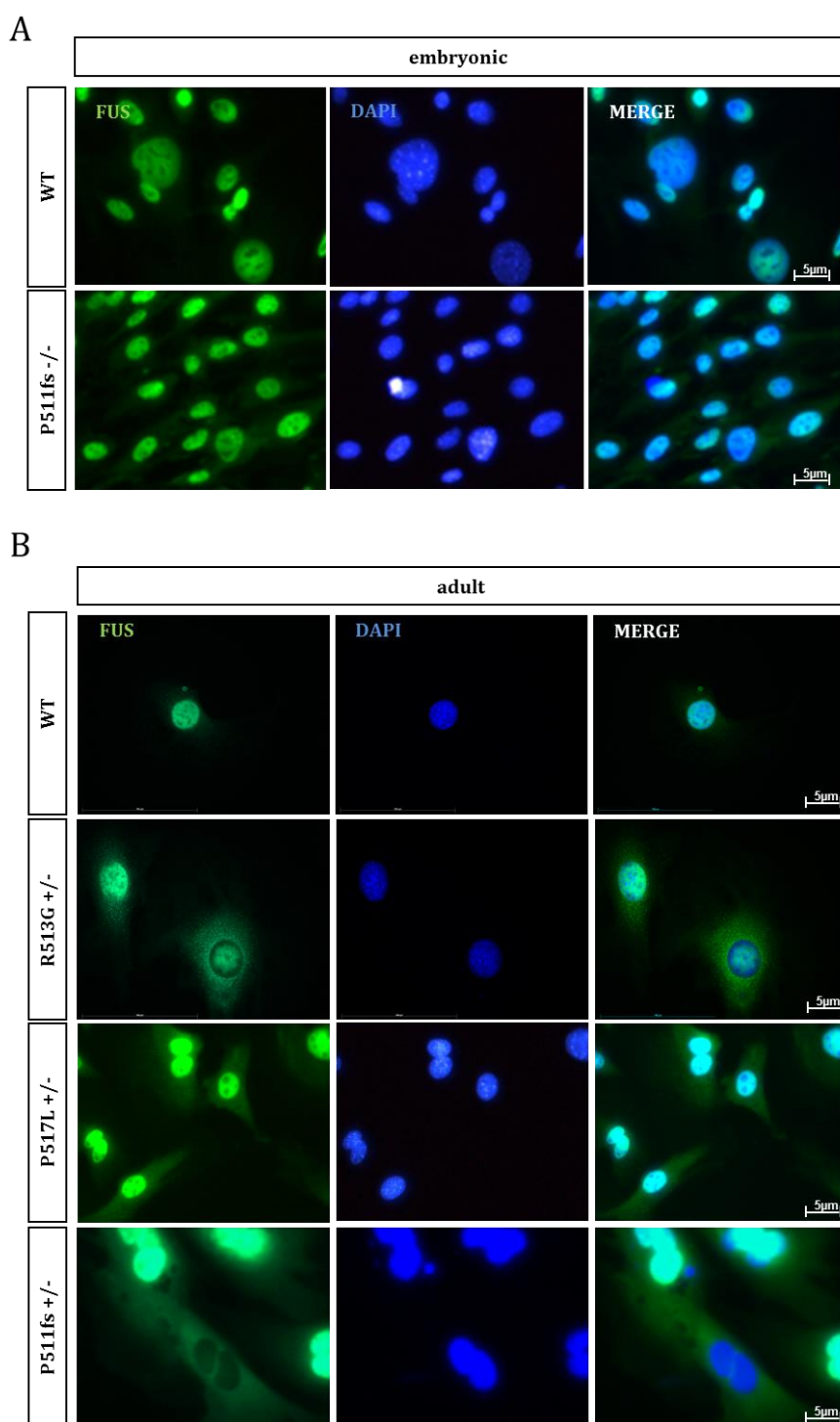


Fig. 27: Slight mislocalization of Fus in fibroblasts derived from adult TALEN mice. (A) In homozygous Fus^{P511fs} MEFs, Fus staining yielded nearly no mislocalization. (B) In fibroblasts from adult mice a slight Fus localization to the cytoplasm could be observed. Thereby, heterozygous Fus^{P511fs} cells showed the strongest cytoplasmic localization. Scale bar: 5 μ m;

In fibroblasts derived from the ear of adult heterozygous mice, a slight shift of Fus from nucleus to cytoplasm was noticed in all three TALEN mouse lines, whereas Fus^{P511fs} cells showed the highest degree of mislocalization (Fig. 27B). However, Fus was still mainly localized to the

nucleus, indicating a milder effect of mutated endogenous Fus than human FUS (for counting see supplementary data, 9.3.2.1).

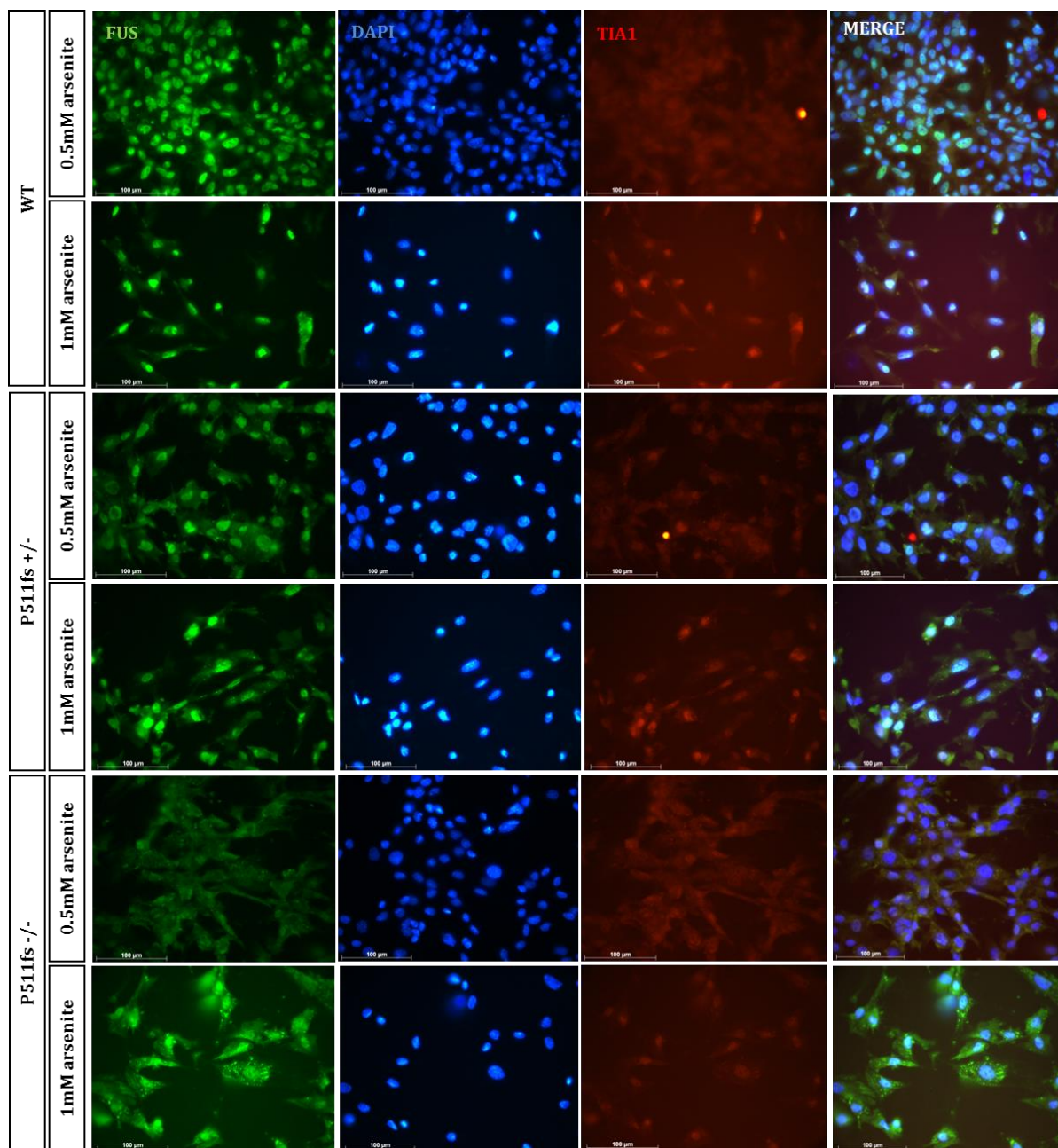


Fig. 28: Shift of Fus protein to the cytoplasm and recruitment into granules upon oxidative stress. Applying 0.5 or 1 mM sodium arsenite for 1 hour yielded a change in localization of Fus protein from nucleus to cytoplasm in MEFs derived from Fus^{P511fs} mouse line. Additionally, stress granule formation was observed and Fus was recruited into these granules, especially in homozygous Fus^{P511fs} cells. Scale bar: 100 μ m; pictures by Sudeepta Panda;

6.1.3.4 Pathological analysis of Fus TALEN mice

To investigate the effects of mutations in the murine *Fus* gene, the same experiments were performed like already described for the humanized mouse model (see chapter 6.1.2.5). Since the *Fus*^{P517L} mouse line was established later than the other two, only a few analyses were done with these mice.

First of all, a possible neuronal mislocalization of Fus protein should be analyzed. Therefore, mice were perfused, brain and SC were cut, and immunostained for Fus. As the *Fus*^{R513G} and *Fus*^{P511fs} mouse lines were available almost one year later than hFUS^{R521G} and the *Fus*^{P517L} even 1.5 years later, only young mice could be examined in this thesis. Staining of aged mice was not possible due to the time limit. Nevertheless, four months old heterozygous mice of all three TALEN lines did not exhibit any abnormalities concerning Fus localization in brain and/or SC. This was also true for a four months old homozygous *Fus*^{R513G} mouse and the single born homozygous *Fus*^{P511fs}, which was sacrificed with 1.5 months of age and used for brain and SC sections (Fig. 29B). Additionally, no inclusion formation could be detected in any of the mice. Fractionation in soluble and insoluble protein from brains of eight months old *Fus*^{R513G} mice did also not result in any differences between WT and heterozygous littermates (Fig. 29E).

Brain and SC sections were additionally stained for p62 and Ubiquitin, since these proteins were found to be colocalized in FUS inclusions (Mizuno et al., 2006; Dormann and Haass, 2013). Though, no inclusions could be found in the cytoplasm of mutant mice (Fig. 29C, D). Further, a marker for DNA damage, γ H₂AX, did not yield any conspicuousness, nor did Nissl staining or staining for neurons in general by NeuN or neuroinflammation by Gfap (data not shown; for Western Blot see Fig. 31). A Western Blot for γ H₂AX from brain and SC of seven months old mice with lung and testis as a control confirmed this finding (Fig. 29F). Strikingly, for *Fus*^{P517L} mice, no band was detected in brain or SC lysates, but in lung. This could be a hint towards enhanced lethality in this line (Tab. 10).

Since these results were not really promising concerning features of ALS and FTLD and due to lack of time, from this point on only *Fus*^{R513G} mice were further analyzed in order to compare them with hFUS^{R521G} mice.

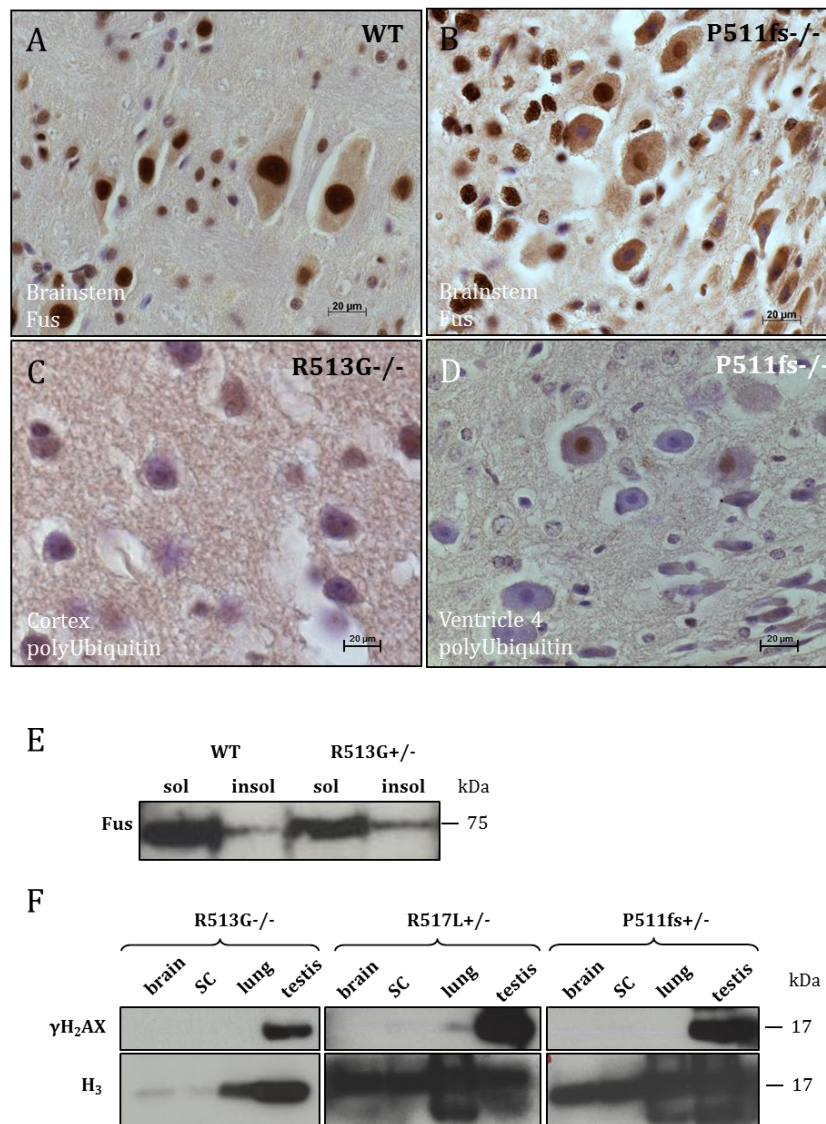


Fig. 29: No inclusion formation, insoluble Fus, or DNA damage in Fus TALEN mice. (A, B) Example for Fus-immunostainings of the brainstem from a 1.5 months old mouse, being homozygous for the most severe mutation P511fs, and a WT control. No differences could be observed concerning Fus localization between WT (A) and mutant (B) mouse. Scale bar: 20 μ m; (C, D) Exemplary immunostaining of mutant brains for polyUbiquitin. No inclusions could be found in a four months old homozygous Fus^{R513G} (C) or a 1.5 months old homozygous Fus^{P511fs} mouse (D). Scale bar: 20 μ m; (E) Exemplary Western Blot for Fus with soluble and insoluble brain lysates. No differences could be observed between an eight months old Fus^{R513G} mouse and a WT littermate. (F) Western Blot for γ H₂AX from protein lysates of brain, SC, lung, and testis purified from seven months old TALEN mice. No signal indicating DNA damage could be detected in the brain or SC. H₃ served as a loading and protein from testis and lung as positive and negative controls.

Loss of motor neurons is a typical feature of ALS. Staining for the neuronal marker NeuN of brain and SC sections from 4 months old Fus^{R513G} mice did not yield changes between WT and mutants (data not shown). However, also aged mice should be analyzed and motor neurons should be quantified. For this reason, 15 months old Fus^{R513G} mice were perfused, SC were prepared, and cut in 40 μ m sections from vertebra C2 on. Furthermore, sections were stained with motor neuron marker Hsp27 (Plumier et al., 1997) and motor neurons innervating the fore-paw

muscles were counted blindly (Fig. 30). No degeneration of motor neurons could be observed in heterozygous animals compared to WT, whereas homozygous littermates showed a trend towards fewer motor neurons, in average 3.5 per section, what was not significant due to the small number of available aged mice (Fig. 30E). Additionally, one of the two examined homozygotes exhibited a swelling of nuclei, which indicates cell death, as swelling was found in premature aged cells (Kobayashi et al., 2008). Enlarged nuclei, identified by shrunken stained cytoplasm, where Hsp27 is expressed, were particularly detected in those regions where a lot of motor neurons were located (Fig. 30D). Other motor neurons looked as if the cell body was already destroyed. There was no clear boundary obvious between the compartments (Fig. 30C).

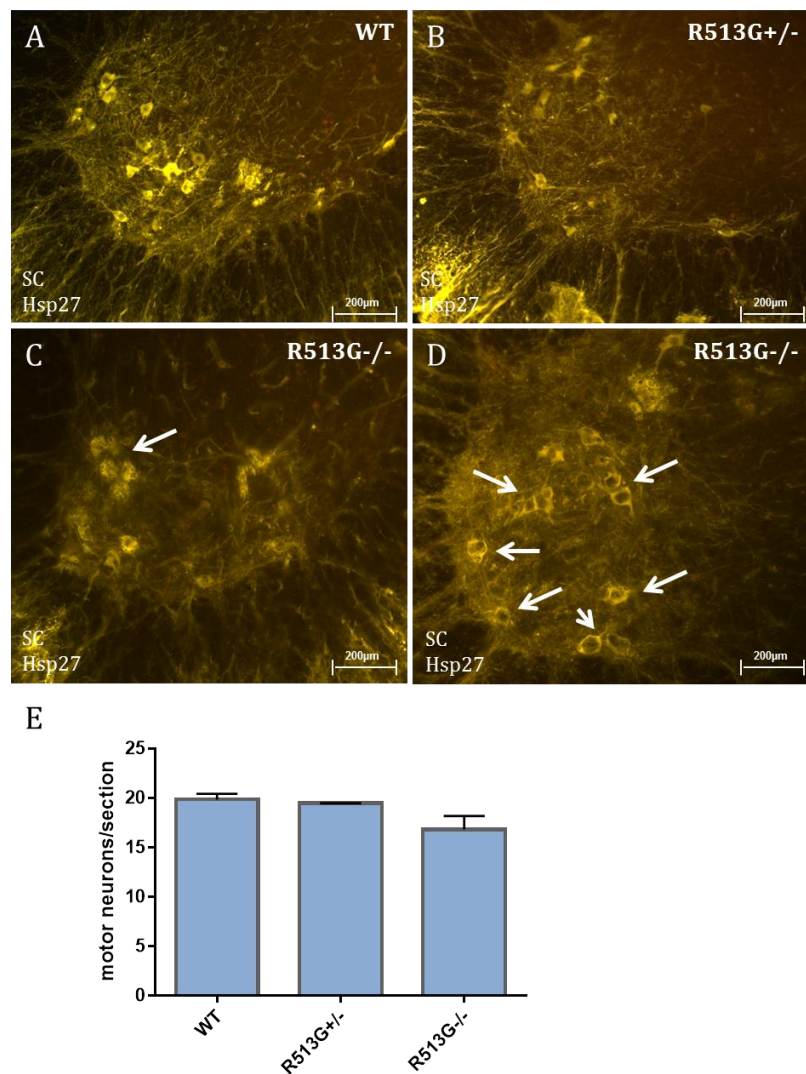


Fig. 30: Tendency of motor neuron degeneration in the cervical SC of $Fus^{R513G-/-}$ mice. Examples of Hsp27 staining of SCs from WT (A), heterozygous (B) and homozygous (C, D) mice. One homozygote exhibited damaged cell structure (C) and swollen nuclei (D). (E) Blind counting of motor neurons yielded a trend towards fewer neurons in homozygotes. (Error bars represent S.D.. One-way ANOVA was performed. $n=2/genotype$; $p=0.07$;) scale bar: 200 μ m;

To check, whether this reduced amount of motor neurons could be due to apoptosis or neuroinflammation, AIF and Gfap levels were examined via Western Blot from brain and SC lysates of 15 months old mice (Fig. 31A). In both tissues, an increase of AIF could be detected in heterozygous *Fus*^{R513G} mice and, to a greater extent, in homozygotes: in the SC protein levels were enhanced by 42% and 70% respectively and in the brain they were more than doubled (Fig. 31A, B), whereas Gfap levels were unchanged in the SC (Fig. 31A, D). In the brain even less Gfap was observed, which did not reach statistical significance due to high variation in WT controls (Fig. 31A, D). Amounts of p62 protein, an autophagy marker (Rusten and Stenmark, 2010), were also determined in Western Blot and again, an increase could be detected in SC, which was significant for homozygous mice (58%), when quantified in relation to the loading control. Brain levels were not changed (Fig. 31A, C).

Western Blot for *Fus* from brain and SC lysates of 15 months old *Fus*^{R513G} mice yielded significant higher *Fus* levels in the SC, more than double in heterozygotes and nearly the fourfold in homozygotes, pointing towards an aggregation of *Fus* (Fig. 32A, B). In brain lysates, *Fus* levels were unchanged, apart from one homozygote, which had very sparse protein (Fig. 32A, B). Investigation of the methylation status of *Fus* in the brain and SC gave contrary outcomes: in mutant brain, levels of Me*Fus* relative to total *Fus* were increased compared to WT, whereas in SC there was a significant decrease (Fig. 32A, C). In embryos, levels of *Fus* were enhanced in heterozygotes as well as homozygotes by 15.1% and 13.3% respectively compared to a WT littermate (Fig. 32D, E), whereas methylation of *Fus* was decreased to 75.9% and 91.6% (Fig. 32D, F), indicating a compensation of the mutation as in h*Fus*^{R521G} embryos (see chapter 6.1.2.5).

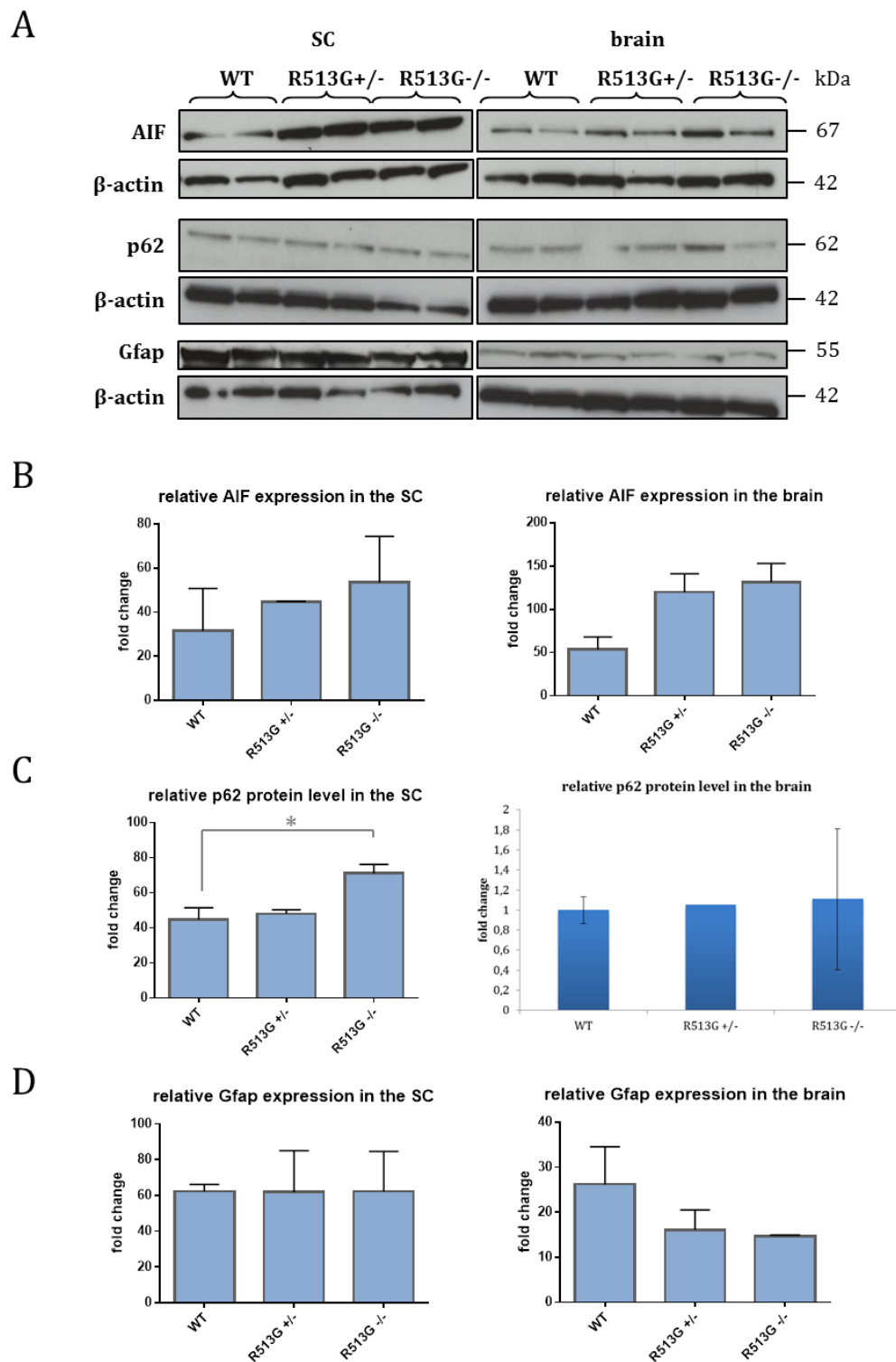


Fig. 31: Enhanced levels of p62 and AIF in the SC of 15 months old homozygous *Fus*^{R513G} mice. (A) Western Blot of brain and SC lysates from 15 months old *Fus*^{R513G} mice and WT controls with the corresponding loading controls (β -actin). Used antibodies are indicated. (B-D) Quantification of Western Blots (A) in relation to the loading control; Error bars represent S.D.. One-way ANOVA was performed. n/genotype=2; (B) AIF levels were tendentially elevated in SC and brain of mutant mice. (C) Enhanced levels of p62 in the SC of homozygotes ($p=0.02$) were measured, but not in the brain. Concerning brain analysis, the first heterozygous mouse could not be elevated due to a bleb and therefore, Student's t-test was performed. (D) No alterations could be observed concerning Gfap levels in the SC. In the brain, levels were tendentially decreased.

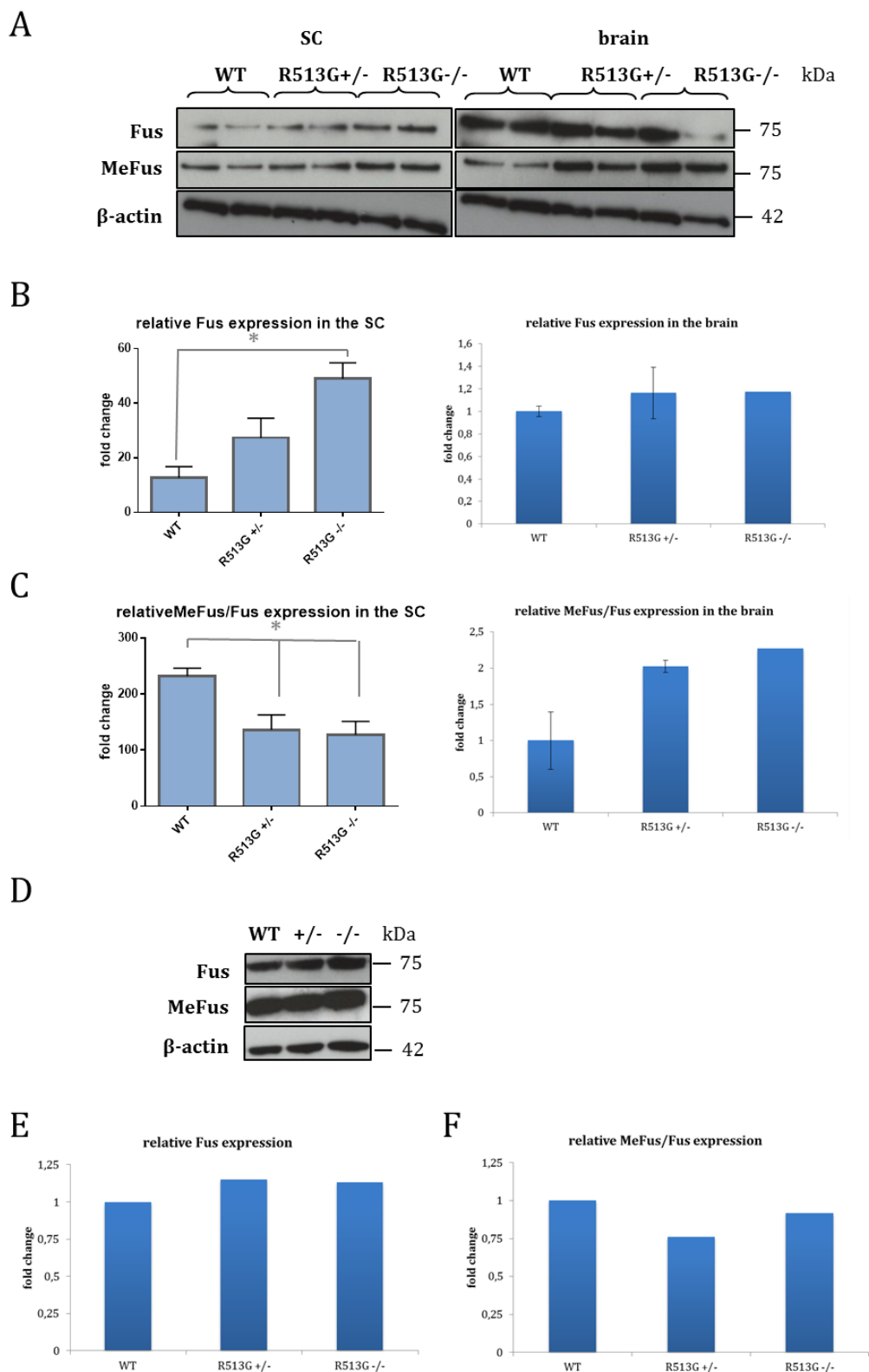


Fig. 32: Accumulation of Fus in the SC of adult Fus^{R513G} mice and decreased Fus methylation in embryos. (A) Western Blot of brain and SC lysates from 15 months old Fus^{R513G} mice and WT controls. Used antibodies are indicated. (B, C) Quantification of Western Blots (A) in relation to the loading control (B) or to Fus (C). Error bars represent S.D.. One-way ANOVA was performed (SC). $n/genotype=2$; Concerning brain analysis, the second homozygous mouse was not considered due to a bleb and Student's t-test was performed. (B) Fus levels were dramatically higher in SC of homozygotes ($p<0.02$) and less in brain ($p=0.4$). (C) Investigation of methylation status revealed opposing results: in the SC there was significant less methylation in both heterozygotes and homozygotes

($p_{het}=0.04$; $p_{hom}=0.03$), whereas in the brain methylation was increased ($p=0.07$). (D) Exemplary Western Blot of head lysates from E14.5 embryos. Used antibodies are indicated. (E, F) Quantification of Western Blots (D) in relation to the loading control (E) or Fus (F); $n/genotype=1$ due to distribution in litter. Total Fus levels were increased (E), whereas methylation of Fus was decreased (F).

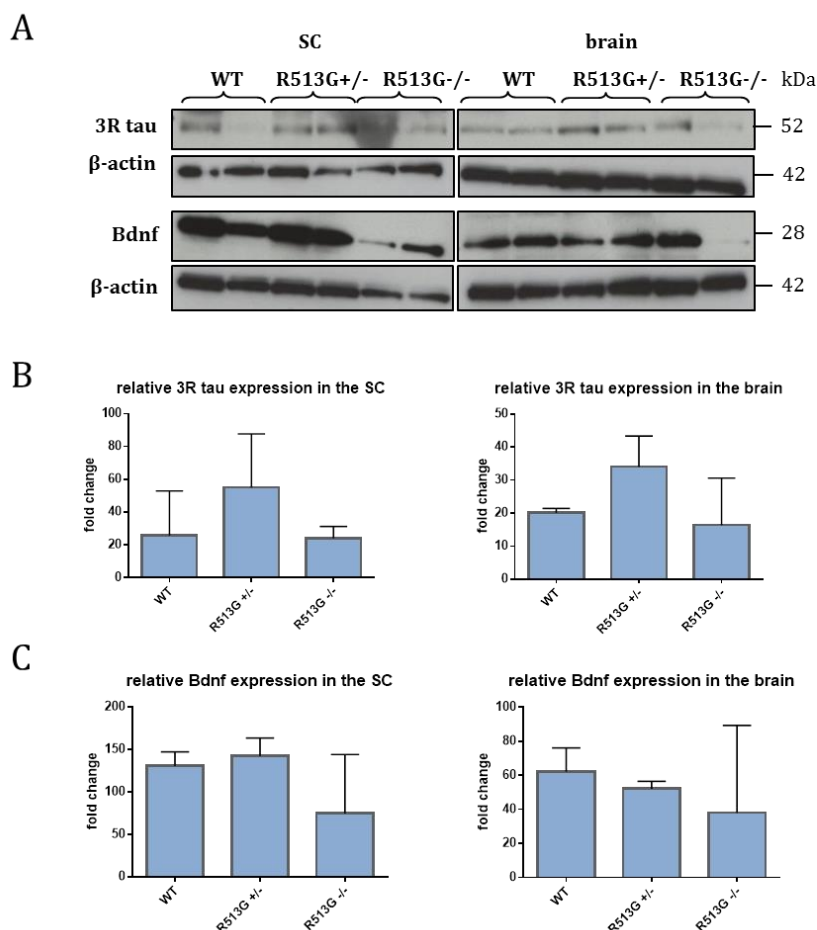


Fig. 33: Hints towards changed levels of Fus splicing targets in Fus^{R513G} mice. (A) Western Blot of brain and SC lysates from 15 months old Fus^{R513G} mice and WT controls with the corresponding loading controls (β -actin). Used antibodies are indicated. (B-C) Quantification of Western Blots (A) in relation to the loading control; Error bars represent S.D.. One-way ANOVA was performed. $n/genotype=2$; Levels of 3R tau (B) and Bdnf (C) were tendentially changed. However, due to high deviation, differences did not reach significance.

Bdnf was found to be a splicing target of Fus and to play a role in dendritic growth and synapse formation. Overexpression of hR521G mutation in rodents led to decreased levels of Bdnf protein (Qiu et al., 2014). Western Blot revealed a tendency towards decreased levels in brain and SC, especially of homozygous Fus^{R513G} mice, though with a high deviation (Fig. 33A, C). Levels of 3R tau, another splicing target of Fus (Orozco et al., 2012), were tendentially elevated in heterozygotes and reached again WT niveau in homozygotes. However, levels were very inhomogenous (Fig. 33A, B). It was striking, that for both splicing targets very low protein levels were observed in the brain of exactly that homozygote, which also had very low Fus levels in the

brain (Fig. 32), supporting their role as splicing targets. In Fig. 32 and 33, different blots are shown, so that it could not be a loading or blotting problem. Additionally, the loading control did not reveal less amounts of loaded protein.

6.1.3.5 Phenotypical analysis of $Fus^{R513G+/-}$ mice

For phenotypical analysis, only heterozygous Fus^{R513G} mice were tested in the GMC in order to compare the results with those of the corresponding humanized mouse line (see chapter 6.1.2.6). Due to unavailability of a comparable number of age matched WT (and also homozygous) littermates, controls from the hFUS^{R521G} cohort were used for calculations. Hence, the analyzed cohort consisted of seven heterozygous males and eleven females, and one male and four female Fus^{R513G} WT controls. Together with the hFUS^{R521G} controls, eight male and 14 female controls were evaluated (Tab. 11). Mice looked healthy and agile. Compared to the matched controls, heterozygous Fus^{R513G} mice were heavier, especially females (Fig. 34A).

Tab. 11: Summary of behavioral analyses of Fus^{R513G} mice in the German Mouse Clinic.

Behavior test	Parameter measured	Fus^{R513G} 8 WT M/7 het M/14 WT F/11 het F	
		Age (months)	Result
SHIRPA (Fig. 34B)	General health and autonomous functions, reflexes, locomotor activity, posture and movement	6	n.d.
Grip Strength (Fig. 34C)	Muscle function	6	n.d.
Rotarod (Fig. 34D)	Coordination and balance	6.5	n.d.
Balance Beam	Motor coordination and balance	6.5	n.d.
Beam Ladder (Fig. 34E, F)	Motor coordination	6.5	Less hindpaw slips, slightly less traversing time; no differences in stops

Inverted Grid	Sensorimotor function	7.5	n.d.
Open field	Locomotion (Fig. 35A)	9	Spontaneous activity ↑ males ↓ females (p=0.003)
	Exploration (Fig. 35B)	9	Increased rearing activity (p=0.03)
	Anxiety-related (Fig. 35C)	9	Time spent in center ↑ males ↓ females (p=0.003)
Balance Beam 2 nd time (Fig. 34G)	Motor coordination and balance	9	Slightly less time and less slips
Inverted Grid 2 nd time	Sensorimotor function	12.5	trend to reduced lastencies
Grip Strength 2 nd time	Muscle function	12.5	n.d.
Y maze (Fig. 35D)	Working memory	13	Trend towards more spontaneous alterations in males
Social discrimination (Fig. 35E)	Olfaction-based social memory/discrimination	13.5	Trend towards more social discrimination in males

n.d., no difference; het, heterozygous; hom, homozygous; F, female; M, male; in red: significant

In terms of grip strength (Fig. 34C) and all motoric and balance based challenges, like Inverted Grid (Supplementary Data, chapter 9.3.2.2), Balance Beam (data not shown), or Rotarod (Fig. 34D), no clear genotype effects could be detected in six to 7.5 months old mice (Tab. 11). In the Beam Ladder test, even a tendency towards less hindpaw slips (Fig. 34E) and slightly less traversing time (Fig. 34F) was noticed, but no difference in stops. A repetition of Balance Beam and Inverted Grid with the same cohort at an age of nine and 12.5 months respectively yielded a trend to slightly less time (Fig. 34G) and less slips in the Beam and to reduced lastencies in Inverted Grid (Supplementary Data, chapter 9.3.2.2).

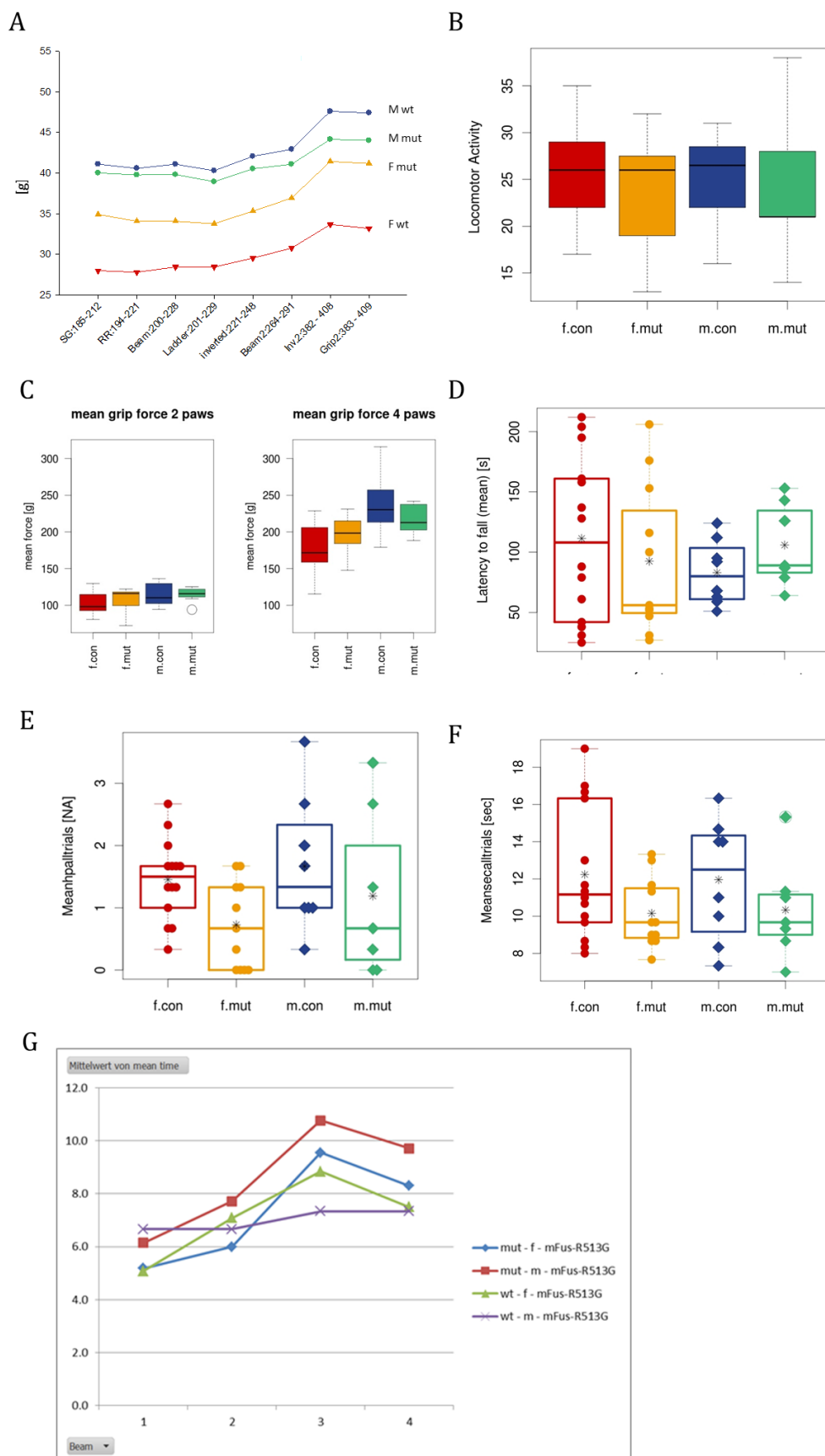


Fig. 34: *Fus*^{R513G} mice did not show any impairments in muscle function or motor coordination. (A) During the different tests, mutants were always heavier than WT controls. Ages (days) are depicted. (B-G) SHIRPA (B), Grip

Strength (C), Rotarod (D), Beam Ladder (E, F), and Balance Beam (G) yielded no significant genotype specific differences in activity, muscle function, or motor coordination. In the Beam Ladder test, mutants showed a tendency towards less hindpaw slips (E) and slightly less traversing time (F). (Error bars represent S.E.M. Two-way ANOVA was performed. n(WT F)=14; n(het F)=11; n(WT M)=8; n(het M)=7;) Graphs by Lore Becker;

Assessment of activity revealed no differences in SHIRPA (Fig. 34B). However, in the Open Field male heterozygotes showed an increase in total distance travelled, whereas females did the opposite (Fig. 35A). Furthermore, total rearing activity was enhanced in both sexes (Fig. 35B). Referring to anxiety-related behavior, also determined by the Open Field, male TALEN mice spent more time in the center, whereas females spent less (Fig. 35C). Working (Fig. 35D) and social memory challenges (Fig. 35E) did not result in any genotype specific behavior.

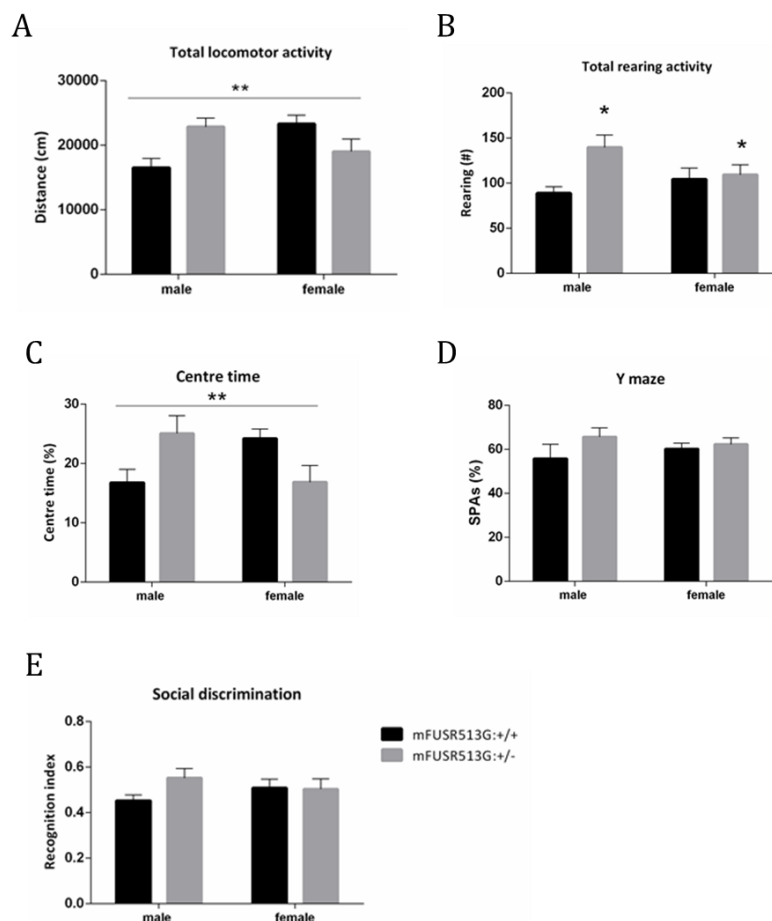


Fig. 35: Sex specific behavior concerning activity and anxiety in Fus^{R513G} mice. (A) Sex specific change in locomotor activity. Males travelled more distance, whereas females did less. $p=0.003$; (B) Regarding exploratory activity, both sexes showed an increase in rearing activity. $p=0.03$; (C) Testing anxiety-related behavior, again males spent more time in the central zone, whereas females did less. $p=0.003$; (D) Y-maze for testing working memory did not yield significant changes between genotypes. (E) The same was observed concerning social discrimination. In the olfaction-based social memory test, males showed tendentially more social discrimination. (Error bars represent S.E.M. Two-way ANOVA was performed. n(mFUSR513G^{+/+} female)=14; n(mFUSR513G^{+/-} female)=11; n(mFUSR513G^{+/+} male)=8; n(mFUSR513G^{+/-} male)=7;) mFUSR513G^{+/+} =WT; Graphs by Lillian Garrett;

6.2 *TMEM106B* MOUSE MODELS

Elevated levels of *TMEM106B* have been reported from FTLD-TDP patients (Van Deerlin et al., 2010; Chen-Plotkin et al., 2012). In order to model the effects of an enhanced *TMEM106B* expression *in vivo*, transgenic mice were generated and crossed with a model carrying the ALS-associated *TARDBP* mutation A315T.

6.2.1 *TRANSGENIC OVEREXPRESSION OF TMEM106B IN VIVO*

6.2.1.1 Generation of *Tmem106b* transgenic mice

Using a bacterial artificial chromosome (BAC), mice should be generated carrying additional *Tmem106b* gene copies (*Tmem106b*^x^{BAC}_{tg}, whereas “x” depicts the **additional** copy number). For this purpose the BAC clone bMQ263o13, containing a 131 kb Sv129 mouse genomic fragment including *Tmem106b*, was purchased from Source BioScience Life Sciences (Fig. 36A). Regulatory elements of the *Tmem106b* locus still remain to be detected. To overcome this and to achieve an endogenous-like expression, approximately 85 kb upstream and 27 kb downstream of the genomic sequence of *Tmem106b* were left in the construct. No additional genes were located in this sequence apart from a processed pseudo gene without known function 13.2 kb upstream of the *Tmem106b* locus and a small nucleolar (sno) RNA gene 22 kb downstream (Fig. 36A).

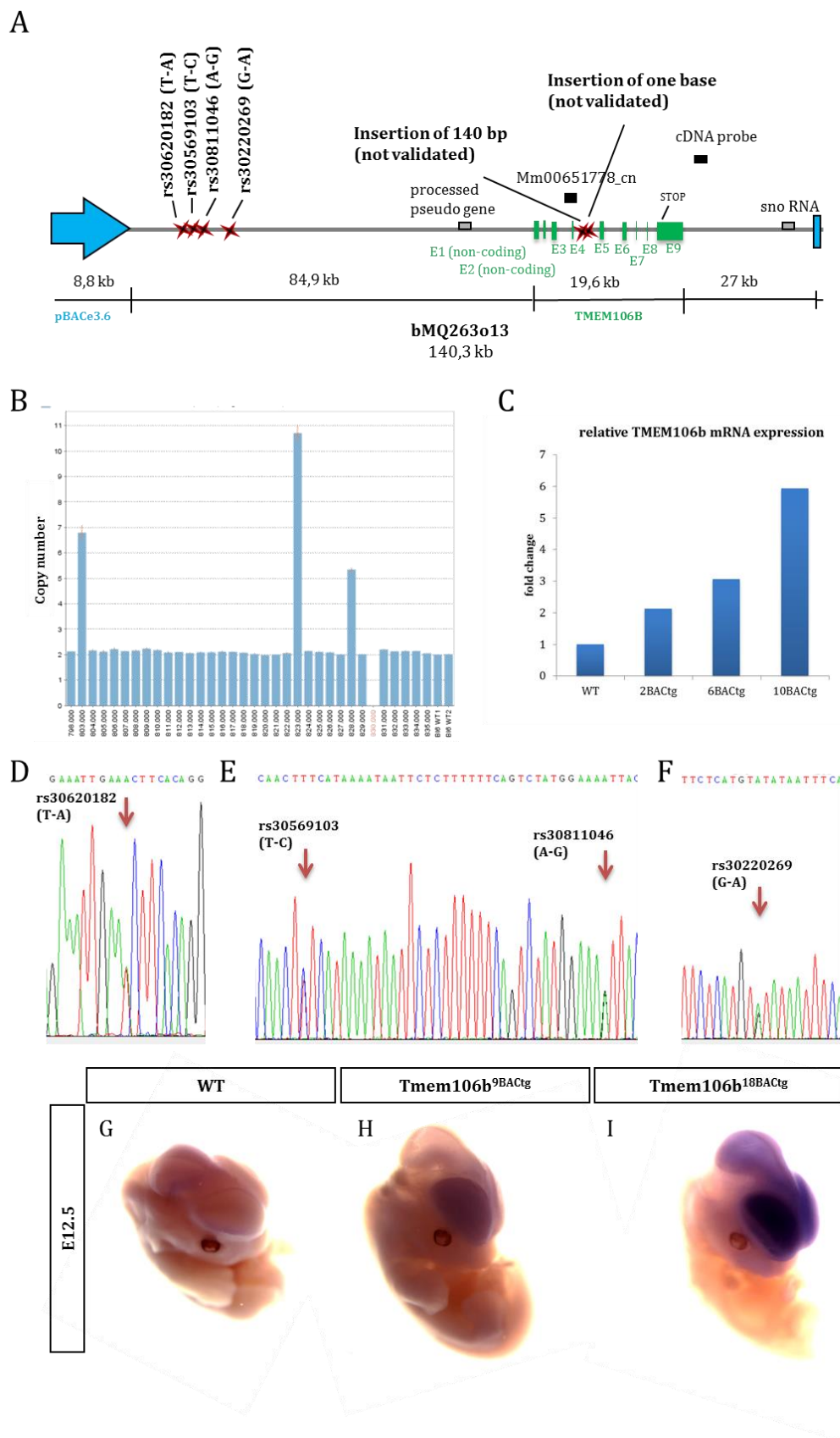


Fig. 36: Transgenic expression of *Tmem106b* in vivo. (A) Map of the 129S7AB2.2 BAC clone bMQ263o13. The 140 kb BAC consists of the pBACe3.6 backbone and a genomic Sv129 fragment containing *Tmem106b*. The plasmid was linearized and brought into a B6 background. The four Sv129-B6 SNPs rs30620182, rs30569103, rs30811046 and

rs30220269 >62kb upstream of *Tmem106b* and two insertions in the coding regions are tagged. *Tmem106b* consists of nine exons, of which exons 1 and 2 are non-coding. The first in-frame STOP codon in exon 9 is depicted. The location of the DNA probe used for *Tmem106b* genotyping is indicated. Besides the *Tmem106b* locus the plasmid contains a processed pseudo gene upstream and a snoRNA (MGI Symbol Gm24985) downstream. (B) Copy Number assay for *Tmem106b* of 34 *Tmem106b*^{BACtg} F1 and two WT control mice with the Taqman Assay Mm00651778_cn in intron 3 and exon 4 (A). Three founder mice could be identified with seven, eleven, and five copy numbers respectively. (C) qRT-PCR analysis of mRNA isolated from adult brains of a WT mouse and three transgenic mice genotyped with four, eight and twelve copies of *Tmem106b*. Compared to WT, transgenic mice showed double, three-, or six-fold *Tmem106b* expression. n/genotype=1; (D-F) SNP genotyping of the founder mouse #828 with three Sv129 sequence insertions. All four SNPs between B6 and Sv129 lying upstream of *Tmem106b* were detected. (G-I) BAC expression in an E12.5 WT embryo (G) and transgenic littermates with eleven (H) and 20 copies (I) of the gene by Whole Mount *in Situ* Hybridization. An increase of expression levels could be detected from WT over the *Tmem106b*^{9BACtg} mouse to the one with 18 additional copies.

The plasmid was purified, linearized, and injected into C57Bl6 (B6) oocytes at the MPI in Dresden (Vintersten et al., 2008) and 69 pups were born. One or more copies of the sequence could be integrated in the genome and thus an enhanced expression of *Tmem106b* should be achieved. B6 mice were chosen as recipient strain to identify possible founder mice by genotyping of SNPs that differ between Sv129 and B6 mouse strains (Fig. 36A). By sequence comparison via Ensembl database, six sequence variants were recognized: four SNPs (rs30620182, rs30569103, rs30811046, and rs30220269) >62 kb upstream of *Tmem106b* with B6 genotypes T, T, A, and G and A, C, G, and A in Sv129 mouse strain and insertions of one base and of 140 bp in Intron 4 in Sv129 mice. Since the predicted insertions in *Tmem106b* could not be validated in the BAC sequence, this was not an appropriate way for tagging positive founder mice, only for an audit, if the whole BAC sequence was integrated. For this reason, a DNA probe homologous to intron 5 was PCR-amplified, Southern Blot was performed for an initial analysis, and two mice were identified to have more than the two WT copies (data not shown). To determine the exact number of insertions a copy number assay was done (Fig. 36B). The two possible positive animals were confirmed carrying five (#803; *Tmem106b*^{5BACtg}) and nine (#823; *Tmem106b*^{9BACtg}) additional copies of *Tmem106b*. A third one was genotyped with five copies altogether (#828; *Tmem106b*^{3BACtg}). Further, this method was used for routine genotyping. As mentioned above, SNPs upstream of *Tmem106b* were genotyped to determine whether the entire Sv129 sequence was integrated. In all three founder mice Sv129 alleles could be detected (Fig. 36D-F).

6.2.1.2 Expression levels of *Tmem106b* in transgenic mice

To find out whether *Tmem106b* was expressed from the additional copies, mRNA and protein levels were determined and quantified.

Therefore, a litter of stage E12.5 was dissected and Whole Mount *in Situ* Hybridization (WISH) was performed (Fig. 36G-I). A probe binding in the coding sequence gave too much background. Therefore, a probe inside the BAC sequence, 2 kb downstream of *Tmem106b* was applied. Staining reactions were stopped simultaneously to compare a WT staining with such of *Tmem106b*^{BACtg} embryos. Transgenic embryos exhibited stronger staining than WT littermates. For instance, staining intensity increased from WT (Fig. 36G) to an embryo with eleven (Fig. 36H) and more to one with 20 copies (Fig. 36I) in a linear fashion. To further determine *Tmem106b* expression and to quantify mRNA levels, brains from adult *Tmem106b*^{BACtg} with four, eight, and twelve copies, respectively, and a WT control were used for RNA purification and following qRT-PCR with a Gene Expression Assay spanning exons 3 and 4 (Fig. 36C). Transgenic mice showed elevated expression of *Tmem106b* dependent on copy numbers.

A Western Blot with brain lysates from three months old transgenic mice, carrying ten or eleven BAC insertions, and WT littermates validated enhanced *Tmem106b* expression (Fig. 40A). Quantification revealed about eight-fold increased protein levels compared to WT controls (Fig. 40B).

6.2.1.3 Subcellular localization of TDP-43 in *Tmem106b*^{BACtg} mice

Since *TMEM106B* was elevated in brains of FTL-D-TDP patients (Van Deerlin et al., 2010; van der Zee et al., 2011) and FTL-D-TDP is characterized by nuclear clearance and cytoplasmic protein inclusions containing ubiquitinated TDP-43 (Neumann et al., 2006; Mackenzie et al., 2010), the effects of ectopic *Tmem106b* expression on TDP-43 localization in neurons and/or glial cells should be investigated. For this reason, brain and SC of eight months old *Tmem106b*^{BACtg} mice were prepared, fixed, and cut for immunostaining. In the motorcortex and cerebellum, predominantly of those mice with a high number of *Tmem106b* copies, mislocalized TDP-43 could be detected in the cytoplasm. However, no TDP-43 positive inclusions were observed (Fig. 37).

Western Blot for TDP-43 with brain lysates of three months old mice with twelve or 13 *Tmem106b* copies altogether (Fig. 40A) revealed a significant decrease in TDP-43 protein levels to about 70.8% compared to WT littermates (Fig. 40D).

Further analysis regarding effects on GRN, C9orf72, or endo-/lysosomal proteins are presented in chapter 6.2.2.

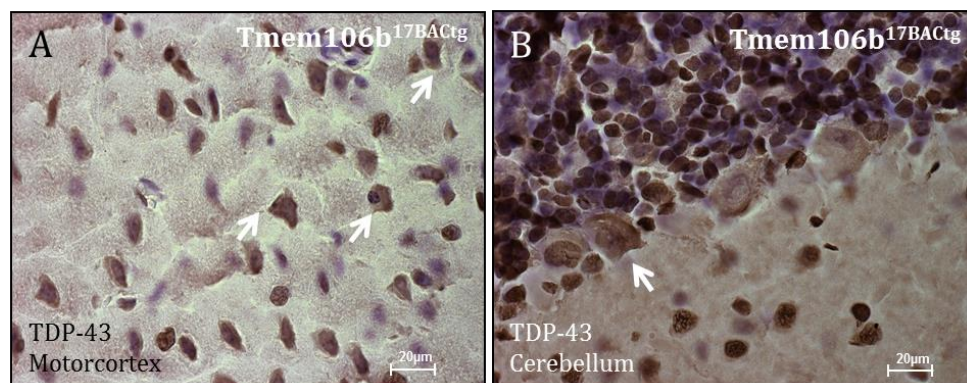


Fig. 37: Cytoplasmic TDP-43 in eight months old *Tmem106b*^{17BACtg} mouse. Immunostaining for TDP-43 yielded occasional mislocalization in cells of the motorcortex (A) and cerebellum (B), but no TDP-43 inclusions. Scale bar: 20 μ m

6.2.1.4 TEM analysis of *Tmem106b*^{BACtg} mice

As an endo-/lysosomal protein, TMEM106b was reported to regulate lysosomal size, morphology, migration, trafficking, and function (Brady et al., 2013; Schwenk et al., 2014; Stagi et al., 2014). That is why Transmission Electron Microscopy (TEM) was performed on sections from cerebellum and frontal cortex of transgenic mice by the pathological institute (Fig. 38). Though, no differences were observed in terms of lysosomal morphology between 17 months old *Tmem106b*^{BACtg} mice carrying 13 or 20 copies of *Tmem106b* and a WT littermate (Fig. 38A-C). Instead, considerable abnormalities were found regarding mitochondria, both in cerebellum and more in the frontal cortex of transgenic mice compared to WT control. This blebbing of mitochondria was obvious in myelinated (Fig. 38E-G), as well as unmyelinated neurons (Fig. 38H-J) of the frontal cortex. Moreover, no increase of abnormal mitochondria could be detected between the mouse with 13 (Fig. 38F, I) and the one with 20 copies (Fig. 38G, J).

Further analysis regarding effects on mitochondrial proteins are presented in chapter 6.2.2.

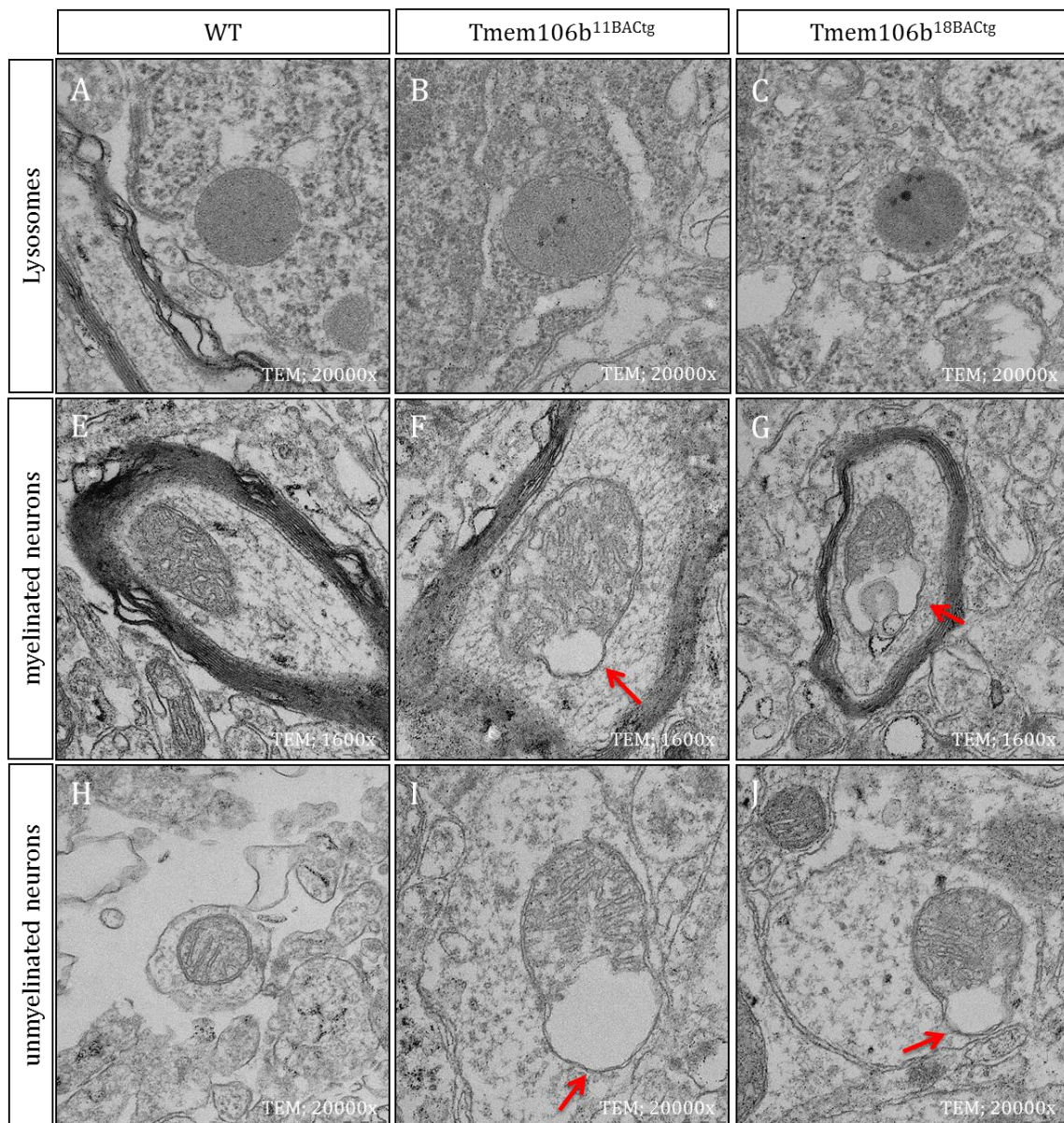


Fig. 38: Blebbing of mitochondria in the frontal cortex of Tmem106b^{BACtg} mice. Transmission Electron Microscopy of lysosomes (A-C), myelinated (E-G), and unmyelinated neurons (H-J) of the frontal cortex of 17 months old transgenic mice carrying eleven or 18 BAC copies and a WT littermate. No changes concerning morphology or size could be observed in lysosomes. However, compared to WT control, transgenic mice showed a blebbing of mitochondria of both, myelinated and unmyelinated neurons. Magnification: 20000x; Pictures by Michaela Aichler;

6.2.2 OVEREXPRESSION OF *TMEM106B* ON A MUTANT *HTDP-43^{A315TKi}* BACKGROUND

Recently, it was demonstrated that overexpression of human TDP-43^{A315T} in mice (hTDP-43^{A315TKi}) led to reduced body weight, mitochondrial dysfunction, insoluble TDP-43 protein, and a decrease in number of motor neurons (Stribl et al., 2014). To further analyze a possible role of *TMEM106B* in the development of FTL-D-TDP, hTDP-43^{A315TKi} mice and *Tmem106b^{BACtg}* mice were intercrossed and studied concerning TDP-43 localization and influence on Grn, C9orf72, mitochondria, and endo-/lysosomal proteins.

First, *Tmem106b* levels were determined in double transgenic mice by Western Blot (Fig. 40A, B). In total brain lysates of three months old mice, *Tmem106b* protein levels were decreased compared to those of *Tmem106b^{BACtg}* littermates considering different copy numbers. Quantification yielded in average an eight-fold elevated *Tmem106b* level in *Tmem106b^{BACtg}* mice with ten or eleven additional copies (see also chapter 6.2.1.2), but only a six-fold increase in compound mutants with eight, eleven, or twelve additional copies. However, this did not reach statistical significance (student's t-test: $p=0.06$). Protein levels in hTDP-43^{A315TKi} mice were comparable to those of WT littermates (Fig. 40A, B).

6.2.2.1 Effects of ectopic *Tmem106b* levels on TDP-43

To analyze the effects of enhanced *Tmem106b* expression on TDP-43 localization also on the hTDP-43^{A315TKi} background, immunostaining was performed on brain and SC sections of two months old compound mice using a human-specific monoclonal antibody for TDP-43 (Fig. 39). Occasionally, cytoplasmic mislocalization, but no inclusion formation could be found in cortical cells (Fig. 39C) and in motor neurons of the SC (Fig. 39B). In *Tmem106b^{BACtg}* (total TDP-43 antibody; data not shown) and hTDP-43^{A315TKi} (Fig. 39A) animals of this age, higher amounts of cytoplasmic TDP-43 could not be observed. Additionally, Western Blot with soluble and insoluble protein fractions of about 3 months old single and compound mice yielded no insoluble total TDP-43, but insoluble human TDP-43 in hTDP-43^{A315TKi} and compound animals due to overexpression (Fig. 39D). This corresponds to the results for the hTDP-43^{A315TKi} mouse line (Stribl et al., 2014). Heterozygotes displayed high amounts of insoluble total TDP-43 at the age of 12 months.

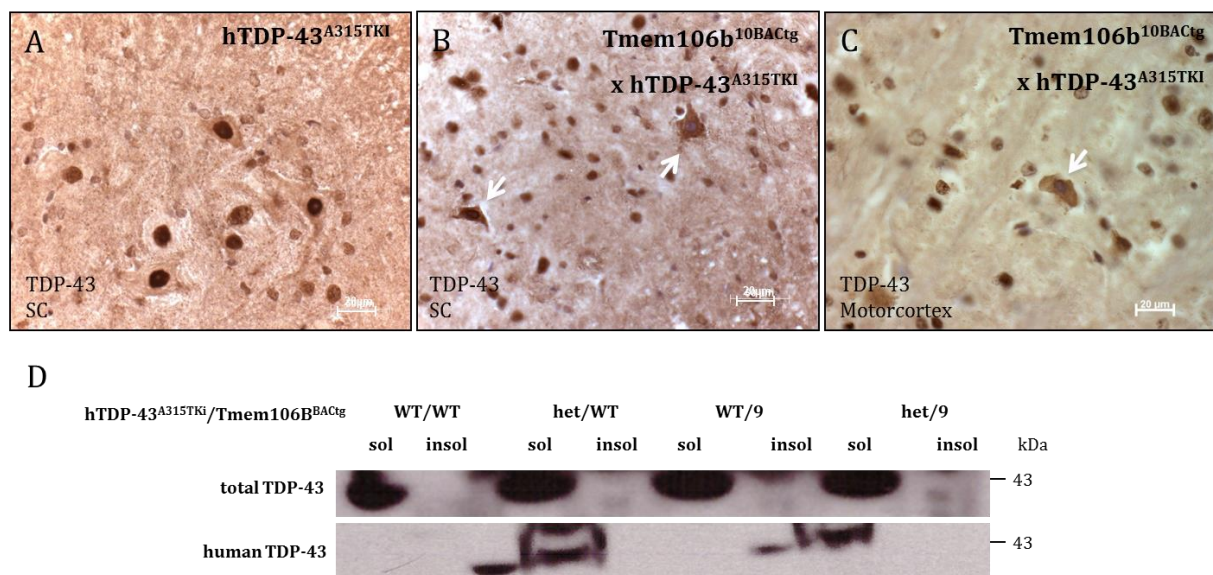
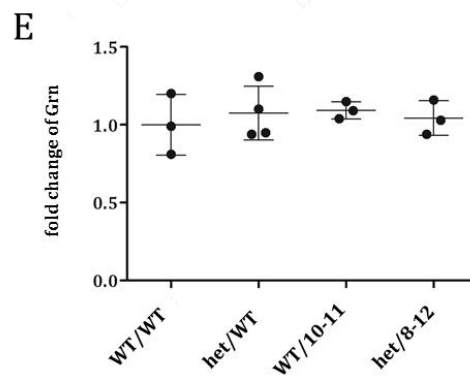
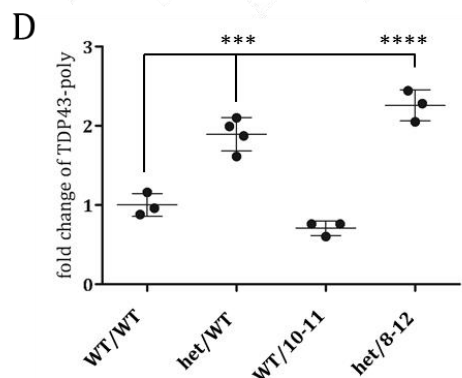
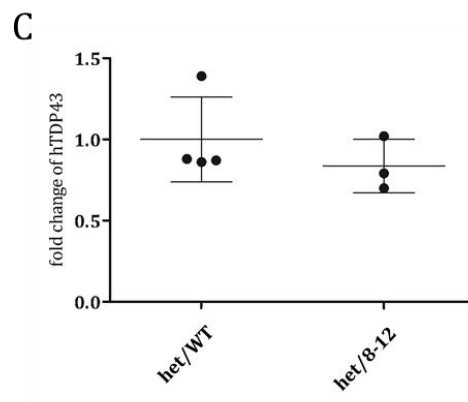
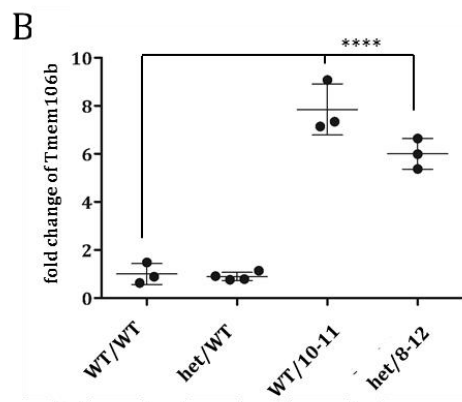
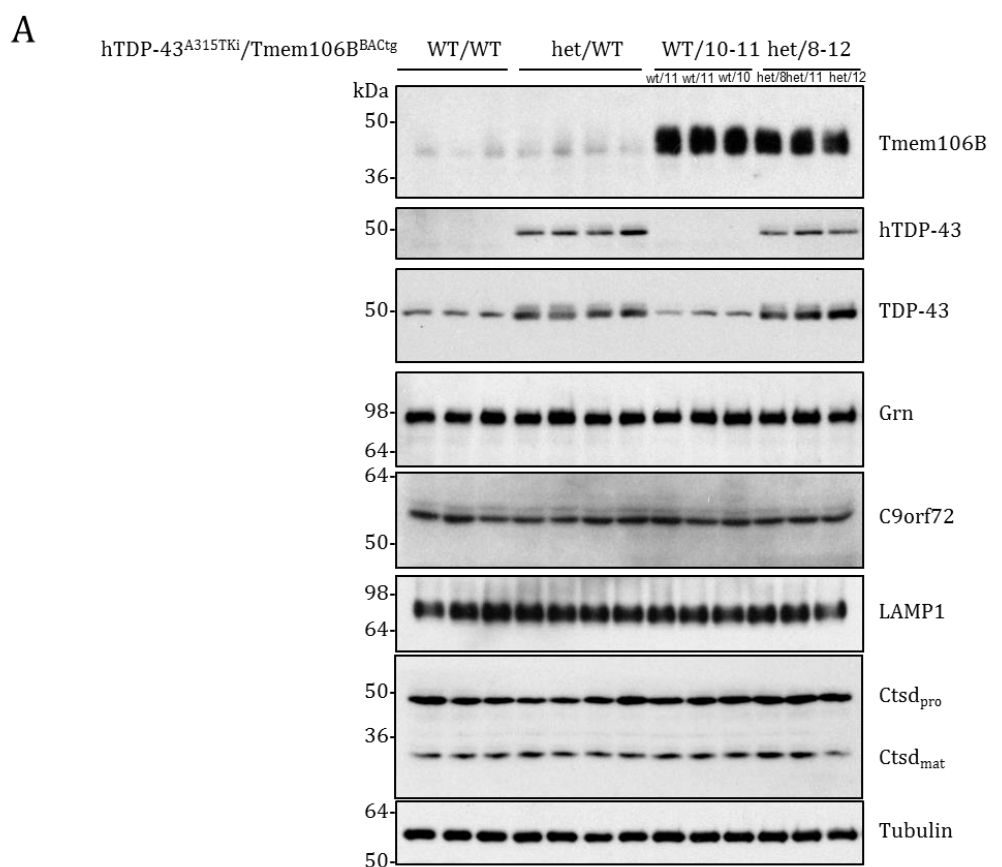


Fig. 39: Cytoplasmic hTDP-43 in *Tmem106b*^{BACtg} and hTDP-43^{A315TKi} compound mice, but no inclusion formation. Immunostaining for hTDP-43 revealed no mislocalization in the SC of a two months old hTDP-43^{A315TKi} animal (A). In compound littermates, cytoplasmic hTDP-43 could be detected in motor neurons of the SC (B) and in cortical cells (C), but no inclusion formation. Scale bar: 20 μ m; (D) Insoluble human TDP-43 could be detected in brain lysates of about three months old hTDP-43^{A315TKi} or compound mutant mice. sol, soluble; insol, insoluble;

Quantification of TDP-43 by Western Blot yielded a significant decrease in *Tmem106b*^{BACtg} mice with ten or eleven additional *Tmem106b* copies to about 70.8% compared to WT littermates (see also chapter 6.2.1.3). Concerning total TDP-43 protein levels, hTDP-43^{A315TKi} mice showed about twice as much in total brain lysates compared to WT controls as described before (Stribl et al., 2014) (Fig. 40A, D). Three months old compound littermates carrying eight, eleven, or twelve additional copies of the transgene displayed even a higher increase: compared to WT, TDP-43 levels were elevated to a value of 2.3 in average (Fig. 40A, D). hTDP-43 could only be detected in hTDP-43^{A315TKi} and compound mice as expected, not in WT or *Tmem106b*^{BACtg} littermates (Fig. 40A, C). Thereby, levels in compound mutant mice appeared to be a bit decreased, but not significantly.



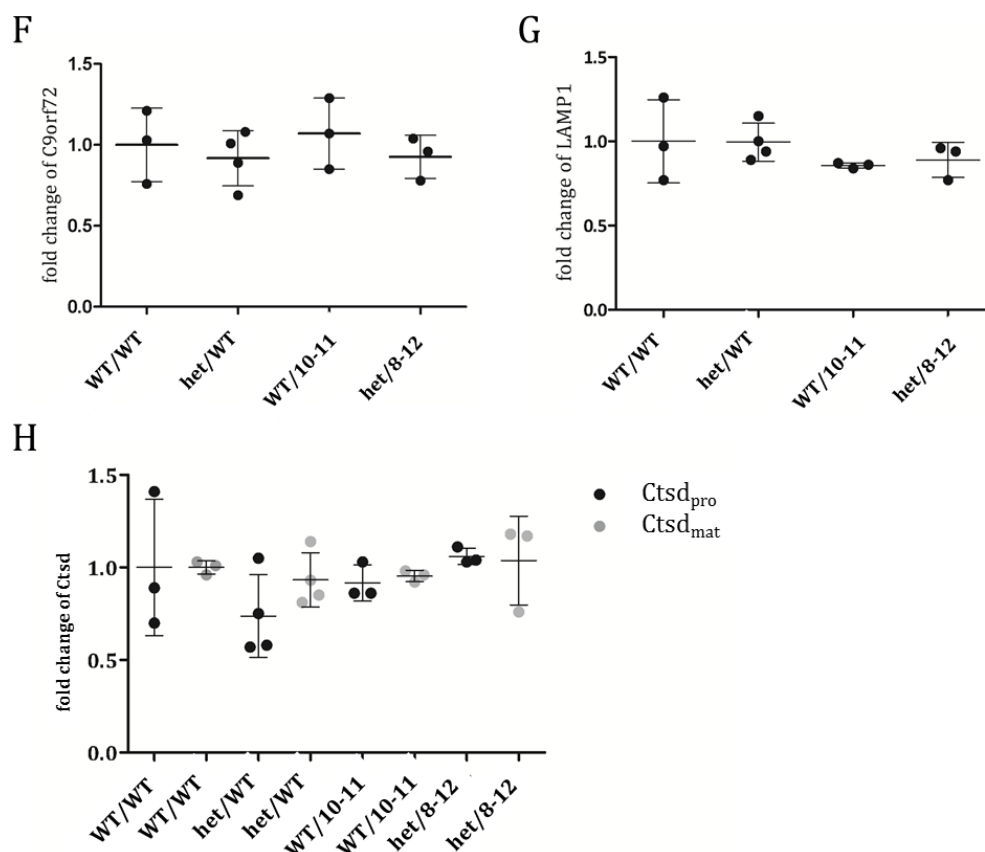


Fig. 40: Elevated levels of total TDP-43, but no changes in Grn, C9orf72, or endo-/lysosomal protein levels upon ectopic Tmem106b expression. (A) Western Blot from total brain lysates of three months old WT, hTDP-43^{A315TKi}, Tmem106b^{BACtg} carrying ten or eleven additional copies of *Tmem106b*, and compound mice with eight to twelve additional copies. Used antibodies are indicated. (B-H) Quantification of (A); Error bars represent S.D.. One-way ANOVA was performed (Except for hTDP-43: Student's t-test;). n(WT; WT/10-11; het/8-12)=3; n(het/WT)=4; Compared to WT and hTDP-43^{A315TKi} mice, Tmem106b^{BACtg} and compound animals showed a six- to eight-fold increase of Tmem106b levels corresponding to the copy number ($p_1=1.0$; $p_2<0.0001$; $p_3<0.0001$;) (B). hTDP-43 was only detected in hTDP-43^{A315TKi} and compound mice (C), whereas total TDP-43 levels were elevated in these animals due to overexpression of hTDP-43^{A315T} ($p_1=0.0002$; $p_2=0.2$; $p_3<0.0001$;) (D). No genotype specific changes could be observed regarding Grn (E), C9orf72 (F), LAMP1 (G), and Cathepsin D (H) protein levels. Graphs by Julia Götzl;

6.2.2.2 Effects of ectopic Tmem106b on protein levels

With respect to a possible interaction of TMEM106b and GRN (Van Deerlin et al., 2010; Cruchaga et al., 2011; Finch et al., 2011; van der Zee et al., 2011; Chen-Plotkin et al., 2012; Lang et al., 2012; Brady et al., 2013; Busch et al., 2013; Nicholson et al., 2013; Gotz et al., 2014; Lattante et al., 2014; Premi et al., 2014), Grn levels were quantified by Western Blot and ELISA. Western blotting of brain lysates from three months old WT, hTDP-43^{A315TKi}, Tmem106b^{BACtg}, and compound mice did not result in any differences (Fig. 40A, E). Quantification of Grn levels in

serum using ELISA yielded a decrease in single mutant mice and levels similar to WT in hTDP-43^{A315TKi} x *Tmem106b*^{BACtg} double mutant animals (Fig. 41).

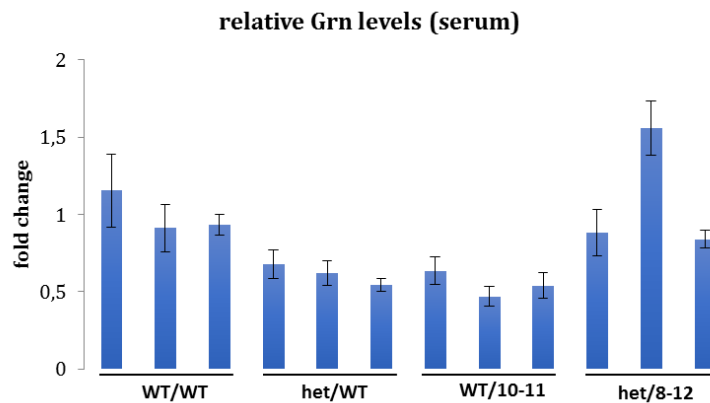


Fig. 41: No clear genotype specific differences in serum Grn levels. ELISA with serum derived from three months old WT, hTDP-43^{A315TKi}, *Tmem106b*^{BACtg} with twelve or 13 copies of *Tmem106b*, and compound mice with 10, 13 or 14 copies. A slight decrease was obvious in single mutant mice, whereas compound animals reached WT levels. Error bars represent S.D.. One-way Anova was performed; n/genotype=3; Graph by Julia Götzl;

In terms of a proposed relationship between TMEM106B and C9orf72 (Gallagher et al., 2014; van Blitterswijk et al., 2014), Western Blot did not reveal any genotype specific variations (Fig. 40A, F). The same applied to Western Blot for the endo-/lysosomal markers LAMP1 (Fig. 40A, G) and Cathepsin D (Fig. 40A, H).

6.2.2.3 TEM analysis of *Tmem106b*^{BACtg} x hTDP-43^{A315TKi} mice

In 6.2.1.4 it was shown, that 17 months old *Tmem106b*^{BACtg} displayed blebbing of mitochondria. 18 months old heterozygous hTDP-43^{A315TKi} animals presented also a mitochondrial dysmorphology: in myelinated neurons a highly reduced cristae formation was observed (Stribl et al., 2014). In order to screen also compound mice for mitochondrial dysmorphology, TEM was repeated for this mouse line. Since aged animals were not available yet, three to six months old mice were used. As a control, WT and single transgenic littermates were additionally analyzed (Fig. 42). However, no mitochondrial alterations could be detected in any of the genotypes in both, cerebellum and frontal cortex, pointing towards an aging phenomenon in hTDP-43^{A315TKi} and *Tmem106b*^{BACtg} mice. Myelinated as well as unmyelinated neurons were inconspicuous in

heterozygous hTDP-43^{A315TKi} (Fig. 42B, F), *Tmem106b*^{BACtg} with eleven or 13 *Tmem106b* copies (Fig. 42D, G), and compound mice with eleven or twelve copies (Fig. 42D, H). As expected, no morphological alterations were observed regarding endo- and lysosomes (data not shown).

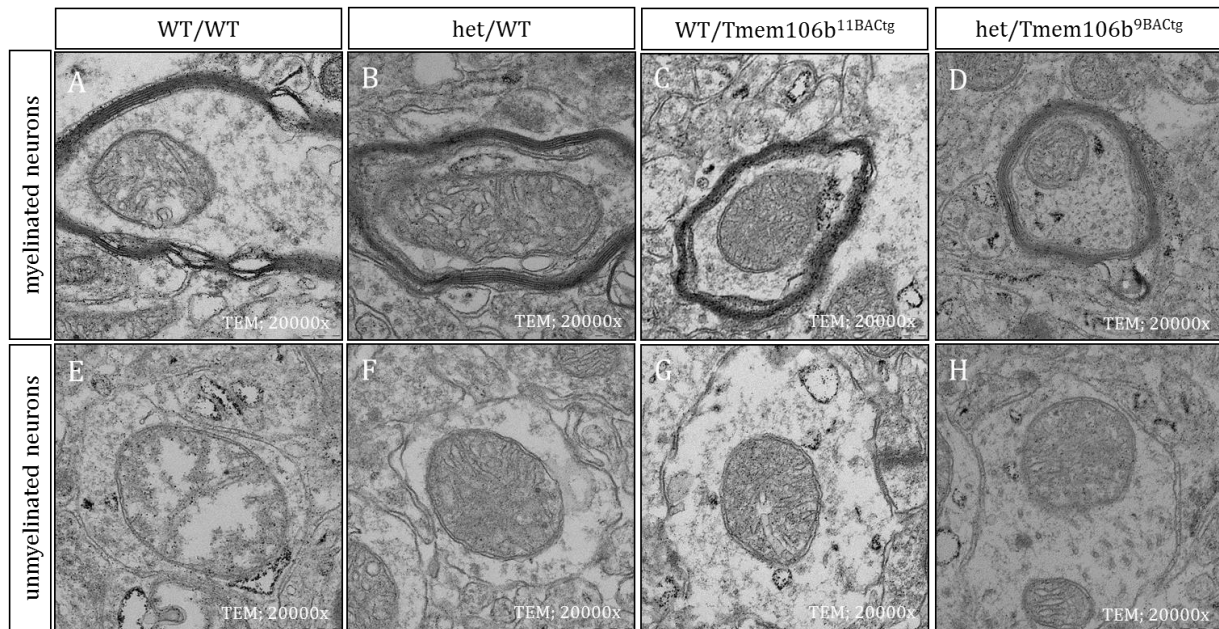
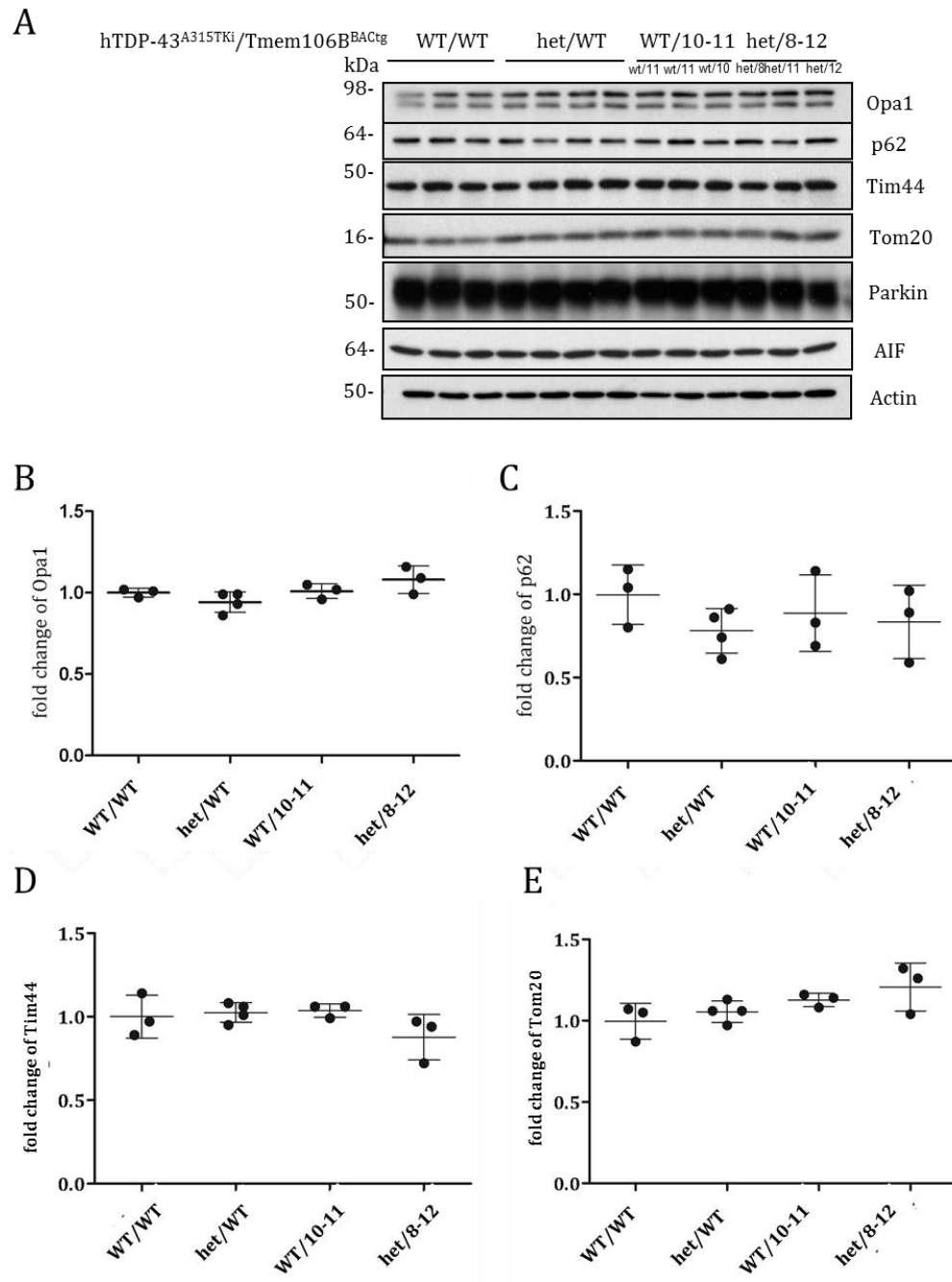


Fig. 42: No mitochondrial dysmorphology in young single and double transgenic mice. Transmission electron microscopy of frontal cortex from three to six months old WT (A, E), hTDP-43^{A315TKi} (B, F), *Tmem106b*^{11BACtg} (C, G), and hTDP-43^{A315TKi}/*Tmem106b*^{9BACtg} (D, H) mice. No genotype specific alterations could be detected. Magnification: 20000x; Pictures by Michaela Aichler;

6.2.2.4 Effects of ectopic *Tmem106b* on mitochondrial proteins and activity

Since the TEM analyses revealed morphological abnormalities of mitochondria at least in aged *Tmem106b*^{BACtg} and hTDP-43^{A315TKi} animals, the effects on proteins involved in mitophagy, the process where mitochondria are targeted for degradation via autophagy pathway, should be investigated, like autophagy marker p62, Opa1 as mitochondrial protein with similarity to dynamin-related GTPases, Parkin being a regulator of mitophagy and Tim and Tom necessary for the protein transport through the mitochondrial membrane. 15 months old hTDP-43^{A315TKi} mice showed a significant reduction of Parkin of about 70%, whereas Opa1 was elevated in three months old mice and decreased in 15 months old animals (Stribl et al., 2014). However, aged mice were not available yet and in three months old mice no genotype specific alterations of protein levels could be detected by Western Blot from total brain lysates (Fig. 43). Autophagy is

closely linked to apoptosis, but there were no hints towards apoptosis as analyzed by western blotting for AIF (Fig. 43A, G). In contrast, AIF levels were reduced in *Tmem106b*^{BACtg} mice (Fig. 43G).



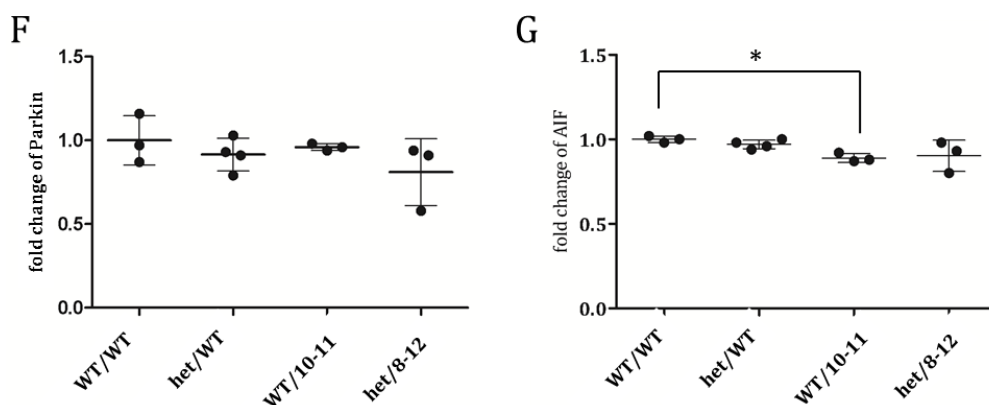


Fig. 43: No genotype specific changes of proteins involved in mitophagy or apoptosis upon ectopic *Tmem106b* expression. (A) Western Blot from brain lysates of three months old WT, hTDP-43^{A315Ti}, *Tmem106b*^{BACtg}, and compound mice. Used antibodies are indicated. (B-G) Quantification of (A); Error bars represent S.D.. One-way ANOVA was performed. n(WT; WT/10-11; het/8-12)=3; n(het/WT)=4; There were no changes concerning protein levels of Opa1 (B), p62 (C), Tim (D), Tom (E), or Parkin (F). AIF levels were significantly reduced to 89% in *Tmem106b*^{BACtg} (p=0.5) (G). Graphs by Julia Götzl;

Furthermore, mitochondrial activity was determined by measuring mitochondrial respiration in a Seahorse Mito Stress Test. Therefore, MEF lines were derived from embryos of all genotypes and analyzed by Nicole Exner from the DZNE (Fig. 44). No genotype specific alterations could be observed concerning basal respiration, ATP turnover, proton leak, maximal respiration, or spare respiratory capacity, not even in compound cells with 23 additional *Tmem106b* copies.

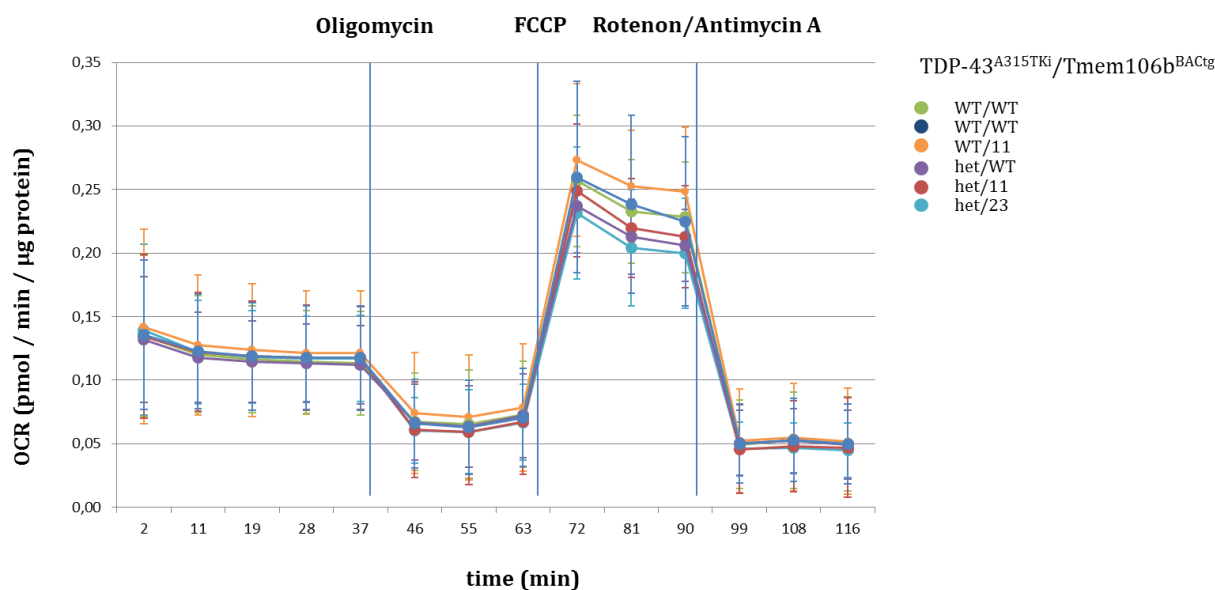


Fig. 44: Ectopic *Tmem106b* expression did not result in any impairment of mitochondrial respiration. Seahorse Mito Stress Test of MEFs derived from WT embryos, an embryo with eleven additional *Tmem106b* gene copies, a heterozygous hTDP-43^{A315TKi} embryo, and compound embryos with eleven or 23 additional copies did not

yield alterations in basal respiration, ATP turnover and proton leak after oligomycin treatment (inhibition of ATP-synthesis), maximal respiration (FCCP; uncoupling agent), or spare respiratory capacity upon rotenon/antimycin A treatment (inhibition of complex I and III). OCR, Oxygen Consumption Rate; FCCP, Carbonyl cyanide-4-(trifluoromethoxy)phenylhydrazone; Error bars represent S.D.. Graph by Nicole Exner;

7 DISCUSSION

ALS and FTLD are adult onset devastating neurodegenerative diseases and *FUS* and *TMEM106B* seem to play an important role in their aetiology. Mutations in the C-terminal NLS of *FUS* lead to a mislocalization to the cytoplasm. Thereby the degree of cytoplasmic *FUS* was in inverse correlation to the age of disease onset in ALS patients (Dormann et al., 2010). It was proposed that mutant *FUS* also draws WT *FUS* out of the nucleus (Vance et al., 2013; Qiu et al., 2014) and that prolonged cellular stress may result in insoluble *FUS* inclusions as found in patients (Dormann et al., 2010; Dormann and Haass, 2013). However, the precise mechanism for the development of ALS waits to be elucidated, as well if it is a loss or a gain of function mechanism. Concerning FTLD, *FUS* inclusions appear to be secondary to a yet unknown disease cascade, which also includes other FET proteins and Transportin.

SNPs in the *TMEM106B* locus were associated with FTLD, but not with ALS (Van Deerlin et al., 2010; van der Zee et al., 2011; Vass et al., 2011; van Blitterswijk et al., 2014). Additionally, *TMEM106B* was found to be elevated in the frontal cortex of FTLD-TDP patients (Van Deerlin et al., 2010; Chen-Plotkin et al., 2012; Gotzl et al., 2014) and that it acts as a modulator of the disease (Adams et al., 2014; Gallagher et al., 2014; Lattante et al., 2014; Premi et al., 2014; van Blitterswijk et al., 2014).

In this study, deeper insights into the development of both, ALS and FTLD, should be gained with the help of mouse models for *FUS* and *TMEM106B*.

7.1 ALS-ASSOCIATED POINT MUTATIONS: LOSS OR GAIN OF FUNCTION?

Since *FUS* mutations result in a mislocalization of *FUS* to the cytoplasm, it was often discussed, whether ALS is caused by a loss of *FUS* function in the nucleus or by a gain of function in the cytoplasm. To answer this question mouse models were generated expressing either human or mouse *Fus* with ALS-associated point mutations. Additionally, a loss of *Fus* model was established to compare it with the mutant ones.

7.1.1 DEPLETION OF *FUS*

Beginning with a conditional gene trap ES cell clone with a β geo cassette inserted in intron 1 of the murine *Fus* gene, mice lacking *Fus* should be generated (Fig. 5). It turned out that homozygous animals were not viable (Tab. 4), except for seven survivor mice with a hypomorphic phenotype ranging from fertile and apparently healthy to stunted sexual organs, impairments in walking, scoliosis and altered brain morphology (Fig. 12). Immunohistochemistry for γ H₂AX (Fig. 14) and karyotyping of chromosomes (Tab. 6) indicated possible defects in DNA repair and recombinations as it had been reported before from *Fus* deficient mice (Hicks et al., 2000; Kuroda et al., 2000). Additionally, infertility was reported in males and, to a smaller extent, also in females (Kuroda et al., 2000). Hicks and colleagues observed perinatal lethality of homozygotes (Hicks et al., 2000), whereas Kuroda et al. obtained homozygous animals on an outbred background (Kuroda et al., 2000). However, homozygotes were smaller and lighter. On an inbred 129svev background, they also noticed perinatal death with survivor animals, which did not reach adulthood (Kuroda et al., 2000), pointing towards genetic background effects on the phenotype. In this study, survival of individual mice could also be due to the genetic background or the leakiness of the gene trap cassette with a varying degree. However, the remaining *Fus* expression could not be assessed due to the small number of available mice, which were all sacrificed for immunostainings and therefore perfused. After perfusion, no RNA or protein could be gained for expression analysis. Moreover, four of the seven survivors were offsprings of the same mating pair. This suggests the assumption that the genetic background was the driving factor. Further, it has to be elucidated, whether the skeletal impairments were due to the stunted muscles or the other way round. Till now, *Fus* was not connected to skeletal function. Though, mice overexpressing the human oncoprotein FUS-CHOP were found to suffer skeletal defects like scoliosis and curvature (Perez-Losada et al., 2000). Homozygous survivors showed a reduction in activity and strength (Fig. 13), but no changes in number of motor neurons (Fig. 14). Thus, the observed phenotype could also be a result of health impairment and weakness. Since Hicks and Kuroda published their mice before FUS was connected to ALS, sensorimotor function was not determined in these *Fus* deficient mice. To draw a clear picture, more homozygous animals have to be analyzed. Though, till now, no more homozygotes followed the seven survivors.

Concerning heterozygous mice, both, Hicks and Kuroda, reported a phenotype that was indistinguishable from those of WT littermates (Hicks et al., 2000; Kuroda et al., 2000) and a *trans*-dominant biological activity was suggested for *Fus* (Hicks et al., 2000). This was also true for the *Fus* GT mice analyzed in this study. Heterozygous animals were not obviously impaired in

health, motoric function or fertility. Adult heterozygous mice displayed reduced Fus protein levels to 60% compared to WT controls and even 87% in embryos (Fig. 6). It was found that FUS protein regulates its own expression by a feedback loop (Lagier-Tourenne et al., 2012; Zhou et al., 2013; Dini Modigliani et al., 2014). FUS binds to its own pre-mRNA and causes differential splicing of exon 7 (Lagier-Tourenne et al., 2012; Zhou et al., 2013). The exon 7-skipped splice variant undergoes NMD and therefore Fus expression is repressed (Zhou et al., 2013). Another hypothesis was declined by Dini Modigliani and colleagues, saying that FUS controls the expression of the two microRNAs miR-141/200a, which, in turn, bind to the 3' UTR of FUS and repress protein synthesis (Dini Modigliani et al., 2014). However, homozygous embryos had still 11% remaining Fus protein compared to WT (Fig. 6), indicating that the gene trap was leaky due to alternative splicing around the insertion cassette for instance. Thus, the 60% remaining Fus in adult heterozygotes could also arise from the leakiness, not from a feedback. Though, higher levels in heterozygous embryos point towards an autoregulation. Fus expression is crucial in embryogenesis, as shown by perinatal death of most homozygous mice, and so it is upregulated in embryonic stages. Later 60% Fus seem to be sufficient for survival and health. Methylation status, which plays a defining role in shuttling of FUS (Dormann et al., 2012), was not changed, whereas PRMT1 levels were significantly reduced to 58% in adult brains (Fig. 6). This contradicts recent findings that FUS is methylated by PRMT1 (Tradewell et al., 2012; Yamaguchi and Kitajo, 2012; Scaramuzzino et al., 2013). However, these were all *in vitro* studies. *In vivo*, other methyltransferases could overtake methylation of Fus.

Further, no disturbed DNA repair, apoptosis, or enhanced neuroinflammation was observed (Fig. 9). On mRNA level, changes in splicing regarding exon inclusion or exclusion upon a lack of Fus reported before (Lagier-Tourenne et al., 2012; Orozco et al., 2012; Qiu et al., 2014) could be confirmed, on protein level no alterations in the amounts of tau or Bdnf were detected (Fig. 8; Supplementary Data, chapter 9.3.3.3). The shift towards the 4R tau isoform, which was found after depletion of FUS in hippocampal neurons and is associated with neurodegeneration (Orozco et al., 2012), could not be observed *in vivo* (Fig. 8). Protein levels of Bdnf, another splicing target of Fus, which was downregulated in FUS-R521C expressing mice and led to a reduced signaling via TrkB receptor (Qiu et al., 2014), were also not changed (Fig. 8). Basically, FUS indeed regulates splicing, as one homozygous Fus^{R513G} mouse with very low Fus levels (Fig. 32) – this will be discussed in chapter 7.1.3 – displayed also very low levels of Bdnf and 3R tau (Fig. 33). However, this could have been important for homozygous deficient mice, though in heterozygotes no grave defects could be assigned to specific targets of Fus. Nevertheless, autophagy seems to be disturbed in these mice, indicated by elevated levels of p62 to more than 150% (Fig. 9). P62/SQSTM1 binds to polyubiquitinated protein aggregates and so induces their degradation in autophagosomes (Pankiv et al., 2007). Therefore, it also interacts directly with

LC3 (Microtubule-associated protein 1A/1B-light chain 3) (Pankiv et al., 2007), a soluble protein, which is recruited to autophagosomes (Tanida et al., 2008). P62 accumulates along with these aggregates if autophagy is disturbed (Pankiv et al., 2007; Rusten and Stenmark, 2010). An impaired autophagy was associated with a number of neurodegenerative diseases, like AD, PD, Lewy bodies disease, HD, and ALS/FTLD (Zatloukal et al., 2002; Mizuno et al., 2006; Kuusisto et al., 2008; Dormann and Haass, 2013). Concerning AD, Beclin 1, as a key player in autophagy, was suggested to be the reason for amyloid- β plaques, since it was found to be reduced in AD brains and deletion *in vitro* and *in vivo* triggered the deposition of amyloid- β peptides (Pickford et al., 2008; Salminen et al., 2013). It was also suggested that impairment of autophagy may contribute to the development of ALS. Recently, ALS/FTLD-linked mutations were reported for OPTN, an autophagy receptor for damaged mitochondria in parkin-mediated mitophagy, which is disrupted upon mutation (Wong and Holzbaur, 2014) and p62/SQSTM1, which reduce or disrupt the binding ability to LC3 (Fecto et al., 2011; Rubino et al., 2012). *VCP*, *CHMP2B*, *FIG4*, *Alsin*, and *UBQLN2*, other genes with reported ALS-/FTLD-linked mutations, are also involved in different steps of autophagy (Otomo et al., 2012). *In vivo* expression of p62 mutants led to cytoplasmic inclusions positive for p62 and ubiquitin (Ichimura et al., 2008). Genetic inactivation of *Sqstm1* resulted in accumulation of hyperphosphorylated tau and neurodegeneration (Ramesh Babu et al., 2008). SOD1-G93A mice, a published model for ALS, showed a progressive increase of LC3 and p62 levels in the SC (Li et al., 2008). Food restriction in order to induce autophagy reduced p62 and mutant SOD1 levels at onset stage of ALS in these mice (Zhang et al., 2013). Injecting trehalose into mutant SOD1 transgenic mice, a substance that increases autophagy levels in motor neurons, reduced SOD1 aggregation and enhanced motor neuron survival, what could be helpful in treatment of ALS patients (Castillo et al., 2013). The same was observed concerning TDP-aggregates (Barmada et al., 2014) and FUS-positive stress granules after autophagy induction (Ryu et al., 2014).

A sensorymotor test battery in the GMC yielded increased number of fore paw slips in the Beam Ladder test, as well as an increased traversing time and slightly more slips in the Balance Beam and a reduced latency to fall down in the Inverted Grid test (Fig. 10; Tab. 5). This could be a hint towards impairments of motor coordination and balance typical for ALS. Since the first performance of Balance Beam with eight months old mice did not give any genotype alterations, what was changed in the repetition at the age of 9.5 months, motor deficits seem to worsen over time. Beam walking is more sensitive than the Rotarod (Stanley et al., 2005), what could explain that there no difference was detected. In working and discrimination memory, tested mice revealed a tendency to better cognitive skills.

Taken together, heterozygous *Fus* GT mice displayed some features of ALS (but not FTL) concerning motor impairment and pathological analysis suggested that a loss of *Fus* function in the nucleus could disturb autophagy and therefore the degeneration of aggregated *Fus*.

7.1.2 HUMANIZED *FUS* MOUSE MODEL

To achieve a mouse model expressing human WT *FUS* or described ALS-associated mutations, an EUCOMM *Fus* GT ES cell clone was used to generate ES cells, harboring the human *FUS* cDNA in intron 1 of the murine *Fus* locus (Fig. 15). The only construct that reached germline transmission was hFUS^{R521G}. Despite of 14 male chimeras (up to 100% chimerism) out of 21 injections into blastocysts, hFUS^{WT} construct did not result in stable inheritance (Tab. 7). The same was observed for the respective human WT TDP-43 construct (Stribl et al., 2014). This low efficiency could point towards a general technical problem or issues of recombination sites. Concerning the human WT, also toxicity of both proteins would be a possibility. Human *FUS* or *TARDBP* cDNA were brought into the endogenous locus without regulatory elements. When injected after excision of hygromycin cassette, that means that hFUS expression was active, only two chimeras were born out of twelve injections. Mitchell et al. observed cytoplasmic *FUS* inclusions, loss of motor neurons and extreme motor deficits in mice with death at the age of twelve weeks upon overexpression of human WT *FUS* (Mitchell et al., 2013). Loss of neurons was confirmed by another group in rats overexpressing the human WT, along with impairments in spatial learning and memory (Huang et al., 2011). The group of Qiu was also successful in generating transgenic mice expressing human FUS^{R521G}, but failed with the corresponding WT control (Qiu et al., 2014). Already low expression levels of human WT *FUS* additional to the endogenous *Fus* resulted in motor deficits, neuroinflammation, and denervation of neuromuscular junctions to a higher degree than in the corresponding human R521G transgenic mice (Sephton et al., 2014). These observations suggest that human WT *FUS* could be toxic in mice.

Homozygous offspring of the hFUS^{R521G} mouse line was not viable (Tab. 8). Human *FUS* was expressed at very low levels shown by qRT-PCR and Western Blot (Fig. 16). This could also be the reason for embryonic lethality – a general lack of *Fus* in these mice. On the other hand, expression in adult brain was higher (78%; Fig. 16) than in *Fus* deficient mice (60%; Fig. 6) and in homozygous MEFs, a remarkable amount of *FUS* protein could be detected, which was found to be mislocalized to the cytoplasm upon the mutation. In heterozygous embryonic cells,

mislocalization was not yet observed (Fig. 17). No species specific antibodies were available and no human specific Taqman Gene Expression Assay, as the only one binds to exon 1, which is non-coding and not integrated in the gene trap cassette. Additionally, for Western Blot and Immunofluorescence two distinct antibodies were used. The one applied for Western Blot recognizes the C-terminus of FUS, where the mutation is located. Santa Cruz does not give precise informations about the binding site, hence the recognition of human FUS could be reduced due to the mutation and expression levels are actually higher. This is supported by the detected embryonic FUS levels: heterozygous and homozygous *Fus* GT embryos had 87% and 11% remaining *Fus* levels respectively compared to WT, whereas hFUS^{R521G} embryos had only 54% and 10%. If the human FUS would not be expressed and it was a knock-out model, levels of endogenous *Fus* should be upregulated by the reported feedback loops, as it was observed in *Fus* GT embryos (Lagier-Tourenne et al., 2012; Zhou et al., 2013; Dini Modigliani et al., 2014). This suggests the assumption that mutant FUS is not recognized to 100%. Further, fibroblasts of heterozygotes displayed a remarkable mislocalization of FUS to the cytoplasm, but only after hygromycin excision, when human FUS expression was activated. Cells still containing the hygromycin cassette looked like the WT, supporting the basic functionality of the mutation (Fig. 17). It has to be mentioned that the phenotype in fibroblasts was not always that drastic in cells gained from other heterozygous TG mice despite comparable ages, advancing additional factors for the development of the phenotype or varying levels of mutated FUS protein. However, analyses of aged heterozygous animals yielded no cytoplasmic FUS or FUS inclusions in the brain and SC (Fig. 19). Additionally, no DNA damage, neuroinflammation, apoptosis (tendency towards more apoptosis) (Fig. 20), or loss of motor neurons (Fig. 21) was detected, nor motoric ALS-like impairments (Tab. 9). Except for embryonic lethality of hFUS^{R521G}^{-/-} mice, human *FUS* mutation did not seem to affect health or motoric function when expressed heterozygously. Nevertheless, besides homozygous lethality, in F1 generation also heterozygous lethality was observed. Among ten heterozygous mice, four died within five to nine months. That raises the question, if these animals had higher human FUS expression levels. Surviving of the left six mice until dissection with 15 months indicates a milder phenotype. Since the mentioned four mice died without reproducing, this implicates that the missing phenotype is due to selection in the first generation.

In published transgenic humanized FUS mouse models several features of ALS, including mislocalized FUS protein, partly insoluble inclusions, loss of neurons, neuroinflammation, DNA damage, motor phenotypes, and also cognitive deficits were monitored (Huang et al., 2011; Huang et al., 2012; Verbeeck et al., 2012; Shelkovnikova et al., 2013; Qiu et al., 2014). However, these animals displayed an overexpression of human R521C FUS (Huang et al., 2011; Huang et al., 2012) or endogenous like expression levels, but additionally to the endogenous *Fus* (Qiu et

al., 2014). Sephton et al. expressed the human WT or R521G FUS at low levels, also additional to the endogenous Fus. Mice had severe motor deficits, along with neuronal impairments, but without mislocalization and aggregation of FUS or motor neuron loss (Sephton et al., 2014). Other mouse models harbored very severe *FUS* mutations, lacking the NLS (Verbeeck et al., 2012) or additionally RGG and zinc finger domains (Shelkovnikova et al., 2013). Verbeeck and colleagues injected recombinant AAV1 encoding FUS WT, FUS R521C, or FUS Δ 14 in the brain of newly born mice (Verbeeck et al., 2012). None of these models expressed human *FUS* mutations under the endogenous promoter, as it was achieved in this study. Thus, described phenotypes can be due to overexpression or an aberrant expression. Nevertheless, in this study, expression levels of human mutant FUS could not be assessed proofly. Likely, they are lower than endogenous Fus and therefore total FUS levels are also decreased. This is why an obvious phenotype could not be monitored.

Qiu and colleagues observed a significant decrease of brain-derived neurotrophic factor BDNF and less activation of the receptor pTrkB, resulting in dendritic and synaptic defects upon expression of human R521C FUS (Qiu et al., 2014). In this study, only a tendency towards less *Bdnf* expression and enhanced activation of TrkB could be observed due to high deviations (Fig. 22). Additionally, reported splicing changes for tau and the shift towards more 4R tau (Orozco et al., 2012) could also not be confirmed. Both isoforms of tau, 3R and 4R tau, were significantly reduced (Fig. 22). Concerning tau, all alterations in splicing were *in vitro* observations and after deletion of FUS (Lagier-Tourenne et al., 2012; Orozco et al., 2012). This implicates that *in vivo* FUS mutations do not correspond to a loss of Fus.

Interesting was the observed distinct mislocalization pattern in fibroblasts derived from embryonic or adult heterozygous hFUS^{R521G} mice (Fig. 17) and the reduced levels of FUS methylation to 75% in embryos compared to WT littermates (Fig. 21). By contrast, in heterozygous brain tissue methylation was increased by 72%. Considering the probably reduced binding of the anti-FUS antibody due to the mutation, the changes could even be more drastic in embryos, and less in adults. The antibody for detection of methylated Fus is against meFUS473–503 (Dormann et al., 2012) and therefore is not affected by the mutation. Methylation status of FUS was reported to play a defining role in shuttling between the nucleus and cytoplasm so that unmethylated FUS has a second binding site for Transportin and FUS aggregates dissipated after inhibition, depletion or overexpression of methyltransferases (Dormann et al., 2012; Tradewell et al., 2012; Yamaguchi and Kitajo, 2012; Scaramuzzino et al., 2013). Reducing methylation status could be a countering mechanism to *FUS* mutations. However, this seems to work only in embryonic or young animals, indicating again that FUS expression is crucial during embryogenesis (compare Fus expression levels in Fus GT embryos). Later, the opposite effect

was noticed. This could be an explanation, additional to the second hit hypothesis (Dormann et al., 2010), why ALS is an adult onset disease. In youth, mutation carriers can compensate *FUS* mutations by demethylation. Ongoing changes in methylation during aging and binding of mutated *FUS* to WT *FUS*, increases mislocalized *FUS* protein levels in the cytoplasm and permanent cellular stress or environmental factors then lead to inclusion formation and disease. Though, in this work, no evidence could be supplied that this process is implemented by PRMT1, as suggested before (Tradewell et al., 2012; Yamaguchi and Kitajo, 2012; Scaramuzzino et al., 2013). PRMT1 levels did again not correlate with methylation status of *FUS* (compare also *Fus* GT mice). Conversely, PRMT1 appeared to be significantly reduced to 80% upon loss of *FUS* in the nucleus (Fig. 23). The same was observed in *Fus* GT mice: PRMT1 was even reduced to 58% (Fig. 7). Recently, it was suggested that accumulation of *FUS* in the cytoplasm causes nuclear depletion of PRMT1, resulting in a loss of function including methylation of histones (Tibshirani et al., 2015). Hence, *Fus* could also directly regulate the expression of PRMT1.

Behavioral analyses in the German Mouse Clinic to assess basic neurological functions yielded reduced locomotor activity of heterozygous *hFUS^{R521G}* transgenic mice in the SHIRPA test, but no genotype differences in the Open Field (Fig. 24, 25; Tab. 9). The Open Field is fitted to test behavior in a novel environment and is more a cognitive test, whereas the SHIRPA test considers general health and autonomous functions. Hence, reduced activity is caused by the overall condition, not by reduced curiosity. In the Inverted Grid test heterozygotes fell from the grid after shorter latencies than WT controls (Fig. 24). This was observed in 13.5 months old mice and also already with 8 months of age. The Inverted Grid is a simple method to judge muscle force needed to prevent from falling from a grid. Since other muscle force and coordination tasks were unobscured and female mutants were heavier than their WT littermates, the Inverted Grid was applied in consideration of body mass effects. Increased body mass is rather an advantage for the Grip Strength test for example, as heavier mice are used to support their weight during live and locomotion. By contrast, for the Inverted Grid increased body weight is a disadvantage. There the latency is measured, how long the mice are able to support the attachment of their weight directly to the grid. However, male mutant mice were lighter than WT controls and showed also reduced latencies, which suggests that results are due to a reduced muscle force. The Open Field is a test of spontaneous activity in a novel environment. Heterozygous *hFus^{R521G}* mice revealed increased rearing activity in the absence of clear alterations in forward locomotor activity, pointing towards more exploration in a novel environment. Furthermore, heterozygotes spent more time in the center, suggesting that these animals had impaired emotional reactivity to this mild novelty stress. However, when sexes were pooled these effects were not obvious anymore (Supplementary Data, chapter 9.3.2.2).

Taken together, these results indicate an embryonic countering mechanism to *FUS* mutations driven by *FUS* methylation. In a battery of sensorimotor challenges, heterozygous animals displayed less activity, a reduced muscle force, and changes in emotionality and exploratory activity without clear alterations in the aspects of cognition, meaning working memory and short-term olfactory memory in a social context. However, no clear ALS related pathology or phenotype could be assessed, as reduced activity and muscle force could also be the result of health impairment. Motor coordination was not changed. Additionally, no loss of motor neurons could be observed. The higher body weight of females would also be more contradictive for a neurodegenerative disease phenotype. ALS patients normally lose weight due to disease.

7.1.3 *FUS* TALEN MICE

Effects of ALS-associated *FUS* mutations should also be analyzed in an endogenous context. Therefore, mice were generated by Panda et al., carrying the corresponding murine *Fus* mutations R513G, P517L, and P511fs to the human mild R521G mutation, the severe P525L exchange, and a delta NLS modification (Fig. 26) (Panda et al., 2013). A correlation of mutation severity and viability could be observed, that way that homozygous *Fus*^{P517L} and *Fus*^{P511fs} mice were not viable whereas homozygous *Fus*^{R513G} animals did not show any health impairments in adulthood (Tab. 10). This was confirmed by Immunofluorescence for *Fus* on fibroblasts derived from adult mice: a slight increase of *Fus* mislocalization to the cytoplasm could be observed in cells harboring the R513G mutation over those with the P517L exchange to P511fs cells (Fig. 27). In embryonic fibroblasts localization pattern was solely nuclear (Fig. 27), but upon oxidative stress, mislocalization was also seen in MEFs (Fig. 28). However, in neurons of four months old mice no genotype differences could be observed concerning *Fus* localization. Additionally, no inclusion formation or DNA damage was detected (Fig. 29). Certainly, this has to be repeated with aged mice, since ALS is an adult onset disease. *Fus* protein levels were elevated, slightly in brain of 15 months old *Fus*^{R513G} mice, but especially in SC lysates to more than double of the WT in heterozygous and nearly fourfold in homozygous animals (Fig. 32). The real levels could even be higher, as the applied anti-FUS antibody recognizes the C-terminus of *Fus*, where the point mutation was placed. Hence, detection of mutated *Fus* could be reduced (compare also the humanized FUS mouse model, chapter 7.1.2). Two different feedback loops were reported for FUS by binding to its own mRNA and following alternative splicing and via microRNAs binding in the 3' UTR of FUS (Lagier-Tourenne et al., 2012; Zhou et al., 2013; Dini Modigliani et

al., 2014). Progressive mislocalization of Fus to the cytoplasm in the SC and brain of these aged mice and the linked loss of Fus in the nucleus could therefore lead to an upregulation of Fus. Constantly increasing levels of Fus then result in aggregates. However, in 15 months old mice, no insoluble Fus protein could be detected, or rather not more than in the WT, what is probably ascribed to the isolation method (Fig. 29). Isolation of soluble protein yielded very low Fus levels in the brain of one homozygous mouse, with normal levels of the loading control (Fig. 32). Splicing targets of Fus, *Bdnf* and *tau*, were also downregulated on differential blots, excluding a loading or blotting problem (Fig. 33). This could point towards a beginning of inclusion formation with insoluble protein at the age of 15 months in homozygous mice. Levels of p62 protein, being colocalized to Fus in inclusions, were also elevated, mainly in SC tissue of homozygous mice (Fig. 31), pointing towards a lack of autophagy (Pankiv et al., 2007; Rusten and Stenmark, 2010). P62/SQSTM1 was also associated with several neurodegenerative diseases including ALS, as, among other autophagy regulators, mutations in *Sqstm1* were found in ALS patients (Fecto et al., 2011; Rubino et al., 2012) (see also chapter 7.1.1). P62 binds to ubiquitinated protein aggregates, interacts with LC3 and therefore targets them for degradation (Pankiv et al., 2007). Thus, upon a FUS mutation and constant increase of FUS expression due to the feedback loop, more and more FUS aggregates are forged, which are bound by p62. The second hit, corresponding to the hypothesis by Dormann et al. (Dormann et al., 2010), is then a disturbed autophagy. Aggregates are not degraded and insoluble inclusions arise, which are positive for Fus, Ubiquitin and p62, as they are found in patients. A decrease in autophagy is a naturally occurring phenomenon during aging (Rubinsztein et al., 2011). Changes in autophagy could also emerge upon genetic reasons and, for that matter, environmental factors were found to influence autophagy like virus infection, fasting, or coffee (Alirezaei et al., 2008; Alirezaei et al., 2010; Alirezaei et al., 2011; Pietrocola et al., 2014). *In vitro* expression of ALS-linked FUS(R521C) mutation caused FUS-positive stress granules, which were observed to be colocalized with LC3-positive autophagosomes (Ryu et al., 2014). Fus GT mice also showed elevated levels of p62, arguing for a lack of autophagy. It would be interesting to analyze, if the expression of autophagy regulating genes is changed upon deficiency of Fus.

Analyses concerning methylation of Fus revealed contradicting results: in the SC methylated Fus levels were significantly reduced to 50%, whereas in the brain levels were doubled (Fig. 32). Thereby, no difference was apparent between hetero- and homozygous mice. In embryos, a tendency towards less methylation was found (Fig. 32), as also observed for the humanized FUS mouse model (Fig. 21). Again, the differences could be more drastic in embryos and SC of adult mice and fewer in adult brain due to a reduced recognition of mutated Fus upon mutation, in contrast to methylated Fus (compare also humanized FUS mouse model, chapter 7.1.2). As mentioned before, methylation contributes to the shuttling of FUS between the nucleus and the

cytoplasm and demethylation can counteract a mutation in the NLS (Dormann et al., 2012). Thus, during embryogenesis, demethylation seems to be a strategy to bring mutated Fus back into the nucleus. In adults, this mechanism is not reliable anymore or even reversed (compare also hFUS^{R521G}). Differences between SC and brain could be due to the extent of mislocalization in distinct kinds of neurons. In pure ALS, only motor neurons are affected by degeneration. Hence, demethylation is induced only in those neurons. Another point could be the use of whole brain samples. Separating of brain regions would perhaps define these results.

Protein levels of the Fus splicing targets tau and Bdnf (Lagier-Tourenne et al., 2012; Orozco et al., 2012; Qiu et al., 2014) were not significantly changed due to a high deviation (Fig. 32). Bdnf was tendentially reduced in SC and brain lysates of hetero- and homozygous Fus^{R513G} mice, as it was reported from human R521C expressing mice (Qiu et al., 2014). Apart from this, no neuroinflammation (Fig. 31), but a decreased number of motor neurons could be detected in homozygous Fus^{R513G} animals (Fig. 30), as well as elevated levels of AIF in hetero- and even more in homozygotes (Fig. 31). Apoptosis-inducing factor AIF was found to be elevated in SC lysates of 15 months old homozygous mice to about 170% and especially in brain lysates, where the levels were more than doubled compared to WT (Fig. 31). Heterozygous AIF levels reached nearly homozygous niveau in the brain, whereas in the SC levels were only slightly increased (Fig. 31). These results correlate with enhanced methylation levels in the brain and decreased levels in the SC, supporting the hypothesis above that neurons in the SC, probably particularly motor neurons, are first protected by demethylation. AIF is a mitochondrial intermembrane flavoprotein and induces a caspase-independent cascade to programmed cell death, which is preferred in neurons (Susin et al., 1999). This happens by a change in AIF localization from mitochondria to the nucleus leading to chromatin condensation, DNA fragmentation, and finally apoptosis (Daugas et al., 2000). Not only dysfunction of autophagy, but also of apoptosis was already associated with neurodegenerative diseases like AD, PD, as well as ALS (Martin, 2010; Ghavami et al., 2014). In SC tissue of SOD1 G93A transgenic mice evidence for an activation and translocation of AIF from mitochondria to the nucleus of motor neurons was found (Oh et al., 2006). In patients, degeneration of motor neurons was ascribed to dysregulation of intracellular Ca²⁺ and excitotoxicity (Martin, 2010; Ghavami et al., 2014). Autophagy and apoptotic cell death pathways are linked: inhibition of apoptosis can transform cell death into autophagy and on the other hand, reduction of autophagy leads to apoptosis upon cellular stress (Ogier-Denis and Codogno, 2003). The latter could be an explanation for the decreased number of motor neurons in the SC of homozygous Fus^{R513G} mice (in average 3.5 per section; Fig. 30). However, aged homozygotes were not available in an appropriate number for behavioral tests and heterozygotes were rather inconspicuous regarding phenotypical as well as pathological analyses, indicating that for this mouse model homozygosity is necessary to see a clear

phenotype. To challenge homozygous animals in sensorimotor tests would be of interest in order to evaluate, whether the decreased number of motor neurons in the SC correlates with motoric impairments. It would be also necessary to check, if the reduced number is a progressive phenomenon due to degeneration or if homozygous Fus^{R513G} mice are born with lesser motor neurons. Swollen nuclei of one homozygote (Fig. 30) would be a hint towards degeneration. Swelling of cell nuclei is a common feature in cancer (Edens et al., 2013; Jevtic and Levy, 2014) and was also observed in premature senescent fibroblasts prior to cell death (Kobayashi et al., 2008). Though, this was only observed in one of two analyzed homozygotes, as well as reduced Fus protein levels in the brain discussed above, what points towards modulating effects in these mice like genetic background.

Heterozygous mice had a comparable number of motor neurons like WT littermates (Fig. 30). P62 levels were not changed and AIF levels in the SC were only slightly increased (Fig. 31). Behavioral tests did not reveal any significant alterations between WT and heterozygotes concerning motor coordination or strength (Fig. 34; Tab. 11). In the Open Field, nine months old Fus^{R513G} animals displayed opposed results in males and females: males showed an increased spontaneous activity and spent more time in the center, whereas females did less (Fig. 35). Rearing activity was elevated in both sexes (Fig. 35). Differences in center time may be indicative of altered anxiety-related behavior, but could also be an impact secondary to the locomotor changes. To determine whether this is a true effect on anxiety, additional anxiety-related tests should be performed such as the elevated plus maze and light/dark box test. After pooling of sexes, these effects were not longer seen, but instead a significant increase in social investigation time, without changes in social discrimination memory (Supplementary Data, chapter 9.3.2.2). A problem in these behavioral tests was the unappropriate number of WT controls. Only one male and a few females were available in that age. For that, WT controls of the $hFUS^{R521G}$ mouse line were used, what could be the explanation for the contradicting results. To clear this, a new cohort, preferably including homozygotes, should be challenged again in this test battery.

Summarizing, one could say that first results were promising concerning Fus^{R513G} mice. Some results did not reach significance due to the low number of analyzed mice. Though, in 15 months old homozygous mice, elevated levels of Fus, p62, and AIF were observed, indicating an aggregation of Fus, a dysfunction of autophagy, and increased apoptosis. Along with a reduction of motor neurons this could point towards neurodegeneration in Fus^{R513G} animals. However, in mice, a homozygous mutation seems to be necessary to result in the described effects, whereas human mutations are dominant.

7.1.4 COMPARISON OF MOUSE MODELS FOR ALS-ASSOCIATED POINT MUTATIONS

In this study, mice were generated carrying the ALS-associated *FUS* mutation R521G, on the one hand a RMCE mouse model with the human *FUS* cDNA, on the other hand a TALEN mouse model with the corresponding murine *Fus* mutation R513G. Analyses of these mice yielded partly different results: humanized mice were embryonic lethal when bred to homozygosity and heterozygotes displayed a reduced muscle force and changes in emotionality and exploratory activity. Additionally, methylation of *FUS* was reduced in embryos and increased in adult mice. The same was detected in fibroblasts derived from embryos or ears of adult animals. Additionally, MEFs did not show a cytoplasmic mislocalization of *FUS*, whereas fibroblasts derived from adult animals did. The same pattern of *Fus* localization was observed in TALEN MEFs and fibroblasts, and furthermore a tendency towards less methylation in hetero- and homozygous embryos and the SC of adult animals, whereas in the brain methylation was enhanced. Reduced methylation of *FUS* seems to be a protective mechanism during embryogenesis to counteract the mutation (see also chapters 7.1.2 and 7.1.3). Phenotypically, no motor deficits could be monitored in heterozygotes, instead hints towards cognitive changes. However, Western Blots yielded elevated levels of *Fus*, AIF and p62 in the spinal cord of *Fus*^{R513G} mice and, at least homozygotes, had a decreased number of motor neurons. A tendency to more AIF was also found in heterozygous h*FUS*^{R521G} mice.

These results indicate that mutated human *FUS* and murine *Fus* act different: the effects of mutated human *FUS* seem to be more drastic, even though it seems to be expressed at lower levels. The first article is that homozygotes are viable concerning TALEN mice, whereas there was only one humanized survivor which died right after weaning age. Second, despite of similarities in *FUS* localization pattern, meaning the change from embryonic fibroblasts to adult ones, mislocalization of *FUS* was more radical in humanized fibroblasts than in TALEN fibroblasts. Counting of cells with *FUS* only in the nucleus or cytoplasm and cells where *FUS* was observed in both compartments revealed for humanized fibroblasts no single cell that had *FUS* only in the nucleus. 71% of cells showed nuclear and cytoplasmic and 29% exclusively cytoplasmic localization. Among heterozygous *Fus*^{R513G} cells, 28% each harbored *Fus* only in the nucleus or cytoplasm. In 44% *Fus* was detected in both, nucleus and cytoplasm (Supplementary Data, chapter 9.3.2.1).

In a behavioral test battery to assess basic neurological functions, effects in humanized mice concerning motor coordination were also more bold than those in *Fus*^{R513G} mice, whereas for the latter ones the tests were not that clear and meaningful due to the lack of an appropriate number of WT controls. Some tests were repeated at later time points to evaluate a potential

phenotype progression or later onset (Supplementary Data, chapter 9.3.2.2 and 9.3.3.1). hFUS^{R521G} mice were less active compared to controls in the SHIRPA test for general health and movement, while this was unchanged in Fus^{R513G} mice (Fig. 46B). Humanized FUS mice also showed muscle weakness in the Inverted Grid. For Fus^{R513G} mice an intermediate effect was measured which did not reach statistical significance (Fig. 46C). In the Open Field, no clear effect in forward (Fig. 46D) or horizontal (Fig. 46E) exploratory activity, or anxiety related behavior (Fig. 46F) was observed for the two mouse models when controls and sexes were pooled. However, while there was no clear phenotype regarding social discrimination memory (Fig. 46H), an increase in amount of social investigation time was monitored for the Fus^{R513G} mice (Fig. 46G). Weighing during the tests indicated that body mass of hFUS^{R521G} males was decreased, whereas both, humanized and TALEN females were heavier than WT controls, which is contra-intuitive to motor neuron disease (Fig. 46A). Thus, phenotypically, heterozygous hFUS^{R521G} mice were more conspicuous than heterozygous Fus^{R513G} animals, although human FUS appeared to be expressed to a lower extend. The phenotype in the humanized mouse model could therefore also be caused by a reduction of total Fus levels (see also chapter 7.1.5).

As mentioned before, Fus, p62 and AIF protein levels were elevated in Fus^{R513G} mice, in hFUS^{R521G} animals a tendency towards more AIF was determined (Fig. 48). The latter had reduced FUS levels due to reasons we could not clear in detail. Levels in analyzed mice could be actually higher, since no human specific assay was available to quantify mRNA levels and the used anti-FUS antibody, which solely gave specific bands, recognized the C-terminus, where the mutation is located. Nevertheless, a selection took probably place in the F1 generation upon the death of animals with a more severe phenotype without reproducing. Another point could be that the human cDNA is expressed without possible regulatory elements localized in introns or upstream or downstream of *FUS*. As mentioned before, FUS levels are modulated via a distinct feedback loops (see also chapters 7.1.1 and 7.1.3). In 2013, it was published that FUS regulates its own exon 7 splicing and that the exon 7-skipped splice variant is subject to NMD (Zhou et al., 2013). Overexpression of FUS led to excision of exon 7 and reduced endogenous FUS protein. Knockdown of FUS protein or expression of ALS-associated mutations had the opposite effect (Zhou et al., 2013), which is probably the reason for enhanced Fus levels in Fus^{R513G} mice (see also chapter 7.1.3). Autoregulation of Fus takes place in the nucleus. A mislocalization of mutant Fus to the cytoplasm corresponds to a loss of Fus and therefore an upregulation of Fus expression. Another feedback loop was uncovered by Dini Modigliani et al. (Dini Modigliani et al., 2014). They found that the expression of microRNAs miR-141 and miR-200a is adjusted by FUS. Conversely, miR-141/200a recognize the 3' UTR of FUS and therefore repress FUS (Dini Modigliani et al., 2014). Lack of the 3' UTR resulted in accumulation of a recombinant FUS-RFP (red fluorescence protein) fusion protein and reduction of endogenous FUS mRNA and protein

in vitro (Dini Modigliani et al., 2014). FUS G48A mutation, which was identified in ALS patients, is located in the 3' UTR at one binding site of miR-141/200a. *In vitro* expression reduced regulation and led to enhanced FUS levels (Dini Modigliani et al., 2014). Overexpression of FUS upon distinct mutations gives rise to more and more aggregation of Fus and finally inclusion formation. However, in the humanized FUS mouse model, this autoregulation cannot work for the human cDNA, as 3' UTR and flanking introns of exon 7 are necessary (Zhou et al., 2013; Dini Modigliani et al., 2014). Heterozygous mice had 78.1% remaining FUS protein compared to WT controls. Since there is no antibody available that distinguishes between human and mouse, it cannot be clarified, which amount of the remaining FUS protein is human and which amount mouse and therefore, if the mouse Fus is regulated somehow. The contraversing FUS protein levels in the both mouse models, overexpression on the one hand and reduction on the other hand, may lead to different pathways, including autophagy, and therefore different phenotypes. In Fus^{R513G} mice, autophagy was reduced and apoptosis enhanced (see also chapter 7.1.3), whereas in hFUS^{R521G} mice also a tendency towards more apoptosis could be observed. Thus, overexpression of Fus could indirect contribute to disturbed autophagy and following reduced degradation of aggregated Fus.

What could also be crucial between human and mouse FUS is a difference in phosphorylation status. Deng and colleagues reported that in human cell lines phosphorylation of FUS is involved in the development of FTLD, this way that FUS gets phosphorylated upon DNA damage and is then exported to the cytoplasm (Deng et al., 2014b). Thereby, an important part of FUS translocation is effected by multiple phosphorylation sites on the N terminus of FUS (Deng et al., 2014b). Comparing the amino acid sequence of human and mouse Fus revealed an interesting variance: just at the N-terminus, namely in the QGSY-rich and the RGG1 domain, the mouse Fus protein contains nine lesser serin and two lesser threonins, which are typical phosphorylation sites (Supplementary Data, chapter 9.3.2.3). This seems to be an evolutionary phenomenon, since almost all eleven additional phosphorylation sites were also found in chimp and Neanderthal. Hence, in the humanized mouse model phosphorylation can play a complementary role to the mutation: upon DNA damage due to less FUS protein or due to the mutation FUS gets phosphorylated and is exported to the cytoplasm. Therefore, DNA damage response is induced and we did not find evidence for a disturbance in seven months old mice. Then, in the cytoplasm, FUS cannot bind to Transportin because of the mutation in the NLS and consequently cannot be transported back to the nucleus. This is then a worsening impact. It would be of interest to look for DNA damage again in much more older mice. Against this, the murine Fus lacks eleven phosphorylation sites (Supplementary Data, chapter 9.3.2.3) and the mutation seems to be the prominent effector.

Summarizing, hFUS^{R521G} and Fus^{R513G} mouse models displayed conformity concerning localization pattern of FUS due to the mutation. However, the following mechanisms were probably influenced by distinct expression levels. Additionally, phosphorylation could play a role in the development of a phenotype. The change of localization pattern from embryos to adult mice supplies evidence that in both mouse models mislocalization is a progressive phenotype and perhaps mice have to be older to observe symptoms. In humanized mice, repetition of behavioral tests at older ages confirmed this.

7.1.5 LOSS OR GAIN OF FUS FUNCTION?

Today, the mechanism of mutations in *FUS* leading to ALS waits to be solved. Since *FUS* functions predominantly in the nucleus a loss of function model is possible. However, published *Fus* deficient mice did not suffer an obvious neuronal or motoric phenotype, but genomic instability (Hicks et al., 2000; Kuroda et al., 2000). Perhaps, other FET proteins can overtake *FUS* function, as *EWS* was higher expressed upon *FUS* knockdown *in vitro* (Ward et al., 2014). Due to mislocalization of *FUS* and aggregation in the cytoplasm, a gain of misfunction in the cytoplasm is also thinkable, like aberrant binding of cytoplasmic RNA targets (Hoell et al., 2011). Qiu and colleagues suggested a gain of function model in their *FUS*-R521C mice affected by DNA damage and splicing defects (Qiu et al., 2014). Most other rodent models reflected features of ALS like motor impairment upon transgenic overexpression of human *FUS* mutations and also WT *FUS* (Huang et al., 2011; Mitchell et al., 2013). Additionally, mutations in the 3' UTR of *FUS* were identified in ALS patients leading to an overexpression of *FUS* (Sabatelli et al., 2013).

To define, if phenotypes of possible mouse models for ALS are due to loss or gain of *FUS* function, mice deficient for *Fus* were additionally generated. These mice showed motoric impairments, especially homozygous survivor animals. Normally, homozygosity was perinatal lethal. A test battery for strength and motor coordination yielded muscle weakness of heterozygotes in the Inverted Grid, which was also observed for hFUS^{R521G} mice and a trend in 12.5 months old Fus^{R513G} mice, but not five months earlier, indicating a progressive phenotype (Supplementary Data, chapter 9.3.3.1). Further, problems in motor coordination and balance were monitored by Balance Beam and Beam Ladder tests. Humanized *FUS* mice showed slightly more time and slips in the Balance Beam test, but that did not reach significance. Concerning Beam Ladder, both models with ALS-associated mutation performed even slightly better. Effects

on emotionality and exploratory activity were not detected for *Fus* deficient mice, but in both mouse lines with *FUS* mutation. All three models displayed a trend towards more social discrimination (Supplementary Data, Chapter 9.3.3.1). However, besides memory, also smelling could play a role in this test. Taken together, the different models repeated some features of ALS concerning motoric function, but did not match in all points. However, *Fus* deficient mice even presented the clearest motor phenotype without cognitive changes, what would argue for a loss of *FUS* function model in ALS patients.

Pathologically, in brain lysates of heterozygous GT mice elevated levels of p62 of about 50% compared to WT controls were found (Supplementary Data, chapter 9.3.3.2). The same degree of increase was detected in SC lysates of homozygous *Fus*^{R513G} mice, whereas in heterozygotes and in brain tissue levels were comparable to WT (Supplementary Data, chapter 9.3.3.2). In the SC of h*FUS*^{R521G} animals there was even a trend to less p62. That is consistent with a finding from Ryu et al.. They reported that autophagic degradation was not disturbed by *FUS*(R521C) expression *in vivo* (Ryu et al., 2014). Though, codeposition of p62 and Ubiquitin in *FUS* positive inclusions suggests an impact of dysfunctional autophagy and protein degradation on the development of ALS (Dormann and Haass, 2013), which can then lead to apoptosis (Ogier-Denis and Codogno, 2003). In *Fus*^{R513G} and h*FUS*^{R521G} mice induction of apoptosis seems to be enhanced. In *Fus* GT mice, however, apoptosis was not changed (Supplementary Data, chapter 9.3.3.2). These results support the assumption of different pathomechanisms in h*FUS*^{R521G} and *Fus*^{R513G} mouse models (see also chapter 7.1.4). However, none of them is in full conformity with *Fus* deficient mice, arguing against a loss of function in ALS patients. Methylation status of *FUS* was only changed in mouse models with ALS-associated point mutation, not in *Fus* deficient mice, strengthening the hypothesis that modification of methylation status depends on the mutation and counteracts it (Supplementary Data, chapter 9.3.3.2).

Lagier-Tourenne and colleagues identified a lot of splicing targets of *FUS* that were partially changed after TDP-43 and/or *FUS* depletion (Lagier-Tourenne et al., 2012). In brain tissues from *Fus* GT mice, some of these targets could be verified like *Ptk2b*, *hnRNP-D*, *Tia1*, or *Ndr2* by RT-PCR using the primers depicted in the paper (see also chapter 7.1.1). For *Sort1* more exon exclusion was detected in *Fus* GT mice. Lagier-Tourenne found only an effect upon TDP-43 depletion, not *FUS* depletion. *Ptk2b* is a cytoplasmic protein tyrosine kinase, which is involved in calcium-induced regulation of ion channels and activation of the map kinase signaling pathway. *HnRNP-D* belongs to the subfamily of ubiquitously expressed heterogeneous nuclear ribonucleoproteins (hnRNPs). The hnRNPs are nucleic acid binding proteins and they complex with heterogeneous nuclear RNA (hnRNA). These proteins are associated with pre-mRNAs in the nucleus and appear to influence pre-mRNA processing and other aspects of mRNA metabolism

and transport. While all of the hnRNPs are present in the nucleus, some seem to shuttle between the nucleus and the cytoplasm. Sort1, a trans-Golgi network (TGN) transmembrane protein, binds a number of unrelated ligands that participate in a wide range of cellular processes. N-myc downstream-regulated gene 2 (*Ndr2*) is implicated in neurodegenerative diseases and is expressed in astrocytes and mis-accumulated in Alzheimer's disease. Analyses were repeated with MEFs or brain tissue from hFUS^{R521G} and Fus^{R513G} mouse lines and three of these five chosen targets showed the same splicing changes as in Fus GT mice (Supplementary Data, chapter 9.3.3.3, Fig. 49). *Tia1* did not work and for *Ptk2b* more exclusion events of exon 24 could not be confirmed. These results suggest again a loss of function in the nucleus caused by *FUS* mutations in the NLS and following mislocalization of FUS protein to the cytoplasm. However, on protein level, both isoforms of tau, 3R and 4R tau, were significantly reduced in hFUS^{R521G} mice, whereas in Fus GT and Fus^{R513G} animals levels were not changed or tendentially elevated (Supplementary Data, chapter 9.3.3.3, Fig. 50). This contradicts other studies, where there was a shift towards 4R tau upon Fus depletion (Orozco et al., 2012). *Bdnf* was tendentially reduced in all three lines (Supplementary Data, chapter 9.3.3.3, Fig. 50), as it was also observed in a FUS R521C expressing rodent model (Qiu et al., 2014).

Comparison of all three mouse models can not definitely clarify, if ALS is caused by a loss or gain of function model. Varying phenotypical and pathological results are aggravated by the backgrounds of the three mouse models. Fus GT and hFUS^{R521G} mice were originated from E14 stem cells and were injected into Balb-C and C57Bl6 blastocysts respectively. To achieve Fus^{R513G} mice, one-cell embryos were obtained by mating of (DBA/2 x C57BL/6)F1 and injected with the TALEN Fus construct (Panda et al., 2013). Zygotes for all three mouse lines were transferred into pseudopregnant CD1 female mice and chimeras were bred with C57Bl6 mice. Thus, all three models have a very mixed background, but not the same mix, what for sure contributes to the phenotype.

This study suggests an interaction of loss and gain of function, especially the results for Fus^{R513G} mice. The first step is the loss of Fus in the nucleus due to the mutation, which causes splicing and expression changes of differential Fus regulated genes, among these Fus itself and perhaps also autophagy regulating genes. The latter is supported by less autophagy in Fus deficient mice (see also chapter 7.1.1). The consequence of the Fus autoregulation is an upregulation of Fus expression and more and more mislocalization, which causes gain of Fus function and finally an aggregation of Fus in the cytoplasm. Lack of autophagy, due to genetic or environmental reasons, inhibits degradation of ubiquitinated and p62-bound Fus aggregates and leads to insoluble inclusions, positive for Fus, p62 and Ubiquitin, as found in patients. Combination of loss and gain of function was already proposed in some reviews (Armstrong and Drapeau, 2013; Dormann

and Haass, 2013). In a zebrafish model, for instance, both, loss and gain of FUS function by knockdown of *fus* or expression of human WT or R521H FUS, led to defective presynaptic function at neuromuscular junctions and impaired motor activity (Armstrong and Drapeau, 2013).

7.2 OVEREXPRESSION OF TMEM106B *IN VIVO*

TMEM106B was found to be a modulator of FTLT-DTP and in patients elevated protein levels were detected in the frontal cortex (Van Deerlin et al., 2010; Chen-Plotkin et al., 2012). To mimic a *Tmem106b* overexpression *in vivo*, mice were generated carrying additional copies of *Tmem106b* (Fig. 36). To enhance possible effects *Tmem106b* was also overexpressed on a mutant TDP-43 background. Therefore, *Tmem106b*^{BACtg} mice were bred with hTDP-43^{A513TKi} animals, characterized with reduced body weight, mitochondrial dysfunction, insoluble TDP-43 protein, and a decrease in number of motor neurons (Stribl et al., 2014). Protein and mRNA levels of *Tmem106b* were elevated in correlation to the copy number (Fig. 36; 40). However, both mouse lines did not display any impairment on viability or health. Eight months old *Tmem106b*^{BACtg} animals with a high copy number of *Tmem106b* showed a slight mislocalization of TDP-43 to the cytoplasm of neurons (Fig. 37), although protein levels of TDP-43 were reduced in brain lysates of three months old mice to about 71% (Fig. 40), indicating a regulatory impact of *Tmem106b* on TDP-43. In aged mice (17 months) a blebbing of mitochondria was observed in neurons, especially in the frontal cortex, whereas morphology of endo- and lysosomes was not altered (Fig. 38). Thereby, this phenotype was not enhanced by a higher copy number. In myelinated neurons of 18 months old heterozygous hTDP-43^{A315TKi} mice a highly reduced cristae formation was observed (Stribl et al., 2014). Though, in younger mice (3 months) of both lines, mitochondria looked normal (Fig. 42), indicating a progressive phenotype. At point of thesis submission, only young hTDP-43^{A315TKi} x *Tmem106b*^{BACtg} mice were available. Mitochondria in brains of three months old animals had a normal shape (Fig. 42) and there were no changes in protein levels of endo-/lysosomal markers or mitochondrial proteins in brain lysates (Fig. 40, 43). Measurements of mitochondrial respiration by Seahorse in MEFs were also inconspicuous (Fig. 41). The same was true for the two single mutant mouse lines (Fig. 40, 42, 43).

Total TDP-43 levels were doubled in the brain of hTDP-43^{A315TKi} mice as reported before (Stribl et al., 2014), and even tendentially higher in compound mutant animals (Fig. 40). Human TDP-

43 was only detected in hTDP-43^{A315TKi} and compound mutant mice as expected, with a little decrease in compound mutants (Fig. 40), indicating that the endogenous TDP-43 was higher in these mice and that the impact of mutant human TDP-43 disturbed the observed regulation by Tmem106b. TDP-43 levels are autoregulated by a negative feedback loop by binding to its own 3' UTR (Ayala et al., 2011; Polymenidou et al., 2011) and human TDP-43 was found to be overexpressed due to missing 3' UTR and endogenous TDP-43 levels downregulated in hTDP-43^{A315TKi} mice (Stribl et al., 2014). Tmem106b seems to interfere in this autoregulation, as in Tmem106b^{BACtg} mice endogenous TDP-43 was reduced compared to WT and in compound mutants it was elevated compared to hTDP-43^{A315TKi} animals. These results suggest that the regulation by Tmem106b is disrupted by the TDP-43 mutation. Cytoplasmic TDP-43, but no inclusions, was found in motor neurons in the SC and cortical cells of young compound mutant animals (Fig. 39). Only small amounts of insoluble hTDP-43 were detected in brains of three months old hTDP-43^{A315TKi} and compound mutant mice due to overexpression, but no insoluble total TDP-43 in all three lines (Fig. 39), which is in correspondence with published results for the hTDP-43^{A315TKi} mouse line, where higher amounts of insoluble protein were found at the age of twelve months (Stribl et al., 2014). Mitochondrial abnormalities in aged but not in young Tmem106b overexpressing and hTDP-43^{A513TKi} mice (Stribl et al., 2014) and progressive accumulation of TDP-43 in hTDP-43^{A513TKi} mice (Stribl et al., 2014) suggest the assumption that impairments in these mice are progressive and age dependent. Thus, analyses of protein levels of mitochondrial proteins should be repeated with aged single and double transgenic mice, as well as TEM analysis with aged compound mice. Blebbing of mitochondria was especially found in the frontal cortex and less in the cerebellum and not all mitochondria were affected. A lot of normal shaped mitochondria were also found. Thus, for repetition of Western Blots single brain regions should be prepared. 17 months old Tmem106^{BACtg} mice looked healthy before dissection meaning the mitochondrial abnormalities were not critical. However, it was interesting that blebbing of mitochondria was mainly apparent in the frontal cortex, where from patients elevated levels of TMEM106B were reported and which is highly affected in FTLD (Geser et al., 2009; Van Deerlin et al., 2010).

Mitochondrial dysfunction, for instance of the respiratory chain, was connected before with several neurodegenerative diseases such as AD, PD and ALS (Martin, 2010; Swerdlow, 2011; Palomo and Manfredi, 2014). Besides the hTDP-43^{A513TKi} mouse model (Stribl et al., 2014), other publications of TDP rodent models claimed an association of mitochondria and disease (Shan et al., 2010; Braun et al., 2011). SOD1 is a ubiquitous cytoplasmic and mitochondrial enzyme and accounts for about 20% of familial ALS cases (Robberecht and Philips, 2013). In several transgenic rodent models expressing mutant SOD1, mitochondrial dysfunctions like changes in respiratory chain activity, mitochondrial protein composition, or mitochondrial morphology

were observed. Additionally, the animals recapitulated many features of ALS, such as axonal dysfunction, motor neuron loss, and progressive neuromuscular malfunction (Gurney et al., 1994; Ripps et al., 1995; Bruijn et al., 1997; Dal Canto and Gurney, 1997; Nagai et al., 2001; Mattiazzi et al., 2002; Chang-Hong et al., 2005; Li et al., 2010). Expression of human mutant VCP in mice led to TDP-43 aggregates, which were also positive for ubiquitin and colocalized with aggregated mitochondria (Yin et al., 2012) or an accumulation of mitochondrial proteins (Nalbandian et al., 2012). In this study, a blebbing of mitochondria was noticed in aged mice. 'Blebbing' of the cell surface appears early upon hypoxic and toxic injury to cells, for example due to changes in Ca^{2+} levels. Another SOD1(G93A) mouse model was characterized with increased vulnerability of mitochondria and perturbation of Ca^{2+} homeostasis (Jaiswal and Keller, 2009). However, till now no link was forged between mitochondrial dysfunction and FTL. One possible scenario can be that TMEM106b is a modulator of FTL by regulating mitochondrial function.

One point is often discussed concerning TMEM106B - its connection to GRN, a secreted glycoprotein, how this connection is mannered, and whether TMEM106B is up- or downstream of GRN. GRN can be cleaved into granulins, a family of active 6 kDa peptides, which are implicated, along with GRN, in a range of biological processes including development, wound repair, inflammation and tumorigenesis. To date, more than 69 different *GRN* mutations have been identified, which lead to haploinsufficiency and that finally to FTL with TDP-43 inclusions (Sieben et al., 2012). *TMEM106B* was identified as a risk locus for the development of FTL-TDP especially in *GRN* mutation carriers (Van Deerlin et al., 2010; Finch et al., 2011; van der Zee et al., 2011; Lattante et al., 2014). Götzl and colleagues measured increased levels of *Tmem106b* in *Grn* deficient mice (Götzl et al., 2014). These results indicate that GRN is upstream of TMEM106B. Contrary, Finch et al. also found an association of *TMEM106B* SNPs and GRN levels in patients (Finch et al., 2011) and another study reported that the top SNP rs1990622 regulates the age of disease onset in *GRN* mutation carriers this way that they get ill 13 years earlier (Cruchaga et al., 2011). The scientists reported that individuals carrying the protective allele have higher levels of GRN (Cruchaga et al., 2011). *In vitro*, GRN levels were elevated upon TMEM106B overexpression (Chen-Plotkin et al., 2012; Brady et al., 2013; Nicholson et al., 2013). These studies suggest that GRN is downstream of TMEM106B. Other groups could not find a link between the two proteins (Lang et al., 2012; Serpente et al., 2014). In this study no differences could be detected between WT, *Tmem106b*^{BACtg}, hTDP-43^{A513TKi}, or compound mutant mice in Western Blots (Fig. 40). *Grn* mRNA levels were also not changed in hTDP-43^{A513TKi} (see PhD thesis of Carola Stribl). However, an ELISA analysis of serum yielded decreased *Grn* levels in single transgenic mice and WT levels in compound mice (Fig. 41). Measurements did not reach significance due to very high levels in one compound mouse, what could be due to an infection.

In contrast to Brady, Nicholson and Chen-Plotkin, who observed an elevation of GRN due to TMEM106B overexpression (Chen-Plotkin et al., 2012; Brady et al., 2013; Qiu et al., 2014), Grn levels were downregulated in *Tmem106b^{BACtg}* mice. However, in patients carrying the protective allele associated with lower TMEM106B expression, higher levels of GRN were measured (Cruchaga et al., 2011) and Finch suggested that *TMEM106B* SNPs increase its own protein expression and lead to a decrease in GRN levels and such conferring enhanced risk for the development of FTLD (Finch et al., 2011). The question rises, why changes in Grn levels are only obvious in serum of mice and not in brain lysates. First, ELISA is much more sensitive than a Western Blot of whole brain samples. Second, modulation of Grn levels in the blood do not have to be driven by modulation of Grn expression. Cruchaga and colleagues also observed changes in GRN plasma levels without alterations in mRNA and protein levels (Cruchaga et al., 2011). Thus, overexpression of *Tmem106b* and TDP-43 alone seem to influence Grn levels, whereas a combination of both has somehow a compensatory effect.

Taken together, overexpression of *Tmem106b* *in vivo* did not affect life or health of mice, confirming the modulating and not causing role of TMEM106B in FTLD-TDP. However, mitochondrial abnormalities in aged *Tmem106b^{BACtg}* animals are promising and these mice should be bred with Grn or *C9orf72* transgenic mouse models.

7.3 LESSONS FROM MOUSE MODELS GENERATED FOR ALS AND FTLD

In this study different mouse models for ALS and FTLD should be generated and analyzed. Noticeable were the abnormalities in autophagy and mitochondrial morphology. Mitochondria are involved in several stages of autophagy from initial formation of autophagosome to regulation of autophagy, and finally the autophagy-mediated cell death (Rubinsztein et al., 2012). It was suggested that mitochondrial dysfunction and apoptosis play a role in the development of ALS, as degeneration of motor neurons were connected with dysregulation of intracellular Ca^{2+} and excitotoxicity (Ghavami et al., 2014). In 2014, Palomo and Manfredi published a review which is mainly dealing with a possible defective mitochondrial quality control (MQC) in ALS (Palomo and Manfredi, 2014). MQC is the mechanism to clear damaged proteins through proteostasis and to eliminate irreparably damaged organelles through mitophagy (Palomo and Manfredi, 2014), the specific autophagic degradation of mitochondria

(Youle and Narendra, 2011). In ALS, an accumulation of damaged mitochondria in motor neurons is pointing towards a defective MQC (Palomo and Manfredi, 2014).

Not only SOD1, TDP-43, and VCP, but also FUS were associated with mitochondrial dysfunction. The R521C FUS rat model of Huang and group, published in 2011, did not show FUS inclusions, but instead Ubiquitin-positive inclusions, which colocalized with selected mitochondrial proteins, indicating that damaged mitochondria might be degraded upon ubiquitination (Huang et al., 2011). For their FUS rat model recapitulating some features of FTLD they also reported aggregation of mitochondria in degenerating neurons (Huang et al., 2012). For mitophagy an ubiquitin-binding adapter is needed. p62/SQSTM1 was reported to act as such an adapter and to recruit mitochondria to the autophagosome (Palomo and Manfredi, 2014). P62 again interacts with HDAC6 (Histone Deacetylase 6) for the recognition of ubiquitinated mitochondria (Yan et al., 2013), and *HDAC6* mRNA in turn was found to be co-regulated by TDP-43 and FUS (Kim et al., 2010). In this study, an overexpression of *Tmem106b* led to morphological abnormalities in mitochondria and in *Fus* deficient and *Fus*^{R513G} mice p62 was elevated, indicating a lack of auto-, as well as mitophagy. Maybe, mitochondria and mitophagy could be the missing link between ALS and FTLD.

Summarizing, although all models recapitulated single features of neurodegenerative diseases concerning autophagy, mitochondrial abnormalities or motor deficits, none would be sufficient for elucidating disease mechanisms or modeling ALS or FTLD in therapeutic approaches. ALS and FTLD are not caused by one single gene mutation. Both are multifactorial diseases, where several genes and environmental factors act together. This leads to a high variation in age of onset, phenotype, and severity. Hence, it will be very difficult to find a model that really recapitulates ALS or FTLD.

8 REFERENCES

- Adams, H.H., Verhaaren, B.F., Vrooman, H.A., Uitterlinden, A.G., Hofman, A., van Duijn, C.M., van der Lugt, A., Niessen, W.J., Vernooij, M.W., and Ikram, M.A. (2014). **TMEM106B Influences Volume of Left-Sided Temporal Lobe and Interhemispheric Structures in the General Population.** *Biological psychiatry* 76, 503-508.
- Ahmeti, K.B., Ajroud-Driss, S., Al-Chalabi, A., Andersen, P.M., Armstrong, J., Birve, A., Blauw, H.M., Brown, R.H., Bruijn, L., Chen, W., *et al.* (2013). **Age of onset of amyotrophic lateral sclerosis is modulated by a locus on 1p34.1.** *Neurobiology of aging* 34, 357.e357-319.
- Al-Chalabi, A., Jones, A., Troakes, C., King, A., Al-Sarraj, S., and van den Berg, L.H. (2012). **The genetics and neuropathology of amyotrophic lateral sclerosis.** *Acta neuropathologica* 124, 339-352.
- Alirezaei, M., Kiosses, W.B., and Fox, H.S. (2008). **Decreased neuronal autophagy in HIV dementia: a mechanism of indirect neurotoxicity.** *Autophagy* 4, 963-966.
- Alirezaei, M., Kembal, C.C., Flynn, C.T., Wood, M.R., Whitton, J.L., and Kiosses, W.B. (2010). **Short-term fasting induces profound neuronal autophagy.** *Autophagy* 6, 702-710.
- Alirezaei, M., Kembal, C.C., and Whitton, J.L. (2011). **Autophagy, inflammation and neurodegenerative disease.** *The European journal of neuroscience* 33, 197-204.
- Alzheimer, A. (1911). **Über eigenartige Krankheitsfälle des späteren Alters.** *Zeitschrift für die gesamte Neurologie und Psychiatrie* 4, 356-385.
- Andersen, P.M., and Al-Chalabi, A. (2011). **Clinical genetics of amyotrophic lateral sclerosis: what do we really know?** *Nature reviews Neurology* 7, 603-615.
- Anderson, P., and Kedersha, N. (2009). **Stress granules.** *Current biology : CB* 19, R397-398.
- Aoki, N., Higashi, S., Kawakami, I., Kobayashi, Z., Hosokawa, M., Katsuse, O., Togo, T., Hirayasu, Y., and Akiyama, H. (2012). **Localization of fused in sarcoma (FUS) protein to the post-synaptic density in the brain.** *Acta neuropathologica* 124, 383-394.
- Armstrong, G.A., and Drapeau, P. (2013). **Loss and gain of FUS function impair neuromuscular synaptic transmission in a genetic model of ALS.** *Human molecular genetics* 22, 4282-4292.

Ayala, Y.M., De Conti, L., Avendano-Vazquez, S.E., Dhir, A., Romano, M., D'Ambrogio, A., Tollervey, J., Ule, J., Baralle, M., Buratti, E., *et al.* (2011). **TDP-43 regulates its mRNA levels through a negative feedback loop.** *EMBO J* 30, 277-288.

Baechtold, H., Kuroda, M., Sok, J., Ron, D., Lopez, B.S., and Akhmedov, A.T. (1999). **Human 75-kDa DNA-pairing protein is identical to the pro-oncoprotein TLS/FUS and is able to promote D-loop formation.** *The Journal of biological chemistry* 274, 34337-34342.

Baker, M., Mackenzie, I.R., Pickering-Brown, S.M., Gass, J., Rademakers, R., Lindholm, C., Snowden, J., Adamson, J., Sadovnick, A.D., Rollinson, S., *et al.* (2006). **Mutations in progranulin cause tau-negative frontotemporal dementia linked to chromosome 17.** *Nature* 442, 916-919.

Barmada, S.J., Serio, A., Arjun, A., Bilican, B., Daub, A., Ando, D.M., Tsvetkov, A., Pleiss, M., Li, X., Peisach, D., *et al.* (2014). **Autophagy induction enhances TDP43 turnover and survival in neuronal ALS models.** *Nature chemical biology* 10, 677-685.

Baumer, D., Hilton, D., Paine, S.M., Turner, M.R., Lowe, J., Talbot, K., and Ansorge, O. (2010). **Juvenile ALS with basophilic inclusions is a FUS proteinopathy with FUS mutations.** *Neurology* 75, 611-618.

Belly, A., Moreau-Gachelin, F., Sadoul, R., and Goldberg, Y. (2005). **Delocalization of the multifunctional RNA splicing factor TLS/FUS in hippocampal neurones: exclusion from the nucleus and accumulation in dendritic granules and spine heads.** *Neuroscience letters* 379, 152-157.

Bendotti, C., Marino, M., Cheroni, C., Fontana, E., Crippa, V., Poletti, A., and De Biasi, S. (2012). **Dysfunction of constitutive and inducible ubiquitin-proteasome system in amyotrophic lateral sclerosis: implication for protein aggregation and immune response.** *Progress in neurobiology* 97, 101-126.

Bennion Callister, J., and Pickering-Brown, S.M. (2014). **Pathogenesis/genetics of frontotemporal dementia and how it relates to ALS.** *Experimental neurology*.

Bentmann, E., Neumann, M., Tahirovic, S., Rodde, R., Dormann, D., and Haass, C. (2012). **Requirements for stress granule recruitment of fused in sarcoma (FUS) and TAR DNA-binding protein of 43 kDa (TDP-43).** *The Journal of biological chemistry* 287, 23079-23094.

Bentmann, E., Haass, C., and Dormann, D. (2013). **Stress granules in neurodegeneration-- lessons learnt from TAR DNA binding protein of 43 kDa and fused in sarcoma.** *The FEBS journal* 280, 4348-4370.

Bertolotti, A., Lutz, Y., Heard, D.J., Chambon, P., and Tora, L. (1996). **hTAF(II)68, a novel RNA/ssDNA-binding protein with homology to the pro-oncoproteins TLS/FUS and EWS is associated with both TFIID and RNA polymerase II.** *EMBO J* 15, 5022-5031.

Bertolotti, A., Bell, B., and Tora, L. (1999). **The N-terminal domain of human TAFII68 displays transactivation and oncogenic properties.** *Oncogene* 18, 8000-8010.

Bertrand, P., Akhmedov, A.T., Delacote, F., Durrbach, A., and Lopez, B.S. (1999). **Human POMp75 is identified as the pro-oncoprotein TLS/FUS: both POMp75 and POMp100 DNA homologous pairing activities are associated to cell proliferation.** *Oncogene* 18, 4515-4521.

Boillee, S., Vande Velde, C., and Cleveland, D.W. (2006). **ALS: a disease of motor neurons and their nonneuronal neighbors.** *Neuron* 52, 39-59.

Bosco, D.A., Lemay, N., Ko, H.K., Zhou, H., Burke, C., Kwiatkowski, T.J., Jr., Sapp, P., McKenna-Yasek, D., Brown, R.H., Jr., and Hayward, L.J. (2010). **Mutant FUS proteins that cause amyotrophic lateral sclerosis incorporate into stress granules.** *Human molecular genetics* 19, 4160-4175.

Bradley, W.G., and Mash, D.C. (2009). **Beyond Guam: the cyanobacteria/BMAA hypothesis of the cause of ALS and other neurodegenerative diseases.** *Amyotrophic lateral sclerosis : official publication of the World Federation of Neurology Research Group on Motor Neuron Diseases* 10 Suppl 2, 7-20.

Brady, O.A., Zheng, Y., Murphy, K., Huang, M., and Hu, F. (2013). **The frontotemporal lobar degeneration risk factor, TMEM106B, regulates lysosomal morphology and function.** *Human molecular genetics* 22, 685-695.

Brady, O.A., Zhou, X., and Hu, F. (2014). **Regulated intramembrane proteolysis of the frontotemporal lobar degeneration risk factor, TMEM106B, by signal peptide peptidase-like 2a (SPPL2a).** *The Journal of biological chemistry* 289, 19670-19680.

Brandt, R., Hundelt, M., and Shahani, N. (2005). **Tau alteration and neuronal degeneration in tauopathies: mechanisms and models.** *Biochimica et biophysica acta* 1739, 331-354.

Braun, R.J., Sommer, C., Carmona-Gutierrez, D., Khoury, C.M., Ring, J., Buttner, S., and Madeo, F. (2011). **Neurotoxic 43-kDa TAR DNA-binding protein (TDP-43) triggers mitochondrion-dependent programmed cell death in yeast.** *The Journal of biological chemistry* 286, 19958-19972.

Brelstaff, J., Lashley, T., Holton, J.L., Lees, A.J., Rossor, M.N., Bandopadhyay, R., and Revesz, T. (2011). **Transportin1: a marker of FTL-D-FUS.** *Acta neuropathologica* 122, 591-600.

Broustal, O., Camuzat, A., Guillot-Noel, L., Guy, N., Millecamps, S., Deffond, D., Lacomblez, L., Golfier, V., Hannequin, D., Salachas, F., et al. (2010). **FUS mutations in frontotemporal lobar degeneration with amyotrophic lateral sclerosis.** *Journal of Alzheimer's disease : JAD* 22, 765-769.

Bruijn, L.I., Becher, M.W., Lee, M.K., Anderson, K.L., Jenkins, N.A., Copeland, N.G., Sisodia, S.S., Rothstein, J.D., Borchelt, D.R., Price, D.L., *et al.* (1997). **ALS-linked SOD1 mutant G85R mediates damage to astrocytes and promotes rapidly progressive disease with SOD1-containing inclusions.** *Neuron* 18, 327-338.

Burd, C.G., and Dreyfuss, G. (1994). **Conserved structures and diversity of functions of RNA-binding proteins.** *Science* 265, 615-621.

Burrell, J.R., Kiernan, M.C., Vucic, S., and Hodges, J.R. (2011). **Motor neuron dysfunction in frontotemporal dementia.** *Brain : a journal of neurology* 134, 2582-2594.

Busch, J.I., Martinez-Lage, M., Ashbridge, E., Grossman, M., Van Deerlin, V.M., Hu, F., Lee, V.M., Trojanowski, J.Q., and Chen-Plotkin, A.S. (2013). **Expression of TMEM106B, the frontotemporal lobar degeneration-associated protein, in normal and diseased human brain.** *Acta neuropathologica communications* 1, 36.

Calvio, C., Neubauer, G., Mann, M., and Lamond, A.I. (1995). **Identification of hnRNP P2 as TLS/FUS using electrospray mass spectrometry.** *Rna* 1, 724-733.

Capell, A., Liebscher, S., Fellerer, K., Brouwers, N., Willem, M., Lammich, S., Gijssels, I., Bittner, T., Carlson, A.M., Sasse, F., *et al.* (2011). **Rescue of progranulin deficiency associated with frontotemporal lobar degeneration by alkalinizing reagents and inhibition of vacuolar ATPase.** *The Journal of neuroscience : the official journal of the Society for Neuroscience* 31, 1885-1894.

Carter, R.J., Morton, J., and Dunnett, S.B. (2001). **Motor coordination and balance in rodents.** *Current protocols in neuroscience / editorial board, Jacqueline N Crawley [et al] Chapter 8, Unit 8* 12.

Castillo, K., Nassif, M., Valenzuela, V., Rojas, F., Matus, S., Mercado, G., Court, F.A., van Zundert, B., and Hetz, C. (2013). **Trehalose delays the progression of amyotrophic lateral sclerosis by enhancing autophagy in motoneurons.** *Autophagy* 9, 1308-1320.

Chang-Hong, R., Wada, M., Koyama, S., Kimura, H., Arawaka, S., Kawanami, T., Kurita, K., Kadoya, T., Aoki, M., Itoyama, Y., *et al.* (2005). **Neuroprotective effect of oxidized galectin-1 in a transgenic mouse model of amyotrophic lateral sclerosis.** *Experimental neurology* 194, 203-211.

Charcot, J.-M., and Joffroy, A. (1869). Deux cas d'atrophie musculaire progressive: avec lésions de la substance grise et des faisceaux antérolatéraux de la moelle épinière (Masson).
Chen-Plotkin, A.S., Unger, T.L., Gallagher, M.D., Bill, E., Kwong, L.K., Volpicelli-Daley, L., Busch, J.I., Akle, S., Grossman, M., Van Deerlin, V., *et al.* (2012). **TMEM106B, the risk gene for frontotemporal dementia, is regulated by the microRNA-132/212 cluster and affects progranulin pathways.** *The Journal of neuroscience : the official journal of the Society for Neuroscience* 32, 11213-11227.

Chen, S., Sayana, P., Zhang, X., and Le, W. (2013). **Genetics of amyotrophic lateral sclerosis: an update.** *Molecular neurodegeneration* 8, 28.

Chen, Y.Z., Bennett, C.L., Huynh, H.M., Blair, I.P., Puls, I., Irobi, J., Dierick, I., Abel, A., Kennerson, M.L., Rabin, B.A., *et al.* (2004). **DNA/RNA helicase gene mutations in a form of juvenile amyotrophic lateral sclerosis (ALS4).** *American journal of human genetics* 74, 1128-1135.

Chio, A., Logroscino, G., Hardiman, O., Swingler, R., Mitchell, D., Beghi, E., Traynor, B.G., and Eurals, C. (2009). **Prognostic factors in ALS: A critical review.** *Amyotrophic lateral sclerosis : official publication of the World Federation of Neurology Research Group on Motor Neuron Diseases* 10, 310-323.

Chow, C.Y., Landers, J.E., Bergren, S.K., Sapp, P.C., Grant, A.E., Jones, J.M., Everett, L., Lenk, G.M., McKenna-Yasek, D.M., Weisman, L.S., *et al.* (2009). **Deleterious variants of FIG4, a phosphoinositide phosphatase, in patients with ALS.** *American journal of human genetics* 84, 85-88.

Crozat, A., Aman, P., Mandahl, N., and Ron, D. (1993). **Fusion of CHOP to a novel RNA-binding protein in human myxoid liposarcoma.** *Nature* 363, 640-644.

Cruchaga, C., Graff, C., Chiang, H.H., Wang, J., Hinrichs, A.L., Spiegel, N., Bertelsen, S., Mayo, K., Norton, J.B., Morris, J.C., *et al.* (2011). **Association of TMEM106B gene polymorphism with age at onset in granulin mutation carriers and plasma granulin protein levels.** *Archives of neurology* 68, 581-586.

Cruts, M., Gijselinck, I., Van Langenhove, T., van der Zee, J., and Van Broeckhoven, C. (2013). **Current insights into the C9orf72 repeat expansion diseases of the FTLD/ALS spectrum.** *Trends in neurosciences* 36, 450-459.

Cushman, M., Johnson, B.S., King, O.D., Gitler, A.D., and Shorter, J. (2010). **Prion-like disorders: blurring the divide between transmissibility and infectivity.** *Journal of cell science* 123, 1191-1201.

Dal Canto, M.C., and Gurney, M.E. (1997). **A low expressor line of transgenic mice carrying a mutant human Cu,Zn superoxide dismutase (SOD1) gene develops pathological changes that most closely resemble those in human amyotrophic lateral sclerosis.** *Acta neuropathologica* 93, 537-550.

Das, R., Yu, J., Zhang, Z., Gygi, M.P., Krainer, A.R., Gygi, S.P., and Reed, R. (2007). **SR proteins function in coupling RNAP II transcription to pre-mRNA splicing.** *Molecular cell* 26, 867-881.

Daugas, E., Susin, S.A., Zamzami, N., Ferri, K.F., Irinopoulou, T., Larochette, N., Prevost, M.C., Leber, B., Andrews, D., Penninger, J., *et al.* (2000). **Mitochondrio-nuclear translocation of AIF in apoptosis and necrosis.** *FASEB journal : official publication of the Federation of American Societies for Experimental Biology* 14, 729-739.

DeJesus-Hernandez, M., Mackenzie, I.R., Boeve, B.F., Boxer, A.L., Baker, M., Rutherford, N.J., Nicholson, A.M., Finch, N.A., Flynn, H., Adamson, J., *et al.* (2011). **Expanded GGGGCC hexanucleotide repeat in noncoding region of C9ORF72 causes chromosome 9p-linked FTD and ALS.** *Neuron* 72, 245-256.

Deng, H., Gao, K., and Jankovic, J. (2014a). **The role of FUS gene variants in neurodegenerative diseases.** *Nature reviews Neurology* 10, 337-348.

Deng, H.X., Chen, W., Hong, S.T., Boycott, K.M., Gorrie, G.H., Siddique, N., Yang, Y., Fecto, F., Shi, Y., Zhai, H., *et al.* (2011). **Mutations in UBQLN2 cause dominant X-linked juvenile and adult-onset ALS and ALS/dementia.** *Nature* 477, 211-215.

Deng, Q., Holler, C.J., Taylor, G., Hudson, K.F., Watkins, W., Gearing, M., Ito, D., Murray, M.E., Dickson, D.W., Seyfried, N.T., *et al.* (2014b). **FUS is phosphorylated by DNA-PK and accumulates in the cytoplasm after DNA damage.** *The Journal of neuroscience : the official journal of the Society for Neuroscience* 34, 7802-7813.

Dini Modigliani, S., Morlando, M., Errichelli, L., Sabatelli, M., and Bozzoni, I. (2014). **An ALS-associated mutation in the FUS 3'-UTR disrupts a microRNA-FUS regulatory circuitry.** *Nature communications* 5, 4335.

Doi, H., Koyano, S., Suzuki, Y., Nukina, N., and Kuroiwa, Y. (2010). **The RNA-binding protein FUS/TLS is a common aggregate-interacting protein in polyglutamine diseases.** *Neuroscience research* 66, 131-133.

Dols-Icardo, O., Garcia-Redondo, A., Rojas-Garcia, R., Sanchez-Valle, R., Noguera, A., Gomez-Tortosa, E., Pastor, P., Hernandez, I., Esteban-Perez, J., Suarez-Calvet, M., *et al.* (2014). **Characterization of the repeat expansion size in C9orf72 in amyotrophic lateral sclerosis and frontotemporal dementia.** *Human molecular genetics* 23, 749-754.

Dormann, D., Rodde, R., Edbauer, D., Bentmann, E., Fischer, I., Hruscha, A., Than, M.E., Mackenzie, I.R., Capell, A., Schmid, B., *et al.* (2010). **ALS-associated fused in sarcoma (FUS) mutations disrupt Transportin-mediated nuclear import.** *EMBO J* 29, 2841-2857.

Dormann, D., and Haass, C. (2011). **TDP-43 and FUS: a nuclear affair.** *Trends in neurosciences* 34, 339-348.

Dormann, D., Madl, T., Valori, C.F., Bentmann, E., Tahirovic, S., Abou-Ajram, C., Kremmer, E., Ansorge, O., Mackenzie, I.R., Neumann, M., *et al.* (2012). **Arginine methylation next to the PY-NLS modulates Transportin binding and nuclear import of FUS.** *EMBO J* 31, 4258-4275.

Dormann, D., and Haass, C. (2013). **Fused in sarcoma (FUS): an oncogene goes awry in neurodegeneration.** *Molecular and cellular neurosciences* 56, 475-486.

Du, K., Arai, S., Kawamura, T., Matsushita, A., and Kurokawa, R. (2011). **TLS and PRMT1 synergistically coactivate transcription at the survivin promoter through TLS arginine methylation.** *Biochemical and biophysical research communications* 404, 991-996.

Edens, L.J., White, K.H., Jevtic, P., Li, X., and Levy, D.L. (2013). **Nuclear size regulation: from single cells to development and disease.** *Trends in cell biology* 23, 151-159.

Elden, A.C., Kim, H.J., Hart, M.P., Chen-Plotkin, A.S., Johnson, B.S., Fang, X., Armakola, M., Geser, F., Greene, R., Lu, M.M., *et al.* (2010). **Ataxin-2 intermediate-length polyglutamine expansions are associated with increased risk for ALS.** *Nature* 466, 1069-1075.

Englund, B., Brun, A., Gustafson, L., Passant, U., Mann, D., Neary, D., and Snowden, J. (1994). **Clinical and neuropathological criteria for frontotemporal dementia.** *Journal of neurology, neurosurgery, and psychiatry* 57, 416-418.

Fecto, F., Yan, J., Vemula, S.P., Liu, E., Yang, Y., Chen, W., Zheng, J.G., Shi, Y., Siddique, N., Arrat, H., *et al.* (2011). **SQSTM1 mutations in familial and sporadic amyotrophic lateral sclerosis.** *Archives of neurology* 68, 1440-1446.

Feil, R., Holter, S.M., Weindl, K., Wurst, W., Langmesser, S., Gerling, A., Feil, S., and Albrecht, U. (2009). **cGMP-dependent protein kinase I, the circadian clock, sleep and learning.** *Communicative & integrative biology* 2, 298-301.

Finch, N., Carrasquillo, M.M., Baker, M., Rutherford, N.J., Coppola, G., Dejesus-Hernandez, M., Crook, R., Hunter, T., Ghidoni, R., Benussi, L., *et al.* (2011). **TMEM106B regulates progranulin levels and the penetrance of FTLD in GRN mutation carriers.** *Neurology* 76, 467-474.

Fujii, R., Okabe, S., Urushido, T., Inoue, K., Yoshimura, A., Tachibana, T., Nishikawa, T., Hicks, G.G., and Takumi, T. (2005). **The RNA binding protein TLS is translocated to dendritic spines by mGluR5 activation and regulates spine morphology.** *Current biology : CB* 15, 587-593.

Fujii, R., and Takumi, T. (2005). **TLS facilitates transport of mRNA encoding an actin-stabilizing protein to dendritic spines.** *Journal of cell science* 118, 5755-5765.

Gal, J., Zhang, J., Kwinter, D.M., Zhai, J., Jia, H., Jia, J., and Zhu, H. (2011). **Nuclear localization sequence of FUS and induction of stress granules by ALS mutants.** *Neurobiology of aging* 32, 2323 e2327-2340.

Gallagher, M.D., Suh, E., Grossman, M., Elman, L., McCluskey, L., Van Swieten, J.C., Al-Sarraj, S., Neumann, M., Gelpi, E., Ghetti, B., *et al.* (2014). **TMEM106B is a genetic modifier of frontotemporal lobar degeneration with C9orf72 hexanucleotide repeat expansions.** *Acta neuropathologica* 127, 407-418.

Geser, F., Martinez-Lage, M., Robinson, J., Uryu, K., Neumann, M., Brandmeir, N.J., Xie, S.X., Kwong, L.K., Elman, L., McCluskey, L., *et al.* (2009). **Clinical and pathological continuum of multisystem TDP-43 proteinopathies.** *Archives of neurology* 66, 180-189.

Ghavami, S., Shojaei, S., Yeganeh, B., Ande, S.R., Jangamreddy, J.R., Mehrpour, M., Christoffersson, J., Chaabane, W., Moghadam, A.R., Kashani, H.H., *et al.* (2014). **Autophagy and apoptosis dysfunction in neurodegenerative disorders.** *Progress in neurobiology* 112, 24-49.

Gijselinck, I., Van Langenhove, T., van der Zee, J., Sleegers, K., Philtjens, S., Kleinberger, G., Janssens, J., Bettens, K., Van Cauwenberghe, C., Pereson, S., *et al.* (2012). **A C9orf72 promoter repeat expansion in a Flanders-Belgian cohort with disorders of the frontotemporal lobar degeneration-amyotrophic lateral sclerosis spectrum: a gene identification study.** *The Lancet Neurology* 11, 54-65.

Gitler, A.D., and Shorter, J. (2011). **RNA-binding proteins with prion-like domains in ALS and FTLD-U.** *Prion* 5, 179-187.

Gotzl, J.K., Mori, K., Damme, M., Fellerer, K., Tahirovic, S., Kleinberger, G., Janssens, J., van der Zee, J., Lang, C.M., Kremmer, E., *et al.* (2014). **Common pathobiochemical hallmarks of progranulin-associated frontotemporal lobar degeneration and neuronal ceroid lipofuscinosis.** *Acta neuropathologica* 127, 845-860.

Greenway, M.J., Andersen, P.M., Russ, C., Ennis, S., Cashman, S., Donaghy, C., Patterson, V., Swingler, R., Kieran, D., Prehn, J., *et al.* (2006). **ANG mutations segregate with familial and 'sporadic' amyotrophic lateral sclerosis.** *Nature genetics* 38, 411-413.

Gregory, R.I., Yan, K.P., Amuthan, G., Chendrimada, T., Doratotaj, B., Cooch, N., and Shiekhattar, R. (2004). **The Microprocessor complex mediates the genesis of microRNAs.** *Nature* 432, 235-240.

Groen, E.J., Fumoto, K., Blokhuis, A.M., Engelen-Lee, J., Zhou, Y., van den Heuvel, D.M., Koppers, M., van Diggelen, F., van Heest, J., Demmers, J.A., *et al.* (2013). **ALS-associated mutations in FUS disrupt the axonal distribution and function of SMN.** *Human molecular genetics* 22, 3690-3704.

Gurney, M.E., Pu, H., Chiu, A.Y., Dal Canto, M.C., Polchow, C.Y., Alexander, D.D., Caliendo, J., Hentati, A., Kwon, Y.W., Deng, H.X., *et al.* (1994). **Motor neuron degeneration in mice that express a human Cu,Zn superoxide dismutase mutation.** *Science* 264, 1772-1775.

Haass, C. (2013). **Cellular mechanisms of ALS mutations - a loss or a gain of function?** *Drug research* 63 Suppl 1, S17.

Hackl, W., and Luhrmann, R. (1996). **Molecular cloning and subcellular localisation of the snRNP-associated protein 69KD, a structural homologue of the proto-oncoproteins TLS and EWS with RNA and DNA-binding properties.** *Journal of molecular biology* 264, 843-851.

Hadano, S., Hand, C.K., Osuga, H., Yanagisawa, Y., Otomo, A., Devon, R.S., Miyamoto, N., Showguchi-Miyata, J., Okada, Y., Singaraja, R., *et al.* (2001). **A gene encoding a putative GTPase regulator is mutated in familial amyotrophic lateral sclerosis 2.** *Nature genetics* 29, 166-173.

Haley, R.W. (2003). **Excess incidence of ALS in young Gulf War veterans.** *Neurology* 61, 750-756.

Hand, C.K., Khoris, J., Salachas, F., Gros-Louis, F., Lopes, A.A., Mayeux-Portas, V., Brewer, C.G., Brown, R.H., Jr., Meininger, V., Camu, W., *et al.* (2002). **A novel locus for familial amyotrophic lateral sclerosis, on chromosome 18q.** *American journal of human genetics* 70, 251-256.

Hicks, G.G., Singh, N., Nashabi, A., Mai, S., Bozek, G., Klewes, L., Arapovic, D., White, E.K., Koury, M.J., Oltz, E.M., *et al.* (2000). **Fus deficiency in mice results in defective B-lymphocyte development and activation, high levels of chromosomal instability and perinatal death.** *Nature genetics* 24, 175-179.

Hodges, J.R., Davies, R., Xuereb, J., Kril, J., and Halliday, G. (2003). **Survival in frontotemporal dementia.** *Neurology* 61, 349-354.

Hoell, J.I., Larsson, E., Runge, S., Nusbaum, J.D., Duggimpudi, S., Farazi, T.A., Hafner, M., Borkhardt, A., Sander, C., and Tuschl, T. (2011). **RNA targets of wild-type and mutant FET family proteins.** *Nature structural & molecular biology* 18, 1428-1431.

Horner, R.D., Kamins, K.G., Feussner, J.R., Grambow, S.C., Hoff-Lindquist, J., Harati, Y., Mitsumoto, H., Pascuzzi, R., Spencer, P.S., Tim, R., *et al.* (2003). **Occurrence of amyotrophic lateral sclerosis among Gulf War veterans.** *Neurology* 61, 742-749.

Huang, C., Zhou, H., Tong, J., Chen, H., Liu, Y.J., Wang, D., Wei, X., and Xia, X.G. (2011). **FUS transgenic rats develop the phenotypes of amyotrophic lateral sclerosis and frontotemporal lobar degeneration.** *PLoS genetics* 7, e1002011.

Huang, C., Tong, J., Bi, F., Wu, Q., Huang, B., Zhou, H., and Xia, X.G. (2012). **Entorhinal cortical neurons are the primary targets of FUS mislocalization and ubiquitin aggregation in FUS transgenic rats.** *Human molecular genetics* 21, 4602-4614.

Hutton, M., Lendon, C.L., Rizzu, P., Baker, M., Froelich, S., Houlden, H., Pickering-Brown, S., Chakraverty, S., Isaacs, A., Grover, A., *et al.* (1998). **Association of missense and 5'-splice-site mutations in tau with the inherited dementia FTDP-17.** *Nature* 393, 702-705.

Ichimura, Y., Kumanomidou, T., Sou, Y.S., Mizushima, T., Ezaki, J., Ueno, T., Kominami, E., Yamane, T., Tanaka, K., and Komatsu, M. (2008). **Structural basis for sorting mechanism of p62 in selective autophagy.** *The Journal of biological chemistry* 283, 22847-22857.

Iko, Y., Kodama, T.S., Kasai, N., Oyama, T., Morita, E.H., Muto, T., Okumura, M., Fujii, R., Takumi, T., Tate, S., *et al.* (2004). **Domain architectures and characterization of an RNA-binding protein, TLS.** *The Journal of biological chemistry* 279, 44834-44840.

Ishigaki, S., Masuda, A., Fujioka, Y., Iguchi, Y., Katsuno, M., Shibata, A., Urano, F., Sobue, G., and Ohno, K. (2012). **Position-dependent FUS-RNA interactions regulate alternative splicing events and transcriptions.** *Scientific reports* 2, 529.

Ito, D., Seki, M., Tsunoda, Y., Uchiyama, H., and Suzuki, N. (2011). **Nuclear transport impairment of amyotrophic lateral sclerosis-linked mutations in FUS/TLS.** *Annals of neurology* 69, 152-162.

Jaiswal, M.K., and Keller, B.U. (2009). **Cu/Zn superoxide dismutase typical for familial amyotrophic lateral sclerosis increases the vulnerability of mitochondria and perturbs Ca²⁺ homeostasis in SOD1G93A mice.** *Molecular pharmacology* 75, 478-489.

Jevtic, P., and Levy, D.L. (2014). **Mechanisms of nuclear size regulation in model systems and cancer.** *Advances in experimental medicine and biology* 773, 537-569.

Johnson, J.K., Diehl, J., Mendez, M.F., Neuhaus, J., Shapira, J.S., Forman, M., Chute, D.J., Roberson, E.D., Pace-Savitsky, C., Neumann, M., *et al.* (2005). **Frontotemporal lobar degeneration: demographic characteristics of 353 patients.** *Archives of neurology* 62, 925-930.

Johnson, J.O., Mandrioli, J., Benatar, M., Abramzon, Y., Van Deerlin, V.M., Trojanowski, J.Q., Gibbs, J.R., Brunetti, M., Gronka, S., Wu, J., *et al.* (2010). **Exome sequencing reveals VCP mutations as a cause of familial ALS.** *Neuron* 68, 857-864.

Josephs, K.A. (2008). **Frontotemporal dementia and related disorders: deciphering the enigma.** *Annals of neurology* 64, 4-14.

Josephs, K.A., Hodges, J.R., Snowden, J.S., Mackenzie, I.R., Neumann, M., Mann, D.M., and Dickson, D.W. (2011). **Neuropathological background of phenotypical variability in frontotemporal dementia.** *Acta neuropathologica* 122, 137-153.

Juneja, T., Pericak-Vance, M.A., Laing, N.G., Dave, S., and Siddique, T. (1997). **Prognosis in familial amyotrophic lateral sclerosis: progression and survival in patients with glu100gly and ala4val mutations in Cu,Zn superoxide dismutase.** *Neurology* 48, 55-57.

Kim, S.H., Shanware, N.P., Bowler, M.J., and Tibbetts, R.S. (2010). **Amyotrophic lateral sclerosis-associated proteins TDP-43 and FUS/TLS function in a common biochemical complex to co-regulate HDAC6 mRNA.** *The Journal of biological chemistry* 285, 34097-34105.

King, O.D., Gitler, A.D., and Shorter, J. (2012). **The tip of the iceberg: RNA-binding proteins with prion-like domains in neurodegenerative disease.** *Brain research* 1462, 61-80.

Kino, Y., Washizu, C., Aquilanti, E., Okuno, M., Kurosawa, M., Yamada, M., Doi, H., and Nukina, N. (2011). **Intracellular localization and splicing regulation of FUS/TLS are variably affected by amyotrophic lateral sclerosis-linked mutations.** *Nucleic acids research* 39, 2781-2798.

Knopman, D.S., Petersen, R.C., Edland, S.D., Cha, R.H., and Rocca, W.A. (2004). **The incidence of frontotemporal lobar degeneration in Rochester, Minnesota, 1990 through 1994.** *Neurology* 62, 506-508.

Kobayashi, Y., Sakemura, R., Kumagai, A., Sumikawa, E., Fujii, M., and Ayusawa, D. (2008). **Nuclear swelling occurs during premature senescence mediated by MAP kinases in normal human fibroblasts.** *Bioscience, biotechnology, and biochemistry* 72, 1122-1125.

Kuhn, R., and Wefers, B. (2014). **Editing and investigating genomes with TALE and CRISPR/Cas systems: Genome engineering across species using TALENs.** *Methods* 69, 1.

Kuroda, M., Sok, J., Webb, L., Baechtold, H., Urano, F., Yin, Y., Chung, P., de Rooij, D.G., Akhmedov, A., Ashley, T., *et al.* (2000). **Male sterility and enhanced radiation sensitivity in TLS(-/-) mice.** *EMBO J* 19, 453-462.

Kuusisto, E., Kauppinen, T., and Alafuzoff, I. (2008). **Use of p62/SQSTM1 antibodies for neuropathological diagnosis.** *Neuropathology and applied neurobiology* 34, 169-180.

Kwiatkowski, T.J., Jr., Bosco, D.A., Leclerc, A.L., Tamrazian, E., Vanderburg, C.R., Russ, C., Davis, A., Gilchrist, J., Kasarskis, E.J., Munsat, T., *et al.* (2009). **Mutations in the FUS/TLS gene on chromosome 16 cause familial amyotrophic lateral sclerosis.** *Science* 323, 1205-1208.

Lagier-Tourenne, C., and Cleveland, D.W. (2009). **Rethinking ALS: the FUS about TDP-43.** *Cell* 136, 1001-1004.

Lagier-Tourenne, C., Polymenidou, M., and Cleveland, D.W. (2010). **TDP-43 and FUS/TLS: emerging roles in RNA processing and neurodegeneration.** *Human molecular genetics* 19, R46-64.

Lagier-Tourenne, C., Polymenidou, M., Hutt, K.R., Vu, A.Q., Baughn, M., Huelga, S.C., Clutario, K.M., Ling, S.C., Liang, T.Y., Mazur, C., *et al.* (2012). **Divergent roles of ALS-linked proteins FUS/TLS and TDP-43 intersect in processing long pre-mRNAs.** *Nature neuroscience* 15, 1488-1497.

Lagier-Tourenne, C., Baughn, M., Rigo, F., Sun, S., Liu, P., Li, H.R., Jiang, J., Watt, A.T., Chun, S., Katz, M., *et al.* (2013). **Targeted degradation of sense and antisense C9orf72 RNA foci as therapy for ALS and frontotemporal degeneration.** *Proceedings of the National Academy of Sciences of the United States of America* 110, E4530-4539.

Landers, J.E., Melki, J., Meininger, V., Glass, J.D., van den Berg, L.H., van Es, M.A., Sapp, P.C., van Vught, P.W., McKenna-Yasek, D.M., Blauw, H.M., *et al.* (2009). **Reduced expression of the**

Kinesin-Associated Protein 3 (KIFAP3) gene increases survival in sporadic amyotrophic lateral sclerosis. *Proceedings of the National Academy of Sciences of the United States of America* 106, 9004-9009.

Lang, C.M., Fellerer, K., Schwenk, B.M., Kuhn, P.H., Kremmer, E., Edbauer, D., Capell, A., and Haass, C. (2012). **Membrane orientation and subcellular localization of transmembrane protein 106B (TMEM106B), a major risk factor for frontotemporal lobar degeneration.** *The Journal of biological chemistry* 287, 19355-19365.

Lanson, N.A., Jr., and Pandey, U.B. (2012). **FUS-related proteinopathies: lessons from animal models.** *Brain research* 1462, 44-60.

Lattante, S., Le Ber, I., Galimberti, D., Serpente, M., Rivaud-Pechoux, S., Camuzat, A., Clot, F., Fenoglio, C., French research network on, F.T.D., Ftd, A.L.S., *et al.* (2014). **Defining the association of TMEM106B variants among frontotemporal lobar degeneration patients with GRN mutations and C9orf72 repeat expansions.** *Neurobiology of aging* 35, 2658 e2651-2655.

Lee, B.J., Cansizoglu, A.E., Suel, K.E., Louis, T.H., Zhang, Z., and Chook, Y.M. (2006). **Rules for nuclear localization sequence recognition by karyopherin beta 2.** *Cell* 126, 543-558.

Lerga, A., Hallier, M., Delva, L., Orvain, C., Gallais, I., Marie, J., and Moreau-Gachelin, F. (2001). **Identification of an RNA binding specificity for the potential splicing factor TLS.** *The Journal of biological chemistry* 276, 6807-6816.

Li, L., Zhang, X., and Le, W. (2008). **Altered macroautophagy in the spinal cord of SOD1 mutant mice.** *Autophagy* 4, 290-293.

Li, Q., Vande Velde, C., Israelson, A., Xie, J., Bailey, A.O., Dong, M.Q., Chun, S.J., Roy, T., Winer, L., Yates, J.R., *et al.* (2010). **ALS-linked mutant superoxide dismutase 1 (SOD1) alters mitochondrial protein composition and decreases protein import.** *Proceedings of the National Academy of Sciences of the United States of America* 107, 21146-21151.

Lillo, P., and Hodges, J.R. (2009). **Frontotemporal dementia and motor neurone disease: overlapping clinic-pathological disorders.** *Journal of clinical neuroscience : official journal of the Neurosurgical Society of Australasia* 16, 1131-1135.

Ling, S.C., Polymenidou, M., and Cleveland, D.W. (2013). **Converging mechanisms in ALS and FTD: disrupted RNA and protein homeostasis.** *Neuron* 79, 416-438.

Livak, K.J., and Schmittgen, T.D. (2001). **Analysis of relative gene expression data using real-time quantitative PCR and the 2(-Delta Delta C(T)) Method.** *Methods* 25, 402-408.

Logroscino, G., Traynor, B.J., Hardiman, O., Chio, A., Mitchell, D., Swingler, R.J., Millul, A., Benn, E., Beghi, E., and Eurala (2010). **Incidence of amyotrophic lateral sclerosis in Europe.** *Journal of neurology, neurosurgery, and psychiatry* 81, 385-390.

Lomen-Hoerth, C., Anderson, T., and Miller, B. (2002). **The overlap of amyotrophic lateral sclerosis and frontotemporal dementia.** *Neurology* 59, 1077-1079.

Lomen-Hoerth, C., Murphy, J., Langmore, S., Kramer, J.H., Olney, R.K., and Miller, B. (2003). **Are amyotrophic lateral sclerosis patients cognitively normal?** *Neurology* 60, 1094-1097.

Lu, R.C., Wang, H., Tan, M.S., Yu, J.T., and Tan, L. (2014). **TMEM106B and APOE polymorphisms interact to confer risk for late-onset Alzheimer's disease in Han Chinese.** *Journal of neural transmission* 121, 283-287.

Luke, G.A., de Felipe, P., Lukashev, A., Kallioinen, S.E., Bruno, E.A., and Ryan, M.D. (2008). **Occurrence, function and evolutionary origins of '2A-like' sequences in virus genomes.** *The Journal of general virology* 89, 1036-1042.

Mackenzie, I.R., Foti, D., Woulfe, J., and Hurwitz, T.A. (2008). **Atypical frontotemporal lobar degeneration with ubiquitin-positive, TDP-43-negative neuronal inclusions.** *Brain : a journal of neurology* 131, 1282-1293.

Mackenzie, I.R., Neumann, M., Bigio, E.H., Cairns, N.J., Alafuzoff, I., Kril, J., Kovacs, G.G., Ghetti, B., Halliday, G., Holm, I.E., *et al.* (2009). **Nomenclature for neuropathologic subtypes of frontotemporal lobar degeneration: consensus recommendations.** *Acta neuropathologica* 117, 15-18.

Mackenzie, I.R., Rademakers, R., and Neumann, M. (2010). **TDP-43 and FUS in amyotrophic lateral sclerosis and frontotemporal dementia.** *The Lancet Neurology* 9, 995-1007.

Mackenzie, I.R., Ansorge, O., Strong, M., Bilbao, J., Zinman, L., Ang, L.C., Baker, M., Stewart, H., Eisen, A., Rademakers, R., *et al.* (2011a). **Pathological heterogeneity in amyotrophic lateral sclerosis with FUS mutations: two distinct patterns correlating with disease severity and mutation.** *Acta neuropathologica* 122, 87-98.

Mackenzie, I.R., Munoz, D.G., Kusaka, H., Yokota, O., Ishihara, K., Roeber, S., Kretschmar, H.A., Cairns, N.J., and Neumann, M. (2011b). **Distinct pathological subtypes of FTL-D-FUS.** *Acta neuropathologica* 121, 207-218.

Mackenzie, I.R., and Neumann, M. (2012). **FET proteins in frontotemporal dementia and amyotrophic lateral sclerosis.** *Brain research* 1462, 40-43.

Mandillo, S., Tucci, V., Holter, S.M., Meziane, H., Banhaabouchi, M.A., Kallnik, M., Lad, H.V., Nolan, P.M., Ouagazzal, A.M., Coghill, E.L., *et al.* (2008). **Reliability, robustness, and reproducibility in**

mouse behavioral phenotyping: a cross-laboratory study. *Physiological genomics* 34, 243-255.

Martin, L.J. (2010). **Mitochondrial and Cell Death Mechanisms in Neurodegenerative Diseases.** *Pharmaceuticals* 3, 839-915.

Maruyama, H., Morino, H., Ito, H., Izumi, Y., Kato, H., Watanabe, Y., Kinoshita, Y., Kamada, M., Nodera, H., Suzuki, H., *et al.* (2010). **Mutations of optineurin in amyotrophic lateral sclerosis.** *Nature* 465, 223-226.

Mastrocola, A.S., Kim, S.H., Trinh, A.T., Rodenkirch, L.A., and Tibbetts, R.S. (2013). **The RNA-binding protein fused in sarcoma (FUS) functions downstream of poly(ADP-ribose) polymerase (PARP) in response to DNA damage.** *The Journal of biological chemistry* 288, 24731-24741.

Mattiazzi, M., D'Aurelio, M., Gajewski, C.D., Martushova, K., Kiaei, M., Beal, M.F., and Manfredi, G. (2002). **Mutated human SOD1 causes dysfunction of oxidative phosphorylation in mitochondria of transgenic mice.** *The Journal of biological chemistry* 277, 29626-29633.

McGoldrick, P., Joyce, P.I., Fisher, E.M., and Greensmith, L. (2013). **Rodent models of amyotrophic lateral sclerosis.** *Biochimica et biophysica acta* 1832, 1421-1436.

McKhann, G.M., Albert, M.S., Grossman, M., Miller, B., Dickson, D., Trojanowski, J.Q., Work Group on Frontotemporal, D., and Pick's, D. (2001). **Clinical and pathological diagnosis of frontotemporal dementia: report of the Work Group on Frontotemporal Dementia and Pick's Disease.** *Archives of neurology* 58, 1803-1809.

Mercy, L., Hodges, J.R., Dawson, K., Barker, R.A., and Brayne, C. (2008). **Incidence of early-onset dementias in Cambridgeshire, United Kingdom.** *Neurology* 71, 1496-1499.

Merner, N.D., Girard, S.L., Catoire, H., Bourassa, C.V., Belzil, V.V., Riviere, J.B., Hince, P., Levert, A., Dionne-Laporte, A., Spiegelman, D., *et al.* (2012). **Exome sequencing identifies FUS mutations as a cause of essential tremor.** *American journal of human genetics* 91, 313-319.

Mitchell, J.C., McGoldrick, P., Vance, C., Hortobagyi, T., Sreedharan, J., Rogelj, B., Tudor, E.L., Smith, B.N., Klasen, C., Miller, C.C., *et al.* (2013). **Overexpression of human wild-type FUS causes progressive motor neuron degeneration in an age- and dose-dependent fashion.** *Acta neuropathologica* 125, 273-288.

Mizuno, Y., Amari, M., Takatama, M., Aizawa, H., Mihara, B., and Okamoto, K. (2006). **Immunoreactivities of p62, an ubiquitin-binding protein, in the spinal anterior horn cells of patients with amyotrophic lateral sclerosis.** *Journal of the neurological sciences* 249, 13-18.

Mori, K., Weng, S.M., Arzberger, T., May, S., Rentzsch, K., Kremmer, E., Schmid, B., Kretzschmar, H.A., Cruts, M., Van Broeckhoven, C., *et al.* (2013). **The C9orf72 GGGGCC repeat is translated into aggregating dipeptide-repeat proteins in FTLN/ALS.** *Science* 339, 1335-1338.

Morlando, M., Dini Modigliani, S., Torrelli, G., Rosa, A., Di Carlo, V., Caffarelli, E., and Bozzoni, I. (2012). **FUS stimulates microRNA biogenesis by facilitating co-transcriptional Drosha recruitment.** *EMBO J* 31, 4502-4510.

Munch, C., Sedlmeier, R., Meyer, T., Homberg, V., Sperfeld, A.D., Kurt, A., Prudlo, J., Peraus, G., Hanemann, C.O., Stumm, G., *et al.* (2004). **Point mutations of the p150 subunit of dynactin (DCTN1) gene in ALS.** *Neurology* 63, 724-726.

Nagai, M., Aoki, M., Miyoshi, I., Kato, M., Pasinelli, P., Kasai, N., Brown, R.H., Jr., and Itoyama, Y. (2001). **Rats expressing human cytosolic copper-zinc superoxide dismutase transgenes with amyotrophic lateral sclerosis: associated mutations develop motor neuron disease.** *The Journal of neuroscience : the official journal of the Society for Neuroscience* 21, 9246-9254.

Nalbandian, A., Llewellyn, K.J., Kitazawa, M., Yin, H.Z., Badadani, M., Khanlou, N., Edwards, R., Nguyen, C., Mukherjee, J., Mozaffar, T., *et al.* (2012). **The homozygote VCP(R(1)(5)(5)H/R(1)(5)(5)H) mouse model exhibits accelerated human VCP-associated disease pathology.** *PloS one* 7, e46308.

Neary, D., Snowden, J.S., Gustafson, L., Passant, U., Stuss, D., Black, S., Freedman, M., Kertesz, A., Robert, P.H., Albert, M., *et al.* (1998). **Frontotemporal lobar degeneration: a consensus on clinical diagnostic criteria.** *Neurology* 51, 1546-1554.

Neumann, M., Sampathu, D.M., Kwong, L.K., Truax, A.C., Micsenyi, M.C., Chou, T.T., Bruce, J., Schuck, T., Grossman, M., Clark, C.M., *et al.* (2006). **Ubiquitinated TDP-43 in frontotemporal lobar degeneration and amyotrophic lateral sclerosis.** *Science* 314, 130-133.

Neumann, M., Rademakers, R., Roeber, S., Baker, M., Kretzschmar, H.A., and Mackenzie, I.R. (2009a). **A new subtype of frontotemporal lobar degeneration with FUS pathology.** *Brain : a journal of neurology* 132, 2922-2931.

Neumann, M., Roeber, S., Kretzschmar, H.A., Rademakers, R., Baker, M., and Mackenzie, I.R. (2009b). **Abundant FUS-immunoreactive pathology in neuronal intermediate filament inclusion disease.** *Acta neuropathologica* 118, 605-616.

Neumann, M., Bentmann, E., Dormann, D., Jawaid, A., DeJesus-Hernandez, M., Ansorge, O., Roeber, S., Kretzschmar, H.A., Munoz, D.G., Kusaka, H., *et al.* (2011). **FET proteins TAF15 and EWS are selective markers that distinguish FTLN with FUS pathology from amyotrophic lateral sclerosis with FUS mutations.** *Brain : a journal of neurology* 134, 2595-2609.

Neumann, M., Valori, C.F., Ansorge, O., Kretzschmar, H.A., Munoz, D.G., Kusaka, H., Yokota, O., Ishihara, K., Ang, L.C., Bilbao, J.M., *et al.* (2012). **Transportin 1 accumulates specifically with**

FET proteins but no other transportin cargos in FTLD-FUS and is absent in FUS inclusions in ALS with FUS mutations. *Acta neuropathologica* 124, 705-716.

Nicholson, A.M., Finch, N.A., Wojtas, A., Baker, M.C., Perkerson, R.B., 3rd, Castanedes-Casey, M., Rousseau, L., Benussi, L., Binetti, G., Ghidoni, R., *et al.* (2013). **TMEM106B p.T185S regulates TMEM106B protein levels: implications for frontotemporal dementia.** *Journal of neurochemistry* 126, 781-791.

Nishimura, A.L., Mitne-Neto, M., Silva, H.C., Richieri-Costa, A., Middleton, S., Cascio, D., Kok, F., Oliveira, J.R., Gillingwater, T., Webb, J., *et al.* (2004). **A mutation in the vesicle-trafficking protein VAPB causes late-onset spinal muscular atrophy and amyotrophic lateral sclerosis.** *American journal of human genetics* 75, 822-831.

Niu, C., Zhang, J., Gao, F., Yang, L., Jia, M., Zhu, H., and Gong, W. (2012). **FUS-NLS/Transportin 1 complex structure provides insights into the nuclear targeting mechanism of FUS and the implications in ALS.** *PLoS one* 7, e47056.

Ogier-Denis, E., and Codogno, P. (2003). **Autophagy: a barrier or an adaptive response to cancer.** *Biochimica et biophysica acta* 1603, 113-128.

Oh, Y.K., Shin, K.S., and Kang, S.J. (2006). **AIF translocates to the nucleus in the spinal motor neurons in a mouse model of ALS.** *Neuroscience letters* 406, 205-210.

Orlacchio, A., Babalini, C., Borreca, A., Patrono, C., Massa, R., Basaran, S., Munhoz, R.P., Rogaeva, E.A., St George-Hyslop, P.H., Bernardi, G., *et al.* (2010). **SPATACSIN mutations cause autosomal recessive juvenile amyotrophic lateral sclerosis.** *Brain : a journal of neurology* 133, 591-598.

Orozco, D., Tahirovic, S., Rentzsch, K., Schwenk, B.M., Haass, C., and Edbauer, D. (2012). **Loss of fused in sarcoma (FUS) promotes pathological Tau splicing.** *EMBO reports* 13, 759-764.

Otomo, A., Pan, L., and Hadano, S. (2012). **Dysregulation of the autophagy-endolysosomal system in amyotrophic lateral sclerosis and related motor neuron diseases.** *Neurology research international* 2012, 498428.

Palomo, G.M., and Manfredi, G. (2014). **Exploring new pathways of neurodegeneration in ALS: The role of mitochondria quality control.** *Brain research.*

Panda, S.K., Wefers, B., Ortiz, O., Floss, T., Schmid, B., Haass, C., Wurst, W., and Kuhn, R. (2013). **Highly efficient targeted mutagenesis in mice using TALENs.** *Genetics* 195, 703-713.

Pankiv, S., Clausen, T.H., Lamark, T., Brech, A., Bruun, J.A., Outzen, H., Overvatn, A., Bjorkoy, G., and Johansen, T. (2007). **p62/SQSTM1 binds directly to Atg8/LC3 to facilitate degradation of ubiquitinated protein aggregates by autophagy.** *The Journal of biological chemistry* 282, 24131-24145.

Parkinson, N., Ince, P.G., Smith, M.O., Highley, R., Skibinski, G., Andersen, P.M., Morrison, K.E., Pall, H.S., Hardiman, O., Collinge, J., *et al.* (2006). **ALS phenotypes with mutations in CHMP2B (charged multivesicular body protein 2B)**. *Neurology* 67, 1074-1077.

Pasinelli, P., and Brown, R.H. (2006). **Molecular biology of amyotrophic lateral sclerosis: insights from genetics**. *Nature reviews Neuroscience* 7, 710-723.

Perez-Losada, J., Pintado, B., Gutierrez-Adan, A., Flores, T., Banares-Gonzalez, B., del Campo, J.C., Martin-Martin, J.F., Battaner, E., and Sanchez-Garcia, I. (2000). **The chimeric FUS/TLS-CHOP fusion protein specifically induces liposarcomas in transgenic mice**. *Oncogene* 19, 2413-2422.

Perry, D.C., and Miller, B.L. (2013). **Frontotemporal dementia**. *Seminars in neurology* 33, 336-341.

Pick, A. (1892). **Über die Beziehungen der senilen Hirnatrophie zur Aphasie**. *Prag Med Wochenschr* 17, 165-167.

Pickford, F., Masliah, E., Britschgi, M., Lucin, K., Narasimhan, R., Jaeger, P.A., Small, S., Spencer, B., Rockenstein, E., Levine, B., *et al.* (2008). **The autophagy-related protein beclin 1 shows reduced expression in early Alzheimer disease and regulates amyloid beta accumulation in mice**. *The Journal of clinical investigation* 118, 2190-2199.

Pietrocola, F., Malik, S.A., Marino, G., Vacchelli, E., Senovilla, L., Chaba, K., Niso-Santano, M., Maiuri, M.C., Madeo, F., and Kroemer, G. (2014). **Coffee induces autophagy in vivo**. *Cell cycle* 13, 1987-1994.

Plato, C.C., Garruto, R.M., Galasko, D., Craig, U.K., Plato, M., Gamst, A., Torres, J.M., and Wiederholt, W. (2003). **Amyotrophic lateral sclerosis and parkinsonism-dementia complex of Guam: changing incidence rates during the past 60 years**. *American journal of epidemiology* 157, 149-157.

Plumier, J.C., Hopkins, D.A., Robertson, H.A., and Currie, R.W. (1997). **Constitutive expression of the 27-kDa heat shock protein (Hsp27) in sensory and motor neurons of the rat nervous system**. *The Journal of comparative neurology* 384, 409-428.

Polymenidou, M., Lagier-Tourenne, C., Hutt, K.R., Huelga, S.C., Moran, J., Liang, T.Y., Ling, S.C., Sun, E., Wancewicz, E., Mazur, C., *et al.* (2011). **Long pre-mRNA depletion and RNA missplicing contribute to neuronal vulnerability from loss of TDP-43**. *Nature neuroscience* 14, 459-468.

Powers, C.A., Mathur, M., Raaka, B.M., Ron, D., and Samuels, H.H. (1998). **TLS (translocated-in-liposarcoma) is a high-affinity interactor for steroid, thyroid hormone, and retinoid receptors**. *Molecular endocrinology* 12, 4-18.

- Prasad, D.D., Ouchida, M., Lee, L., Rao, V.N., and Reddy, E.S. (1994). **TLS/FUS fusion domain of TLS/FUS-erg chimeric protein resulting from the t(16;21) chromosomal translocation in human myeloid leukemia functions as a transcriptional activation domain.** *Oncogene* 9, 3717-3729.
- Premi, E., Formenti, A., Gazzina, S., Archetti, S., Gasparotti, R., Padovani, A., and Borroni, B. (2014). **Effect of TMEM106B polymorphism on functional network connectivity in asymptomatic GRN mutation carriers.** *JAMA neurology* 71, 216-221.
- Qiu, H., Lee, S., Shang, Y., Wang, W.Y., Au, K.F., Kamiya, S., Barmada, S.J., Finkbeiner, S., Lui, H., Carlton, C.E., *et al.* (2014). **ALS-associated mutation FUS-R521C causes DNA damage and RNA splicing defects.** *The Journal of clinical investigation* 124, 981-999.
- Rabbitts, T.H., Forster, A., Larson, R., and Nathan, P. (1993). **Fusion of the dominant negative transcription regulator CHOP with a novel gene FUS by translocation t(12;16) in malignant liposarcoma.** *Nature genetics* 4, 175-180.
- Rademakers, R., Neumann, M., and Mackenzie, I.R. (2012). **Advances in understanding the molecular basis of frontotemporal dementia.** *Nature reviews Neurology* 8, 423-434.
- Ramesh Babu, J., Lamar Seibenhener, M., Peng, J., Strom, A.L., Kemppainen, R., Cox, N., Zhu, H., Wooten, M.C., Diaz-Meco, M.T., Moscat, J., *et al.* (2008). **Genetic inactivation of p62 leads to accumulation of hyperphosphorylated tau and neurodegeneration.** *Journal of neurochemistry* 106, 107-120.
- Rappsilber, J., Ryder, U., Lamond, A.I., and Mann, M. (2002). **Large-scale proteomic analysis of the human spliceosome.** *Genome research* 12, 1231-1245.
- Ratnavalli, E., Brayne, C., Dawson, K., and Hodges, J.R. (2002). **The prevalence of frontotemporal dementia.** *Neurology* 58, 1615-1621.
- Ravenscroft, T.A., Baker, M.C., Rutherford, N.J., Neumann, M., Mackenzie, I.R., Josephs, K.A., Boeve, B.F., Petersen, R., Halliday, G.M., Kril, J., *et al.* (2013). **Mutations in protein N-arginine methyltransferases are not the cause of FTLD-FUS.** *Neurobiology of aging* 34, 2235 e2211-2233.
- Renton, A.E., Majounie, E., Waite, A., Simon-Sanchez, J., Rollinson, S., Gibbs, J.R., Schymick, J.C., Laaksovirta, H., van Swieten, J.C., Myllykangas, L., *et al.* (2011). **A hexanucleotide repeat expansion in C9ORF72 is the cause of chromosome 9p21-linked ALS-FTD.** *Neuron* 72, 257-268.
- Renton, A.E., Chio, A., and Traynor, B.J. (2014). **State of play in amyotrophic lateral sclerosis genetics.** *Nature neuroscience* 17, 17-23.

Riedl, L., Mackenzie, I.R., Forstl, H., Kurz, A., and Diehl-Schmid, J. (2014). **Frontotemporal lobar degeneration: current perspectives.** *Neuropsychiatric disease and treatment* 10, 297-310.

Ringholz, G.M., Appel, S.H., Bradshaw, M., Cooke, N.A., Mosnik, D.M., and Schulz, P.E. (2005). **Prevalence and patterns of cognitive impairment in sporadic ALS.** *Neurology* 65, 586-590.

Ripps, M.E., Huntley, G.W., Hof, P.R., Morrison, J.H., and Gordon, J.W. (1995). **Transgenic mice expressing an altered murine superoxide dismutase gene provide an animal model of amyotrophic lateral sclerosis.** *Proceedings of the National Academy of Sciences of the United States of America* 92, 689-693.

Robberecht, W., and Philips, T. (2013). **The changing scene of amyotrophic lateral sclerosis.** *Nature reviews Neuroscience* 14, 248-264.

Rogelj, B., Easton, L.E., Bogu, G.K., Stanton, L.W., Rot, G., Curk, T., Zupan, B., Sugimoto, Y., Modic, M., Haberman, N., *et al.* (2012). **Widespread binding of FUS along nascent RNA regulates alternative splicing in the brain.** *Scientific reports* 2, 603.

Rollinson, S., Mead, S., Snowden, J., Richardson, A., Rohrer, J., Halliwell, N., Usher, S., Neary, D., Mann, D., Hardy, J., *et al.* (2011). **Frontotemporal lobar degeneration genome wide association study replication confirms a risk locus shared with amyotrophic lateral sclerosis.** *Neurobiology of aging* 32, 758 e751-757.

Rosen, D.R., Siddique, T., Patterson, D., Figlewicz, D.A., Sapp, P., Hentati, A., Donaldson, D., Goto, J., O'Regan, J.P., Deng, H.X., *et al.* (1993). **Mutations in Cu/Zn superoxide dismutase gene are associated with familial amyotrophic lateral sclerosis.** *Nature* 362, 59-62.

Rosso, S.M., Donker Kaat, L., Baks, T., Joosse, M., de Koning, I., Pijnenburg, Y., de Jong, D., Dooijes, D., Kamphorst, W., Ravid, R., *et al.* (2003). **Frontotemporal dementia in The Netherlands: patient characteristics and prevalence estimates from a population-based study.** *Brain : a journal of neurology* 126, 2016-2022.

Rubino, E., Rainero, I., Chio, A., Rogaeva, E., Galimberti, D., Fenoglio, P., Grinberg, Y., Isaia, G., Calvo, A., Gentile, S., *et al.* (2012). **SQSTM1 mutations in frontotemporal lobar degeneration and amyotrophic lateral sclerosis.** *Neurology* 79, 1556-1562.

Rubinsztein, D.C., Marino, G., and Kroemer, G. (2011). **Autophagy and aging.** *Cell* 146, 682-695.

Rubinsztein, D.C., Shpilka, T., and Elazar, Z. (2012). **Mechanisms of autophagosome biogenesis.** *Current biology : CB* 22, R29-34.

Rulten, S.L., Rotheray, A., Green, R.L., Grundy, G.J., Moore, D.A., Gomez-Herreros, F., Hafezparast, M., and Caldecott, K.W. (2014). **PARP-1 dependent recruitment of the amyotrophic lateral sclerosis-associated protein FUS/TLS to sites of oxidative DNA damage.** *Nucleic acids research* 42, 307-314.

Rusten, T.E., and Stenmark, H. (2010). **p62, an autophagy hero or culprit?** *Nature cell biology* 12, 207-209.

Rutherford, N.J., Zhang, Y.J., Baker, M., Gass, J.M., Finch, N.A., Xu, Y.F., Stewart, H., Kelley, B.J., Kuntz, K., Crook, R.J., *et al.* (2008). **Novel mutations in TARDBP (TDP-43) in patients with familial amyotrophic lateral sclerosis.** *PLoS genetics* 4, e1000193.

Rutherford, N.J., Carrasquillo, M.M., Li, M., Bisceglia, G., Menke, J., Josephs, K.A., Parisi, J.E., Petersen, R.C., Graff-Radford, N.R., Younkin, S.G., *et al.* (2012). **TMEM106B risk variant is implicated in the pathologic presentation of Alzheimer disease.** *Neurology* 79, 717-718.

Ryu, H.H., Jun, M.H., Min, K.J., Jang, D.J., Lee, Y.S., Kim, H.K., and Lee, J.A. (2014). **Autophagy regulates amyotrophic lateral sclerosis-linked fused in sarcoma-positive stress granules in neurons.** *Neurobiology of aging*.

Sabatelli, M., Moncada, A., Conte, A., Lattante, S., Marangi, G., Luigetti, M., Lucchini, M., Mirabella, M., Romano, A., Del Grande, A., *et al.* (2013). **Mutations in the 3' untranslated region of FUS causing FUS overexpression are associated with amyotrophic lateral sclerosis.** *Human molecular genetics* 22, 4748-4755.

Saftig, P., Hetman, M., Schmahl, W., Weber, K., Heine, L., Mossmann, H., Koster, A., Hess, B., Evers, M., von Figura, K., *et al.* (1995). **Mice deficient for the lysosomal proteinase cathepsin D exhibit progressive atrophy of the intestinal mucosa and profound destruction of lymphoid cells.** *EMBO J* 14, 3599-3608.

Sah, N.K., Khan, Z., Khan, G.J., and Bisen, P.S. (2006). **Structural, functional and therapeutic biology of survivin.** *Cancer letters* 244, 164-171.

Salminen, A., Kaarniranta, K., Kauppinen, A., Ojala, J., Haapasalo, A., Soininen, H., and Hiltunen, M. (2013). **Impaired autophagy and APP processing in Alzheimer's disease: The potential role of Beclin 1 interactome.** *Progress in neurobiology* 106-107, 33-54.

Sapp, P.C., Hosler, B.A., McKenna-Yasek, D., Chin, W., Gann, A., Genise, H., Gorenstein, J., Huang, M., Sailer, W., Scheffler, M., *et al.* (2003). **Identification of two novel loci for dominantly inherited familial amyotrophic lateral sclerosis.** *American journal of human genetics* 73, 397-403.

Satoh, J., Kino, Y., Kawana, N., Yamamoto, Y., Ishida, T., Saito, Y., and Arima, K. (2014). **TMEM106B expression is reduced in Alzheimer's disease brains.** *Alzheimer's research & therapy* 6, 17.

Scaramuzzino, C., Monaghan, J., Milioto, C., Lanson, N.A., Jr., Maltare, A., Aggarwal, T., Casci, I., Fackelmayer, F.O., Pennuto, M., and Pandey, U.B. (2013). **Protein arginine methyltransferase 1 and 8 interact with FUS to modify its sub-cellular distribution and toxicity in vitro and in vivo.** *PloS one* 8, e61576.

Schebelle, L., Wolf, C., Stribl, C., Javaheri, T., Schnutgen, F., Ettinger, A., Ivics, Z., Hansen, J., Ruiz, P., von Melchner, H., *et al.* (2010). **Efficient conditional and promoter-specific in vivo expression of cDNAs of choice by taking advantage of recombinase-mediated cassette exchange using FLEX gene traps.** *Nucleic acids research* 38, e106.

Schmidhofer, T. (2007). Ludwig II. von Bayern - nicht schizophren, sondern ... (Pressestelle, Klinikum rechts der Isar der Technischen Universität München).
Schwenk, B.M., Lang, C.M., Hogg, S., Tahirovic, S., Orozco, D., Rentzsch, K., Lichtenthaler, S.F., Hoogenraad, C.C., Capell, A., Haass, C., *et al.* (2014). **The FTL risk factor TMEM106B and MAP6 control dendritic trafficking of lysosomes.** *EMBO J* 33, 450-467.

Seelaar, H., Kamphorst, W., Rosso, S.M., Azmani, A., Masdjedi, R., de Koning, I., Maat-Kievit, J.A., Anar, B., Donker Kaat, L., Breedveld, G.J., *et al.* (2008). **Distinct genetic forms of frontotemporal dementia.** *Neurology* 71, 1220-1226.

Seelaar, H., Rohrer, J.D., Pijnenburg, Y.A., Fox, N.C., and van Swieten, J.C. (2011). **Clinical, genetic and pathological heterogeneity of frontotemporal dementia: a review.** *Journal of neurology, neurosurgery, and psychiatry* 82, 476-486.

Sephton, C.F., Tang, A.A., Kulkarni, A., West, J., Brooks, M., Stubblefield, J.J., Liu, Y., Zhang, M.Q., Green, C.B., Huber, K.M., *et al.* (2014). **Activity-dependent FUS dysregulation disrupts synaptic homeostasis.** *Proceedings of the National Academy of Sciences of the United States of America* 111, E4769-4778.

Serpente, M., Fenoglio, C., Clerici, F., Bonsi, R., Arosio, B., Cioffi, S.M., Rotondo, E., Franceschi, M., Boneschi, F.M., Mari, D., *et al.* (2014). **Transmembrane Protein 106B Gene (TMEM106B) Variability and Influence on Progranulin Plasma Levels in Patients with Alzheimer's Disease.** *Journal of Alzheimer's disease : JAD.*

Shan, X., Chiang, P.M., Price, D.L., and Wong, P.C. (2010). **Altered distributions of Gemini of coiled bodies and mitochondria in motor neurons of TDP-43 transgenic mice.** *Proceedings of the National Academy of Sciences of the United States of America* 107, 16325-16330.

Shelkovernikova, T.A. (2013). **Modelling FUSopathies: focus on protein aggregation.** *Biochemical Society transactions* 41, 1613-1617.

Shelkovernikova, T.A., Peters, O.M., Deykin, A.V., Connor-Robson, N., Robinson, H., Ustyugov, A.A., Bachurin, S.O., Ermolkevich, T.G., Goldman, I.L., Sadchikova, E.R., *et al.* (2013). **Fused in sarcoma (FUS) protein lacking nuclear localization signal (NLS) and major RNA binding motifs triggers proteinopathy and severe motor phenotype in transgenic mice.** *The Journal of biological chemistry* 288, 25266-25274.

Shelkovernikova, T.A., Robinson, H.K., Southcombe, J.A., Ninkina, N., and Buchman, V.L. (2014). **Multistep process of FUS aggregation in the cell cytoplasm involves RNA-dependent and RNA-independent mechanisms.** *Human molecular genetics* 23, 5211-5226.

Siddique, T., Figlewicz, D.A., Pericak-Vance, M.A., Haines, J.L., Rouleau, G., Jeffers, A.J., Sapp, P., Hung, W.Y., Bebout, J., McKenna-Yasek, D., *et al.* (1991). **Linkage of a gene causing familial amyotrophic lateral sclerosis to chromosome 21 and evidence of genetic-locus heterogeneity.** *The New England journal of medicine* 324, 1381-1384.

Sieben, A., Van Langenhove, T., Engelborghs, S., Martin, J.J., Boon, P., Cras, P., De Deyn, P.P., Santens, P., Van Broeckhoven, C., and Cruts, M. (2012). **The genetics and neuropathology of frontotemporal lobar degeneration.** *Acta neuropathologica* 124, 353-372.

Skibinski, G., Parkinson, N.J., Brown, J.M., Chakrabarti, L., Lloyd, S.L., Hummerich, H., Nielsen, J.E., Hodges, J.R., Spillantini, M.G., Thusgaard, T., *et al.* (2005). **Mutations in the endosomal ESCRTIII-complex subunit CHMP2B in frontotemporal dementia.** *Nature genetics* 37, 806-808.

Snowden, J.S., Hu, Q., Rollinson, S., Halliwell, N., Robinson, A., Davidson, Y.S., Momeni, P., Baborie, A., Griffiths, T.D., Jaros, E., *et al.* (2011). **The most common type of FTL-D-FUS (aFTLD-U) is associated with a distinct clinical form of frontotemporal dementia but is not related to mutations in the FUS gene.** *Acta neuropathologica* 122, 99-110.

Sreedharan, J., Blair, I.P., Tripathi, V.B., Hu, X., Vance, C., Rogelj, B., Ackerley, S., Durnall, J.C., Williams, K.L., Buratti, E., *et al.* (2008). **TDP-43 mutations in familial and sporadic amyotrophic lateral sclerosis.** *Science* 319, 1668-1672.

Stagi, M., Klein, Z.A., Gould, T.J., Bewersdorf, J., and Strittmatter, S.M. (2014). **Lysosome size, motility and stress response regulated by fronto-temporal dementia modifier TMEM106B.** *Molecular and cellular neurosciences* 61, 226-240.

Stanley, J.L., Lincoln, R.J., Brown, T.A., McDonald, L.M., Dawson, G.R., and Reynolds, D.S. (2005). **The mouse beam walking assay offers improved sensitivity over the mouse rotarod in determining motor coordination deficits induced by benzodiazepines.** *Journal of psychopharmacology* 19, 221-227.

Stribl, C., Samara, A., Trumbach, D., Peis, R., Neumann, M., Fuchs, H., Gailus-Durner, V., Hrabe de Angelis, M., Rathkolb, B., Wolf, E., *et al.* (2014). **Mitochondrial dysfunction and decrease in body weight of a transgenic knock-in mouse model for TDP-43.** *The Journal of biological chemistry* 289, 10769-10784.

Susin, S.A., Lorenzo, H.K., Zamzami, N., Marzo, I., Snow, B.E., Brothers, G.M., Mangion, J., Jacotot, E., Costantini, P., Loeffler, M., *et al.* (1999). **Molecular characterization of mitochondrial apoptosis-inducing factor.** *Nature* 397, 441-446.

Suzuki, N., Kato, S., Kato, M., Warita, H., Mizuno, H., Kato, M., Shimakura, N., Akiyama, H., Kobayashi, Z., Konno, H., *et al.* (2012). **FUS/TLS-immunoreactive neuronal and glial cell inclusions increase with disease duration in familial amyotrophic lateral sclerosis with an R521C FUS/TLS mutation.** *Journal of neuropathology and experimental neurology* 71, 779-788.

Swerdlow, R.H. (2011). **Role and treatment of mitochondrial DNA-related mitochondrial dysfunction in sporadic neurodegenerative diseases.** *Current pharmaceutical design* 17, 3356-3373.

Takeuchi, R., Toyoshima, Y., Tada, M., Shiga, A., Tanaka, H., Shimohata, M., Kimura, K., Morita, T., Kakita, A., Nishizawa, M., *et al.* (2013). **Transportin 1 accumulates in FUS inclusions in adult-onset ALS without FUS mutation.** *Neuropathology and applied neurobiology* 39, 580-584.

Tan, A.Y., and Manley, J.L. (2009). **The TET family of proteins: functions and roles in disease.** *Journal of molecular cell biology* 1, 82-92.

Tan, A.Y., Riley, T.R., Coady, T., Bussemaker, H.J., and Manley, J.L. (2012). **TLS/FUS (translocated in liposarcoma/fused in sarcoma) regulates target gene transcription via single-stranded DNA response elements.** *Proceedings of the National Academy of Sciences of the United States of America* 109, 6030-6035.

Tanida, I., Ueno, T., and Kominami, E. (2008). **LC3 and Autophagy.** *Methods in molecular biology* 445, 77-88.

Testa, D., Lovati, R., Ferrarini, M., Salmoiraghi, F., and Filippini, G. (2004). **Survival of 793 patients with amyotrophic lateral sclerosis diagnosed over a 28-year period.** *Amyotrophic lateral sclerosis and other motor neuron disorders : official publication of the World Federation of Neurology, Research Group on Motor Neuron Diseases* 5, 208-212.

Tibshirani, M., Tradewell, M.L., Mattina, K.R., Minotti, S., Yang, W., Zhou, H., Strong, M.J., Hayward, L.J., and Durham, H.D. (2015). **Cytoplasmic sequestration of FUS/TLS associated with ALS alters histone marks through loss of nuclear protein arginine methyltransferase 1.** *Human molecular genetics* 24, 773-786.

Tolino, M., Kohrmann, M., and Kiebler, M.A. (2012). **RNA-binding proteins involved in RNA localization and their implications in neuronal diseases.** *The European journal of neuroscience* 35, 1818-1836.

Tradewell, M.L., Yu, Z., Tibshirani, M., Boulanger, M.C., Durham, H.D., and Richard, S. (2012). **Arginine methylation by PRMT1 regulates nuclear-cytoplasmic localization and toxicity of FUS/TLS harbouring ALS-linked mutations.** *Human molecular genetics* 21, 136-149.

Traynor, B.J., Nalls, M., Lai, S.L., Gibbs, R.J., Schymick, J.C., Arepalli, S., Hernandez, D., van der Brug, M.P., Johnson, J.O., Dillman, A., *et al.* (2010). **Kinesin-associated protein 3 (KIFAP3) has no effect on survival in a population-based cohort of ALS patients.** *Proceedings of the National Academy of Sciences of the United States of America* 107, 12335-12338.

Tsuiji, H., Iguchi, Y., Furuya, A., Kataoka, A., Hatsuta, H., Atsuta, N., Tanaka, F., Hashizume, Y., Akatsu, H., Murayama, S., *et al.* (2013). **Spliceosome integrity is defective in the motor neuron diseases ALS and SMA.** *EMBO molecular medicine* 5, 221-234.

Udan, M., and Baloh, R.H. (2011). **Implications of the prion-related Q/N domains in TDP-43 and FUS.** *Prion* 5, 1-5.

Uez, N., Lickert, H., Kohlhase, J., de Angelis, M.H., Kuhn, R., Wurst, W., and Floss, T. (2008). **Sall4 isoforms act during proximal-distal and anterior-posterior axis formation in the mouse embryo.** *Genesis* 46, 463-477.

Uranishi, H., Tetsuka, T., Yamashita, M., Asamitsu, K., Shimizu, M., Itoh, M., and Okamoto, T. (2001). **Involvement of the pro-oncoprotein TLS (translocated in liposarcoma) in nuclear factor-kappa B p65-mediated transcription as a coactivator.** *The Journal of biological chemistry* 276, 13395-13401.

Urwin, H., Josephs, K.A., Rohrer, J.D., Mackenzie, I.R., Neumann, M., Authier, A., Seelaar, H., Van Swieten, J.C., Brown, J.M., Johannsen, P., *et al.* (2010). **FUS pathology defines the majority of tau- and TDP-43-negative frontotemporal lobar degeneration.** *Acta neuropathologica* 120, 33-41.

van Blitterswijk, M., Mullen, B., Nicholson, A.M., Bieniek, K.F., Heckman, M.G., Baker, M.C., DeJesus-Hernandez, M., Finch, N.A., Brown, P.H., Murray, M.E., *et al.* (2014). **TMEM106B protects C9ORF72 expansion carriers against frontotemporal dementia.** *Acta neuropathologica* 127, 397-406.

Van Deerlin, V.M., Sleiman, P.M., Martinez-Lage, M., Chen-Plotkin, A., Wang, L.S., Graff-Radford, N.R., Dickson, D.W., Rademakers, R., Boeve, B.F., Grossman, M., *et al.* (2010). **Common variants at 7p21 are associated with frontotemporal lobar degeneration with TDP-43 inclusions.** *Nature genetics* 42, 234-239.

van der Zee, J., Van Langenhove, T., Kleinberger, G., Slegers, K., Engelborghs, S., Vandenberghe, R., Santens, P., Van den Broeck, M., Joris, G., Brys, J., *et al.* (2011). **TMEM106B is associated with frontotemporal lobar degeneration in a clinically diagnosed patient cohort.** *Brain : a journal of neurology* 134, 808-815.

van der Zee, J., Gijssels, I., Dillen, L., Van Langenhove, T., Theuns, J., Engelborghs, S., Philtjens, S., Vandenberghe, M., Slegers, K., Sieben, A., *et al.* (2013). **A pan-European study of the C9orf72 repeat associated with FTL: geographic prevalence, genomic instability, and intermediate repeats.** *Human mutation* 34, 363-373.

van der Zee, J., and Van Broeckhoven, C. (2014). **Dementia in 2013: frontotemporal lobar degeneration-building on breakthroughs.** *Nature reviews Neurology* 10, 70-72.

Van Hoecke, A., Schoonaert, L., Lemmens, R., Timmers, M., Staats, K.A., Laird, A.S., Peeters, E., Philips, T., Goris, A., Dubois, B., *et al.* (2012). **EPHA4 is a disease modifier of amyotrophic lateral sclerosis in animal models and in humans.** *Nature medicine* 18, 1418-1422.

Van Langenhove, T., van der Zee, J., Slegers, K., Engelborghs, S., Vandenberghe, R., Gijssels, I., Van den Broeck, M., Mattheijssens, M., Peeters, K., De Deyn, P.P., *et al.* (2010). **Genetic contribution of FUS to frontotemporal lobar degeneration.** *Neurology* 74, 366-371.

Van Langenhove, T., van der Zee, J., and Van Broeckhoven, C. (2012). **The molecular basis of the frontotemporal lobar degeneration-amyotrophic lateral sclerosis spectrum.** *Annals of medicine* 44, 817-828.

Vance, C., Rogelj, B., Hortobagyi, T., De Vos, K.J., Nishimura, A.L., Sreedharan, J., Hu, X., Smith, B., Ruddy, D., Wright, P., *et al.* (2009). **Mutations in FUS, an RNA processing protein, cause familial amyotrophic lateral sclerosis type 6.** *Science* 323, 1208-1211.

Vance, C., Scotter, E.L., Nishimura, A.L., Troakes, C., Mitchell, J.C., Kathe, C., Urwin, H., Manser, C., Miller, C.C., Hortobagyi, T., *et al.* (2013). **ALS mutant FUS disrupts nuclear localization and sequesters wild-type FUS within cytoplasmic stress granules.** *Human molecular genetics* 22, 2676-2688.

Vass, R., Ashbridge, E., Geser, F., Hu, W.T., Grossman, M., Clay-Falcone, D., Elman, L., McCluskey, L., Lee, V.M., Van Deerlin, V.M., *et al.* (2011). **Risk genotypes at TMEM106B are associated with cognitive impairment in amyotrophic lateral sclerosis.** *Acta neuropathologica* 121, 373-380.

Verbeeck, C., Deng, Q., Dejesus-Hernandez, M., Taylor, G., Ceballos-Diaz, C., Kocerha, J., Golde, T., Das, P., Rademakers, R., Dickson, D.W., *et al.* (2012). **Expression of Fused in sarcoma mutations in mice recapitulates the neuropathology of FUS proteinopathies and provides insight into disease pathogenesis.** *Molecular neurodegeneration* 7, 53.

Vintersten, K., Testa, G., Naumann, R., Anastassiadis, K., and Stewart, A.F. (2008). **Bacterial artificial chromosome transgenesis through pronuclear injection of fertilized mouse oocytes.** *Methods in molecular biology* 415, 83-100.

Wall, P.M., Blanchard, R.J., Yang, M., and Blanchard, D.C. (2003). **Infralimbic D2 receptor influences on anxiety-like behavior and active memory/attention in CD-1 mice.** *Progress in neuro-psychopharmacology & biological psychiatry* 27, 395-410.

Wang, W.Y., Pan, L., Su, S.C., Quinn, E.J., Sasaki, M., Jimenez, J.C., Mackenzie, I.R., Huang, E.J., and Tsai, L.H. (2013). **Interaction of FUS and HDAC1 regulates DNA damage response and repair in neurons.** *Nature neuroscience* 16, 1383-1391.

Ward, C.L., Boggio, K.J., Johnson, B.N., Boyd, J.B., Douthwright, S., Shaffer, S.A., Landers, J.E., Glicksman, M.A., and Bosco, D.A. (2014). **A loss of FUS/TLS function leads to impaired cellular proliferation.** *Cell death & disease* 5, e1572.

Watts, G.D., Wymer, J., Kovach, M.J., Mehta, S.G., Mumm, S., Darvish, D., Pestronk, A., Whyte, M.P., and Kimonis, V.E. (2004). **Inclusion body myopathy associated with Paget disease of bone**

and frontotemporal dementia is caused by mutant valosin-containing protein. *Nature genetics* 36, 377-381.

Wefers, B., Panda, S.K., Ortiz, O., Brandl, C., Hensler, S., Hansen, J., Wurst, W., and Kuhn, R. (2013). **Generation of targeted mouse mutants by embryo microinjection of TALEN mRNA.** *Nature protocols* 8, 2355-2379.

Wefers, B., Ortiz, O., Wurst, W., and Kuhn, R. (2014). **Generation of targeted mouse mutants by embryo microinjection of TALENs.** *Methods* 69, 94-101.

Wicklund, M.P. (2005). **Amyotrophic lateral sclerosis: possible role of environmental influences.** *Neurologic clinics* 23, 461-484.

Wong, Y.C., and Holzbaur, E.L. (2014). **Optineurin is an autophagy receptor for damaged mitochondria in parkin-mediated mitophagy that is disrupted by an ALS-linked mutation.** *Proceedings of the National Academy of Sciences of the United States of America* 111, E4439-4448.

Woulfe, J., Gray, D.A., and Mackenzie, I.R. (2010). **FUS-immunoreactive intranuclear inclusions in neurodegenerative disease.** *Brain pathology* 20, 589-597.

Wu, C.H., Fallini, C., Ticozzi, N., Keagle, P.J., Sapp, P.C., Piotrowska, K., Lowe, P., Koppers, M., McKenna-Yasek, D., Baron, D.M., *et al.* (2012). **Mutations in the profilin 1 gene cause familial amyotrophic lateral sclerosis.** *Nature* 488, 499-503.

Yamaguchi, A., and Kitajo, K. (2012). **The effect of PRMT1-mediated arginine methylation on the subcellular localization, stress granules, and detergent-insoluble aggregates of FUS/TLS.** *PloS one* 7, e49267.

Yan, J., Seibenhener, M.L., Calderilla-Barbosa, L., Diaz-Meco, M.T., Moscat, J., Jiang, J., Wooten, M.W., and Wooten, M.C. (2013). **SQSTM1/p62 interacts with HDAC6 and regulates deacetylase activity.** *PloS one* 8, e76016.

Yang, Y., Hentati, A., Deng, H.X., Dabbagh, O., Sasaki, T., Hirano, M., Hung, W.Y., Ouahchi, K., Yan, J., Azim, A.C., *et al.* (2001). **The gene encoding alsin, a protein with three guanine-nucleotide exchange factor domains, is mutated in a form of recessive amyotrophic lateral sclerosis.** *Nature genetics* 29, 160-165.

Yin, H.Z., Nalbandian, A., Hsu, C.I., Li, S., Llewellyn, K.J., Mozaffar, T., Kimonis, V.E., and Weiss, J.H. (2012). **Slow development of ALS-like spinal cord pathology in mutant valosin-containing protein gene knock-in mice.** *Cell death & disease* 3, e374.

Yoshimura, A., Fujii, R., Watanabe, Y., Okabe, S., Fukui, K., and Takumi, T. (2006). **Myosin-Va facilitates the accumulation of mRNA/protein complex in dendritic spines.** *Current biology : CB* 16, 2345-2351.

Youle, R.J., and Narendra, D.P. (2011). **Mechanisms of mitophagy**. *Nature reviews Molecular cell biology* 12, 9-14.

Zatloukal, K., Stumptner, C., Fuchsichler, A., Heid, H., Schnoelzer, M., Kenner, L., Kleinert, R., Prinz, M., Aguzzi, A., and Denk, H. (2002). **p62 Is a common component of cytoplasmic inclusions in protein aggregation diseases**. *The American journal of pathology* 160, 255-263.

Zhang, D., Paley, A.J., and Childs, G. (1998). **The transcriptional repressor ZFM1 interacts with and modulates the ability of EWS to activate transcription**. *The Journal of biological chemistry* 273, 18086-18091.

Zhang, K., Shi, P., An, T., Wang, Q., Wang, J., Li, Z., Duan, W., Li, C., and Guo, Y. (2013). **Food restriction-induced autophagy modulates degradation of mutant SOD1 in an amyotrophic lateral sclerosis mouse model**. *Brain research* 1519, 112-119.

Zhang, Z.C., and Chook, Y.M. (2012). **Structural and energetic basis of ALS-causing mutations in the atypical proline-tyrosine nuclear localization signal of the Fused in Sarcoma protein (FUS)**. *Proceedings of the National Academy of Sciences of the United States of America* 109, 12017-12021.

Zhou, Y., Liu, S., Liu, G., Ozturk, A., and Hicks, G.G. (2013). **ALS-associated FUS mutations result in compromised FUS alternative splicing and autoregulation**. *PLoS genetics* 9, e1003895.

Zhou, Y., Liu, S., Ozturk, A., and Hicks, G.G. (2014). **FUS-regulated RNA metabolism and DNA damage repair: Implications for amyotrophic lateral sclerosis and frontotemporal dementia pathogenesis**. *Rare diseases* 2, e29515.

Zhou, Z., Licklider, L.J., Gygi, S.P., and Reed, R. (2002). **Comprehensive proteomic analysis of the human spliceosome**. *Nature* 419, 182-185.

Zinszner, H., Albalat, R., and Ron, D. (1994). **A novel effector domain from the RNA-binding protein TLS or EWS is required for oncogenic transformation by CHOP**. *Genes & development* 8, 2513-2526.

Zinszner, H., Sok, J., Immanuel, D., Yin, Y., and Ron, D. (1997). **TLS (FUS) binds RNA in vivo and engages in nucleo-cytoplasmic shuttling**. *Journal of cell science* 110 (Pt 15), 1741-1750.

9 APPENDIX

9.1 ABBREVIATIONS

°C	Degree centigrade
4R	Four-repeat tau isoform
βgeo	β-galactosidase/neomycinphosphotransferase
γH ₂ AX	Aktivated Histon H ₂ AX
μ	micro (10 ⁻⁶)
A	Purine base Adenine
aa	Amino acid
Actb	Actin, beta
AD	Alzheimer's disease
adSA	Adenoviral splice acceptor
aFTLD-U	Atypical FTLD-U
AIF	Apoptosis inducing factor
ALS	Amyotrophic Lateral Sclerosis
ALS-Ci/Bi	ALS with cognitive or behavioral impairment
ANG	Angiogenin
ANOVA	Analysis of Variance
attB	Attachment site in the donor vector (RMCE)
ATXN2	Ataxin 2

B6	C57Bl6
BAC	Bacterial artificial chromosome
BCA	Bicinchoninic acid
BDNF	Brain-derived neurotrophic factor
BIBD	Basophilic inclusion body disease
bp	Base pair
BSA	Bovine serum albumin
bvFTD	Behavioral-variant frontotemporal dementia
c	centi (10^{-2})
C	Pyrimidine base Cytosine
C	Amino acid Cysteine
C9orf72	C9 open reading frame 72
CaCl ₂	Calcium chloride
CAG	Cytomegalovirus immediate early enhancer-chicken β -actin hybrid
cDNA	Complementary DNA
CHMP2B	Charged multivesicular body protein 2b
CLIP	Crosslinking and immunoprecipitation
CO ₂	Carbon dioxide
C-terminus	Carboxy terminus
CTSD	Cathepsin D
Da	Dalton
DAB	3,3'-diaminobenzidine
DAPI	4',6-diamidino-2-phenylindole

DCTN1	Dynactin
DH5 α	<i>E.coli</i> strain
DNA	Deoxyribonucleic acid
DNA-PK	DNA-dependent protein kinase
DNase	Desoxyribonuclease
dNTP	Deoxynukleosidtriphosphate
DPR	Dipeptide repeat proteins
DZNE	Deutsches Zentrum für Neurodegenerative Erkrankungen
E	Embryonic day
E14	E14Tg2A cells
<i>E. coli</i>	<i>Escherichia coli</i>
e.g.	exempli gratia, for example
ELISA	Enzyme Linked Immunosorbent Assay
ES cells	Embryonic stem cells
EUCOMM	European Conditional Mouse Mutagenesis
EWS	Ewing sarcoma RNA-binding protein
EWSR1	Ewing sarcoma breakpoint region 1
F	Female
FA	Formaldehyde
fALS	Familiar ALS
FCCP	Carbonyl cyanide-4-(trifluoromethoxy)phenylhydrazone
FET	FUS-EWS-TAF15
Fig.	figure

Flp	Flippase
FlpO	Optimized Flippase
FRT	FLP recombinase target
fs	Frameshift
FTD	Frontotemporal dementia
FTLD	Frontotemporal Lobar Degeneration
FTLD-MND	FTLD with motor neuron disease
FTLD-U	FTLD with ubiquitin-positive inclusions
FUS/TLS	Fused in Sarcoma/Translocation in Liposarcoma
fw	Forward
g	Acceleration of gravity (9.81 m/s ²)
G	Purine base Guanine
G	Amino acid Glycine
Gfap	Glial Fibrillary Acidic Protein
GMC	German Mouse Clinic
Grn	Progranulin
GT	Gene trap
GWAS	Genomewide association study
h	Hour(s)
H	Amino acid Histidine
H ₃	Histon H ₃
HCG	Human Chorion Gonadotropin
HD	Huntington's disease

HDAC1	Histone deacetylase 1
HDAC6	Histone Deacetylase 6
het	Heterozygote
hnRNP	Heterogeneous ribonucleoproteins
hom	Homozygote
HR	Homologous recombination
Hsp27	Heat shock protein 27
IAP	Inhibitor of apoptosis protein
IDG	Institute of Developmental Genetics
IHC	Immunohistochemistry
IPTG	Isopropyl- β -D-thiogalactopyranosid
IVC	Individually ventilated cages
k	Kilo
kg	Kilogram
l	Litre
L	Amino acid Leucine
LAMP1	Lysosomal-associated membrane protein 1
LB	Lysogeny broth
LC3	Microtubule-associated protein 1A/1B-light chain 3
LIF	Leukemia inhibiting factor
LMN	Lower motor neurons
loxP	Locus of crossing over of P1 phage
m	Meter

m	Milli (10^{-3})
M	Male
M	Molar
MAP6	Microtubule-associated protein 6
MAPT	Microtubule-associated protein tau
MEFs	Mouse embryonic fibroblasts
MeFUS	Methylated FUS
min	Minute(s)
MND	Motor neuron disease
MQC	Mitochondrial quality control
mRNA	Messenger RNA
n	nano (10^{-9})
n	Sample size
NCI	Neuronal cytoplasmic inclusions
NCL	Neuronal ceroid lipofuscinosis
n.d.	No difference
Ndrp2	N-myc downstream-regulated gene 2
NES	Nuclear export signal
NeuN	Neuronal nuclei
NF- κ B	Nuclear factor κ B
NIFID	Neuronal intermediate filament inclusion disease
NLS	Nuclear localization signal
NMD	Nonsense mediated decay

OCR	Oxygen consumption rate
OD	Optical density
Opa1	Optic atrophy 1
OPTN	Optineurin
Orf	Open reading frame
p	pico (10^{-12})
p	p-value (statistical analysis)
P	Amino acid Proline
p62	Protein with 62 kDa, sequestosome 1
pA	Polyadenylation signal
PARP-1	Poly (ADP-ribose) polymerase
PBS	Phosphate buffered saline
PCR	Polymerase chain reaction
PD	Parkinson's disease
PDC	Parkinson's disease and dementia
PFA	Paraformaldehyde
PFN 1	Profilin 1
PFNA	Progressive non-fluent aphasia
PMSG	Pregnant mare's serum gonadotropin
PPA	Primary progressive aphasia
PRMT1	Protein arginine methyltransferase 1
Ptk2b	Protein tyrosine kinase 2b
PY	Proline-tyrosine nuclear localization signal

Q	Amino acid Glutamine
QGSY	Glutamine-,glycine-,serine-, tyrosine-rich domain
qRT-PCR	quantitative real time polymerase chain reaction
R	Amino acid Arginine
RFP	Red fluorescence protein
RGG	Arginine-glycine-glycine
RIPA buffer	Radioimmunoprecipitation assay buffer
RMCE	Recombinase Mediated Cassette Exchange
RNA	Ribonucleic acid
RNase	ribonuclease
rpm	Rounds per minute
RRM	RNA recognition motif
RT	Room temperature
RT-PCR	reverse transcription polymerase chain reaction
rv	Reverse
S	Amino acid Serine
SA	Splice acceptor
sALS	Sporadic ALS
SBT	Somatic brain transgenesis
SC	Spinal cord
S.D.	Standard deviation
SD	Semantic dementia
SDS	Sodium dodecyl sulfate

SDS-PAGE	Sodium dodecyl sulfate polyacrylamide gel electrophoresis
sec	Second(s)
S.E.M	Standard error of the mean
SETX	Senataxin (SETX)
SMN	survival motor neuron
snoRNA	Small nucleolar RNA
SNP	Single nucleotide polymorphism
SOD1	Superoxide dismutase 1
Sort1	Sortilin 1
SPG	Spatacsin
SPPL2a	Signal peptide peptidase-like 2a
SQSTM1	Sequestosome 1
T	Pyrimidine base Thymine
Tab.	Table
TAE	Tris acetate with EDTA
TAF15	TATA-binding protein-associated factor 15
TARDBP	TAR DNA-binding protein gene
TBS(-T)	Tris buffered saline (with Tween)
TDP-43	Transactive response DNA binding protein 43 kDa
temp.	Temperature
TG	Transgenic
Tia1	Tia1 cytotoxic granule-associated RNA binding protein
Tim	Mitochondrial import inner membrane translocase

	subunit
TMEM106B	Transmembrane Protein 106 B
Tom	Mitochondrial import receptor subunit
Tris	Trishydroxymethyl-aminoethane
U	Pyrimidine base Uracil
U	Unit(s)
UBQLN2	Ubiquilin 2
UMN	Upper motor neurons
UPS	Ubiquitin proteasome system
UTR	Untranslated region
UV	Ultra-violet
V	Volt(s)
VAPB	Vesicle-associated membrane protein-associated protein B and C
VCP	Valosin-containing protein
VE-H ₂ O	Demineralized water
WISH	Whole Mount <i>in Situ</i> Hybridization
WT	Wild type
x	Symbol for crosses between mouse strains
X	STOP-codon
Y	Amino acid Tyrosine
Zn finger	Zink finger motif

9.2 INDICES

9.2.1 TABLES

Tab. 1: Heterogeneity of ALS.....	7
Tab. 2: Heterogeneity of FTLD.....	11
Tab. 3: Common features and differences of ALS-FUS and FTLD-FUS.....	20
Tab. 4: Lethality of <i>Fus</i> ^{-/-} mice.....	84
Tab. 5: Summary of behavioral analyses of <i>Fus</i> GT mice in the German Mouse Clinic.....	93
Tab. 6: Chromosomal Copy Number Assay of homozygous GT survivors.....	95
Tab. 7: Injected <i>hFUS</i> ES cell clones before or after Cre Recombination and resulting germline transmission.....	102
Tab. 8: Lethality of homozygous <i>hFUS</i> ^{R521G} mice.....	103
Tab. 9: Summary of behavioral analyses of <i>Fus</i> GT mice in the German Mouse Clinic.....	115
Tab. 10: Viability of mutant <i>Fus</i> TALEN mice. Depicted are numbers from het x het matings. ..	119
Tab. 11: Summary of behavioral analyses of <i>Fus</i> ^{R513G} mice in the German Mouse Clinic.....	130
Tab. 12: Comparison of heterozygous <i>hFUS</i> ^{R521G} , <i>Fus</i> ^{R513G} and <i>Fus</i> GT mice concerning GMC test battery.....	216

9.2.2 FIGURES

Fig. 1: ALS and FTD as two ends of one disease spectrum.....	12
Fig. 2: Pathological features in ALS-TDP and FTLD-TDP.....	13
Fig. 3: Structure of FUS.....	16
Fig. 4: Pathological features in ALS-FUS and FTLD-FUS.....	19
Fig. 5: Illustration and genotyping of the EUCE0290f05 gene trap mice alleles.....	83
Fig. 6: Embryonic and adult expression levels of <i>Fus</i>	85
Fig. 7: <i>Fus</i> depletion did not change its methylation status.....	86
Fig. 8: Splicing targets were not changed on protein level upon depletion of <i>Fus</i>	87
Fig. 9: No DNA damage or neuroinflammation, but enhanced p62 upon depletion of <i>Fus</i>	88
Fig. 10: Sensorimotor impairments in <i>Fus</i> GT mice.....	90
Fig. 11: No memory deficits in <i>Fus</i> deficient mice.....	92

Fig. 12: Morphological heterogeneity of homozygous survivor mice.....	94
Fig. 13: Phenotypical analysis of homozygous survivors.....	96
Fig. 14: Pathological analysis of homozygous GT survivors.....	97
Fig. 15: Generation of mice carrying ALS-associated <i>hFUS</i> mutations.....	99
Fig. 16: Expression of hFUS ^{R521G} <i>in vivo</i>	104
Fig. 17: Mislocalization of FUS in fibroblasts derived from heterozygous adult mice, but not in embryonic fibroblasts.....	106
Fig. 18: FUS is recruited into stress granules upon oxidative stress.....	108
Fig. 19: No FUS mislocalization or inclusions in hFUS ^{R521G+/-} mice.....	109
Fig. 20: Expression of hFUS mutation R521G <i>in vivo</i> did not cause insoluble FUS, DNA damage, or other pathological features.....	110
Fig. 21: No loss of motor neurons in hFUS ^{R521G+/-} mice.....	111
Fig. 22: Expression of hFUS mutation R521G <i>in vivo</i> did not change levels of the splicing target <i>Bdnf</i>	112
Fig. 23: Differences in FUS methylation status in embryos and adult hFUS ^{R521G+/-} mice.....	113
Fig. 24: hFUS ^{R521G+/-} mice showed hypoactivity but were inconspicuous concerning strength and motor coordination.....	116
Fig. 25: Enhanced curiosity in hFUS ^{R521G+/-} mice.....	117
Fig. 26: Generation of mutant <i>Fus</i> mice applying TALEN technology.....	118
Fig. 27: Slight mislocalization of <i>Fus</i> in fibroblasts derived from adult TALEN mice.;.....	121
Fig. 28: Shift of <i>Fus</i> protein to the cytoplasm and recruitment into granules upon oxidative stress.....	122
Fig. 29: No inclusion formation, insoluble <i>Fus</i> , or DNA damage in <i>Fus</i> TALEN mice.....	124
Fig. 30: Tendential motor neuron degeneration in the cervical SC of <i>Fus</i> ^{R513G-/-} mice.....	125
Fig. 31: Enhanced levels of p62 and AIF in the SC of 15 months old homozygous <i>Fus</i> ^{R513G} mice.....	127
Fig. 32: Accumulation of <i>Fus</i> in the SC of adult <i>Fus</i> ^{R513G} mice and decreased <i>Fus</i> methylation in embryos.....	128
Fig. 33: Hints towards changed levels of <i>Fus</i> splicing targets in <i>Fus</i> ^{R513G} mice.....	129
Fig. 34: <i>Fus</i> ^{R513G} mice did not show any impairments in muscle function or motor coordination.....	132
Fig. 35: Sex specific behavior concerning activity and anxiety in <i>Fus</i> ^{R513G} mice.....	133
Fig. 36: Transgenic expression of <i>Tmem106b</i> <i>in vivo</i>	135
Fig. 37: Cytoplasmic TDP-43 in eight months old <i>Tmem106b</i> ^{17BACtg} mouse.....	138
Fig. 38: Blebbing of mitochondria in the frontal cortex of <i>Tmem106b</i> ^{BACtg} mice.....	139

Fig. 39: Cytoplasmic hTDP-43 in Tmem106b ^{BACtg} and hTDP-43 ^{A315TKi} compound mice, but no inclusion formation.....	141
Fig. 40: Elevated levels of total TDP-43, but no changes in Grn, C9orf72, or endo-/lysosomal protein levels upon ectopic Tmem106b expression..	143
Fig. 41: No clear genotype specific differences in serum Grn levels.....	144
Fig. 42: No mitochondrial dysmorphology in young single and double transgenic mice.....	145
Fig. 43: No genotype specific changes of proteins involved in mitophagy or apoptosis upon ectopic Tmem106b expression.....	147
Fig. 44: Ectopic Tmem106b expression did not result in any impairment of mitochondrial respiration.	147
Fig. 45: Quantification of fibroblasts from adult heterozygous hFUS ^{R521G} and Fus ^{R513G} mice bearing mislocalized FUS.....	212
Fig. 46: Comparison of behavioral analyses of FusR513G and hFUSR521G mouse lines with pooled sexes and controls.	213
Fig. 47: Comparison of FUS protein sequenz from human, Neanderthal, chimp, and mouse.	215
Fig. 48: Comparison of protein levels in adult brains.	219
Fig. 49: Comparison of FUS splicing targets on mRNA level.....	220
Fig. 50: Comparison of FUS splicing targets on protein level.....	221

9.3 SUPPLEMENTARY DATA

9.3.1 VIDEOS OF FUS *GT*^{-/-} SURVIVOR MICE

For videos of homozygous GT survivor mice, see digital appendix.

The first video shows a homozygous EUCE0290f05 mouse with the number 253 at the age of seven weeks, the second video the mouse with the number 274 at the age of three weeks. These were the two survivors with the strongest phenotype. It can be seen that both have a hump and a toddling gait, characterized by bilateral external torsion of the tibia. Additionally, #274 was very small, even for the young age of three weeks.

9.3.2 COMPARISON OF HFUS AND MFUS

9.3.2.1 Subcellular mislocalization of FUS

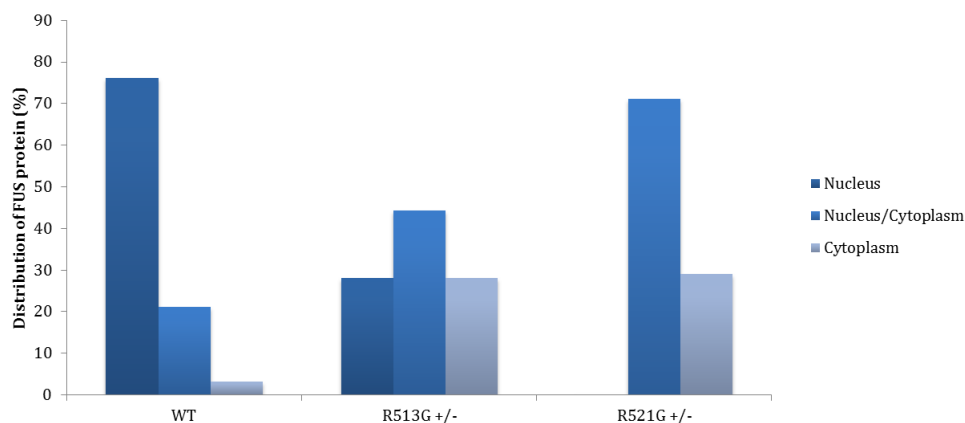


Fig. 45: Quantification of fibroblasts from adult heterozygous hFUS^{R521G} and Fus^{R513G} mice bearing mislocalized FUS. Counted were cells with FUS only in the nucleus or cytoplasm and cells, where FUS was observed in both compartments. Among Fus^{R513G} cells 28% each harbored Fus only in the nucleus or cytoplasm. In 44% Fus was detected in both nucleus and cytoplasm. Concerning hFUS^{R521G} no single cell was found where FUS staining was only found in the nucleus. 71% of cells showed nuclear and cytoplasmic and 29% exclusively cytoplasmic localization. 100 cells/genotype were counted.

9.3.2.2 Comparison of phenotypical analysis

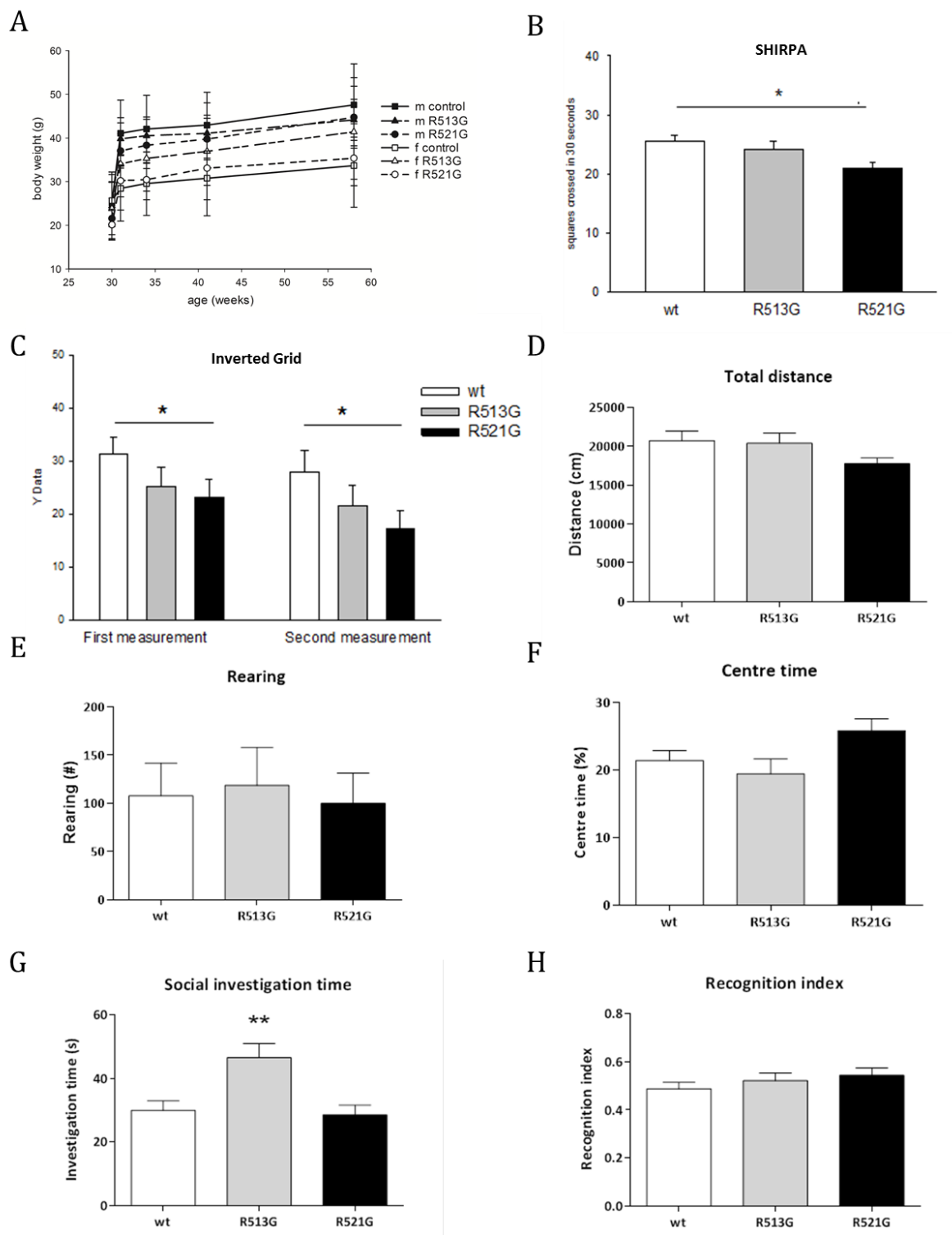


Fig. 46: Comparison of behavioral analyses of Fus^{R513G} and $hFUS^{R521G}$ mouse lines with pooled sexes and controls. (A) Comparison of weight. Mutant R521G females were heavier than mutant R513G females and controls. No body weight loss occurred. (B) Locomotor activity was reduced in $hFUS^{R521G}$ heterozygotes compared to controls (ANOVA $p < 0.05$), while this was unchanged in Fus^{R513G} mice. (C) For the Inverted Grid, shorter latencies were

observed for hFUS^{R521G} mice compared to controls (linear regression, $p < 0.05$; age 8 months). In a second measurement of the same mice at the age of 13 months this effect could be confirmed ($p < 0.05$). Fus^{R513G} mice showed an intermediate phenotype, which did not reach statistical significance. (D-F) In the Open Field, our test of spontaneous activity in a novel environment, neither the hFus^{R521G} nor FUS^{R513G} mice showed clear differences in forward (total distance) (D) or horizontal (total rearing) exploratory activity (E) with pooled sexes. Furthermore, there were no clear differences in terms of anxiety-related behavior (total center time and distance) between the groups (F). (G, H) However, while there were no clear genotype effects on social discrimination memory (H), there was an increase in amount of social investigation time by the Fus^{R513G} mice (ANOVA: $F(2,52) = 7.81$, $p = 0.001$) (G). Error bars represent S.E.M. Graphs and description by Lore Becker and Lillian Garrett;

9.3.2.3 Sequenz comparison

human	1	MASNDYTQQATQSYGAYPTQPGQGYSSQSSQPYGQQSYSS	YSQSTD	SGYGG	SY-SSY	59	
neand	1	MASNDYTQQATQSYGAYPTQPGQGYSSQSSQPYGQQSYSS	YSQSTD	SGYGG	SY-SSY	59	
chimp	1	MASNDYTQQATQSYGAYPTQPGQGYSSQSSQPYGQQSYSS	YQSAD	SGYGG	SYGSSY	59	
mouse	1	MASNDYTQQATQSYGAYPTQPGQGYSSQSSQPYGQQSYSS	YQSAD	SGYGG	SYGSSY	59	
human	60	QSQNTGYGTSTPQGYCSTGGYSSQSSQSSYGGQSSYPGYGQQPAPSTSGSYGSSSQS				119	QGSY
neand	60	QSQNTGYGTSTPQGYCSTGGYSSQSSQSSYGGQSSYPGYGQQPAPSTSGSYGSSSQS				119	
chimp	60	QSQNR---TSPQGYCSIG-YSSQSSQSSYGGQSSYPGYGQQPAPSTLGSYGSSSQS				114	
mouse	60	QSQNTGYGTSTPQGYCSTGGYSSQSSQSSYGGQSSYPGYGQQPAPSTSGSYGSSSQS				120	
human	120	SSYGQPQSGSYSQQPSYGGQQQ-SYGQQQS-YNPPQGYGQQNQYNSSSGGGGGGGGGNY				177	
neand	120	SSYGQPQSGSYSQQPSYGGQQQ-SYGQQQS-YNPPQGYGQQNQYNSSSGGGGGGGGGNY				177	
chimp	115	SSYGQPQSGSYSQQPSYGGQQQ-SYGQQQS-YNPPQGYGQQNQYNSSSGGGGGGG---NY				169	
mouse	121	SSYGQPQSGGYGQQ-SYGGQQQSYGQQQS-YNPPQGYGQQNQYNSSSGGGGGGGGG-NY				178	
human	178	GQDQSSMSGGGSGGGTGNQDQSSGGGSGGYG--QDRGGRGRGGSGGGGGGGGGG--YN				233	RGG1
neand	178	GQDQSSMSGGGSGGGTGNQDQSSGGGSGGYG--QDRGGRGRGGSGGGGGGGGGG--YN				233	
chimp	170	GQDQSSMSGGGSGGGTGSQDQSSGGGSGGYG--QDRGGRGRGGSGGGGGGGGGGGYIN				227	
mouse	179	GQDQSSMSGGGSGGGTGNQDQSSGGGSGGYG--QDRGGRGRGGSGGGGGGGGGG--YN				226	
human	234	RSSGGYEPGRGGGRGGRGGMGGSDRGGFNKFGGPRDQGSRHDSEQDNSDNNTIFVQGLG				293	Export
neand	241	RSSGGYEPGRGGGRGGRGGMGGSDRGGFNKFGGPRDQGSRHDSEQDNSDNNTIFVQGLG				293	
chimp	228	RSSGGYEPGRGGGRGGRGGMGGSDRGGFNKFGGPRDQGSRHDSEQDNSDNNTIFVQGLG				298	
mouse	227	RSSGGYEPGRGGGRGGRGGMGGSDRGGFNKFGGPRDQGSRHDSEQDNSDNNTIFVQGLG				286	
human	294	ENVTIESVADYFKQIGIIKTNKKTGQPMINLYTDRETGKLGKGEATVSFDDPPSAKAAIDW				353	RRM
neand	294	ENVTIESVADYFKQIGIIKTNKKTGQPMINLYTDRETGKLGKGEATVSFDDPPSAKAAIDW				353	
chimp	299	ENVTIESVADYFKQIGIIKTNKKTGQPMINLYTDRETGKLGKGEATVSFDDPPSAKAAIDW				358	
mouse	287	ENVTIESVADYFKQIGIIKTNKKTGQPMINLYTDRETGKLGKGEATVSFDDPPSAKAAIDW				346	
human	354	FDGKEFSGNPIKVSFATRRAADFNRGGNGRGGGRGGPMGRGGYGGGGSGGGGRGGFPSPG				413	RGG2
neand	354	FDGKEFSGNPIKVSFATRRAADFNRGGNGRGGGRGGPMGRGGYGGGGSGGGGRGGFPSPG				413	
chimp	359	FDGKEFSGNPIKVSFATRRAADFNRGGNGRGGGRGGPMGRGGYGGGGSGGGGRGGFPSPG				418	
mouse	347	FDGKEFSGNPIKVSFATRRAADFNRGGNGRGGGRGGPMGRGGYGGGGSGGGGRGGFPSPG				406	
human	414	GGGGGQQRAGDWKCPNPTCENMNF SWRNECNQCKAPKPDGPPGGP GGSHMGGNYGDDRR				473	RGG3
neand	414	GGGGGQQRAGDWKCPNPTCENMNF SWRNECNQCKAPKPDGPPGGP GGSHMGGNYGDDRR				473	
chimp	419	GGGGGQQRAGDWKCPNPTCENMNF SWRNECNQCKAPKPDGPPGGP GGSHMGGNYGDDRR				467	
mouse	407	GGGGGQQRAGDWKCPNPTCENMNF SWRNECNQCKAPKPDGPPGGP GGSHMGGNYGDDRR				466	
human	474	GGGGYDRGGYRGGDRGGFRGGGGDRGGFGPGKMDSRGEHRQDRRERPY				526	PY
neand	474	GGGGYDRGGYRGGDRGGFRGGGGDRGGFGPGKMDSRGEHRQDRRERPY				526	
chimp	468	GGGGYDRGGYRGGDRGGFRGGGGDRGGFGPGKMDSRGEHRQDRRERPY				518	
mouse	467	-GGGGYDRGGYRGGDRGGFRGGGGDRGGFGPGKMDSRGEHRQDRRERPY				518	

sequence-
variations:

sequence-
feature:

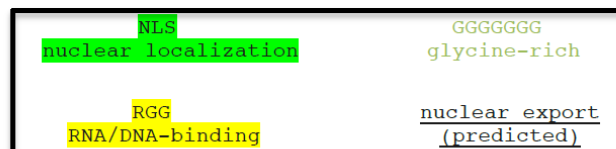
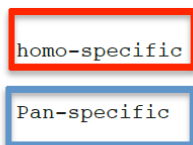


Fig. 47: Comparison of FUS protein sequenz from human, Neanderthal, chimp, and mouse. Neanderthals and humans exhibit eleven additional phosphorylation sites (nine serins and two threonins) at the N-terminus of FUS compared to murine amino acid sequence. Protein domains and mutations in discussed mouse models are depicted. (Thomas Floss)

9.3.3 COMPARISON OF *FUS* GT, *FUS*^{R513G} AND *FUS*^{R521G} MOUSE LINES

9.3.3.1 Comparison of GMC data

Tab. 12: Comparison of heterozygous hFUS^{R521G}, Fus^{R513G} and Fus GT mice concerning GMC test battery.

Behavior test	Parameter measured	<i>hFUS</i> ^{R521G}		<i>Fus</i> ^{R513G}		<i>Fus</i> GT	
		7 WT M/9 het M/10 WT F/8 het F		8 WT M/7 het M/14 WT F/11 het F		9 WT M/12 het M/7 WT F/16 het F	
		Age (months)	Result	Age (months)	Result	Age (months)	Result
SHIRPA	General health and autonomous functions, reflexes, locomotor activity, posture and movement	7	Reduced locomotor activity	6	n.d.	7	n.d.
Grip Strength	Muscle function	7	n.d.	6	n.d.	7	n.d.
Rotarod	Coordination and balance	7.5	More falling from the rod	6.5	n.d.	7.5	n.d.
Balance Beam	Motor coordination and balance	7.5	Trend to more time and slips	6.5	n.d.	8	n.d.
Beam Ladder	Motor coordination	7.5	Slightly less traversing time	6.5	Less hindpaw slips	8	Increased number of fore paw slips (p<0.05), no difference in time and

							stops
Inverted Grid	Sensorimotor function	8	Latencies reduction	7.5	n.d.	8	Reduced latency to fall down ($p<0.01$)
Open field	Locomotion	9	n.d.	9	Spontaneous activity ↑ males ↓ females ($p=0.003$)	8	n.d.
	Exploration	9	Increase in total rearing activity ($p=0.01$)	9	Increased rearing activity ($p=0.03$)	8	n.d.
	Anxiety-related	9	More time in the center ($p=0.03$)	9	Time spent in center ↑ males ↓ females ($p=0.003$)	8	n.d.
Balance Beam 2 nd time	Motor coordination and balance	9.5	Slightly more time	9	Slightly less time and less slips	9.5	Increased traversing time and slightly more slips, no difference in stops
Inverted Grid 2 nd time	Sensorimotor function	13.5	Latencies reduction	12.5	trend to reduced lastencies	9.5	Reduced latency to fall down ($p<0.01$)

Grip Strength 2 nd time	Muscle function	13.5	n.d.	12.5	n.d.	9.5	n.d.
Y maze	Working memory	10	n.d.	13	Trend towards more spontaneous alterations in males	13	Trend to less alterations
Social discrimination	Olfaction-based social memory/discrimination	12.5	Trend towards more social discrimination	13.5	Trend towards more social discrimination in males	13.5	Trend to more social discrimination

n.d., no difference; het, heterozygous; hom, homozygous; F, female; M, male; in red: significant

9.3.3.2 Comparison of pathological results

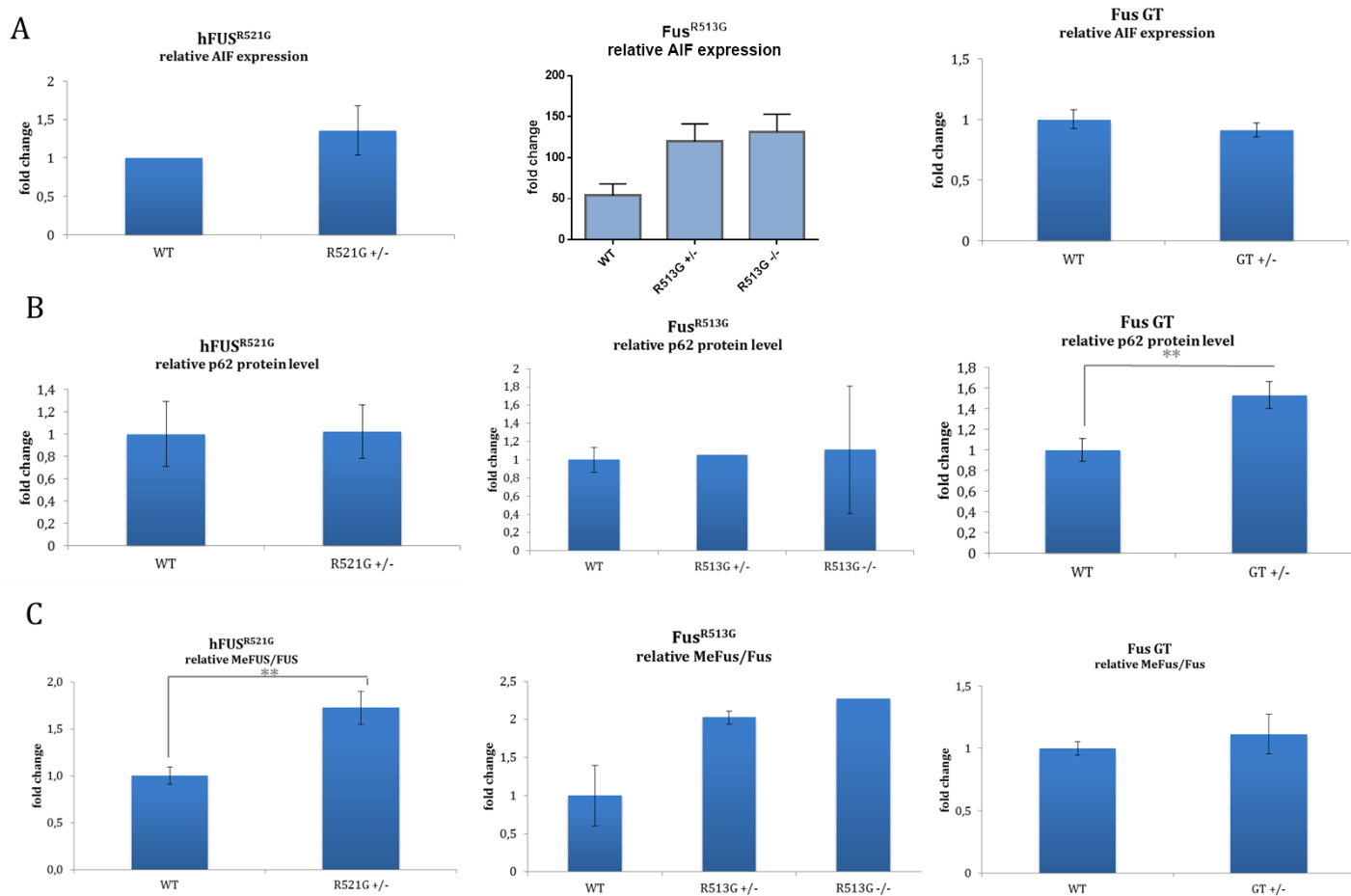


Fig. 48: Comparison of protein levels in adult brains. Changes in AIF and p62 levels, as well as methylation status of FUS were not consistent between the different mouse models. Error bars represent S.D.. Student's t-test was performed (exception: relative AIF expression in Fus^{R513G} mice: One-way ANOVA). For n see detailed figures.

9.3.3.3 Comparison of splicing targets







Gene	Lagier-Tourenne <i>et al.</i> , 2012	My results
Ptk2b	More exclusion (only after depletion of FUS not of TDP-43)	 GT  Mutations
hnRNP-D	More inclusion	
Sort1	Change only TDP-43 dependent	 More exclusion
Ndr2	More exclusion	
Tia1	More inclusion	 In adult GT brain

Fig. 49: Comparison of FUS splicing targets on mRNA level. Changes concerning exon inclusion or exclusion of some splicing targets found in the publication of Lagier-Tourenne et al. (2012) after depletion of FUS are listed. In brains of *Fus* GT mice compared to WT controls, most findings could be confirmed, except for *Sort1* for which Lagier-Tourenne and colleagues observed only TDP-43 dependent changes. In brains or MEFs derived from *hFUS^{R521G}* or TALEN mice, results for *hnRNP-D*, *Sort1* or *Ndr2* were the same as in *Fus* deficient mice. Concerning *Ptk2b*, more exon exclusion could not be observed. *Tia1* worked only in GT mice.

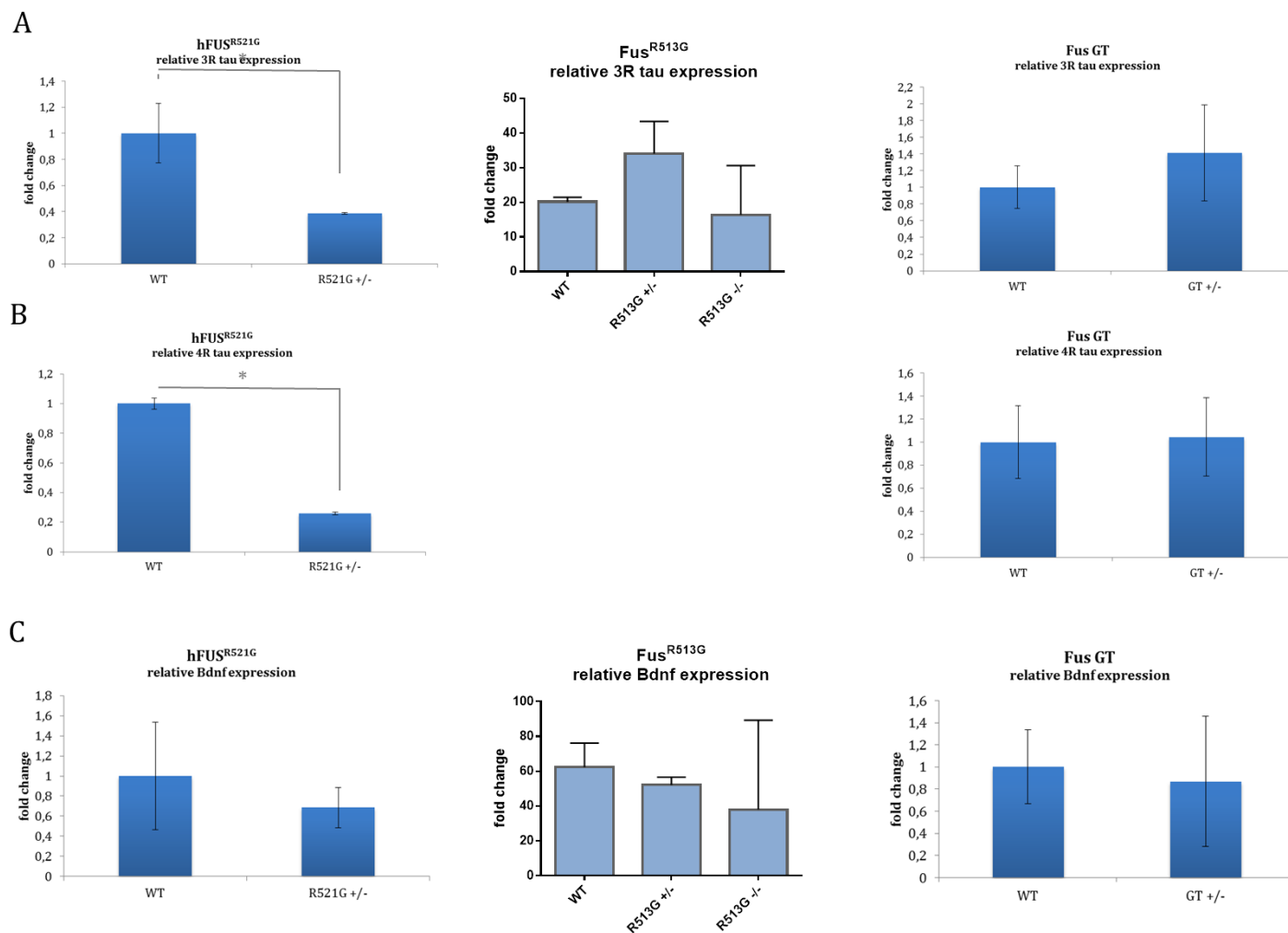


Fig. 50: Comparison of FUS splicing targets on protein level. Levels of tau and Bdnf were reduced in the humanized FUS mouse model, whereas in Fus deficient and TALEN mice tau levels were not changed or tendentially elevated. Bdnf was also tendentially reduced. Error bars represent S.D.. Student's t-test was performed (exception: relative 3R tau and Bdnf expression in Fus^{R513G} mice: One-way ANOVA). For n see detailed figures.

Danksagung

Danke an...

... Prof. Dr. Wolfgang Wurst und Dr. Daniela Vogt Weisenhorn für die Möglichkeit, meine Doktorarbeit am IDG anzufertigen, sowie für das Interesse an meinem Thema und die hilfreichen Ratschläge bei Problemen.

... PD Dr. Thomas Floss für die gute Betreuung meiner Arbeit, die Unterstützung bei Problemen, die entspannte Arbeitsatmosphäre und dass er sich immer Zeit genommen hat, wenn es etwas zu besprechen gab.

... Prof. Dr. Dr. Christian Haass für die Teilnahme an meinem Thesis Committee und die anregenden Diskussionen.

... Prof. Dr. Harald Luksch für die Übernahme des Vorsitzes in der Prüfungskommission.

... Prof. Dr. Heiko Lickert für die Übernahme der Funktion als Zweitprüfer.

... dem Injektionsteam und der GMC für die gute Zusammenarbeit.

... Julia Götzl für die sehr gute Kollaboration und die Zeit und Mühen, die diese in Anspruch genommen hat.

... Theresa Faus-Keßler für die statistische Analyse.

... die liebe Irina, die sich immer um meine Mäuse gekümmert hat!

... Constantin fürs Korrektur lesen.

... Annerose für die Hilfe und Organisation bei so vielen Dingen (insbesondere des Kaffeevorrates ☺) und dem gesamten IDG für die allgegenwärtige Hilfsbereitschaft und die tolle Arbeitsatmosphäre.

... Anke, Carola, Helga, Irina, Susanne, Luise, Constantin, Clara, Bene, Svenja und Anja. Ohne euch wäre die Doktorarbeit nur halb so schön gewesen. Ihr seid nicht nur Kollegen sondern vor allem sehr gute Freunde.

... Caro für den guten Zuspruch und das offene Ohr, vor allem in den letzten Monaten.

... Dani für deine Freundschaft und Unterstützung in allen Lebenslagen! Du bist die Beste!

... Silvio für alles! Für deine endlose Geduld und die ständige Unterstützung, egal was war.

... Mama und Corinna, die immer für mich da sind.

... meine Großeltern, die hoffentlich auf mich stolz sein können.